UNIVERSITA' VITA-SALUTE SAN RAFFAELE

CORSO DI DOTTORATO DI RICERCA INTERNAZIONALE
IN MEDICINA MOLECOLARE

CURRICULUM IN CELLULAR AND MOLECULAR
BIOLOGY

Identifying metabolic alterations in inflammation-driven tumours

DoS: Dr. Simone Cardaci
Second Supervisor: Prof. Giuseppe Filomeni

Tesi di DOTTORATO di RICERCA di Federico Uchenna Stanley
matr. 019832
Ciclo di dottorato XXXVII
SSD BIO11/BIO12

Anno Accademico 2023/2024

UNIVERSITA' VITA-SALUTE SAN RAFFAELE

CORSO DI DOTTORATO DI RICERCA INTERNAZIONALE
IN MEDICINA MOLECOLARE

CURRICULUM IN CELLULAR AND MOLECULAR
BIOLOGY

Identifying metabolic alterations in inflammation-driven tumours

DoS: Dr. Simone Cardaci
Second Supervisor: Prof. Giuseppe Filomeni

Tesi di DOTTORATO di RICERCA di Federico Uchenna Stanley
matr. 019832
Ciclo di dottorato XXXVII
SSD BIO11/BIO12

Anno Accademico 2023/2024

CONSULTAZIONE TESI DI DOTTORATO DI RICERCA

Il sottoscritto Federico Uchenna Stanley

Matricola / registration number 019832

nato/ born at Bologna

il/on 01/07/1994

autore della tesi di Dottorato di ricerca dal titolo / author of the PhD Thesis titled:

Identifying metabolic alterations in inflammation-driven tumours

AUTORIZZA la Consultazione della tesi / AUTHORIZES the public release of the thesis

Data /Date 28/10/2024

Firma /Signature 

DECLARATION

This thesis has been:

- composed by myself and has been used in a previous publication. Throughout the text I use both 'I' and 'We' interchangeably.
- has been written according to the editing guidelines approved by the University.

Images 1, 2, 3, 4, 5, and 8 were obtained from open-access papers, with references provided in their respective figure legends.

All the results presented here were obtained by me, except for:

1) *Computational analyses of experiments performed by me, illustrated in Results, figures 13, 16, 18 (A,B,C), 22 (A,B,C), 23E, 25 (A,B,C), 26 (A,B,C), 27(C,D,E), 28, 29, 31, 32B, 33, 40 (B,C,D), 41, 42 (B,C) were performed by Dr. Tanja Eberhart, Cancer Metabolism Unit, Division of Genetics and Cell Biology, IRCCS San Raffaele Scientific Institute, Milan, Italy*
2) *Histological stainings illustrated in Results, figurse 10A, 10C, 15C, 19B, 23C, 25D, 45, were performed by Dr. Amleto Fiocchi, from the Advanced Light and Electron Microscopy Centre, San Raffaele Hospital, Milan, Italy*
3) *Whole body metabolic analyses of in vivo experiments performed by me, illustrated in Results, figures 20A and 21, were performed by Dr. Sylvia Badurek, Preclinical Phenotyping Facility, Vienna BioCenter Core Facilities (VBCF), member of the Vienna BioCenter (VBC), Vienna, Austria*
4) *Liver proteomic of experiments performed by me, reported in Results, figures 16 and 18 (A, B, C), was carried out by Prof. Angelo D'alessandro lab members Rachel Culp-Hill and Monika Dzieciatkowska, Department of Biochemistry and Molecular Genetics, Anschutz Medical Campus, University of Colorado School of Medicine, Aurora, CO, USA*
5) *Metabolomics of experiments performed by me, descripted in Results, figures 12 (B, D), 14A, 17 (B, C), 18E, 22E, 27A, 30, 32A, 40A, 44B, were performed by Dr. David Sumpton and Engy Shokry, CRUK Beatson Institute, Glasgow, UK*
6) *RNA sequencings of experiments performed by me, descripted in Results, figures 22 (A, B, C), 23E, 25 (A, B, C), 26 (A, B, C), were performed by Dr. Andreas*

Sommer, Next Generation Sequencing Facility, Vienna BioCenter Core Facilities (VBCF), member of the Vienna BioCenter (VBC), Vienna, Austria

7) *16s ribosomal DNA gene sequencings illustrated in Results and in vitro treatments of stools derived from experimental mice and pure bacterial strains with itaconate illustrated in Results, figure 36, were performed by Prof. Nicasio Mancini and Prof. Nicola Clementi lab members Dr. Roberto Ferrarese and Dr. Sofia Sisti, Laboratory of Medical Microbiology and Virology, Vita-Salute San Raffaele University, Milan, Italy, in collaboration with me.*

Except for data illustrated in *Results, figures 43, 44 and 45*, the results presented in this thesis were previously published in a peer-reviewed journal:

***Eberhart, T., *Stanley, F.U.**, Ricci, L. *et al.* ACOD1 deficiency offers protection in a mouse model of diet-induced obesity by maintaining a healthy gut microbiota. *Cell Death Dis* 15, 105 (2024). https://doi.org/10.1038/s41419-024-06483-2 (Eberhart, Stanley et al., 2024) (*co-first authors).

All sources of information are acknowledged by means of reference.

Ackowledgements

First, I would like to thank my Director of Studies, Dr. Simone Cardaci, who firstly welcomed me in the lab and guided me during the three years.

I gratefully acknowledge Professor Giuseppe Filomeni for co-supervising my project.

I want to express my gratitude towards Dr. Tanja Eberhart, who guided and assisted me since her arrival in the lab, whose work has been essential in accomplishing this PhD project and, most importantly, for having my back.

I want to thank my PhD mate, Dr. Luisa Ricci for providing me technical support when needed and for making our days more liveable in the lab.

I would like to thank Dr. Silvia Lence, our master's student intern, for her assistance with technical support and mice colony maintenance during the final phases of this project.

I would also like to thank all my internal and external collaborators, who contributed to my project providing with reagents and technical support.

Last, but not least, Dr. Tiziana Chirico, our former master student, who struggled and worked with me during my first two years of the PhD, helping me obtaining several results.

Abstract

Itaconate is a metabolite with immune-regulatory and anti-microbial functions, which is synthetised by the mitochondrial enzyme ACOD1 (Aconitate Decarboxylase 1) by repurposing cis-aconitate from the tricarboxylic acid (TCA) cycle in the mitochondria. Obesity is characterized by a corrupted pro-inflammatory milieu, elicited by integrated signals resulting from fat overnutrition and it is a risk factor predisposing individuals to the development of inflammatory-driven cancers, such as hepatocellular carcinoma (HCC). Despite itaconate biosynthesis has been found involved in the development of several inflammatory diseases, its role in response to whole-body nutritional perturbations and associated HCC progression remained largely unresolved. By employing integrated multi-omics approaches, we demonstrated that genetic deficiency of *Acod1* promotes gut microbiota-mediated metabolic health in mice. Specifically, abrogation of itaconate biosynthesis protected mice from obesity, altered glucose homeostasis and liver dysfunction by attenuating meta-inflammatory responses elicited by high fat diet (HFD) consumption. Faecal metagenomics and microbiota transplantation experiments demonstrated that such effects were secondary to an amelioration in the composition of the intestinal microbiota, known to participate in the development of metabolic disease. In particular, ablation of itaconate biosynthesis opposed the decline in the *Bacteroidetes/Firmicutes* ratio, a dysbiotic signature induced by HFD feeding associated with obesity and type 2 diabetes both in mice and humans. Specularly to *Acod1* loss, oral administration of supraphysiological doses of itaconate in *wild type* mice magnified the effects of HFD on intestinal microbiota composition and obesity-related outcomes. Furthermore, *in vitro* and *in vivo* experiments showed that itaconate, endogenously produced or exogenously administered, inhibited the growth of *Bacteroides*, a microbial genus belonging to *Bacteroidaceae* family, known to elicit beneficial effects against metabolic syndrome. In line with protection from diet-induced obesity, we demonstrated that *Acod1* loss offers resistance to development of HCC induced in mice following prolonged consumption of a hepatosteatotic diet (Western diet). In conclusion, this study reveals a novel role for itaconate biosynthesis in sustaining changes in intestinal microbiota elicited by dietary lipid overload, thus pointing ACOD1 as a potential target against metabolic disease and associated liver cancer.

Table of contents

Table of contents 1
Acronyms and abbreviations 3
List of figures and tables 9
Introduction 11
Energy Balance Homeostasis 11
Central and peripheral control of energy balance 13
Adipose tissue 15
Adipose Tissue plasticity 17
Adipose tissue endocrine function 21
Obesity 24
Dysfunction of adipose tissues in obesity 24
Chronic low-grade inflammation 26
Comorbidities in obesity 27
Therapeutic strategies in obesity 31
Gut microbiota in health and disease 35
How to study the gut microbiota 38
Cis-Aconitate Decarboxylase 1 and Itaconate 40
Immunoregulatory properties of itaconate 43
Itaconate in host-pathogen interactions 47
The role of itaconate in diseases 48
Aim of the work 52
Results 53
Acod1 deficiency protects mice from diet-induced obesity and associated dysfunction of systemic glucose homeostasis. 53
Analysis of Acod1 expression in mouse and human tissues 59
Itaconate administration abolishes the effects of Acod1 ablation on metabolic responses to HFD 63
Acod1 ablation opposes liver steatosis and associated metabolic dysfunction induced by dietary lipid overload. 65
Acod1 loss positively impacts mice on HFD by enhancing metabolic activity 72
Acod1 loss reduces obesity-associated inflammation in adipose tissues 82
Itaconate biosynthesis promotes gut microbiota changes associated with diet-induced obesity 88
Itaconate supplementation induces an "obesity-like" microbiome 95

Itaconate Biosynthesis: Sustaining Gut Microbiota Alterations and Driving Meta-Inflammation in Metabolic Disease *103*
Acod1 loss protects against hepatocellular carcinoma development induced by Western diet *113*
Discussion *116*
Materials and methods *128*
Mice and treatments *128*
RNA extraction and real-time qPCR *128*
RNA-sequencing (RNA-seq). *129*
Liver Proteomics *129*
Functional Enrichment Analyses *131*
Metabolite extraction and LC-MS *131*
Diglyceride profiling *132*
Measurement of liver triglycerides and NH3 ..... *132*
SCFA measurement *133*
Histology and image analyses *134*
Glycemia and insulinemia determination *135*
Glucose and insulin tolerance test *135*
Indirect calorimetry and activity measurements *135*
Determination of total faecal energy excretion *135*
16s ribosomal DNA gene sequencing and analysis *135*
Treatment of faecal bacterial cultures with itaconate. *137*
Treatment of pure bacterial cultures with itaconate *137*
Plasma metabolic hormones and cytokines determination *138*
Measurement of intestinal permeability *138*
Measurement of faecal bacterial abundance *138*
Faecal microbiota transplantation *138*
In vitro adipogenesis assay *139*
Generation and treatment of BMDMs *139*
Enzyme-linked immunosorbent assay (ELISA). *140*
Human datasets *140*
Ethical approval of animal studies *140*
Statistics and reproducibility *140*
Data availability *141*
References *143*

Acronyms and abbreviations

4-EI: 4-monoethyl itaconate

4-OI: 4-octyl itaconate

5-HT: Serotonin; 5-hydroxytryptamine

5-HTTP: 5-hydroxiltriptophan

ABCG2: ATP-binding cassette transporter G2

ABHD5: Alpha/beta hydrolase domain-containing protein 5

ACC: Acetyl-CoA carboxylase

ACLY: ATP-citrate lyase

ACOD1: aconitato decarboxylase 1

ACTB: Actin beta

AgRP: Agouti-related protein

ALDOA: Aldolase A

AMPK: AMP-activated protein kinase

ARC: Arcuate nucleus

ASS: Argininosuccinate synthetase

ATF3: Activating Transcription Factor 3

ATGL: Adipose triglyceride lipase

ATM: Adipose tissue-resident macrophage

ATP: Adenosine triphosphate

b-AR: Beta adrenergic receptor

BAT: Brown adipose tissue

BMDM: Bone marrow-derived macrophage

BMI: Body mass index

BMP: Bone morphogenetic protein

BMR: Basal metabolic rate

C/EBP: CCAAT/enhancer binding protein

cAMP: Cyclic adenosine triphosphate

CART: Amphetamine-regulated transcript

CAZymes: Carbohydrate-active enzymes

CCK: Cholecystokinin

CCL: chemokine (C-C motif) ligand

CD36: Cluster of differentiation 36

ChREBP: Carbohydrate-responsive element-binding protein

Cidea: Cell Death inducing DFFA like effector A

CLS: Crown-like structure

CLYBL: Citramalyl-CoA lyase

CNS: central nervous system

CO2: Carbon dioxide 2

CPS1: Carbamoyl phosphate synthetase 1

CPT: Carnitine palmitoyltransferase

CVD: Cardiovascular disease

DAG: Diacylglycerol

DI: Dymethil itaconate

DIO: Diet-induced obesity

Dio2: Iodothyronine Deiodinase 2

DNL: De novo lipogenesis

EC: Enterochromaffin cell

EPS: Extracellular polysaccharide

eWAT: Epididymal white adipose tissue

F26BP: Fructose-6-phosphate-2 kinase

FADH2: Flavin adenine dinucleotide

FASN: Fatty acid synthase

FATP: Fatty acid transport protein

FDA: Food and drug administration

FFA: Free fatty acids

FFAR: Free fatty acids receptor

FITC-dextran: Fluorescein isothiocyanate dextran

FMT: Faecal microbiota transplantation

GALT: Gut-associated lymphoid tissue

GAPDH: Glyceraldehyde-3-phoshate

Ghrl: Ghrelin gene

GIT: Gastrointestinal tract

GLP-1: Glucagon-like peptide 1

GLP-1R: Glucagon-like peptide 1 receptor

GLUT: Glucose transporter

GM-CSF: Granulocyte-macrophage colony-stimulating factor

GPCR: G-protein coupled receptor

GR: Glucocorticoid receptor

GSDMD: Gasdermin

H&E: Haematoxylin and eosin

HCC: Hepatocellular carcinoma

HDAC: Hystone deacetylase

HFD: High-fat diet

HSC: Hepatic stellate cell

HSL: Hormone-sensitive lipase

I/R: Ischemia/reperfusion injury

IBS: Irritable bowel syndrome

ICL: Isocitrate lyase

IKK-β: IκB kinase

IL: Interleukin

INFγ: Interferon γ

iNOS: Inducible nitric oxide synthase

IR: Insulin resistance

IRG1: Immune-responsive gene 1

IRS: Insulin receptor substrate

iWAT: Inguinal white adipose tissue

JAK: Janus kinase

JNK: c-Jun N-terminal kinase

KEAP1: Kelch-like ECH-associated protein 1

kJ: kilo Joule

LBP: Lipopolysaccharide binding protein

LCA: Lithocholic acid

LCFA: Long chain fatty acid

LC-MS: Liquid chromatography–mass spectrometry

LD: Lipid droplet

LDHA: Lactate dehydrogenase A

LDL: Low-density lipoprotein

Lep: Leptin gene

Lepr: Leptin receptor

LepRb: Leptin receptor

LPL: Lipoprotein lipase

LPS: Lipopolysaccharide

MAG: Monoacylglycerol lipase

MCM: Methylmalonyl-CoA mutase

MCP1: Monocyte chemoattractant protein 1

MDSC: Myeloid-derived suppressor cells

MGL: Monoglyceride lipase

Mit/TFE: Microphthalmia/transcription factor E

MPO: Myeloperoxidase

mRNA: Messanger RNA

MS: Mass spectrometry

mtDNA: Mitochondrial DNA

Mtorc1: Mechanistic target of rapamycin complex 1

mtROS: Mitochondrial reactive oxygen species

NAD: Nicotinamide adenine dinucleotide

NAFLD: Non-alcoholic fatty liver diseases

NAGS: N-acetylglutamante synthase

NASH: Non-alcoholic steatohepatitis

ND: Normal diet

NE: Noradrenaline

NF-kb: Nuclear factor-kappa B

NFKBIZ: NF-kappa-B inhibitor zeta

NLRP3: NOD-, LRR-, and pyrin domain-containing protein 3

NPY: Neuropeptide Y

NRF: Nuclear respiratory factor

NRF2: Nuclear factor erythroid 2-like 2

NS: Non-significant

NTS: Nucleus of the solitary tract

O2: oxygen

Ob/Ob: mice with leptin gene deficiency

OD: Optical density

OTC: Ornithine transcarbamylase

OXGR: Oxoglutarate receptor

OXPHOS: Oxidative phosphorylation

PAMP: Pathogen-associated molecular pattern

PCA: Principal component analysis

PDGFR: platelet-derived growth factor receptor

PDH: Pyruvate dehydrogenase

PGC1α: Peroxisome proliferator-activated receptor gamma coactivator 1-alpha

PKA: Protein kinase A

PLIN: Perilipin

POMC: Pro-opiomelanocortin

PPAR: Peroxisome proliferator-activated receptor

PVN: Paraventricular nucleus

pWAT: Peritoneal white adipose tissue

PYY: Peptide tyrosine tyrosine

qPCR: quantitative polymerase chain reaction

RER: Respiratory exchange ratio

RET: Reverse electron transport

RNA: Ribonucleic acid

ROS: Reactive oxygen species

RQ: Respiratory quotient

rRNA: Ribosomal RNA

SAS: Statistical analysis system

SCFA: Short chain fatty acids

SCS: Succinyl coenzyme A synthetase

SDH: Succinate dehydrogenase

sem: Standard error of the mean

SNS: Sympathetic nervous system

SREBP-1c: sterol regulatory element-binding protein-1c

STAT: Signal transducer and activator of transcription

STING: Stimulator of interferon genes

T2DM: Type 2 diabetes mellitus

TCA Tricarboxylic acid cycle

TET: Ten-eleven translocation methyl-cytosine dioxygenases

TFEB: Transcription factor EB

TG: Triacylglycerol (triglyceride)

TIN: Tumour infiltrating neutrophil

TLR: Toll-like receptor

TNFα: Tumor necrosis factor alpha

UCP: Uncoupling protein

VCO2: Carbon dioxide production

VLDL: Very-low-density lipoprotein

VO2: Oxygen consumption

WAT: White adipose tissue

WD Western diet

WHO: World Health Organization

ZYKV: Zika virus

α-KG: Alpha ketoglutarate

αMSH: α-melanocyte stimulating hormone

List of figures and tables

Figure 1. Energy balance homeostasis *11*
Figure 2. Morphology of three fat depots in mammals. *17*
Figure 3. Chronic low-grade inflammation *27*
Figure 4. Site of action of FDA approved anti-obesity medications. *34*
Figure 5. Gut microbiota alterations in healthy and obese patients. *38*
Figure 6. ACOD1 catalyses the decarboxylation of cis-aconitate to itaconate *40*
Figure 7. Itaconate family and derivatives. *43*
Figure 8. Targets and mechanisms of action of itaconate and derivatives *47*
Figure 9. Acod1 loss offers protection against diet-induced obesity in mice. *54*
Figure 10. Acod1 deficiency opposes diet-induced changes in adipose tissues. *56*
Figure 11. Acod1 loss opposes alterations in glucose and insulin homeostasis under HFD consumption. *58*
Figure 12. Acod1 expression modulation in tissues. *61*
Figure 13. ACOD1 expression in human tissues. *62*
Figure 14. Itaconate supplementation nullifies the effects of Acod1 ablation on metabolic responses to HFD. *64*
Figure 15. Genetic deficiency of Acod1 opposes diet-induced liver steatosis. *66*
Figure 16. Acod1 deficiency counteracts the impact of dietary lipid overload on hepatic proteome. *68*
Figure 17. Acod1 loss counteracts fatty acids accumulation in the liver of HFD-fed mice. *69*
Figure 18. Acod1 loss rescues urea cycle dysfunctions induced by dietary lipid overload. *71*
Figure 19. Acod1 ablation ameliorates fibrosis in mice under fat overnutrition. *72*
Figure 20. Impact of Acod1 loss on energy balance-regulating processes. *74*
Figure 21. Acod1 deficiency ameliorates metabolic fitness challenged with dietary lipid overload *76*
Figure 22. Acod1 ablation enhances catabolic processes during a high-fat diet in white adipose tissue. *78*
Figure 23. Acod1 loss enhances energy expenditure through activation of thermogenic processes in adipose tissues. *81*
Figure 24. Acod1 impact on inflammation. *83*
Figure 25. Acod1 ablation attenuates HFD-induced meta-inflammation in white adipose tissue. *85*
Figure 26. Acod1 ablation protects from the systemic HFD-driven metabolic inflammation. *87*
Figure 27. Acod1 exacerbates the impact of diet-induced gut dysbiosis. *89*
Figure 28. Acod1 ablation increases the abundance of Bacteroidetes families under high-fat diet. *91*
Figure 29. Acod1 deficiency increases the abundance of the Bacteroides genus under high-fat diet. *92*
Figure 30. Acod1 loss rescues the drop in the abundance of SCFAs induced by HFD. *93*
Figure 31. Acod1 loss does not alter the small intestine microflora. *94*
Figure 32. Itaconate supplementation induces an "obesity-like" gut microbiota. *95*
Figure 33. Itaconate supplementation reduces the abundance of Bacteroidetes families under high-fat diet. *97*
Figure 34. Itaconate supplementation aggravates obesity and associated metabolic outcomes. *99*
Figure 35. Effects of itaconate supplementation on urea cycle gene expression and macrophage accumulation. *100*
Figure 36. Itaconate inhibits the growth of Bacteoidetes-belonging taxa. *102*
Figure 37. Schematic representation of faecal microbiota transplantation (FMT) *103*
Figure 38. Faecal microbiota of Acod1-deficient mice offers transferable protection from metabolic disease and liver dysfunction. *105*
Figure 39. Faecal microbiota of Acod1-deficient mice opposes adipose tissues inflammation and

altered catabolic activity induced by high-fat diet. *106*
Figure 40. Gut microbiota before FMT. *108*
Figure 41. Gut microbiota after FMT. *109*
Figure 42. Effect and correlation of itaconate biosynthesis on gut permeability in mice and humans. *111*
Figure 43. Working model *112*
Figure 44. Acod1 loss protects against diet-induced HCC progression. *113*
Figure 45. Acod1 is modulated by Western diet. *114*
Figure 46. Impact of Acod1 loss on livers after WD/ CCl4 challenge. *115*
Table 1. List of primers used *142*

Introduction

Energy Balance Homeostasis

Energy balance is defined as the difference between the energy absorbed by the intestine following food ingestion and the energy utilized by body's tissues for various activities (Fig. **1**). The primary factors influencing energy balance include energy intake, intestinal energy absorption, energy expenditure, and energy storage. Energy intake encompasses the assimilation of energy from the ingestion of macronutrients (lipids, carbohydrates, and proteins) and their subsequent intestinal absorption and metabolism. Instead, energy expenditure encompasses the basal metabolic rate (BMR), which is the amount of energy expended by the body at rest to maintain essential physiological functions, thermogenesis, and physical activity. Energy expenditure and energy storage fluctuate dynamically, resulting in either a positive or negative energy balance. A positive energy balance occurs when energy intake and assimilation exceed the energy demands of physical and physiological activities. This excess energy is stored as body fat, the primary energy reserve in humans and other mammals, leading to an increase in body weight and fat mass. A long-term positive energy balance may lead to overweight or obesity and associated chronic conditions. Conversely, a prolonged negative energy balance can disrupt energy homeostasis, resulting in chronic disorders such as anorexia and undernutrition. (Hill et al., 2012).

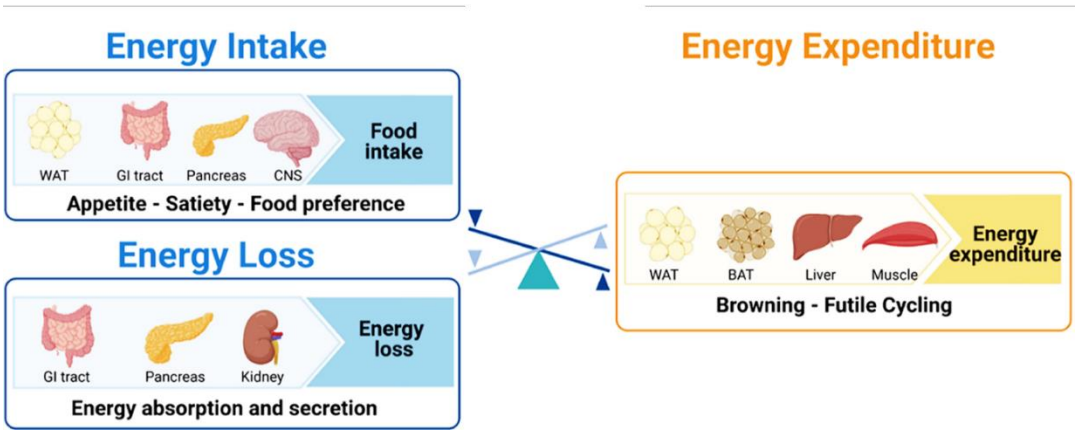

Figure 1. Energy balance homeostasis (Löffler et al., 2021).

In animals, the total daily energy expenditure can be divided into different components. These include the energy spent on basal metabolism, the increase in energy expenditure following food intake, the energy spent on thermoregulation and the energy consumed on physical activity. Beyond physical work, heat is the end-product of all metabolic activities. Therefore, it is possible to calculate energy expenditure by measuring directly heat produced by the animal (direct calorimetry). However, more routinely and easily, whole body energy consumption can be determined indirectly by measuring components of the metabolic processes that generate heat,such as O_2 consumed and CO_2 produced, and hence infer its production indirectly. For instance, the overall equation for glucose oxidation is:

$$\mathbf{C_6H_{12}O_6 + 6\,(H_2O) + 6\,(O_2) \longrightarrow 12(H_2O) + 6(CO_2) + 2820\ kJ}$$

This equation indicates that the animal has used 2,820 kilo Joule of energy for every 6 mol of oxygen consumed or CO_2 produced. When different fuel supplies are utilized, the equation changes in a systemic way depending on the substrate used. This can be inferred from the measured ratio of oxygen consumption to CO_2 production called the respiratory exchange ratio (RER). The actual substrate oxidation at the tissue level is referred to as the respiratory quotient (RQ), a dimensionless number calculated from RER, describing the macronutrients metabolized. If metabolism consists solely of lipids, the respiratory quotient is approximately 0.7, for proteins it is approximately 0.8, and for carbohydrates it is 1.0. Often, energy consumption is composed of both fats and carbohydrates. Therefore, the approximate respiratory quotient of a mixed diet is 0.8 (Speakman, 2013). For measuring energy expenditure in rodents, metabolic cages equipped with several chambers and gas analysers have been developed, allowing researchers to carry out metabolic (indirect calorimetry), behavioural and physiological studies by monitoring individually caged mice in an automated and synchronized manner. Metabolic parameters measured include food and water consumption, oxygen consumption (VO_2), carbon dioxide production (VCO_2), respiratory exchange ratio (RER, VCO_2/VO_2) and ambulatory movements, using a 3- dimensional infrared light-beam (Speakman, 2013). Collectively, such metabolic cages enable researchers to evaluate changes in the

metabolic rate of experimental animals occurring in response to specific interventions and to associate them to either preferential substrate use, feeding behaviour or locomotor activities.

Central and peripheral control of energy balance

The control of energy balance requires a fine interplay between central and peripheral signals. Therefore, one of the most relevant and coordinated pathway involved in energy homeostasis is the control of satiety, which is defined as the physiological state at the end of a meal when further eating is inhibited by 'fullness' (Amin & Mercer, 2016). Central signals originating from the brain integrate information regarding energy status and modulate appetite, satiety, and energy expenditure. In particular, the hypothalamus plays a key role in the regulation of feeding behaviour. The hypothalamus is divided into several nuclei which are closely connected with various brain regions (cerebral cortex, limbic system, and autonomic nervous system). Nutrients, vagal afferent signalling from the gut and adiposity related signals stimulate the arcuate nucleus (ARC), which is the primary site for processing and integrating peripheral signals of hunger and satiety and is characterized by orexigenic (appetite-increasing) first-order neurons secreting neurohormones such as neuropeptide Y (NPY) and agouti-related peptide (AgRP) and anorexigenic (appetite-decreasing) first-order neurons (S. Li et al., 2023), producing pro-opiomelanocortin (POMC) and cocaine- and amphetamine-regulated transcript (CART) (Roh & Kim, 2016). These neurohormones act on second-order neurons in other areas of the hypothalamus, such as the paraventricular nucleus and lateral hypothalamus, as well as in the nucleus of the solitary tract (NTS) in the brainstem, thereby influencing appetite regulation and energy balance. (Camilleri, 2014).

Peripheral signals provide feedback to the brain regarding the body's energy stores and current metabolic needs. Throughout the body, several organs participate in the production of these signals, among which the gastrointestinal tract (GIT), the adipose tissue, the liver, pancreas and skeletal muscles. This intricate communication network between hormonal and neuroendocrine systems ensures that energy intake, storage, and expenditure are finely tuned to maintain homeostasis and body weight within a narrow range. Based on the luminal content, enteroendocrine cells, which are specialized cells found throughout the GIT, produce hormones such as ghrelin, cholecystokinin (CCK),

glucagon-like peptide 1 and peptide YY (GLP-1 and PYY respectively) whose function is to regulate energy balance (Perry & Wang, 2012). Ghrelin is secreted before a meal and stimulates the production of the orexigenic neuropeptides NPY and AgrP (Hong-Zai et al., 2010), promoting food intake and suppressing thermogenesis (Wren et al., 2000; Yasuda et al., 2003). CCK, produced mainly by intestinal I cells in the duodenum and jejunum and in a small part in the central nervous system (CNS), is released during food ingestion. CCK has an anorexigenic effect and acts as a satiety-stimulator by suppressing gastric emptying and transit through a direct action on the stomach and by inhibiting food intake through the communication with the brain (Beglinger, 1994; Matzinger et al., 1999). GLP-1 is a 30 amino acid hormone produced by intestinal L cells found in the distal ileum and colon and is considered as an incretin hormone due to its ability to stimulate the proliferation of the insulin-secretor β-pancreatic cells. In addition, GLP-1 inhibits the pancreatic secretion of glucagon (Ramracheya et al., 2018). In parallel, GLP-1 determines an anorexigenic effect by reducing food intake after binding with its receptor (Bugarith et al., 2005). PYY, a 36 amino acid protein belonging to the pancreatic polypeptide-fold family of peptides, is secreted by L-type endocrine cells mainly found along the terminal ileum and colon and acts as an anorexigenic hormone.

Adipose tissue

The adipose tissue is a specialized connective tissue originating from mesenchymal cells and composed mostly by adipocytes, whose primary function is to store energy in the form of lipids. Within the adipose tissue, a wide range of cell populations are found, such as mesenchymal, endothelial and immune cells (mainly macrophages) as well as pre-adipocytes. Based on its morphology (Fig. **2**), the adipose tissue can be subdivided into three main categories: white, brown and beige adipose tissues.

White adipose tissue (WAT) is the most abundant fat tissue and major energy reservoir in mammals, playing a crucial role in maintaining whole-body energy homeostasis. Based on their anatomical location, the WATs are categorized into subcutaneous, found beneath the skin and representing most of the total fat mass, and visceral white adipose tissue, located around organs in the peritoneal cavity. White adipocytes are spherical, white cells, characterized by the presence of a large unilocular lipid droplet that occupies most of the cell volume and few mitochondria. In mouse models, the inguinal adipose depot (iWAT) and the epididymal (eWAT) adipose depot are the predominant models of subcutaneous and visceral adipose tissue, respectively.

Mature white adipocytes develop from a series of finely tuned cellular events named adipogenesis, which is divided in two sequential steps. The process begins with the "commitment" phase, where a multipotent, fibroblast-like mesenchymal precursor, characterized by the expression of platelet-derived growth factor receptors (PDGFRα and/or PDGFRβ) commits to the adipocyte lineage forming a pre-adipocyte. This phase is regulated by specific signalling pathways and transcription factors, such as Wnt and Bone morphogenetic proteins (BMP2 and BMP4). Subsequently, pre-adipocytes enter a differentiation phase characterized by mitotic clonal expansion allowing the generation of a sufficient number of cells until growth arrest. This phase is then followed by morphological and biochemical alterations, leading to the formation of a mature adipocyte. During the differentiation stage, the induction of several transcription factors is essential in regulating this finely tuned process. Peroxisome proliferator-activated receptor γ (PPARγ) and CCAAT/enhancer binding protein α (C/EBPα) are the primary regulators of the adipogenic program (Audano et al., 2022).

Brown adipose tissue (BAT) is a highly vascularized specialized type of adipose tissue primarily found in mammals, including humans, composed by brown adipocytes, where its primary function is thermogenesis through the uncoupling of mitochondrial respiration. As a thermogenic organ, BAT is essential in maintaining body temperature and consuming the excessive energy. Brown adipocytes are distinguished from their white counterparts by their characteristic features: the presence of numerous small lipid droplets and a dense population of mitochondria rich in iron, which imparts the tissue its distinctive brown colour. The high mitochondrial density enables brown adipocytes to produce heat through non-shivering thermogenesis, a process driven by the expression of uncoupling protein 1 (UCP1) (Jung et al., 2019). UCP1 is found in the inner mitochondrial membrane of brown and beige adipocytes and uncouples the electron transport chain from ATP synthesis, allowing protons to leak across the mitochondrial inner membrane and dissipate energy as heat instead of producing ATP. The heat generated by UCP1-mediated thermogenesis in brown and beige adipocytes can be dissipated to the rest of the body, increasing overall energy expenditure. UCP1 activation is primarily regulated by sympathetic nervous system (SNS) signalling in response to cold exposure or other stimuli. This stimulation leads to the release of norepinephrine from sympathetic nerve terminals, which binds to β3-adrenergic receptor on the surface of brown adipocytes. Activation of beta-adrenergic receptors initiates a signalling cascade that increases intracellular levels of cyclic AMP (cAMP). Elevated cAMP activates protein kinase A (PKA), which phosphorylates and activates UCP1. Importantly, UCP1 activation can also be influenced by other factors such as diet, hormones (like thyroid hormones) and physical activity (X. Liu et al., 2022).

In addition to UCP1, brown adipocytes specifically express a set of thermogenic genes that support uncoupled respiration and high levels of fatty acid and/or glucose oxidation. This BAT-specific signature includes genes such as PPARα (Barberá et al., 2001), Cell Death inducing DFFA like effector A (CIDEA), Iodothyronine Deiodinase 2 (DIO2) and Peroxisome proliferator-activated receptor gamma coactivator 1-alpha (PGC-1α) involved in FA metabolism, lipid droplet remodelling, thyroid hormone metabolism and mitochondrial biogenesis, respectively (Tabuchi & Sul, 2021; Villarroya et al., 2017).

Beige adipocytes are a distinct type of adipocytes that exhibits characteristics of both white and brown adipocytes (Tiraby et al., 2003). These cells emerge within the white

adipose tissue depots through a process called “browning”, which can be induced by various stimuli such as cold exposure, β -adrenergic receptor stimulation and exercise (Cousin et al., 1992). Beige adipocytes arise from trans differentiation of white adipocytes, with the ability to de-differentiate back into white unilocular cells (Bartelt & Heeren, 2013). These cells share some similarities with classical brown adipocytes, particularly in their ability to dissipate energy as heat through thermogenesis, by expressing UCP1. Morphologically, beige adipocytes often exhibit a multilocular appearance with smaller lipid droplets and a higher density of mitochondria compared to typical white adipocytes. They also display a distinct gene expression profile, including increased levels of UCP1 and PGC-1α. Functionally, beige adipocytes contribute to energy expenditure and metabolic regulation, like brown adipocytes. Their presence and activation have been associated with improved glucose metabolism, increased insulin sensitivity, and protection against obesity in animal models and humans (Jung et al., 2019; Shinde et al., 2021).

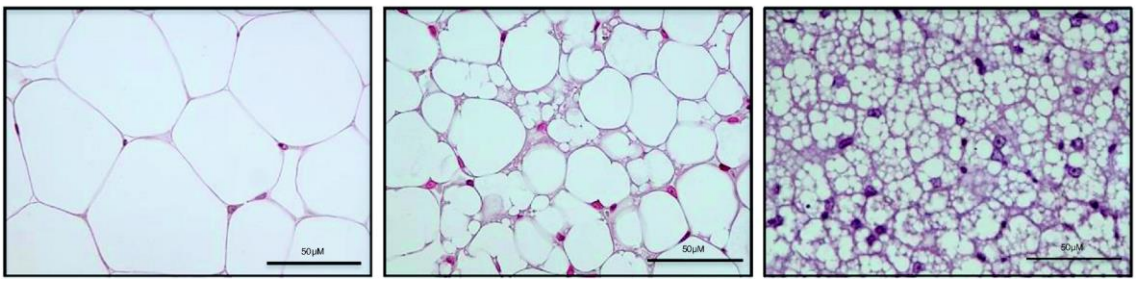

Figure 2. Morphology of three fat depots in mammals.
Hematoxylin and eosin staining of (A) white, (B) beige and (C) brown adipocytes. Scale bars 50μm) (Keipert & Jastroch, 2014).

Adipose Tissue plasticity

White adipocytes exhibit significant metabolic plasticity, allowing them to adapt to various physiological states. This plasticity is crucial for maintaining energy balance and overall metabolic health.

In times of energy surplus, such as after eating, white adipocytes store excess energy deriving from FAs in the form of triglycerides (TGs), which in turn accumulate in intracellular organelles named lipid droplets (LD). Upon binding to its receptor, insulin,

a key regulatory hormone, facilitates glucose uptake via glucose transporter 4 (GLUT4) and enhances lipogenesis by activating the phosphoinositide 3-kinase (PI3K)/AKT signalling cascade. Specifically, AKT stimulates GLUT4 translocation from the intracellular store to the plasma membrane (Summers et al., 1998). Glucose is converted into glycerol, providing the backbone for fatty acid esterification into TGs. Mechanistically, fatty acids are either taken up from circulating lipoproteins (chylomicrons and VLDL) through the action of insulin-stimulated lipoprotein lipase (LPL) or synthesized de novo from carbohydrates via de novo lipogenesis (DNL). LPL hydrolyses TGs into non-esterified fatty acids (NEFAs), which then enter white adipocytes through fatty acid transporters such as CD36 and fatty acid transport protein-1 (FATP1). In response to insulin signalling, FATP1 translocates to the cell membrane and facilitates the uptake of long-chain fatty acids (LCFAs) (Q. Wu et al., 2006).

De novo lipogenesis (DNL) represents a pivotal metabolic pathway within white adipocytes, where non-lipid precursors, such as carbohydrates, are synthesized into fatty acids. This process plays a crucial role in energy homeostasis by converting excess glucose into TGs for storage. Insulin stimulates glucose uptake into adipocytes, which then enters glycolysis and is converted into pyruvate. Subsequently, pyruvate dehydrogenase (PDH) decarboxylates pyruvate to produce acetyl-CoA, a key precursor for lipogenesis. After the condensation of acetyl-CoA with the tricarboxylic acid cycle (TCA)- derived oxaloacetate, the newly formed citrate is exported from the mitochondria into the cytosol where it is cleaved by ATP-citrate lyase (ACLY) to yield acetyl-CoA and oxaloacetate again. Acetyl-CoA, derived from both mitochondrial and cytosolic pools, serves as the starting point for the synthesis of malonyl-CoA. This critical step is catalysed by acetyl-CoA carboxylase 1 (ACC1), an enzyme sensitive to hormonal and nutritional signals. Malonyl-CoA acts as the primary building block for fatty acid elongation, facilitated by fatty acid synthase (FASN), culminating in the formation of palmitate (C16:0), the predominant end-product of DNL in white adipocytes. Palmitate undergoes further modifications, including elongation and desaturation, leading to the generation of diverse fatty acids such as stearic acid, oleic acid, and palmitoleic acid. These fatty acids are esterified to glycerol-3-phosphate to form TGs, which are stored within lipid droplets as a reservoir of metabolic fuel. The regulation of DNL in white adipocytes is finely tuned

by hormonal, nutritional, and transcriptional factors. Insulin exerts a pivotal role by enhancing the expression and activity of lipogenic enzymes, thereby promoting lipogenesis in response to elevated glucose levels (Sakers et al., 2022). Transcription factors such as sterol regulatory element-binding protein-1c (SREBP-1c) and carbohydrate-responsive element-binding protein (ChREBP) orchestrate the transcriptional activation of genes involved in DNL, ensuring adaptive responses to fluctuating nutritional states (Song et al., 2018).

In the fasted state, white adipocyte metabolism undergoes a significant transformation aimed at mobilizing stored energy reserves to meet metabolic demands through a process called lipolysis. The initiation of lipolysis is orchestrated by a series of enzymatic reactions within adipocytes. Initially, adenylate cyclase is activated, leading to increased cyclic AMP (cAMP) levels. Elevated cAMP levels activate protein kinase A (PKA), which in turn phosphorylates and activates key lipolytic enzymes such as adipose triglyceride lipase (ATGL), the key limiting step of lipolysis, and hormone-sensitive lipase (HSL).

After interaction with its co-activator alpha/beta hydrolase domain-containing protein 5 (ABHD5), which is normally bound to perilipin 1 (PLIN1), ATGL becomes activated and hydrolyses TGs into diacylglycerol (DAG) and the first free fatty acid (FFA). Next, HSL further breaks down DAG into monoacylglycerol (MAG) and subsequent FFAs. Finally, monoacylglycerol lipase (MGL) completes the process by converting MAG into glycerol and the third FFA molecule. These FFAs are then released into the bloodstream, serving as essential energy substrates for various tissues and organs (Yang & Mottillo, 2021).

This process is finely regulated by catecholamines like epinephrine and norepinephrine, released from the adrenal glands and sympathetic nervous system, which activate β-adrenergic receptors (β-ARs) coupled to stimulatory G proteins (Gs). In addition, hormones such as glucagon, secreted by pancreatic α-cells in response to low blood glucose levels, influence adipocyte metabolism during fasting by stimulating lipolysis via increasing cAMP levels within adipocytes. This hormonal response promotes the breakdown of TGs into FFAs and glycerol, facilitating energy provision to tissues. Conversely, insulin mediates the transcriptional downregulation of *PNPLA2,* the gene encoding for ATGL via FOXO1 phosphorylation (Grabner & Xie, 2020.).

Physiologically, the released FFAs play critical roles in metabolic processes. In muscle cells, FFAs undergo β-oxidation to generate acetyl-CoA, which fuels the citric acid cycle (TCA cycle) and oxidative phosphorylation to produce ATP (Fritzen et al., 2020). In the liver, glycerol derived from adipocyte lipolysis is used for gluconeogenesis, helping to maintain blood glucose at a regular level which is essential for brain function and other glucose-dependent tissues (Rui, 2014).

Another catabolic process taking place in the adipocyte is fatty acid β-oxidation, which occurs in the mitochondria and involves several key enzymatic steps. Released FFAs are first converted into fatty acyl-CoA derivatives in the cytosol and the resulting acyl-CoA molecules are then transported into the mitochondrial matrix through a carnitine-dependent shuttle system. On the outer mitochondrial membrane, carnitine palmitoyltransferase I (CPT1) converts acyl-CoA to acyl-carnitine. Acyl-carnitine is transported across the inner mitochondrial membrane by a translocase enzyme and carnitine palmitoyltransferase II (CPT2) on the inner membrane then reconverts it back to acyl-CoA within the mitochondrial matrix. Once inside the mitochondria, fatty acyl-CoA undergoes β-oxidation, a cyclical series of reactions that systematically cleave two-carbon units from the acyl chain. Each cycle of β-oxidation involves four key steps: oxidation by acyl-CoA dehydrogenase, hydration by enoyl-CoA hydratase, a second oxidation by hydroxyacyl-CoA dehydrogenase and thiolysis by ketoacyl-CoA thiolase. These steps produce acetyl-CoA, NADH and FADH2 (Houten & Wanders, 2010). Acetyl-CoA enters the citric acid cycle (TCA cycle) for further oxidation, generating additional NADH and FADH2, which are critical for ATP production through the electron transport chain (Adeva-Andany et al., 2019).

The regulation of β-oxidation in adipocytes is tightly controlled by hormonal and nutritional signals. Insulin inhibits β-oxidation by promoting the dephosphorylation and activation of acetyl-CoA carboxylase (ACC), which catalyses the formation of malonyl-CoA which, in turni, inhibits CPT1 (Wakil & Abu-Elheiga, 2009). Conversely, during fasting, decreased insulin levels and increased glucagon levels activate AMP-activated protein kinase (AMPK), which phosphorylates and inactivates ACC, thereby lowering malonyl-CoA levels and enhancing CPT1 activity, promoting β-oxidation (Kahn et al., 2005).

Adipose tissue endocrine function

Despite its role in energy storage and lipid metabolism, the adipose tissue is also recognized for its endocrine function, by secreting a variety of bioactive molecules (adipokines) as well as regulatory lipid species (lipokines). These signalling molecules play crucial roles in regulating systemic metabolism, inflammation, and overall homeostasis. The endocrine function of WAT is highly dynamic and responsive to various physiological states. For instance, during periods of energy surplus, WAT expands and alters its secretion profile, often leading to an increase in pro-inflammatory adipokines and a decrease in insulin-sensitizing adipokines. Conversely, weight loss and reduced adiposity can reverse these changes, improving metabolic outcomes.

Adipokines have hormone-like functions and act as growth factors that modulate insulin resistance, fat and glucose metabolism, inflammatory responses and mediate the endocrine, paracrine and autocrine signalling between adipose tissue and other organs like the liver, muscle, brain and immune system. Among the most well-studied adipokines are leptin, adiponectin, and resistin.

Leptin, primarily secreted by adipocytes, is involved in regulating energy balance by inhibiting hunger through its actions on the hypothalamus, thereby playing a critical role in body weight regulation. Genetically obese mouse models, such as ob/ob mice, lacking the leptin gene (*LEP)* and db/db mice, lacking the leptin receptor (*LEPR),* are widely used to study the molecular basis of obesity. These mice develop early-onset of obesity due to hyperphagia and low energy expenditure (Kleinert et al., 2018). In both rodents and humans, plasma levels of leptin are positively correlated with fat tissue mass, and it is mostly regulated at the transcriptional level (Scheja & Heeren, 2019). LEPR is a type I cytokine receptor and is expressed both in the central nervous system, predominantly the hypothalamus, and in the periphery. Upon binding to its receptor, leptin triggers the janus kinase (JAK) 2- signal transducer and activator of transcription (STAT) 3 pathway, regulating appetite by acting on the nucleus arcuatus of the hypothalamus, either by activating anorexigenic and inhibiting orexigenic neurons (Obradovic et al., 2021). Additionally, leptin engages the PI3K-AKT and MAPK pathways, crucial for glucose metabolism and cellular growth (Garcia-Galiano et al., 2019). Beyond central effects, leptin enhances insulin sensitivity and reduces lipid accumulation in the liver while

promoting fatty acid oxidation and glucose uptake in skeletal muscle (Margetic et al., 2002; Scheja & Heeren, 2019).

Adiponectin enhances insulin sensitivity and has anti-inflammatory properties, making it essential for maintaining glucose and lipid metabolism. The importance of adiponectin signalling in regulating insulin sensitivity has been demonstrated by observing that adiponectin-deficient mice develop insulin resistance (Fasshauer & Blüher, 2015; T. M. D. Nguyen, 2020). Both obese humans and rodents exhibit low circulating levels of this adipokine, although the underlying mechanisms remain incompletely understood. Adiponectin exerts its effects through two main receptors, AdipoR1 and AdipoR2, which are widely expressed in various tissues, including muscle, liver and adipose tissue (Ruan & Dong, 2016). Upon binding to its receptors, adiponectin activates several intracellular signalling pathways, among which the AMP-activated protein kinase (AMPK) pathway, which increases fatty acid oxidation and glucose uptake in skeletal muscle and inhibits gluconeogenesis in the liver. Moreover, adiponectin activates the peroxisome proliferator-activated receptor alpha (PPARα) pathway in the liver, promoting the expression of genes involved in fatty acid transport and β-oxidation, reducing lipid accumulation, and enhancing lipid metabolism (Clemente-Suárez et al., 2023). Furthermore, adiponectin inhibits the c-Jun N-terminal kinase (JNK) and nuclear factor-kappa B (NF-κB) pathways, both associated with inflammation and insulin resistance, thus reducing inflammatory responses and improving insulin signalling (Gamberi et al., 2018).

Resistin is a protein secreted by macrophages in both humans and rodents (also from mouse adipocytes) which plays an important role in insulin resistance and inflammation. Circulating levels of this protein are elevated in obese humans and rodents (Schwartz & Lazar, 2011). Resistin interferes with insulin signalling pathways by inhibiting insulin-stimulated glucose uptake in skeletal muscle cells and adipocytes. At the molecular level, resistin activates intracellular signalling cascades that disrupt insulin receptor substrate (IRS) signalling, impairing downstream AKT activation, and ultimately reducing glucose uptake. In addition to its effects on insulin sensitivity, resistin functions as a pro-inflammatory cytokine. It promotes the production of inflammatory mediators such as tumor necrosis factor (TNF)-α and interleukin (IL)-6, contributing to chronic low-grade inflammation observed in obesity and metabolic syndrome (Jamaluddin et al., 2012;

Scheja & Heeren, 2019).

Lipokines, a subclass of lipid-derived signalling molecules, have emerged as important regulators of metabolic processes (Hernández-Saavedra & Stanford, 2019). Notable examples are fatty acids, like palmitoleic acid and oleic acid, as well as oxidized lipids, each with distinct molecular structures that differently influence insulin sensitivity and inflammation. Certain oxidized lipids act as pro-inflammatory mediators, stimulating the release of cytokines and chemokines from adipose tissue, contributing to chronic low-grade inflammation observed in obesity and metabolic syndrome.

Obesity

Obesity is a chronic condition characterized by the excessive accumulation of body fat, negatively influencing health and well-being. As mentioned in chapter 1, obesity results from a long-term positive disruption of energy balance. Overweight and obesity are typically diagnosed by the measurement of the body mass index (BMI). A BMI over 25 is considered being overweight while a BMI over 30 is regarded as being obese. Moreover, other factors such as waist circumference and body composition are also considered. Globally, the obesity prevalence has reached epidemic proportions, driven by sedentary lifestyles, high-calorie diets, and socioeconomic factors. According to a study published by Lancet in 2024, more than 1 billion people are living with obesity and, worldwide, obesity has more than doubled since 1990 among adults (Phelps et al., 2024). In line, obesity has also become a major health and economic burden in Italy, with total costs amounted to 13.34 billion euros attributable to obesity in 2020 (d'Errico et al., 2022). Obesity is linked to an elevated risk of several medical conditions, including cardiovascular disease, hypertension, non-alcoholic steatohepatitis (NASH) and metabolic consequences including type 2 diabetes mellitus (T2DM), insulin resistance and dyslipidaemia. In addition, obesity significantly increases the risk of developing various types of cancer such as breast, colon and rectum, oesophagus, stomach, gallbladder, uterus, pancreas and liver among others (Pati et al., 2023).

Dysfunction of adipose tissues in obesity

During conditions of a prolonged positive energy balance, the capacity of adipocytes to safely store excess lipids reaches its limit, leading to significant disturbances of the adipose tissue. Firstly, adipocytes expand by increasing their size (hypertrophy) and number (hyperplasia) to accommodate the elevated influx of lipids. This in turn, leads to alteration of cellular functions, including augmented basal lipolysis, impaired mitochondrial functions and metabolic abberations.

Once adipocytes are unable to store additional lipids, these excess fats accumulate in non-adipose tissues regulating glucose metabolism such as the liver, muscle and pancreas. This process results in detrimental effects referred to as "lipotoxicity". Then, the impaired insulin sensitivity and increased secretion of pro-inflammatory cytokines, contribute to the development of a pro-inflammatory state within the adipose tissue. Moreover, the

overflow of free fatty acids (FFAs) from hypertrophic adipocytes into the bloodstream increases circulating lipid levels, contributing to dyslipidaemia. Elevated FFAs in the blood impair insulin signalling in peripheral tissues, exacerbate systemic insulin resistance, and increase the risk of cardiovascular diseases (Longo et al., 2019).

One of the alterations is the dysregulated secretion of adipokines, which are critical hormones involved in energy homeostasis, inflammation, and insulin sensitivity. In obese individuals, adipose tissue produces elevated levels of leptin, leading to leptin resistance and impaired satiety signalling, thus perpetuating overeating (Lönnqvist et al., 1995). Conversely, adiponectin levels are markedly reduced, negatively impacting insulin sensitivity and lipid metabolism (Kadowaki et al., 2006). Moreover, adiponectin has been demonstrated to polarize adipose tissue-resident macrophages toward an alternative activated M2-like phenotype (Ohashi et al., 2010).

In addition to these metabolic disturbances, the overwhelmed storage capacity of adipocytes triggers adipose tissue remodelling. This includes the development of fibrosis, characterized by excessive deposition of extracellular matrix components such as collagen. Fibrosis further impairs the expandability and function of adipose tissue, promoting a vicious cycle of inflammation and metabolic dysfunction (Khan et al., 2009).

Obesity is also accompanied by significant mitochondrial dysfunctions in adipocytes. One key aspect of mitochondrial dysfunction in obese adipocytes is the reduction in mitochondrial biogenesis, which is regulated by a network of transcription factors and coactivators, including PGC-1α and nuclear respiratory factors (NRFs) (S. Kleiner et al., 2012). As obesity progresses, the expression and activity of PGC-1α and NRFs are diminished, leading to a decrease in the number and function of mitochondria (Lahera et al., 2017; Rong et al., 2007). Chronic inflammation and elevated levels of pro-inflammatory cytokines such as TNF-α and IL-6 also affect mitochondria functions. In addition, impaired oxidative phosphorylation (OXPHOS) leads to elevated reactive oxygen species (ROS) levels (Bhatti et al., 2017; Schrauwen & Hesselink, 2004), causing oxidative damage to mitochondrial DNA (mtDNA), proteins and lipids, further impairing mitochondrial function and exacerbating oxidative stress (Hernández-Aguilera et al., 2013).

Chronic low-grade inflammation

A hallmark of obesity is the development of a persistent, chronic low-grade inflammation, termed meta-inflammation, affecting all tissues involved in energy balance. Enlarged adipocytes and increased infiltration of immune cells, such as macrophages and T lymphocytes, contribute to the secretion of pro-inflammatory cytokines like TNF-α, IL-6 and monocyte chemoattractant protein-1 (MCP-1) (Hildebrandt et al., 2022a). This inflammatory cascade disrupts adipocyte function and compromises insulin sensitivity. Moreover, adipose tissue inflammation contributes to the dysregulation of adipokine secretion, including elevated levels of leptin and resistin, and decreased levels of adiponectin (Sam & Mazzone, 2014). Meta-inflammation not only impacts local adipose tissue health but also exacerbates systemic inflammation, linking obesity to a higher risk of metabolic disorders such as type 2 diabetes, cardiovascular diseases and non-alcoholic fatty liver disease (NAFLD) (Hotamisligil, 2006).

Myeloid cells are part of the innate immune system and represent the most abundant immune cells in the white adipose tissue. Adipose tissue-resident macrophages (ATM), who are the first immune cells seeding the adipose tissue (Hassnain Waqas et al., 2017; Schulz et al., 2012), are the most abundant myeloid population and play a significant role both under homeostatic conditions and in the development of the obesity-induced inflammation. In a lean adipose tissue, ATMs represent 10% of cells present in the adipose tissue and provide housekeeping functions by regulating dead cell clearance, systemic glucose homeostasis and metabolic adaptation to nutrient surplus (D. Thomas & Apovian, 2017). Tissue-resident macrophages exhibit an alternatively activated M2 phenotype, characterized by the expression of anti-inflammatory cytokines such as IL-10, Arg1 and IL-1 (Lumeng, Bodzin, et al., 2007). Conversely, as obesity progresses, ATMs shift from an anti-inflammatory M2-like phenotype to a pro-inflammatory M1 phenotype, characterized by the secretion of cytokines such as TNF-α, IL-1β and IL-6. These pro-inflammatory mediators have been reported to interfere with insulin signalling by promoting the serine phosphorylation of insulin receptor substrate (IRS) proteins via activation of stress kinases such as c-Jun N-terminal kinase (JNK) and IκB kinase (IKK-β) and by inducing GLUT4 downregulation (Lumeng, Deyoung, et al., 2007; Uysal et al., 1997). Furthermore, macrophages can comprise up to 40% of the cell population in the

obese adipose tissue. This increase is driven by the secretion of chemoattractant signals like MCP-1) and chemokine (C-C motif) ligand 2 (CCL2) by hypertrophic adipocytes that recruit circulating monocytes differentiating into M1 macrophages within the adipose tissue (Weisberg et al., 2003). A major hallmark of the inflamed adipose tissue is the formation of clusters of macrophages surrounding dead adipocytes named crown-like structures (CLSs) (Cinti et al., 2005).

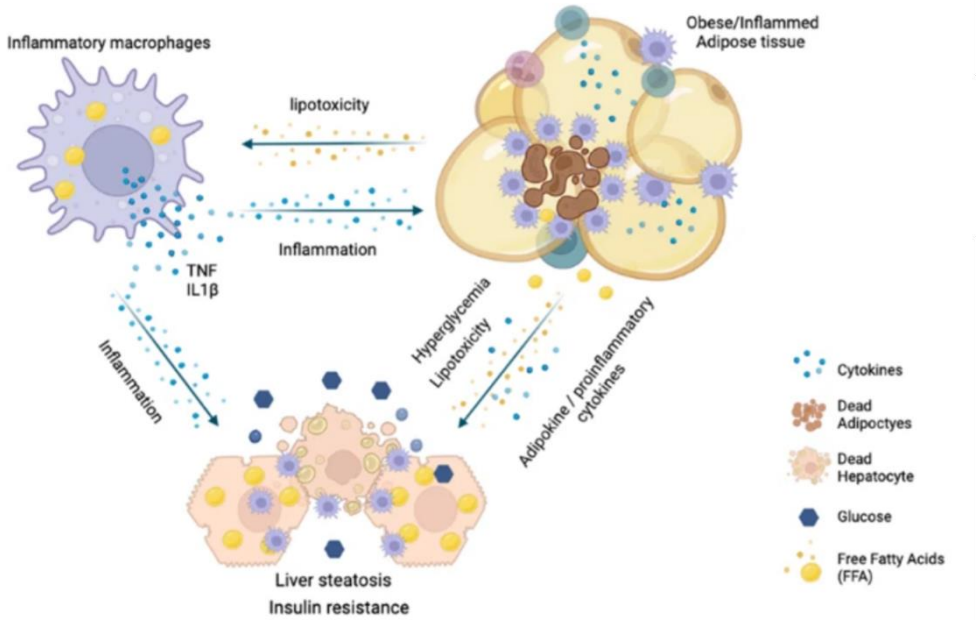

Figure 3. Chronic low-grade inflammation (Hildebrandt et al., 2022b).

Comorbidities in obesity

Obesity is a complex metabolic disorder that increases the risk of development of many pathological conditions. Among them, insulin resistance, hypertension, dyslipidaemia, type-2 diabetes (T2DM), cardiovascular disease (CVD), non-alcoholic fatty liver disease (NAFLD) and some type of malignancies such as liver cancer (Kloock et al., 2023).

Insulin resistance. Insulin is a peptide hormone produced by pancreatic β-cells and it regulates glucose homeostasis. Briefly, under physiological conditions, increased glycemia leads to augmented insulin secretion and levels, promoting glucose uptake into peripheral tissues and suppressing hepatic gluconeogenesis. Mechanistically, upon insulin binding, the insulin receptor undergoes a conformational change, leading to the

activation of its tyrosine kinase domain which phosphorylates the insulin receptor substrate (IRS) proteins. Then, phosphorylated IRS proteins act as docking sites for several downstream signalling molecules, which are essential in regulating glucose homeostasis. The development of insulin resistance (IR), characterized by the diminished ability of cells, particularly muscle, fat, and liver cells, to respond to the actions of insulin, is a prominent mechanism of obesity-related diseases. Importantly, chronic low-grade inflammation contributes instrumentally to this process. Indeed, hypertrophic adipocytes and infiltrating macrophages produce pro-inflammatory cytokines such as TNF-α, IL-6, and MCP-1, which have been reported to activate stress kinases, including JNK and IKK-β, thereby promoting serine phosphorylation of IRS proteins and disrupting insulin signalling (Uysal et al., 1997).

Another factor contributing to insulin resistance is the occurrence of adipokine imbalance during obesity. Leptin exerts its effect by binding to the leptin receptor and limits insulin production in pancreatic β-cells (Covey et al., 2006). The occurrence of leptin resistance in obesity also impacts insulin signalling by driving the over production of insulin by β-cells (Gray et al., 2010). The elevated leptin levels exacerbate inflammation by stimulating the production of pro-inflammatory mediators via activation of the transcription factor nuclear factor κB (NF-κB) (Aleffi et al., 2005), which, in turn, activates pro-inflammatory genes, thereby contributing to inflammation-induced insulin resistance. In contrast, adiponectin positively impacts on insulin sensitivity, reduces hepatic gluconeogenesis and reduce inflammation by polarizing ATMs into M2-like macrophages, thus contributing to ameliorate insulin sensitivity (Kirichenko et al., 2022). Insulin resistance is further exacerbated by elevated levels of circulating free fatty acids (FFAs) and ectopic lipid accumulation, which activate protein kinase C (PKC), leading to additional serine phosphorylation of IRS proteins (Schmitz-Peiffer & Biden, 2008).

Mitochondrial dysfunction, characterized by increased ROS production and reduced mitochondrial biogenesis, further impairs insulin signalling. Excessive nutrient supply leads to increased mitochondrial activity and elevated ROS production. High levels of ROS disrupt insulin signalling via several mechanisms, for example by PKC, JNK and IKK-β. Furthermore, ROS also promote the production of pro-inflammatory mediators, which in turn influence insulin sensitivity (Bournat & Brown, 2010). Additionally, impaired oxidative phosphorylation and disrupted mitochondrial dynamics exacerbate

insulin resistance (Gonzalez-Franquesa & Patti, 2017).

Non-alcoholic fatty liver disease (NAFLD). When the adipose tissue exceeds its storing capacity, lipids spill out and accumulate in ectopic sites, such as the skeletal muscle and the liver. Lipid deposition in the liver paves the way for the progression of non-alcoholic fatty liver disease, which encompasses a spectrum of liver conditions ranging from a reversible hepatic steatosis to non-alcoholic steatohepatitis (NASH) and can progress to hepatocellular carcinoma (Pouwels et al., 2022). NAFLD is a major cause of liver-related morbidity and mortality. Globally, the prevalence of NAFLD has significantly increased, mirroring the increase in obesity and metabolic syndrome. Currently, NAFLD affects an estimated 30% of the adult population worldwide (Younossi et al., 2023). Insulin resistance is central for the development of NAFLD. Insulin resistance leads to the increased lipolysis in the adipose tissue, resulting in elevated circulating FFAs. Subsequently, the augmented fatty acid uptake by hepatocytes is mediated by the overexpression of fatty acid transporters such as CD36 (Rada et al., 2020). This excessive lipid accumulation leads to lipotoxicity, causing oxidative stress and mitochondrial dysfunction. Another hallmark of NAFLD is the mitochondrial dysregulation resulting from the abnormal influx of FFAs that overwhelms β-oxidation capacity, leading to the production of toxic lipid intermediates and ROS (Day & Saksena, 2002).

In addition, insulin resistance also promotes hepatic de novo lipogenesis, further increasing lipid deposition within the hepatocytes. In patients, diagnosis of NAFLD is usually investigated by histological examination of liver biopsies. In particular, it is defined by the presence of ballooning within hepatocytes, indicating deposition of triglycerides in the form of lipid droplets (Pouwels et al., 2022). NAFLD is also characterized by the development of inflammation in the liver, with pro-inflammatory macrophages being one of the mayor players (Kazankov et al., 2018; Nieto-Vazquez et al., 2008; Sato et al., 2014). In the advanced stages of NAFLD, chronic inflammation and cellular damage stimulate the activation of hepatic stellate cells (HSCs), which produce extracellular matrix proteins, leading to fibrosis. Persistent fibrogenesis can progress to cirrhosis, characterized by extensive scarring of liver tissue and impaired liver function (Divella et al., 2019).

Liver cancer. Primary liver cancer is a significant global health issue, accounting for 9% of all cancer-related deaths worldwide. The most common form is hepatocellular carcinoma (HCC), representing around 80-90% of all cases and being highly aggressive (Kinsey & Lee, 2024; Sohn et al., 2021). Despite the growing understanding of the biological mechanisms underlying the development of liver cancer, treatments remain largely ineffective and outcomes continue to be poor. Liver cancer has been increasingly linked to obesity and NAFLD (Chen et al., 2012; Esposito et al., 2012; Lauby-Secretan et al., 2016). At the molecular level, the progression from NAFLD to HCC involves a complex interplay of metabolic, inflammatory and genetic factors. As already mentioned, obesity is defined by a state of chronic low-grade inflammation, characterized by elevated levels of pro-inflammatory cytokines such as TNF-α, IL-6, and adipokines like leptin (Park et al., 2010). These cytokines activate signalling pathways, including JAK/STAT, NF-κB, and MAPK, which promote hepatocyte proliferation, survival, and resistance to apoptosis (Marra & Bertolani, 2009; Stickel & Hellerbrand, 2010). Concurrently, obesity-associated insulin resistance leads to hyperinsulinemia and increased insulin-like growth factor 1 (IGF-1), further stimulating oncogenic pathways such as PI3K/AKT and RAS/RAF/MEK/ERK (Ohlsson et al., 2009). Moreover, oxidative stress induced by excessive fatty-acid influx, mitochondrial dysfunction and gut dysbiosis foster the development of liver cancer (Yahoo et al., 2023).

Several dietary regimens have been employed to study NAFLD-associated HCC in mice.

Choline-deficient high-fat diet (CD-HFD). The CD-HFD model replicates the full spectrum of liver pathology observed in human patients with NAFLD/NASH-related HCC. This diet combines choline deprivation, which disrupts lipid metabolism, with a high-fat content that exacerbates fat accumulation in the liver. Choline plays a critical role in liver function by supporting the synthesis of phosphatidylcholine, a component of very-low-density lipoprotein (VLDL), which helps export triglycerides from the liver (Flessa et al., 2022). This model has been demonstrated to induce a progressive liver damage, starting with simple steatosis and resulting in a 25% incidence of HCC development after 12 months of diet (Wolf et al., 2014).

Western diet (WD). WD is rich in saturated fats (~ 40% of calories from fat), refined sugars (especially fructose), cholesterol and low in fibres, vitamins, and other essential nutrients (Charlton et al., 2011). The Western diet model closely mimics the dietary habits

and metabolic conditions that contribute to liver disease in human populations, making it a relevant model for studying HCC, with HCC development in 89% of the mice between 8 and 13 months on diet (Asgharpour et al., 2016).

HFD/WD plus carbon tetrachloride (CCl_4). CCl_4 is a chemical compound that has been widely used in experimental models to induce liver injury. It is metabolized in the liver by cytochrome P450 enzymes, producing reactive metabolites that cause oxidative stress, lipid peroxidation, and cellular damage. When combined, these diets and carbon tetrachloride (CCl_4) synergistically promote the development of HCC by accelerating liver damage, resulting in a >50% of incidence of HCC in 6 months (Tsuchida et al., 2018).

Therapeutic strategies in obesity

In clinical practice, diagnosis is assessed by considering an adult's body mass index (BMI) over ≥ 30 kg/m^2 and waist circumference. Obesity treatments focus on achieving sustainable weight loss and addressing obesity-related health issues. The first step typically involves lifestyle interventions such as dietary changes, increased physical activity, and behavioural modifications. Based on gravity and on the presence of comorbidities, obesity treatment should be escalated to anti-obesity medications and/or surgical interventions (Tchang et al., 2021).

Surgical treatments for obesity have emerged as highly effective interventions for individuals struggling with severe or morbid obesity. Bariatric surgery, which encompasses a range of procedures, has become a crucial component of comprehensive weight loss management (N. T. Nguyen et al., 2016). These surgical techniques involve either restricting food intake, limiting food absorption, or a combination of both approaches. The most common bariatric procedures include gastric bypass, gastric sleeve, gastric banding, and vertical gastrectomy (Gulinac et al., 2023; Mechanick et al., 2013). Furthermore, bariatric surgery has been associated with substantial improvements in obesity and obesity-related comorbidities, such as type 2 diabetes, hypertension, and cardiovascular diseases (O'Brien et al., 2019; Sjöström et al., 2012).

While lifestyle modifications, including diet and exercise, form the cornerstone of obesity management, these interventions alone are often insufficient for many individuals.

Therefore, pharmacotherapy is considered an essential adjunct to lifestyle changes for achieving and maintaining significant weight loss. The rationale for using anti-obesity treatments is multifaceted, encompassing the need to enhance weight loss outcomes, mitigate health risks, and improve overall quality of life. Anti-obesity medications provide an additional tool to support weight loss efforts by targeting specific physiological pathways that regulate appetite, metabolism, energy expenditure and fat absorption (Fig. **4**) (Müller et al., 2021).

Appetite suppressants are a class of drugs designed to reduce hunger and increase feelings of fullness, thereby promoting weight loss. These medications work primarily by acting on the central nervous system, influencing neurotransmitter pathways that regulate appetite and satiety. Sympathomimetic agents function by mimicking the activity of the sympathetic nervous system. The hypothalamic paraventricular nucleus (PVN) is innervated by noradrenergic fibres and integrate signals derived from the ARC, thus modulating appetite and eating behaviour (Sayar-Atasoy et al., 2023). Depending on the activation of different adrenergic receptors, noradrenaline can either suppress or increase appetite (Wellman, 2000). Phentermine stimulates the release of noradrenaline and is one of the most prescribed appetite suppressants and often used for short-term weight management in conjunction with diet and exercise (Yanovski & Yanovski, 2014). For long-term use, phentermine is given in combination with topiramate, an anticonvulsant that has weight loss side effects by increasing feelings of fullness and enhance calorie expenditure. Together, they provide a more potent weight loss effect than either drug alone. In controlling appetite, other appetite suppressant drugs have received FDA authorization for the treatment of obesity. The combination of bupropion/naltrexone has received FDA authorization in 2014, and it is widely used (Yanovski & Yanovski, 2015). Bupropion is an antidepressant that also helps reduce appetite by inhibiting noradrenaline and dopamine reuptake and by promoting anorexigenic effects via stimulation of the secretion of the α-melanocyte stimulating hormone (αMSH) from pro-opiomelanocortin-producing hypothalamic cells (Apovian et al., 2013). Instead, naltrexone, an μ-opioid receptor antagonist, is thought to reduce appetite via inhibition of β-endorphin action and by preventing autoinhibition of pro-opiomelanocortin neurons (Kulak-Bejda et al., 2021). Fat absorption inhibitors, specifically lipase inhibitors, function by binding to lipase enzymes within the intestine, halting the breakdown of dietary triglycerides into

monoglycerides and fatty acids. As a result, the absorption of dietary fat is decreased, promoting weight loss and enhancing metabolic well-being. Orlistat is a lipase inhibitor and its mechanism of action involves inhibiting the enzymes gastric and pancreatic lipases, which are responsible for breaking down dietary triglycerides into absorbable free fatty acids and monoglycerides in the intestinal lumen (Bansal et al., 2024; Hill et al., 1999). By inhibiting these lipases, orlistat reduces the absorption of dietary fats by approximately 30% (Muls et al., 2001).

GLP-1 (glucagon-like peptide-1) agonists mimic the actions of the incretin hormone GLP-1, which plays a crucial role in regulating appetite, satiety, and energy homeostasis. By activating GLP-1 receptors, these agonists can induce weight loss through multiple mechanisms, including reducing appetite, slowing gastric emptying, and increasing feelings of fullness. Among them, liraglutide, originally approved for type 2 diabetes in 2010, it has been shown to significantly reduce body weight at higher doses and approved for chronic weight management in 2014. Another GLP-1 receptor agonist approved for type 2 diabetes in 2017 and for obesity at a higher dose under in 2021 is semaglutide (Wang et al., 2023). Tirzepatide, instead, is a dual gastric inhibitory polypeptide GIP/GLP-1 receptor agonist used in the treatment of diabetes and in reducing weight loss (Willard et al., 2020).

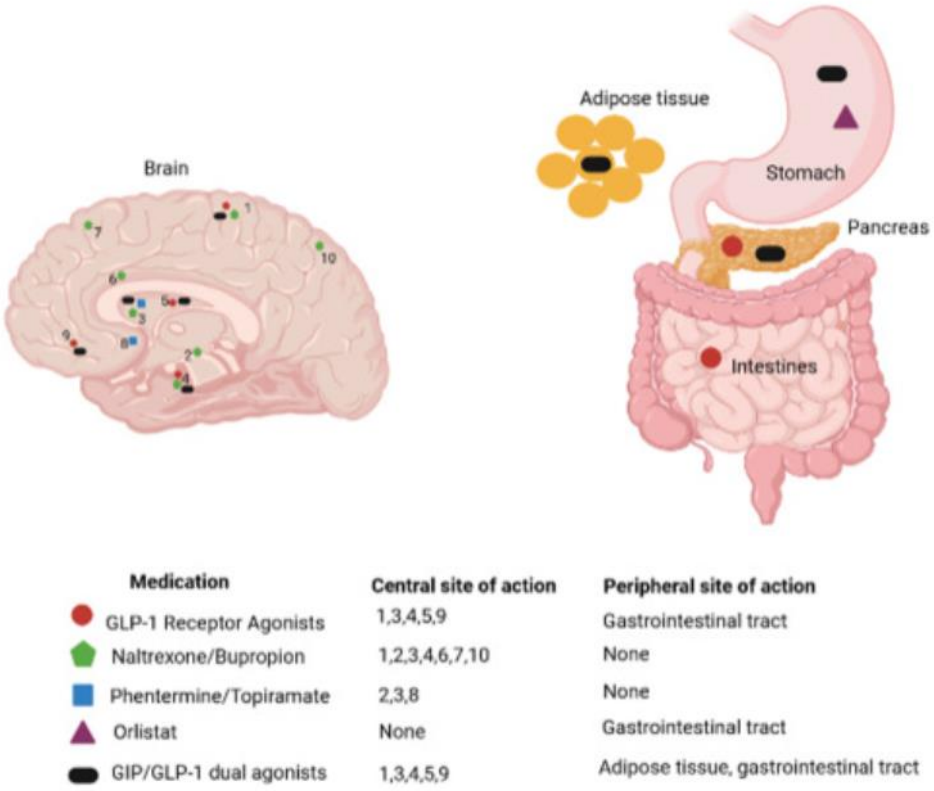

Figure 4. Site of action of FDA approved anti-obesity medications.
GLP-1 Receptor Agonists *(red circles): act on brain regions 1, 3, 4, 5, and 9 and target the gastrointestinal tract.* ***Naltrexone/Bupropion*** *(green pentagons): affect brain regions 1, 2, 3, 4, 6, 7, and 10 without peripheral targets.* ***Phentermine/Topiramate*** *(blue squares): focus on brain regions 2, 3, and 8, with no peripheral action.* ***Orlistat*** *(black triangles): acts only on the gastrointestinal tract, with no central activity.* ***GIP/GLP-1 Dual Agonists*** *(purple diamonds): target brain regions 1, 3, 4, 5, and 9, and influence both the gastrointestinal tract and adipose tissue. (1): parietal cortex, (2) hippocampus, (3) hypothalamus, (4) insula, (5) putamen, (6) dorsal anterior cingulate, (7) superior frontal cortex, (8) nucleus accumbens, (9) orbitofrontal cortex, (10) superior parietal cortex* (Chakhtoura et al., 2023).

Gut microbiota in health and disease

The microbiota is a complex and dynamic ecosystem of an estimated 100 trillion microorganisms living in symbiosis with the host, contributing to homeostasis and immune functions (Hou et al., 2022a; Sender et al., 2016). This intricate community includes a diverse range of bacteria, archaea, viruses, fungi, and protozoa, each contributing to a balanced and functional microbiota. Although the two terms "microbiota" and "microbiome" are usually used interchangeably, it is important to clarify that "microbiota" refers to the living organism residing in the body. Differently, "microbiome" refers to either the microbial genomes within a particular ecological niche or the genomes of the individual microorganisms themselves. Based on its location within the host, the microbiota can be characterized into oral, skin, respiratory and gut microbiota, with the latter being the most studied and the most impactful on human health (Shreiner et al., 2015). As early as 400 BC, Hippocrates stated, "Death sits in the bowels", highlighting the long-recognized significance of the gut in health and disease (Lichtenstein, 2013). The gut microbiota exerts several physiological processes, ranging from the digestion and fermentation of complex carbohydrates, producing short-chain fatty acids (SCFAs) that provide energy for intestinal cells and help regulate systemic inflammation. Additionally, the gut microflora interacts with the host immune system, promoting immune tolerance and protecting against pathogenic infections. It also synthesizes essential vitamins, such as B vitamins and vitamin K, and plays a role in modulating hormone levels that influence appetite and metabolism (Hou et al., 2022a; Shreiner et al., 2015). SCFAs are short-chain monocarboxylic acids among which butyrate, acetate and propionate represent the most abundant and important (Topping & Clifton, 2001). SCFAs are rapidly absorbed by the epithelial cells lining the gastrointestinal tract, with only a small fraction (5-10%) being excreted in the faeces (Anachad et al., 2023; Canfora et al., 2015a). Once absorbed, SCFAs serve as a major energy source for colonocytes and have systemic effects on host metabolism and immune function. SCFAs play a crucial role in maintaining intestinal barrier integrity by enhancing tight junction assembly and mucin production (Mariadason et al., 1997; Suzuki et al., 2008), thereby mitigating bacterial translocation and inflammation. Additionally, SCFAs have systemic effects: acetate and propionate influence lipid and glucose metabolism by modulating liver functions, including the regulation of de novo lipogenesis

and gluconeogenesis. They also impact appetite regulation by stimulating the release of hormones such as PYY and GLP-1, which help to control food intake and body weight (Canfora et al., 2015b). Furthermore, SCFAs modulate immune responses either by regulating the expression of pro-inflammatory mediators, such as IL1-β, IL-6, TNF-α, IFN-Ɣ and by modulating immune recruitment (Vinolo et al., 2011). In addition, these metabolites interact with G protein-coupled receptors (GPCRs) like free fatty-acid receptors (FFAR2 and FFAR3), which are involved in anti-inflammatory signalling and immune cell regulation (Brown et al., 2003; Kim et al., 2013). Finally, SCFAs are natural inhibitors of class I and II HDACs, known regulators of inflammation and immunity, thus facilitating gene expression through histone acetylation and promoting anti-inflammatory effects (Boffa et al., 1978; Sealy & Chalkley, 1978; Shakespear et al., 2011).

The composition of the gut microbiota is remarkably diverse, including *Firmicutes*, *Bacteroidetes*, *Actinobacteria*, *Proteobacteria*, *Fusobacteria*, and *Verrucomicrobia*, with *Firmicutes* and *Bacteroidetes* phyla being the most predominant members (Hou et al., 2022a). The *Firmicutes* phylum, a group of gram-positive bacteria, represents a significant component of the human gut microbiota and is characterized by its ability to ferment dietary carbohydrates (Flint et al., 2012). At a lower taxonomic level, *Firmicutes* include several key bacterial genera such as *Lactobacillus*, *Clostridium*, *Bacillus*, and *Streptococcus*, each of which plays distinct roles in maintaining gut health and influencing metabolic processes (Candela et al., 2010).

The *Bacteroidetes* phylum is a diverse and significant group of gram-negative bacteria found in the human gut microbiota. This phylum includes several genera, such as *Prevotella*, *Porphyromonas* and *Bacteroides* being the most abundantly represented in faecal microbiota (Sghir et al., 2000). A healthy gut microbiota typically exhibits a diverse composition, including a balanced representation of *Bacteroidetes*. This microbial diversity is essential for maintaining metabolic health and preventing dysbiosis, which can lead to obesity and other metabolic issues. Members of the *Bacteroidetes* phylum are particularly adept at breaking down polysaccharides due to their extensive repertoire of carbohydrate-active enzymes (CAZymes). These enzymes include glycoside hydrolases, polysaccharide lyases, and carbohydrate esterases, which collectively enable the degradation of various plant-derived and host-derived polysaccharides (F. Thomas et al., 2011). This enzymatic capability allows *Bacteroidetes* to thrive on a wide range of dietary

fibres and other complex carbohydrates, producing SCFAs as metabolic byproducts, which are key metabolites exerting systemic anti-inflammatory effects.

A well-balanced gut microbiota is critical for maintaining health (Fig. **5**). On the contrary, exposure to several factors such as high-fat diet and pathogens can alter gut microbiota composition and equilibrium (Lecuyer et al., 2021; Luck et al., 2015). Such disruption has been named dysbiosis and is associated with various health issues. Disruptions of the microbiota have been linked to metabolic disorders like obesity and type 2 diabetes, gastrointestinal diseases such as inflammatory bowel disease (IBD) and irritable bowel syndrome (IBS), and even neuropsychiatric conditions through the gut-brain axis (Afzaal et al., 2022). Several studies reported that an increased faecal ratio of *Firmicutes* to *Bacteroidetes* is commonly associated with obesity and metabolic disorders. This dysbiotic signature can lead to enhanced energy extraction from the diet, contributing to weight gain and insulin resistance. For example, studies have found that individuals with obesity often exhibit a higher relative abundance of *Firmicutes*, which is linked to increased levels of pro-inflammatory cytokines such as TNF-α and IL-6, further exacerbating inflammation and metabolic dysfunction (Ciofi et al., 2006; Ley et al., 2005; Turnbaugh et al., 2006). One of the primary mechanisms through which gut dysbiosis contributes to obesity-related inflammation is by affecting the production of SCFAs. During dysbiosis, the production of SCFAs is frequently diminished. Indeed, studies have found reduced levels of SCFAs in faecal samples from dysmetabolic mice, as well as in samples from obese and diabetic human patients (Makki et al., 2018; L. Zhao et al., 2018). Gut microflora alteration leads to compromised gut barrier function, resulting in increased intestinal permeability allowing the translocation of microbial products like lipopolysaccharides (LPS) from the gut lumen into the systemic circulation thus inducing an immune response in the host with the promotion of a pro-inflammatory state. This phenomenon has been defined as “leaky gut”. The loss of gut integrity facilitates the translocation of bacterial components from the intestine to the periphery (Brenchley & Douek, 2012). LPS and other endotoxins can trigger systemic inflammation by activating the immune system, leading to the release of pro-inflammatory cytokines such as TNF-α, IL-6 and IL-1β. This inflammatory response exacerbates insulin resistance and contributes to the development of metabolic disorders. Elevated levels of these cytokines disrupt insulin signalling pathways, impairing glucose uptake and metabolism and

promoting further fat accumulation (Agus et al., 2021; You et al., 2022).

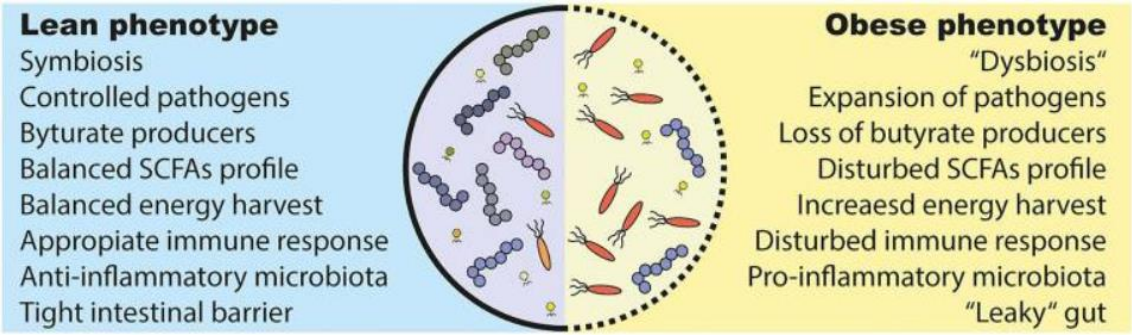

Figure 5. Gut microbiota alterations in healthy and obese patients. *(Scheithauer et al., 2020).*

How to study the gut microbiota

Metagenomics. Metagenomics has become a pivotal tool in microbiome research and among the various techniques employed, the two primary methodologies are 16S rRNA sequencing and shotgun metagenomics. 16S rRNA sequencing focuses on the small 16 ribosomal RNA subunit gene (16S rRNA gene), which contains hypervariable regions useful for identifying and classifying bacterial species within a sample. This technique targets specific gene regions (typically V1-V5) to provide a detailed profile of bacterial diversity and composition (Mancabelli et al., 2017; Van de Peer et al., 1996). Conversely, shotgun metagenomics takes a broader approach by sequencing the entire DNA content from the microbial community, including not only bacteria but also archaea, viruses, fungi, and other microorganisms. This method fragments the total DNA into smaller pieces and then sequences these fragments to reconstruct the genomes of all present microbes (Quince et al., 2017). While 16S rRNA sequencing offers a focused view of bacterial taxonomy and diversity, shotgun metagenomics provides a more comprehensive overview of the functional potential and interactions within the microbiome, revealing insights into microbial genes, metabolic pathways, and potential interactions between different microbial groups.

Mouse models. Given the crucial role of gut microbiota in maintaining homeostasis, a growing number of researchers are focusing on the link between gut microflora and human diseases. Beyond computational studies, the use of mouse models has become

essential for investigating gut microbiota and its effects on health and disease. Mice offer several advantages due to their genetic similarities to humans, controlled breeding environments, and the ability to manipulate their microbiota through diet, antibiotics, or faecal microbiota transplantation (FMT), which facilitates the study of microbiota changes and their effects by transferring faecal material from donor to recipient mice. These models provide invaluable insights into the complex interactions between host and microbiota (Fritz et al., 2013). The gold-standard to study gut microbiota is the usage of germ-free mice which are raised in sterile conditions and provide a clear baseline for studying microbial colonization effects upon microbiota transplantation (Hou et al., 2022b; P. Yi & Li, 2012). Germ-free mice exhibit several distinct physiological features, including an underdeveloped immune system, poorly developed gut-associated lymphoid tissues (GALT), reduced serum immunoglobulin levels, and smaller spleens and mesenteric lymph nodes with low levels of tissue-resident macrophages (Khosravi et al., 2014). Notably, germ-free mice are resistant to diet-induced obesity (Bäckhed et al., 2007). In addition, axenic mice, which are mice with a depleted gut microflora, that received microbiota transplants from obese donors gained more energy from their diet than those receiving microbiota from lean donors (Fei & Zhao, 2012; Ridaura et al., 2013a; Turnbaugh et al., 2006b). Collectively, these findings suggest that the obese phenotype can be transmitted through gut microbiota transplantation, indicating a direct causal relationship between gut microbiota and obesity.

Another strategy often used by researchers is the administration of broad-spectrum antibiotics to mice to either deplete specific bacterial populations or generally reduce the gut microflora, thus favouring microbiota transplantation engraftment (Bokoliya et al., 2021a; Kennedy et al., 2018). This procedure can be easily applied to any mouse genotype or condition and is less expensive than germ-free mice usage.

Finally, genetically modified mice can be used to resemble the phenotype associated with the genetic defect in the disease, allowing researchers to study the role of individual genes in the interaction between the host and its microbiota (Geurts et al., 2011; Peloquin & Nguyen, 2013).

Cis-Aconitate Decarboxylase 1 and Itaconate

Cis-Aconitate Decarboxylase 1 (ACOD1), also known as immune-responsive gene 1 (IRG1), is a mitochondrial enzyme involved in the metabolic reprogramming of immune cells (Degrandi et al., 2009; Hall et al., 2013). ACOD1 catalyses the biosynthesis of the metabolite itaconate via decarboxylation of the Krebs Cycle intermediate cis-aconitate upon inflammatory stimuli (Fig. **6**) (Basler et al., 2006; C. G. L. Lee et al., 1995; Michelucci et al., 2013).

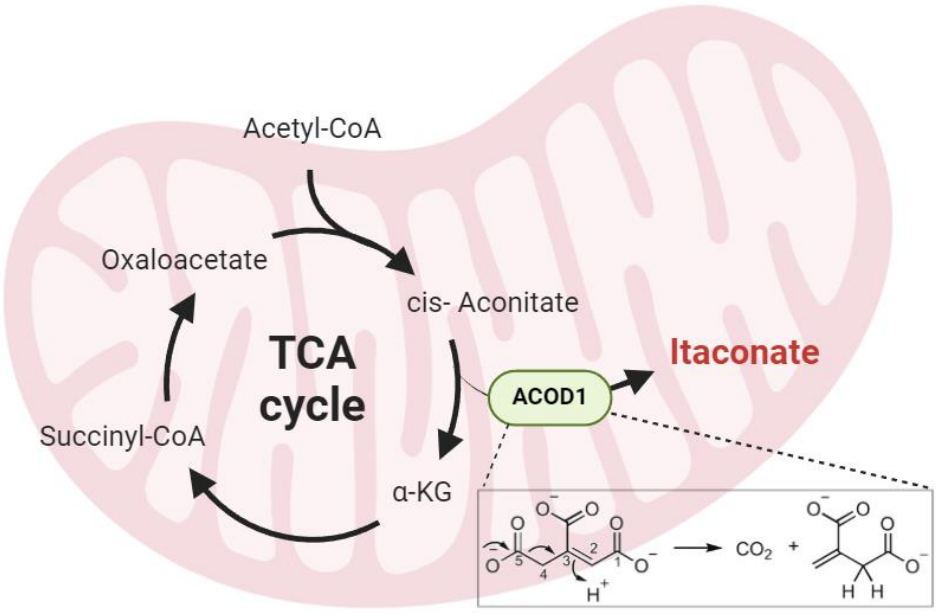

Figure 6. ACOD1 catalyses the decarboxylation of cis-aconitate to itaconate
Created with Biorender.

Although barely detectable under physiological conditions, *Acod1* is drastically induced upon inflammatory stimuli and initially found in classically activated (pro-inflammatory) macrophages (Basler et al., 2006; C. G. L. Lee et al., 1995). For example, the engagement of Toll-like receptors (TLRs) such as TLR2, TLR3, TLR4, TLR5, and TLR9 by various pathogen-associated molecular patterns (PAMPs), including LPS, lipid A, and lipoteichoic acid, induces the expression of *Acod1* in immune cells, predominantly macrophages (Kuo et al., n.d.; Uddin et al., 2016; R. Wu et al., 2020a). Besides TLR ligands, the transcription of the *Acod1* gene is also responsive to several inflammatory cytokines, including IFNβ, IFNγ, TNF, IL1β, granulocyte-macrophage colony-stimulating factor (GM-CSF) (Naujoks et al., 2016; S. Shi et al., 2005; Y. Zhao et al.,

2023) in both immune and non-immune cells (Daniels et al., 2019a; Ren et al., 2016; Z. Yi et al., 2020a). Furthermore, in response to bacterial stimuli, activation of the lysosomal biogenesis factor transcription factor EB (TFEB) promotes the transcription of *Acod1* in macrophages (Schuster et al., 2022).

The human *ACOD1* gene, consisting in 481 amino acids, is located on chromosome 13q22.3 and is significantly conserved across a variety of species (Schmidt & Richter, 2000; Sendra et al., 2020; Xiao et al., 2011). Structural analyses have revealed that ACOD1 operates as a homodimer with its active site composed of eight specific residues, which are critical for its catalytic activity: Asp93, Thr97, His103, His159, Lys207, Lys272, His277, and Tyr318. The catalytic mechanism of ACOD1 involves the opening of the active site by tilting the smaller domain relative to the larger domain (Chun et al., 2020). Despite the conservation of active site residues between mouse and human ACOD1, the mouse enzyme exhibits a higher catalytic rate constant of 4.9 s−1 compared to the human enzyme's 0.9 s−1 (F. Chen et al., 2023). A critical study discovered that the presence of a human-specific residue, Met154, significantly reduces the activity of human ACOD1, whereas other mammals have an isoleucine at this position, resulting in higher enzymatic activity (F. Chen et al., 2023).

Itaconate is a α, β-five-carbon dicarboxylic acid which shares structural similarity with other metabolites such as succinate, fumarate, malonate, phosphoenolpyruvate and α-ketoglutarate. Due to its conjugated unsaturated double bond, itaconate acts as a mild electrophile thereby affecting protein activity and function through a Michael addition reaction. Specifically, it covalently interacts with thiol functional groups, such as free or protein cysteine residues, resulting in a 2,3-dicarboxypropylation reaction, also named as "itaconation" (Brogi et al., 2021; Mills, Ryan, Prag, Dikovskaya, Menon, Zaslona, Jedrychowski, H Costa, et al., 2018). In itaconate-producing cells, itaconate catabolism proceeds through a three-step enzymatic reaction. First, itaconate is converted to itaconyl-CoA by succinyl coenzyme A synthetase (SCS). Next, itaconyl-CoA undergoes hydration to form citramalyl-CoA, catalysed by methylglutaconyl-CoA hydratase (AUH). Finally, citramalyl-CoA is cleaved into acetyl-CoA and pyruvate by citramalyl-CoA lyase (CLYBL) (Adler et al., 1957; X. Shi et al., 2022). As already mentioned, itaconate production occurs in the mitochondrial matrix but to exert its regulatory functions it must

cross the mitochondrial inner membrane. Due to its structural similarity to malate, itaconate is transported across the mitochondrial inner membrane via the dicarboxylate (SLC25A10), citrate (SLC25A1), and oxoglutarate (SLC25A11) carriers (Mills, et al., 2018). Moreover, it has been recently shown that itaconate can be transported from the cytosol to the extracellular space by the ATP-binding cassette transporter G2 (ABCG2) in an ATPase-dependent manner in macrophages (C. Chen et al., 2024).

Itaconate has two naturally occurring isomers differing solely in the position of the double bond and exhibiting immunomodulatory effects in macrophages, named mesaconate and citraconate (Fig. **7**) (Winterhoff et al., 2021). While msaconate has been found to be synthesized from itaconate (W. He et al., 2022), the biosynthetic mechanism of citraconate is still poorly understood. Among the three isomers, citraconate exhibits the most electrophilic properties and has been found as the first naturally occurring ACOD1 inhibitor (F. Chen, Elgaher, et al., 2022).

Given its high polarity, itaconate cannot pass through cell membranes. Therefore, membrane-permeable itaconate derivatives such as dimethyl-itaconate (DI), 4-octyl-itaconate (4-OI) and 4-monoethyl itaconate (4-EI) have been developed: DI has both carboxyl groups methylated, 4-OI contains an octyl group that further increases its lipophilicity and 4-EI has an ethyl ester group at the 4-position (Fig. **7**). Although extensively used, emerging evidence suggests that these derivatives do not fully mimic itaconate functions *in vivo*, because of their increased reactivity towards thiols compared with itaconate (Z. Li et al., 2023; O'Neill & Artyomov, 2019; Swain et al., 2020).

Itaconate exemplifies the significant impact of metabolic reprogramming during immune responses. This metabolite is abundantly synthesized in classically activated macrophages, exerting anti-inflammatory and immunoregulatory effects by modulating numerous metabolic pathways in macrophages in response to inflammatory and stress stimuli. Moreover, several studies have highlighted its role as an antimicrobial agent, capable of inhibiting the growth of various bacterial pathogens and limiting the replication of viruses within cells (O'Neill & Artyomov, 2019). The emerging intricate interactions between itaconate metabolism, host-pathogen interactions, and the regulation of inflammatory and immune responses are discussed in detail in the following paragraphs.

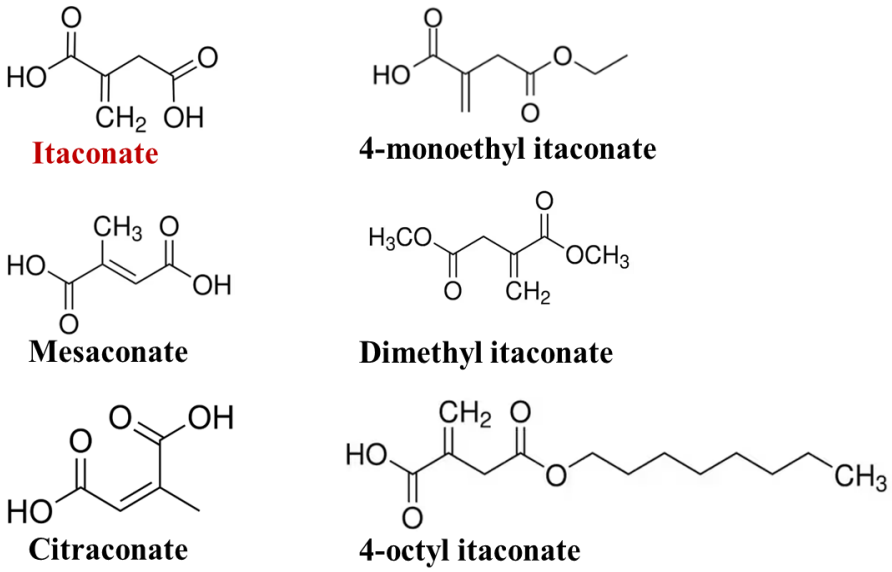

Figure 7. Itaconate family and derivatives.

Immunoregulatory properties of itaconate

Due to its chemical structure, itaconate exihibits several immunoregulatory properties (Fig. **8**)

Itaconate as SDH inhibitor. Succinate dehydrogenase (SDH) forms the mitochondrial complex II, being a key component of the TCA cycle and electron transport chain. The oxidation of succinate to fumarate by SDH contributes to generate mitochondrial reactive oxygen species (mtROS) which sustains the production of inflammatory cytokines. Due to its structural similarity to succinate, itaconate acts as a competitive inhibitor of the enzymatic activity of SDH *in vitro* and *in vivo*. Consequently, the generation of mtROS is inhibited, leading to reduced activity of prolyl hydroxylases. This inhibition interferes with the stabilization of hypoxia-inducible factor (HIF), thereby suppressing the transcription of the pro-inflammatory cytokine IL-1β (Cordes et al., 2016; Lampropoulou et al., 2016a). During ischemia/ reperfusion injury (I/R), the SDH- driven oxidization of succinate aggravates I/R in mice through production of mtROS by reverse electron transport (RET) at mitochondrial complex I (Chouchani et al., 2014). Although it has been not demonstrated yet, itaconate has been argued to block ROS generation from RET via inhibiting SDH activity (Lampropoulou et al., 2016b). Importantly, RET has been shown to aggravates I/R and in line with this, DI administration has been found to reduce ROS production in LPS-activated macrophages, thus protecting against I/R. Further

studies are necessary to investigate the effect of itaconate on RET.

Itaconate as a glycolytic inhibitor. Metabolic reprogramming after proinflammatory stimuli in macrophages includes a switch from oxidative metabolism towards glycolysis. Glyceraldehyde-3-phoshate (GADPH) is a rate-limiting enzyme in aerobic glycolysis and it was demonstrated that 4-OI inactivates GADPH by directly alkylating the cysteine residue at position 22 reducing IL-1β, inducible nitric oxide synthase (iNOS) and TNF production by limiting aerobic glycolysis (Liao et al., 2019). Consequently, the extracellular acidification rate is diminished and the intracellular oxygen consumption increases, leading to activation of anti-inflammatory programs. Furthermore, alkylated cysteine residues have been identified in several other glycolytic enzymes including aldolase A (ALDOA) and lactate dehydrogenase (LDHA). ALDOA is a major player in glycolysis and gluconeogenesis while LDHA converts pyruvate to lactate at the last step. Both these enzymes are modified by itaconate resulting in glycolytic inhibition (Mills et al., 2018; Qin et al., 2019). In addition, it has been reported that itaconate inhibits liver glycolysis by affecting the activity of fructose-6-phosphate-2 kinase (F26BP) (Sakai et al., 2004). In conclusion, itaconate can regulate the activity of several metabolic enzymes via cysteine alkylation.

Itaconate as an electrophilic stress regulator. Nuclear factor erythroid 2-like 2 (NRF2) is a key transcription factor involved in the response to oxidative stress and inflammation. Under normal conditions, kelch-like ECH-associated protein 1 (KEAP1) regulates NRF2 by promoting its degradation via the cullin 3-based E3 ubiquitin ligase complex. However, itaconate covalently alkylates KEAP1 cysteine residues via Michael addition reaction, preventing KEAP1-mediated degradation of NRF2, leading to the activation of NRF2 and its target genes (Mills, et al., 2018). Once in the nucleus, NRF2 promotes the transcription of genes with anti-inflammatory and antioxidant functions. NRF2 activation leads to a decrease in nitrite levels, reduction in iNOS, IL-10, and IL-1β expression and a decrease in cellular ROS production, thereby suppressing HIF-1α (Kobayashi et al., 2016).

In addition to NRF2 activation, itaconate influences the ATF3/IkBζ axis. IkBζ, a nuclear protein encoded by NF-kappa-B inhibitor zeta (NFKBIZ), is the key transcription factor involved in the regulation of secondary transcriptional responses to TLR activation, thus modulating IL-6 but not TNFα production (Yamamoto et al., 2004). Instead, Activating

Transcription Factor 3 (ATF3) is a stress-responsive transcription factor that represses pro-inflammatory gene expression and negatively regulate IkBζ. Itaconate and itaconate derivatives increase ATF3 levels, thus inhibiting IkBζ at the translation level. This leads to the reduction of certain pro-inflammatory cytokines such as IL-6 in an NRF2-independent manner, except for TNFα (Bambouskova et al., 2018). Correspondingly, after LPS treatment and tolerization, ATF3 and IkBζ levels decrease and increase, respectively, in *Acod1*-deficient macrophages compared to *wild type* counterparts.

Additionally, endogenous itaconate and its derivative 4-OI inhibit the NOD-, LRR-, and pyrin domain-containing protein 3 (NLRP3) inflammasome in murine LPS-treated bone marrow-derived macrophages (BMDMs), resulting in reduced production of inflammatory cytokines (Hooftman et al., 2020). This inhibitory mechanism is independent of SDH inhibition and NRF2 activation. Instead, itaconate acts through the alkylation of Cys548 on NLRP3 following LPS stimulation. Recent studies have demonstrated that endogenously produced itaconate is crucial for regulating late NLRP3 inflammasome tolerization and pyroptosis via synergistic interactions with iNOS (Bambouskova et al., 2021). Mechanistically, itaconate post-translationally modifies gasdermin D (GSDMD), preventing the complete activation of caspase-1, thereby regulating cell death and tissue damage (Bambouskova et al., 2021). This regulation of cell death occurs in highly inflamed cells, leading to the secretion of IL-1β.

Transcription factor EB (TFEB), a key regulator of lysosomal biogenesis and autophagy, is a member of the microphthalmia/transcription factor E (MiT/TFE) family of transcription factors. Lysosomes are essential organelles involved in bacterial killing in macrophages. Under nutrient-rich conditions, TFEB is retained in the cytoplasm following phosphorylation by the mechanistic target of rapamycin complex 1 (mTORC1). While during starvation or stress, mTORC1 activity is inhibited, leading to the dephosphorylation and nuclear translocation of TFEB, where it activates target gene transcription (Napolitano & Ballabio, 2016). 4-OI and itaconate inhibit mTOR-mediated phosphorylation and cytosolic retention by alkylating TFEB at a cysteine residue to induce its nuclear localization (Z. Zhang et al., 2022).

Stimulator of interferon genes (STING) plays a pivotal role in macrophage activation and is central in the protection against foreign pathogens. It was already known that itaconate suppresses STING expression in macrophages via activation of NRF2 (Olagnier et al.,

2018). Nevertheless, in 2023 two papers reported a novel NRF2-indipendent inhibition of STING, in which itaconate and 4-OI directly alkylate STING at multiple cysteine residues (W. Li et al., 2023; Su et al., 2023).

It was recently discovered that itaconate and its derivative 4-OI can inhibit IL-4-induced M2 polarization by inhibiting the JAK1/STAT6 pathway (Runtsch et al., 2022). Mechanistically, after being taken up by M2 macrophages, itaconate dampens JAK1 activation through alkylation at cysteines residues 715, 816, 943, and 1130, thereby inhibiting STAT6 phosphorylation. This highlights a potential role for itaconate and its derivatives as therapeutic options in M2 macrophages-driven diseases (Blanco et al., 2022).

Itaconate as an epigenetic regulator. Recently, itaconate has been identified as an inhibitor of a member of the ten-eleven translocation methyl-cytosine dioxygenases family, TET methyl-cytosine dioxygenase 2 (TET2). TET2 is essential for DNA demethylation by oxidizing 5-methylcytosine (5mC) to 5-hydroxymethylcytosine (5hmC) (Cong et al., 2021; Hu et al., 2013). α-KG is an essential co-factor for TET enzymes and due to its structural similarity α-KG, itaconate competitively inhibits TET2. By inhibiting its catalytic activity, itaconate suppresses the expression of LPS-inducible genes in macrophages (L. L. Chen et al., 2022).

Itaconate as a paracrine signalling molecule. Beyond its cell-autonomous functions, itaconate has been found to act as an orthosteric agonist of the GPCR oxoglutarate receptor 1 (OXGR1). OXGR1, also called GPR99, has been an orphan receptor since the discovery that α-ketoglutarate was found to promote OXGR1 signalling (W. He et al., 2004) and it has several important functions in heart pathophysiological processes and mucociliary clearance in the respiratory tract (Bankova et al., 2016; Omede et al., 2016). In a mouse model of pulmonary infection with *Pseudomonas aeruginosa*, itaconate production is induced in activated macrophages. Upon binding to OXGR1, itaconate induce the activation of the canonical intracellular response of Gq thus stimulating Oxgr1-dependent mucus secretion and transport in respiratory epithelium (Zeng et al., 2023).

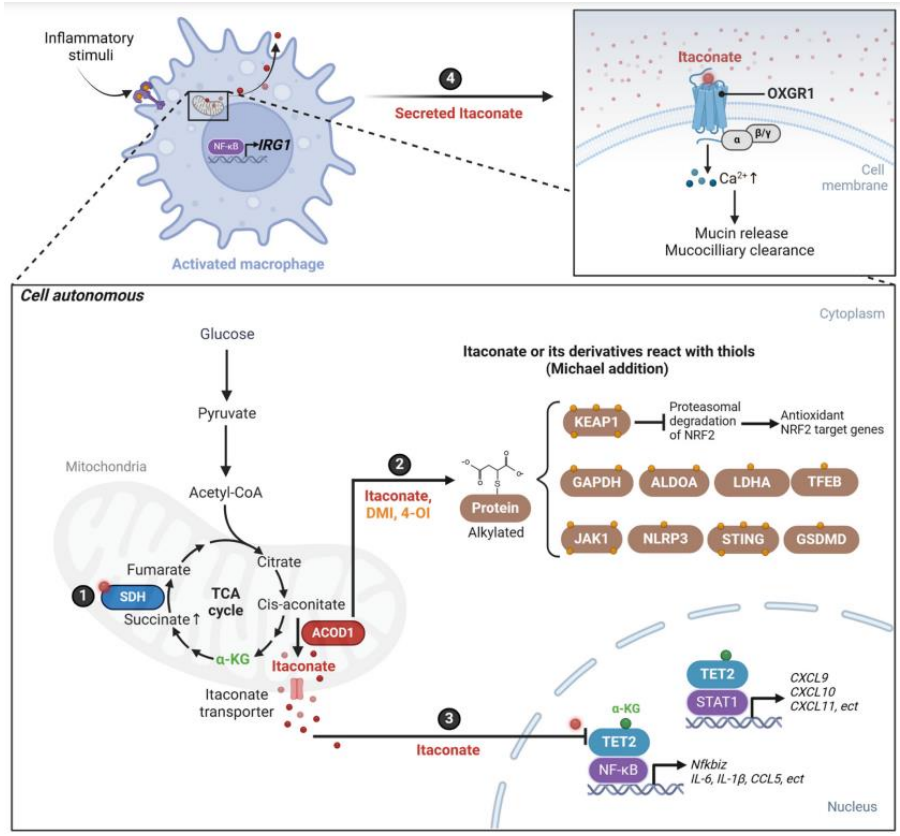

Figure 8. Targets and mechanisms of action of itaconate and derivatives *(Ye et al., 2024a).*

Itaconate in host-pathogen interactions

Itaconate plays significant roles in host-pathogen interactions, primarily by modulating immune responses and exerting antimicrobial effects. It is a natural antimicrobial agent and is essential in restricting replication of many microbes.

The glyoxylate shunt is a variation of the tricarboxylic acid cycle used by bacteria, which is essential for the utilization of acetate and fatty acids as carbon sources during physiological conditions that require gluconeogenesis, necessary for their growth and survival (Lorenz & Fink, 2002; McKinney et al., 2000). One of the major antimicrobial mechanisms of itaconate consists in the inhibition of the isocitrate lyase (ICL), a bacterial enzyme catalysing the cleavage of isocitrate to succinate and glyoxylate in the glyoxylate shunt, thus restricting growth of pathogens depending on ICL activity such as *Pseudomonas Indigofera* (McFadden & Purohit, 1977). In addition, itaconyl-CoA, a by-product of itaconate catabolism, has been found to exert a bactericidal function by restricting the growth of *Mycobacterium tuberculosis* (Ruetz et al., 2019). Specifically,

itaconyl-CoA inhibits methylmalonyl-CoA mutase (MCM), a key enzyme in *M. tuberculosis* metabolism that converts methylmalonyl-CoA to succinyl-CoA, a crucial step in the propionate metabolism pathway (Savvi et al., 2008). Conversely, pathogens such as *Pseudomonas aeruginosa* and *Staphylococcus aureus* can utilize itaconate to enhance their survival. These bacteria exploit host-derived itaconate to directly or indirectly boost the synthesis of extracellular polysaccharide (EPS), which contributes to the formation of protective biofilms, thereby promoting their survival and growth (Riquelme et al., 2020; Tomlinson et al., 2021).

In addition to its known bactericidal functions, itaconate has demonstrated notable antiviral effects, particularly against Zika virus (ZIKV) infections. The expression of *Acod1* is upregulated in a ZBP1/RIPK3/IRF1-dependent manner during ZIKV infection, leading to increased production of itaconate. Then, itaconate inhibits SDH in the infected neurons, resulting in metabolic disturbances and a reduction in viral genome replication in mice (Daniels et al., 2019b). Moreover, the itaconate derivative 4-OI has been shown to reduce SARS-CoV-2 infection and its associated inflammatory complications by activating an antiviral response through the transcription factor NRF2 (Olagnier et al., 2020).

The role of itaconate in diseases

As described above, itaconate exerts its effects through diverse mechanisms, combating both bacterial and viral infections while also mediating immunoregulatory functions across different tissues and pathological conditions. Due to the multifaceted nature of its actions, further research is crucial to fully elucidate its potential clinical applications and therapeutic benefits.

Itaconate as an immunomodulatory metabolite. Psoriasis is a chronic autoimmune disease affecting the joints and the skin and associated both with immunogenic and inflammatory factors (Diskin C., Ryan T. A. J., O'Neill L. A. J. 2020). Polymorphisms in NFKBIZ have been associated with psoriasis (Tsoi LC, et al. 2015) and itaconate inhibits IkBζ (encoded by NFKBIZ) post-translationally. Concomitantly, DI treatment resulted in downregulation of IκBζ target-genes and ameliorated the psoriatic pathology in a psoriasis mouse model.

Sepsis is a life-threating condition characterized by a dysregulated immune response to infection, leading to significant tissue and organ damage. As sepsis progresses, a profound imbalance between inflammation and immune homeostasis occurs, leading to multiple organ failure (Cecconi M., et al., 2018). Following the initial infection, the innate immune system is continuously stimulated to release pro-inflammatory cytokines (Van der Poll T., et al., 2017). While the induction of tolerance is intended to mitigate damage from the infection, prolonged activation can result in immunosuppression or immuno-paralysis, increasing susceptibility to secondary infections (Biswas S. K., Lopez-Collazo E., 2009). In the early stages of infection, the administration of derivatives like DI or 4-OI has been shown to inhibit the excessive inflammation, thereby protecting mice from death and improving the survival rates in LPS-induced sepsis models. However, the strong upregulation of Acod1 during tolerance in LPS-tolerized murine macrophages and human peripheral blood mononuclear cells (PBMCs) following sepsis, suggests that itaconate might also contribute to immuno-paralysis (Li Y., et al., 2013; Dominguez-Andrés J., et al., 2019). Contrarly, recent evidence challenges earlier studies proposing that the ACOD1/itaconate axis might have protective effects in these conditions due to itaconate anti-inflammatory properties. Indeed, it has been found that the itaconate may exert pro-inflammatory effects rather than simply suppress the immune system thus worsening the outcomes of sepsis in different mouse models (F. Chen, Wu, et al., 2022). In this study, Chen and colleagues demonstrated that the STING1/MYD88- mediated increase expression of ACOD1 after LPS exposure, leads to itaconate production which, in turn, induces cell death and DAMPS release, thus aggravating sepsis. In addition, in another study it has been showed that ACOD1 expression mediates polymicrobial sepsis in an itaconate-independent manner by activating a cytokine storm mainly via activation of TNF signalling pathway, thus imparting a profound pro-inflammatory response (R. Wu et al., 2022). Recent findings have uncovered a previously unrecognized role for the ACOD1/itaconate axis, adding new layers of complexity to our understanding of its immunoregulatory functions.

Itaconate as an antioxidant metabolite. Ischemia-reperfusion (I/R) injury is a significant cause of tissue damage following the restoration of blood supply after a period of ischemia and it is characterized by oxidative stress, inflammation, and subsequent cell death (Kalogeris et al., 2016). Due to its anti-inflammatory and antioxidant properties,

itaconate and its derivatives have been investigated as promising candidates to mitigate the damage associated with I/R. It has been shown that itaconate and DI inhibit SDH in murine models of cardiac and cerebral I/R, thus reducing SDH-driven mtROS production and promoting the transcription of antioxidant and anti-inflammatory proteins (Cordes et al., 2020; Lampropoulou et al., 2016b). Moreover, another study demonstrated that in a model of liver I/R itaconate exerts beneficial effects on hepatocytes by modulating the activation of NRF2, leading to a mitigated oxidative damage (Z. Yi et al., 2020b).

Itaconate as a regulator of tumorigenesis. Recently, itaconate has been identified as a metabolite produced within the myeloid compartment of several solid tumours, playing an ambivalent role in the development and progression of malignancies and metastasis formation. One of the first studies to point out a role for the ACOD1/itaconate axis in tumorigenesis showed that *ACOD1* expression was linked to glioma progression both in *vitro* and *in vivo* (Pan et al., 2014). This data was confirmed years later by another study where elevated *Acod1* expression was found in tumour-associated macrophages (TAM) during the progression of glioblastoma in mice (Pires-Afonso et al., 2022). Furthermore, it has been shown that macrophages of peritoneal tumour-bearing mice accumulate itaconate, thereby reducing OXPHOS-driven production of ROS and promoting tumour growth (Weiss et al., 2018). In addition, several studies reported a pro-tumorigenic role of secreted itaconate by myeloid-derived suppressor cells (MDSCs). In HCC, itaconate promotes $CD8^+$ T-cell exhaustion via an epigenetic mechanism (Gu et al., 2023). In several mouse tumour models, *Acod1* deficiency limited tumour growth by reversing the immune-suppressive tumour microenvironment, thereby promoting anti-tumour immunity (Y. J. Chen et al., 2023; H. Zhao et al., 2022). Moreover, activation of the GM-CSF-JAK/STAT5-C/EBPβ pathway has been shown to induce *Acod1* upregulation and production of itaconate in tumour infiltrating neutrophils (TINs) in breast cancer. By modulating NRF2, itaconate stimulated evasion from ferroptosis in TINs, promoting breast cancer-induced lung metastasis (Y. Zhao et al., 2023). Notably, itaconate exerts its pro-tumorigenic functions also by enhancing resistance to chemo- and immunotherapy by modulating the immune microenvironment.

These are just a few examples of diseases in which treatment with itaconate or its derivatives demonstrated promising therapeutic effects. Further studies are necessary to

expand our understanding about itaconate and its mechanisms during inflammatory and immunogenic processes to develop the basis for future therapeutic applications.

Aim of the work

Obesity is a chronic condition characterized by excessive fat accumulation associated with a body mass index (BMI) ≥ 30 kg/m^2. With approximately 30% of the world's population affected, obesity represents a global health concern as it predisposes individuals to the development of noncommunicable diseases including type 2 diabetes, non-alcoholic fatty liver disease and liver cancer, accounting for ~70% of premature deaths worldwide. Therefore, understanding the adaptations of the metabolic machinery to overnutrition might provide targets for therapeutic intervention and prevent life-threatening health conditions. Obesity develops when chronic energy intake exceeds energy expenditure causing the adaptive accumulation of unused nutrients as fat in adipose tissue depots. This results in adipose tissue dysregulation and initiation of a chronic low-grade inflammation (Y. S. Lee & Olefsky, 2021), leading to impaired adipocyte liporegulatory capacities and energy-expenditure processes, including decreased sensitivity to insulin and lipid deposition in ectopic tissues, such as in the liver (Y. S. Lee et al., 2018; Y. S. Lee & Olefsky, 2021). Metabolic changes in cells have instrumental roles in regulating inflammatory responses occurring in obesity. Itaconate is a metabolite synthetized in a reaction of decarboxylation of the tricarboxylic acid (TCA) cycle intermediate cis-aconitate, catalysed by the mitochondrial cis-aconitate decarboxylase 1 (ACOD1) enzyme, also known as immune-responsive gene 1 (IRG1), in animals (Michelucci et al., 2013). Although poorly detectable in resting conditions, ACOD1 and itaconate levels are upregulated in immune (mainly macrophages) and non-immune cells in response to pro-inflammatory and oxidative conditions to sustain immunoregulatory and antioxidant programs by reprogramming cell metabolism. Moreover, itaconate has been found involved in the initiation and progression of several solid tumours. **However, understanding the role of itaconate biosynthesis in whole-body metabolic and meta-inflammatory responses to nutritional perturbations remained largely unexplored.** Therefore, this project aimed at investigating the role of ACOD1 in diet-induced obesity and the development of associated tumours, such as hepatocellular carcinoma (HCC). This work proposes a model in which *Acod1* deficiency protects mice from HFD-induced obesity and associated comorbidities by maintaining a healthy gut microbiota.

Results

Acod1 deficiency protects mice from diet-induced obesity and associated dysfunction of systemic glucose homeostasis.

Itaconate came to the limelight of biomedical research after having been found involved in several conditions such as sepsis, liver ischemia-reperfusion injury and cancer. However, its role in the responses to whole-body nutritional perturbations was incompletely understood. To evaluate whether itaconate biosynthesis had any role in the homeostatic response to fat overnutrition, 5-week years old constitutive *Acod1* knockout (*Acod1*$^{-/-}$) mice were challenged with either standard chow (ND) or standardized high-fat diet (HFD), comprising 60% of calories from fat, for 16 weeks to promote metabolic disease and compared to *wild type (WT)* counterparts under the same dietary regimens. Unexpectedly, *Acod1*$^{-/-}$ mice gained significant less weight compared to their *wild type* littermates upon HFD overload **(**Fig**. 9A, 9B).** Conversely, no difference in body weight gain was imposed by genotype on mice under a regular chow. To corroborate data derived from body weight gain, mice were subjected to necroscopic analysis at the end of the experiment. Consistent with the decreased body weight gain observed in HFD-fed *Acod1*$^{-/-}$ mice, *Acod1* depletion mitigated fat accumulation in adipose tissues in response to HFD, as indicated by the significant decrease in the weight of inguinal (iWAT), epididimal (eWAT) and perirenal (pWAT) white fat depots as well as brown adipose tissue (BAT) isolated from *Acod1*$^{-/-}$ mice compared to their *wild type* counterparts. On the contrary no major differences were detected in the weights of fat depots isolated from *wild type* and *Acod1*$^{-/-}$ mice fed with a normal diet (Fig**. 9C**). Interestingly, the impact of *Acod1* deficiency on body weight was exclusively due to the augmented accumulation of adiposity and not to any increase in the mass of several lean soft tissues (Fig**. 9D**). These data suggested that *Acod1* loss opposed the accumulation of adiposity under fat overnutrition.

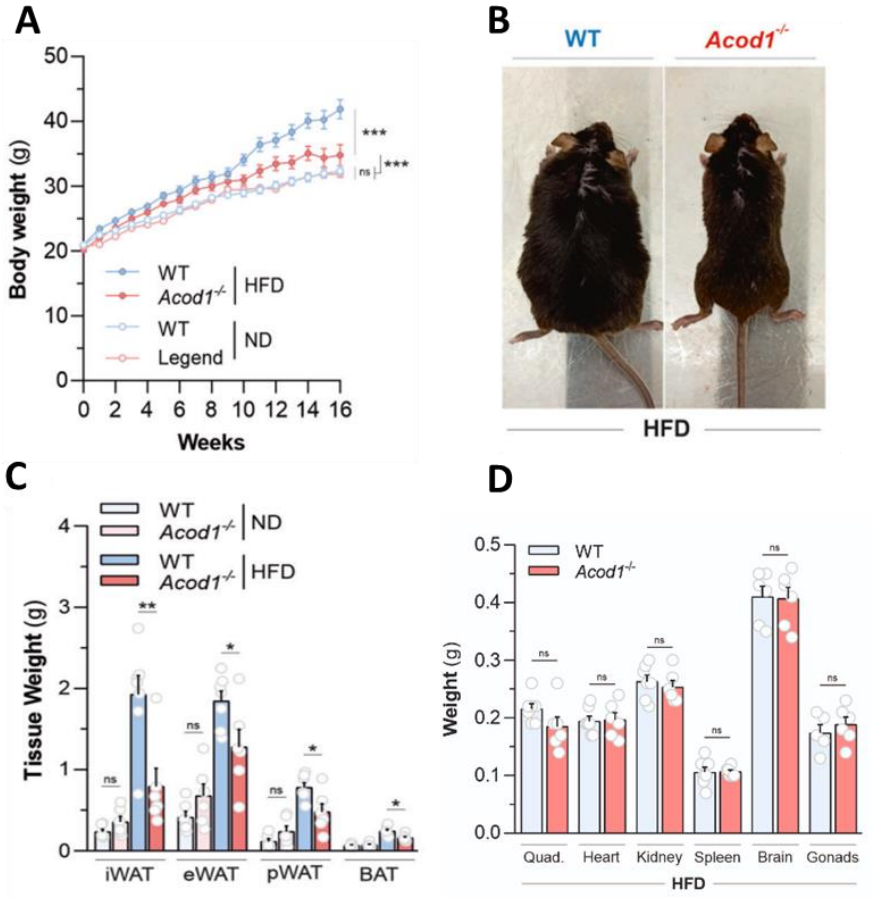

Figure 9. Acod1 loss offers protection against diet-induced obesity in mice.
A*. Body weights of wild type and Acod1$^{-/-}$ mice fed with ND or HFD for 16 weeks. Data as mean ± sem of n = 17 (ND-WT), n = 18 (ND- Acod1$^{-/-}$), n = 26 (HFD-WT) and n = 22 (HFD-Acod1$^{-/-}$) from three experiments independently executed (two-way ANOVA).* ***B****. Representative images of WT and Acod1$^{-/-}$ mice after HFD.* ***C****. Weights (g) of adipose tissues from mice treated as in A at the end of the experiment; ND (n = 6), HFD-WT (n = 7), HFD-Acod1$^{-/-}$ (n = 6). Data as mean ± sem from one representative experiment out of three independently executed (student t-test).* ***D****. Weights (g) of the indicated tissues isolated from WT and Acod1$^{-/-}$ mice after 16 weeks on HFD. Data as mean±s.e.m of n=7 (HFD-fed WT), n=6 (HFD-fed Acod1$^{-/-}$) mice from one representative experiment out of three independently executed (student t-test). *P < 0.05; **P < 0.01; ***P < 0.001; ns not significant.*

Adipocyte hyperplasia and hypertrophy are common hallmarks of the obese adipose tissue. During obesity, fat intake within adipocytes exceeds adipocyte retaining capacity, leading to the occurrence of adipocyte hypertrophy and thus adipose tissue expansion (Horwitz & Birk, 2023). Therefore, histological analyses and quantitative

determination of adipocyte size were performed on white fat depots from mice at end of the experiment. In line with the diminished adiposity, *Acod1* ablation resulted in a marked decrease of adipocyte size in white adipose tissues as demonstrated by a decreased haematoxylin and eosin staining and histomorphometry analysis measured in fat depots derived from *Acod1*$^{-/-}$ mice challenged with HFD, compared to their *wild type* counterparts (Fig**. 10A, 10B**). It has been reported that HFD exposure damages the cytoarchitecture of the brown adipose tissue, leading to the conversion of brown adipocytes into white unilocular cells in a process called "whitening" (Rangel-Azevedo et al., 2022). To determine whether genetic ablation of *Acod1* could protect against HFD-induced morphological changes occurring in BAT, histological analysis of BAT isolated from mice was conducted. Under fat overnutrition, *Acod1* loss decreased BAT whitening (Fig**. 10C, 10D**) with respect to *wild type* controls. Contrarily, *Acod1* was dispensable in regulating fat morphological changes under a normal diet (data not shown**)**. Collectively, these data demonstrated that *Acod1* is a gene having an instrumental role in obesity development.

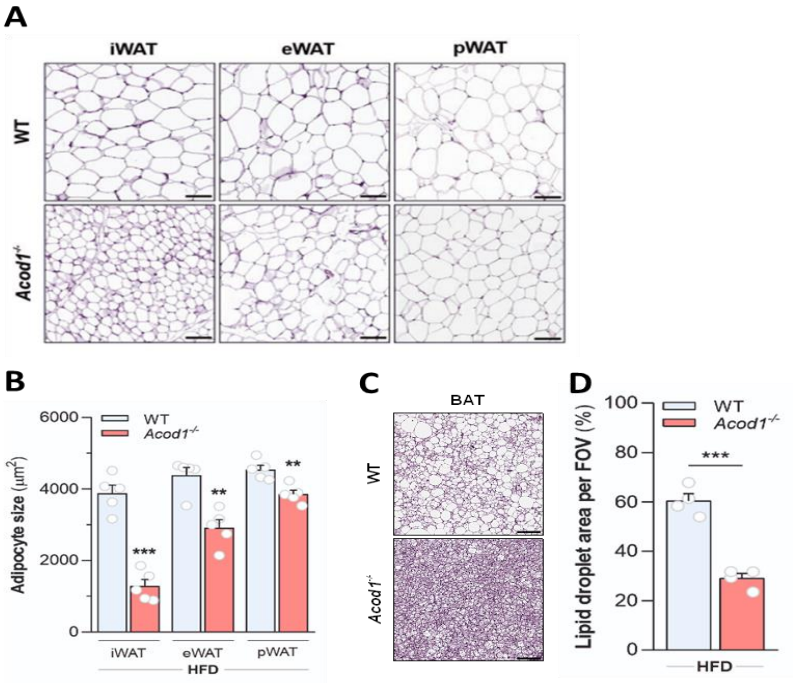

Figure 10. Acod1 deficiency opposes diet-induced changes in adipose tissues.
A*. Representative images of H&E staining of iWAT, eWAT and pWAT from HFD-fed WT and Acod1*$^{-/-}$ *mice and (**B**) quantification of adipocyte size in images described in Fig. 10A. Data as mean±s.e.m. (n = 5 mice per group, average of 5 images each) (student t-test).* ***C****. Representative images of H&E staining of BAT from HFD-fed WT and Acod1*$^{-/-}$ *mice and (**D**) quantification of BAT whitening in images described in Fig. 10C. Data as mean±s.e.m. (n = 4 mice per group, average of 3 images each); FOV, field of vision (student t-test). *P<0.05; **P<0.01; ***P<0.001; ns: not significant.*

Abnormal fat accumulation in tissues following overnutrition results in derangement of glucose and insulin homeostasis. Therefore, to evaluate whether protection from diet-induced obesity offered by *Acod1* loss was associated with an amelioration of systemic glucose homeostasis, fasting blood glucose and insulin levels were measured in *wild type* and *Acod1*$^{-/-}$ mice fed with either with a regular chow or HFD for 16 weeks. In line with their leaner phenotype, HFD-challenged *Acod1*$^{-/-}$ mice exhibited lower fasting glycemia (Fig. **11A**) and insulinemia compared to *wild type* mice (Fig. **11B**). No significant differences in blood glucose and insulin levels were observed between the two genotypes when mice were fed with a regular chow (Fig. **11A, B**). Building on this evidence, the impact of the genotype on mouse responses to intraperitoneal glucose overload was assessed through a glucose tolerance test. Under a regular chow, glucose blood levels of *wild type* and *Acod1*$^{-/-}$ mice did not differ following intraperitoneal glucose injection. In

contrast, genetic ablation of *Acod1* enhanced tolerance to glucose administration in mice fed HFD, compared to their *wild type* counterparts (Fig. **11C**).

Next, to explore whether the enhanced glucose tolerance associated with *Acod1* deficiency in response to HFD was linked to heightened responsiveness of peripheral tissues to insulin signalling, an insulin tolerance test was conducted. As illustrated in Figure **11D**, the presence of *Acod1* exhibited negligible influence on regulating insulin tolerance in mice on a regular diet. Conversely, the absence of *Acod1* resulted in increased sensitivity to insulin action in mice exposed to HFD with respect to *wild type* littermates. Insulin resistance in obesity is regulated by a complex interplay of multiple mechanisms. Among them, neural molecules and adipokines exert several and opposed effects in modulating insulin resistance. To investigate whether the ameliorated insulin sensitivity induced by *Acod1* loss observed under fat overnutrition was secondary to alterations in the signalling of insulin-regulating hormones, plasma levels of GLP-1 and resistin were measured. As illustrated in Figure **11E**, the genotype did not impose any alteration on the plasma levels of neither GLP-1 and resistin under HFD consumption. In summary, these results indicated that genetic deficiency of *Acod1* in mice served as a protective factor against disruptions in glucose homeostasis linked to diet-induced obesity.

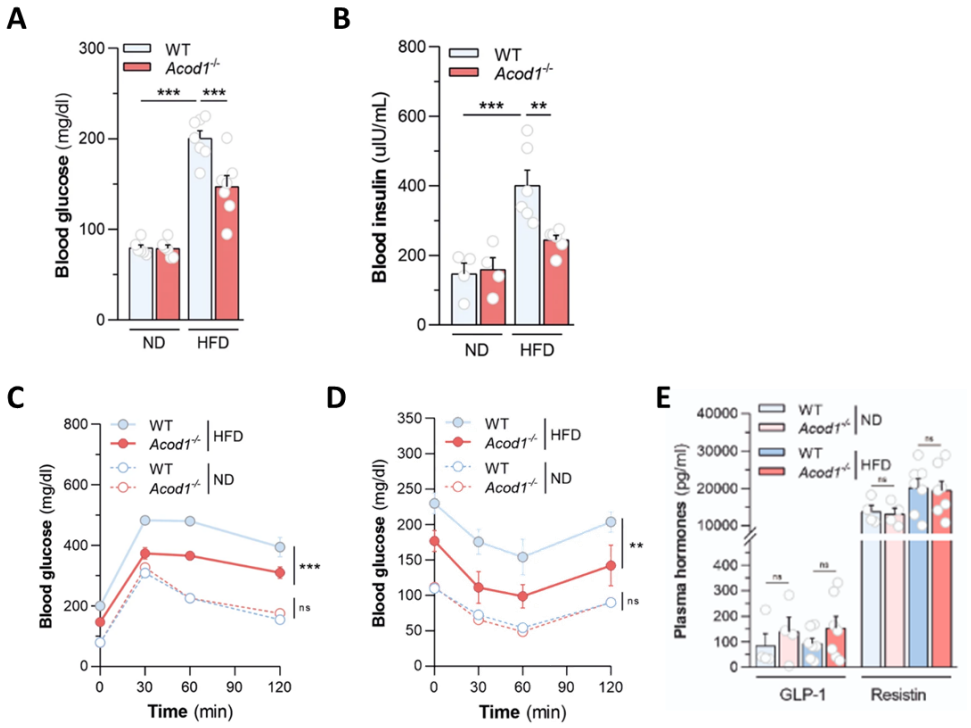

Figure 11. Acod1 loss opposes alterations in glucose and insulin homeostasis under HFD consumption.

A. *Fasting glycemia of wild type and Acod1$^{-/-}$ mice fed with ND or HFD for 16 weeks; ND (n = 6), HFD (n = 7). Data as mean ± sem from one representative experiment out of two independently executed (one-way ANOVA with Dunnett's multiple comparisons test compared to HFD-fed WT mice).* ***B.*** *Fasting insulinemia of in mice treated as in A; ND (n = 4), HFD-WT (n = 7), HFD-Acod1$^{-/-}$ (n = 6). Data as mean ± sem from one representative experiment out of two independently executed (one-way ANOVA with Dunnett's multiple comparisons test compared to HFD-fed WT mice).* ***C.*** *Glucose tolerance test (GTT) in mice treated as in A; ND (n = 6), HFD (n = 7). Data as mean ± sem from one representative experiment out of two independently executed (two-way ANOVA).* ***D.*** *Insulin tolerance test (ITT) in mice described* ***in A****; ND (n = 5), HFD (n = 7). Data as mean ± sem from one representative experiment out of two independently executed (two-way ANOVA).*

E*. Levels of metabolic hormones measured in plasma of WT and Acod1$^{-/-}$ mice after 16 weeks on ND or HFD. Data as mean±s.e.m of n=4 (ND-fed), n=7 (HFD-fed) mice from one experiment (student t-test). * P < 0.05; **P < 0.01; ***P < 0.001; ns not significant.*

Analysis of Acod1 expression in mouse and human tissues

Acod1 is a barely detectable gene in physiological conditions but inducible upon stimuli, such as LPS and pathogens (R. Wu et al., 2020b). Data presented so far demonstrated that genetic ablation of *Acod1* protected mice from obesity and associated alterations in glucose homeostasis. However, whether dietary lipid overload could modulate its expression was not demonstrated yet. To explore the impact of HFD on *Acod1* expression, profiling of *Acod1* expression levels in several tissues involved in the response to dietary lipid overload derived from *Acod1*$^{-/-}$ and *wild type* mice fed either with a ND or HFD was conducted at the end of the experiment. Despite *Acod1* was not modulated in organs such as the iWAT, eWAT and small intestine, HFD significantly upregulated *Acod1* mRNA levels in the BAT, liver and colon of *wild type* mice compared to animals fed a regular chow (Fig. **12A)**. Next, to establish whether the elevated expression of *Acod1* was linked to an increase in itaconate production, liquid chromatography-mass spectrometry (LC-MS) was used. As a result, HFD consumption resulted in heightened itaconate levels, reflecting the increased expression levels of *Acod1* in the same districts (Fig. **12B**), suggesting a prominent role for itaconate biosynthesis in the systemic response to fat overnutrition. On the other hand, neither *Acod1* mRNA nor itaconate levels were detected in knockout animals.

To gain a better understanding on the role of the Acod1/itaconate axis in adipose tissue expansion, a time-resolved profiling at four-week intervals (4-8-12 weeks) of *Acod1* mRNA and itaconate levels was performed. No changes in *Acod1* mRNA levels were observed in all tissues tested upon 4 and 8 weeks of HFD regimen, with respect to ND-fed controls (Fig. **12C**). On the contrary, a significant increase of *Acod1* gene expression was measured in the colon starting at 12 weeks compared to ND-fed controls (Fig. **12C** and Fig. **12A**). Importantly, HFD administration significantly increased itaconate levels in colon matching the corresponding timing of gene induction, thus phenocopying the increased *Acod1* mRNA levels (Fig. **12D** and Fig. **12B**). Notably, the timing of *Acod1* mRNA and itaconate accumulation in the colon coincided with the divergence in body weight gain between *wild type* and *Acod1*$^{-/-}$ mice subjected to HFD. This observation supported the significant role of colonic *Acod1* expression in the metabolic responses of mice to prolonged fat overnutrition.

Since *Acod1* is mainly expressed in macrophages, a time-resolved profiling of the macrophage marker *F4/80* (used as a proxy for or macrophage accumulation) in BAT, liver and colon was performed to elucidate whether *Acod1* upregulation was a result of increased macrophage accumulation in those tissues. Although HFD consumption did not result in a significant increase of *F4/80* mRNA levels in BAT of *wild type* mice throughout the experiment, a significant induction was observed in liver and colon at 16 weeks. (Fig. **12E**). By combining these results with the time-resolved profiling of *Acod1,* the upregulation of *Acod1* mRNA levels in colon and BAT might result from a true up-regulation of its gene expression, whereas it might be considered just a proxy for increased macrophage accumulation in the liver.

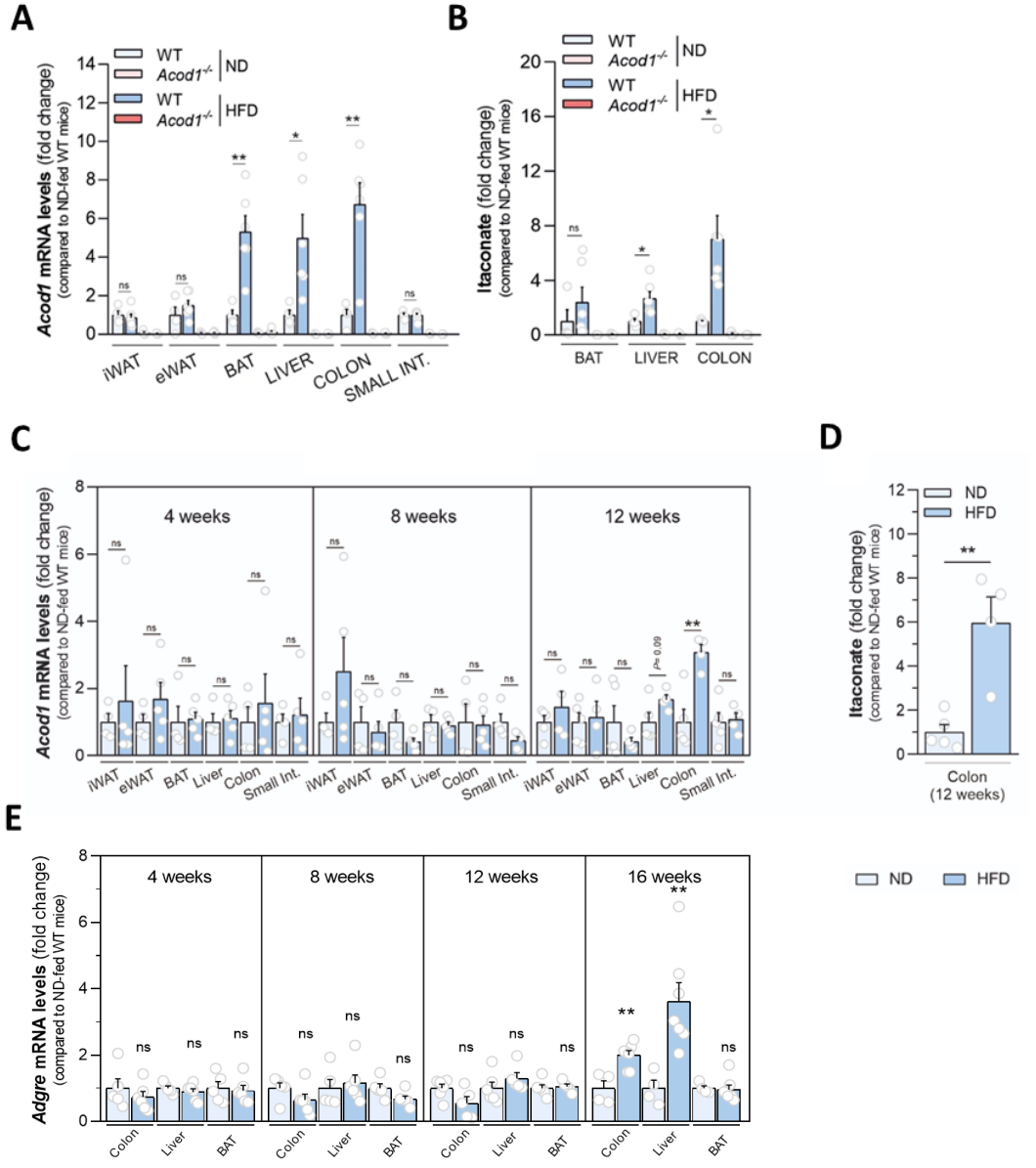

Figure 12. Acod1 expression modulation in tissues.

A. *qPCR analysis of Acod1 mRNA levels in the indicated tissues from WT and Acod1$^{-/-}$ mice fed with ND (n = 4) or HFD (n = 6) for 16 weeks. Data as mean ± sem from one experiment out of two independently executed.* ***B***. *Itaconate levels in indicated tissues from mice as described in A; ND (n = 4), HFD-WT (n = 6), HFD-Acod1$^{-/-}$ (n = 4). Data as mean ± sem from one experiment out of two independently executed.* ***C***. *qPCR analysis of Acod1 mRNA levels in the indicated tissues from WT and Acod1$^{-/-}$ mice fed with ND or HFD for the time indicated. Data as mean±sem of n=4-6 mice per group from one experiment.* ***D***. *Itaconate levels in colon from the indicated mice fed with either ND or HFD for 12 weeks. Data as mean±sem of n=5 (ND-fed) and n=4 (HFD-fed) mice from one experiment.* ***E***. *qPCR analysis of F4/80 (Adgre1) mRNA levels in the indicated tissues from WT mice fed with ND or HFD for the time indicated. Data as mean±sem of n=4-7 mice per group from one experiment. In (A-E): student t-test; *P < 0.05; **P < 0.01; ***P < 0.001; ns not significant*

After, to extend the relevance of data obtained from murine studies to human contexts, *ACOD1* expression was retrieved in publicly available transcriptomic datasets of human subjects with obesity and the associated NAFLD. *ACOD1* mRNA levels were found higher in colon biopsies of obese subjects with respect to healthy counterparts (Fig. **13A**) and correlated with lower tolerance to oral glucose overload (Fig. **13B**). Also, increased *ACOD1* expression was found in livers of NAFLD patients in dependency of disease severity (Fig. **13C**) and hepatic steatosis grades (Fig. **13D**). Collectively, these data demonstrate that *Acod1* is a gene responsive to dietary lipid overload and its expression in the colon might play a crucial role in determining resistance to diet-induced obesity.

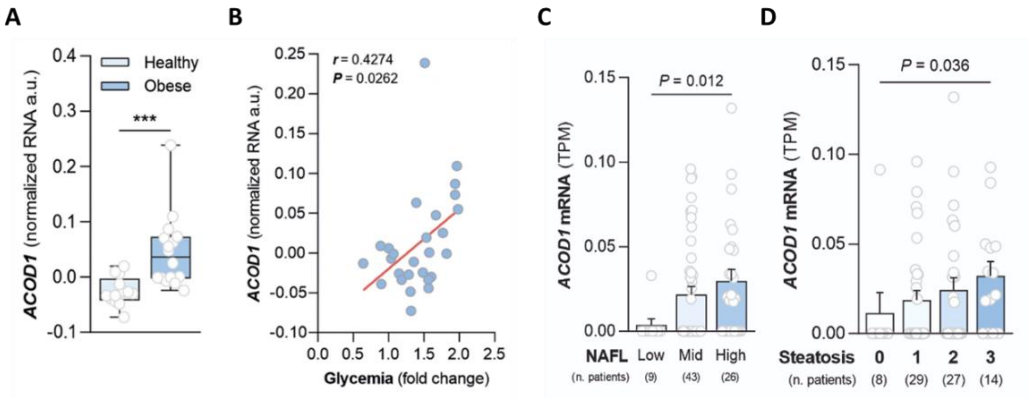

Figure 13. ACOD1 expression in human tissues.
A*. ACOD1 mRNA levels (GSE158237) in colon of healthy (BMI < 25 kg/m^2, n = 13) and obese subjects (BMI > 30 kg/m^2, n = 16). Boxes extend from 25th to 75th percentiles, black lines = median, whiskers=minimum to maximum (student t-test).* ***B****. Correlation analysis between colonic ACOD1 mRNA (GSE158237) and relative changes in plasma glucose levels measured 2 h after oral glucose overload (OGTT) compared with baseline, in human subjects described in Fig. 13A. r = Pearson's correlation coefficient (Pearson correlation).*
C*. ACOD1 mRNA levels (GSE130970) in liver of NAFLD patients categorized according to disease (NAFL) score (Mann-Whitney test).* ***D****. ACOD1 mRNA levels (GSE130970) in liver of NAFLD patients categorized according to hepatic steatosis grade (Mann-Whitney test).*

Itaconate administration abolishes the effects of Acod1 ablation on metabolic responses to HFD

ACOD1 is the mitochondrial enzyme catalysing itaconate biosynthesis due to its capacity to decarboxylate the Krebs cycle's intermediate cis-aconitate upon several inflammatory stimuli (Michelucci et al., 2013). Thus far, data presented in this thesis demonstrated that *Acod1* deficiency in mice confers protection towards high-fat diet-induced obesity and obesity-associated alterations in systemic glucose and insulin homeostasis. Therefore, to elucidate whether the protected phenotype observed in *Acod1*$^{-/-}$ mice challenged with HFD was due to Acod1 catalytic activity, a rescue experiment was set up. In particular, low doses of itaconate (1mM) were administered in drinking water to HFD-fed *Acod1* deficient mice for 16 weeks and compared to their untreated *Acod1*$^{-/-}$ and *wild type* counterparts under the same dietary regimen. Itaconate treatment was sufficient to restore itaconate levels in the large intestine of *Acod1*$^{-/-}$ mice upon fat overnutrition to a comparable level as those measured in stools of *wild type* mice (Fig. **14A**). In addition, itaconate-treated mice gained significantly more weight compared with their *Acod1*$^{-/-}$ counterparts (Fig. **14B**). At the end of the experiment, necroscopic analysis revealed that itaconate-treated mice had an enhanced accumulation of adiposity as demonstrated by the significant increase in the weight of inguinal, epididymal, perirenal white adipose tissues and brown adipose tissue compared to untreated *Acod1*$^{-/-}$ mice (Fig. **14C**). To determine whether the increase body weight conferred by itaconate administration also recapitulates the effect of high-fat diet on systemic insulin homeostasis, an insulin tolerance test was performed. Itaconate supplementation significantly lowered tolerance to insulin overload compared with *Acod1*$^{-/-}$ counterparts (Fig. **14D**). Collectively, these data demonstrated that protection against diet-induced obesity and obesity-associated dysfunctions in glucose homeostasis were due to itaconate biosynthesis.

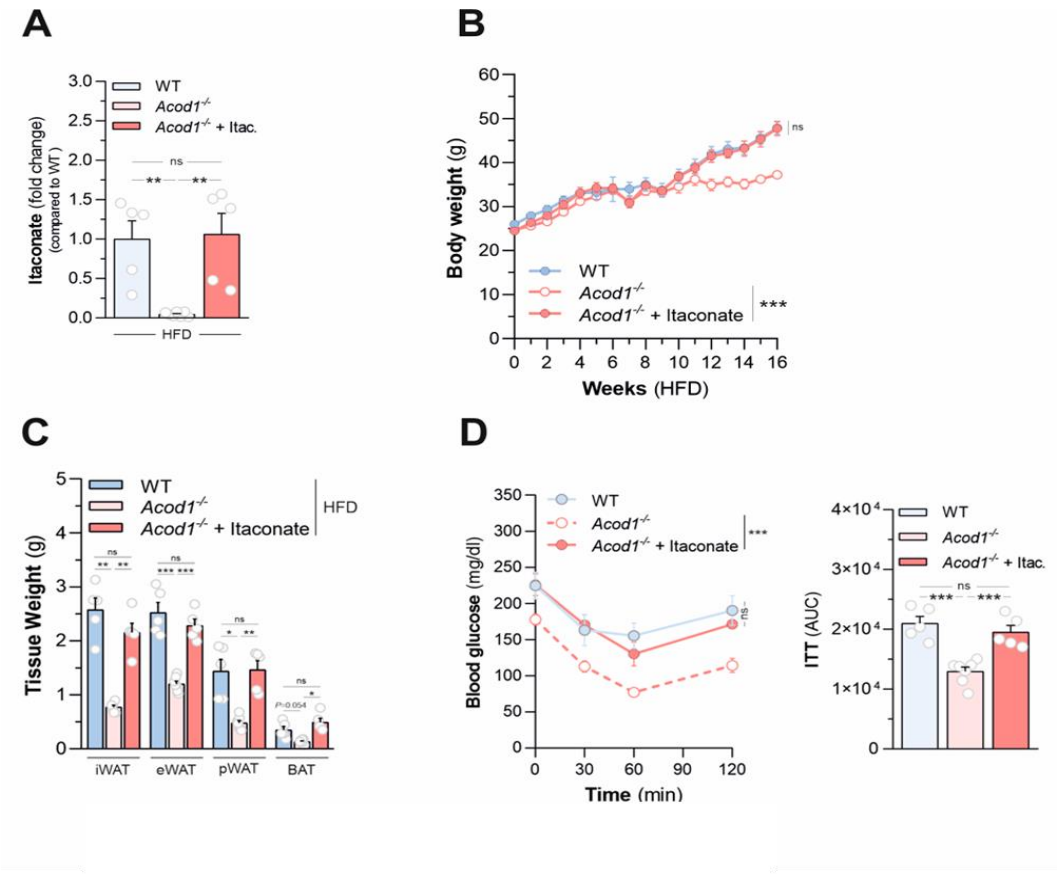

Figure 14. Itaconate supplementation nullifies the effects of Acod1 ablation on metabolic responses to HFD.

A*. Determination of itaconate levels in colon of HFD-fed mice in response to treatment with 1mM itaconate in drinking water for 16 weeks. Data as mean±s.e.m of n=5 (WT), n=7 (Acod1$^{-/-}$) and n=5 (Acod1$^{-/-}$ + Itac.) mice from one experiment.* ***B****. Effect of treatment of 1mM itaconate in drinking water on body weights of Acod1$^{-/-}$ mice fed with HFD for 16 weeks. Data as mean±s.e.m of n=5 (WT), n=7 (Acod1$^{-/-}$) and n=5 (Acod1$^{-/-}$ + Itac.) mice from one experiment.* ***C****. Tissue weights of mice described in (L). Data as mean±s.e.m of n=5 (WT), n=7 (Acod1$^{-/-}$) and n=5 (Acod1$^{-/-}$ + Itac.) mice from one experiment.* ***D****. ITT (left) and AUC of ITT (right) in mice described in (B). Data as mean±s.e.m of n=5 (WT), n=7 (Acod1$^{-/-}$) and n=5 (Acod1$^{-/-}$ + Itac.) mice from one experiment. In (A, C and D-right panel): one-way ANOVA followed by Dunnett's multiple comparisons test. In (B and D-left panel): two-way ANOVA. *P<0.05; **P<0.01; ***P<0.001; ns: not significant (t-test).*

Acod1 ablation opposes liver steatosis and associated metabolic dysfunction induced by dietary lipid overload.

Among the several comorbidities linked to diet-induced obesity, NAFLD stands out as a spectrum of liver pathologies, representing the hepatic manifestation of metabolic disorders. Briefly, dietary lipid overload leads to adipose tissue disfunction, instigating the deposition of fat in ectopic sites, notably the liver. This set the stage for the development of NAFLD, a condition that may evolve into NASH. The progression to NASH is often marked by inflammatory processes and the development of fibrosis culminating in metabolic liver dysfunction, further predisposing individuals to a heightened risk of development of hepatocellular carcinoma (Stickel & Hellerbrand, 2010). Therefore, it has been evaluated whether resistance to diet-induced obesity offered by *Acod1* loss was also associated to protection against liver steatosis. Necroscopic analyses performed at the end of the experiment showed that the genotype did not impose any difference in the weight and colour of the livers isolated from mice fed with a regular chow. On the contrary, under HFD-feeding, livers isolated from *wild type* mice were bigger (Fig. **15A**) and paler in colour (Fig. **15B**) indicative of increased lipid content, with respect to *Acod1*$^{-/-}$ counterparts. Next, histological examination of liver sections stained with haematoxylin and eosin were performed. As shown in Fig. **15C**, no major differences were observed in liver sections between *wild type* and *Acod1*$^{-/-}$ mice fed with normal diet. Contrarily, loss of *Acod1* resulted in an obvious decrease in lipid droplets accumulating within hepatocytes following HFD consumption (Fig. **15C**). To confirm such indications, quantitative determination of hepatic triglyceride content was measured. As a result, *Acod1* ablation clearly attenuated hepatic steatosis, whereas no differences were imposed under a regular chow (Fig. **15D**). These data demonstrate that genetic ablation of *Acod1* protects liver of mice from diet-induced steatosis.

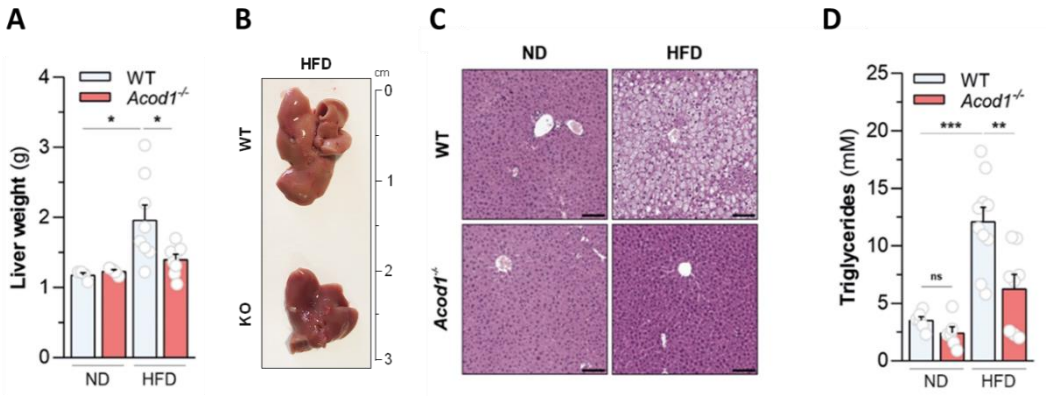

Figure 15. Genetic deficiency of Acod1 opposes diet-induced liver steatosis.
A. *Weights of livers from WT and Acod1$^{-/-}$ mice fed with ND (n = 4) or HFD (n = 8) for 16 weeks. Data as mean±s.e.m. from one experiment out of three independently executed.* ***B.*** *Representative images of livers isolated from mice fed with HFD after 16 weeks.* ***C.*** *Representative H&E staining of livers from mice described in A, Bar = 100 µm.* ***D.*** *Liver triglycerides in mice described in A; ND (n = 6), HFD-WT (n = 10), HFD-Acod1$^{-/-}$ (n = 8). Data as mean±s.e.m. from two independent experiments.*
*In (A) one-way ANOVA with Dunnett's multiple comparisons test compared to HFD-fed WT mice; In (D) t-test. *P < 0.05; **P < 0.01; ***P < 0.001; ns not significant.*

The accumulation of triglycerides within the hepatic milieu may arise from alterations in diverse hepatic metabolic processes. These alterations encompass potential changes in the processes of uptake, de novo synthesis, oxidation of fatty acids and/or the balance between the biosynthesis and degradation of acylglycerols. Moreover, the accumulation of fat in the liver may also be attributed to perturbations in the assembly and secretion of lipoproteins, contributing to the dynamic fluxes of lipids between the liver and peripheral tissues. Therefore, to conduct a more in-depth exploration into the impact of *Acod1* deficiency on hepatic responses to HFD, untargeted label-free quantitative proteomics was conducted on liver specimens obtained from both *wild type* and *Acod1*$^{-/-}$ mice subjected to either a regular chow or HFD. As shown in Fig. **16A**, principal component analysis (PCA) displayed an obvious separation between the hepatic proteome of mice challenged with HFD compared with their controls. Furthermore, a sub-clustering was observed exclusively in HFD-challenged mice, and not in their respective counterparts under normal dietary conditions (Fig. **16A**). This implied that the absence of *Acod1* elicited a distinct proteomic signature in response to elevated dietary fat intake. Specifically, *Acod1* deficiency counteracted the impact of dietary lipid overload on the hepatic proteome, as underscored by the significant negative correlation between

alterations in protein abundances induced by HFD in the livers of *wild type* mice and those orchestrated by the loss of *Acod1* under the same dietary regimen (Fig. **16B**). In particular, HFD challenge significantly elicited the levels of 130 proteins in the livers of *wild type* mice compared to their ND-fed controls (Fig. **16C**). Intriguingly, almost half of these proteins (58) underwent a significant down-regulation in response to the loss of *Acod1*, as illustrated in the Venn diagram in Figure **16C**. To identify known biological functions of these 58 proteins, functional enrichment analysis was performed, revealing that the enriched metabolic categories within the restored proteome were linked to fatty acid biosynthesis and processing pathways (Fig. **16D**). Notably, *Acod1* loss was accompanied by the counteraction of HFD-induced hepatic accumulation of perilipins (Plin2, Plin3, Plin4). Perilipins play a crucial role in NAFLD by participating in the regulation of lipid metabolism within hepatocytes. These proteins are primarily involved in sequestering lipids within lipid droplets in hepatocytes to prevent the excessive breakdown of stored triglycerides due to lipase action. A further contribution to the amelioration of HFD-induced liver steatosis consisted in the decreased protein levels of enzymes responsible for peroxisomal fatty acid β-oxidation (Acox1, Hsd17b4, Scp2, Crat, Acot2, Acot4, Decr2). In NAFLD, dysregulation of this pathway can lead to an accumulation of fatty acids in the liver, exacerbating hepatic steatosis. Importantly, the products of peroxisomal fatty acid β-oxidation can inhibit hepatic lipophagy (A. He et al., 2020), a cellular process responsible for the breakdown of lipid droplets. In addition, among the list of the 58 proteins displayed in the heatmap (Fig. **16E**), Cd36 (cluster of differentiation 36), which is a plasma membrane transporter responsible for facilitating free fatty acids (FFAs) uptake by the liver, was the second most significantly rescued protein by *Acod1* ablation.

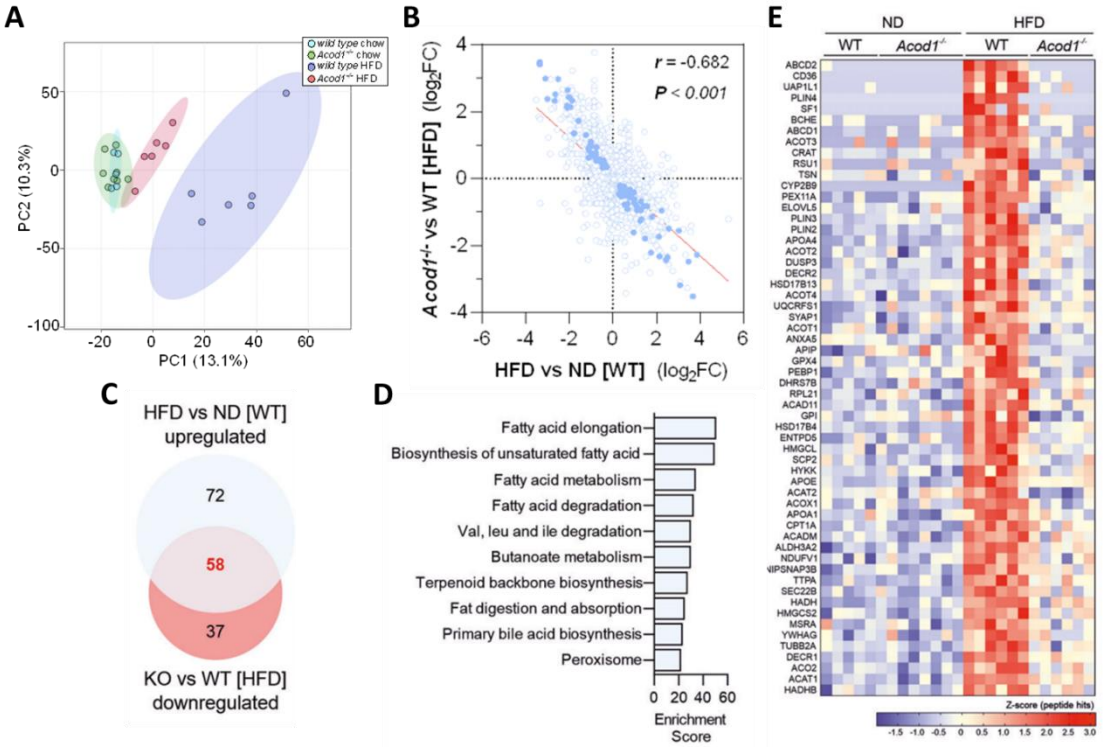

Figure 16. Acod1 deficiency counteracts the impact of dietary lipid overload on hepatic proteome.

A*. Principal component analysis (PCA) comparing liver proteome of WT and Acod1$^{-/-}$ mice fed with either ND or HFD for 16 weeks. Data derive from n=5 ND-fed (WT), n=8 (ND-fed Acod1$^{-/-}$) and n=6 (HFD-fed) mice from two independent experiments.* ***B.*** *Pearson`s correlation analysis between changes in the abundance of liver proteins imposed by dietary lipid overload in WT mice (HFD vs ND [WT]) and those determined by Acod1 loss in mice on HFD (Acod1$^{-/-}$ vs WT [HFD]. Statistically significantly altered proteins (FRD < 0.1) are illustrated in blue, not statistically significantly altered proteins in white. FC: fold change. Data derive from n=5 ND-fed (WT), n=8 (ND-fed Acod1$^{-/-}$) and n=6 (HFD-fed) mice from two independent experiments.* ***C.*** *Venn diagram and KEGG-based functional enrichment analysis (**D**) of upregulated proteins in livers of WT mice fed with HFD compared with ND-fed mice (HFD vs ND [WT]) and rescued by Acod1 loss (Acod1$^{-/-}$ vs WT [HFD]). Data derive from n = 5 ND-fed (WT), n = 8 (ND-fed Acod1$^{-/-}$) and n = 6 (HFD-fed) mice from two independent experiments.* ***E.*** *Heatmap of protein levels described in* ***C.***

To investigate whether Cd36 protein level was rescued also at the transcriptional level, its gene expression was measured by real-time qPCR. *Acod1* loss counteracted the HFD-induced upregulation of *Cd36* gene expression in the liver of *Acod1*$^{-/-}$ mice compared to their counterparts. On the contrary, no major differences in *Cd36* mRNA levels were observed under a regular chow (Fig. **17A**). CD36 is a key mediator of fatty acid uptake in the liver. Therefore, to evaluate whether changes in Cd36 protein expression correlated with alterations in the accumulation of diverse free-fatty acids (FFAs), the abundance of

several FFAs was measured by ultra-high pressure-liquid chromatography-mass spectrometry (UHPLC-MS) in the livers of *wild type* and *Acod1* $^{-/-}$ mice under both dietary regimens. Consistent with the attenuation of Cd36 content at both the proteomic and transcriptomic levels, *Acod1* expression significantly negatively correlated with the increased levels of FFAs accumulated upon HFD regimen in the livers of *wild type* mice (Fig. **17B**). After their activation, fatty acids serve as precursors for the synthesis of diacylglycerols (DAGs). Therefore, the levels of these species in the same livers were quantified. As a result, the loss of *Acod1* reduced the abundance of the corresponding diacylglycerol species when compared to the levels observed in *wild type* livers (Fig. **17C**). These data demonstrated that *Acod1* deficiency opposed the HFD-induced steatotic phenotype observed in *wild type* mice.

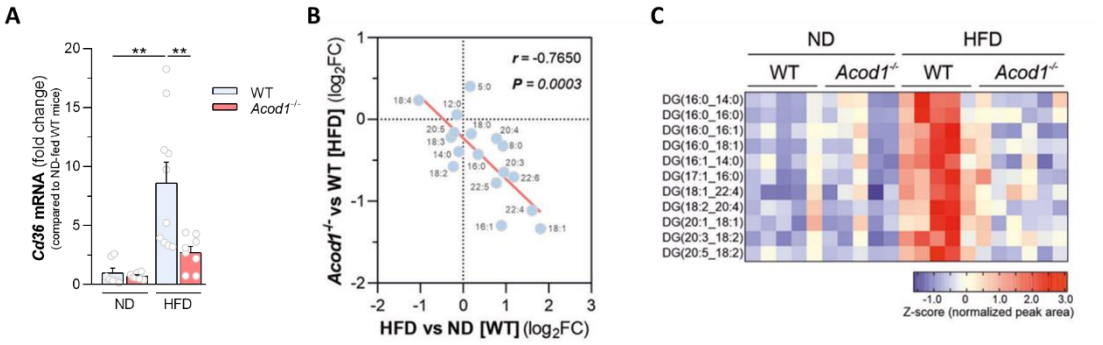

Figure 17. Acod1 loss counteracts fatty acids accumulation in the liver of HFD-fed mice. ***A.*** *qPCR analysis of Cd36 mRNA levels in livers of mice fed either with a ND or HFD for 16 weeks. Data are presented as mean±s.e.m of n=7 (ND-fed), n=10 (HFD-fed WT) and n=8 (HFD-fed Acod1*$^{-/-}$*) mice.* ***B.*** *Pearson's correlation between changes in liver free fatty acid (FFA) levels in HFD-fed WT mice (HFD vs ND [WT]) and by Acod1 loss (Acod1*$^{-/-}$ *vs WT [HFD]); n = 6 pre group. Data from two independent experiments.* ***C.*** *Heatmap depicting diacylglycerol levels in livers of mice treated as in 15A. Data derive from n = 5 (ND-fed), n = 5 (HFD-fed WT), n = 6 (HFD-fed Acod1*$^{-/-}$*) mice from one experiment. In (A) student t-test. *P < 0.05; **P < 0.01; ***P < 0.001; ns not significant.*

Next, the abundance of 46 proteins was significantly reduced in response to HFD challenge in the hepatic milieu of *wild type* mice and conversely augmented by the genetic ablation of *Acod1* (Fig. **18A**). Intriguingly, functional enrichment analysis underscored that the urea cycle was the most altered pathway under HFD regimen, a perturbation that was effectively rescued in *Acod1*$^{-/-}$ mice (Fig. **18B**). The urea cycle is a metabolic route

crucial for ammonia detoxification and this is particularly relevant in the context of NAFLD experimental models and patients, where hepatic fatty acid accumulation can impair the urea cycle (De Chiara et al., 2018), leading to compromised ammonia detoxification and contributing to the development of hepatic fibrosis (De Chiara et al., 2020). In particular, the heatmap displayed four specific enzymes- ornithine transcarbamylase (Otc), carbamoyl phosphate synthetase 1 (Cps1), argininosuccinate synthetase 1 (Ass1), and N-acetylglutamate synthase (Nags) (Fig. **18C**)- that emerged as altered. The alterations in the levels of these urea cycle-associated proteins imposed by the genotype were primarily observed following HFD administration and not under normal chow conditions (Fig. **18C**). Building upon these observations, the impact of *Acod1* loss on the expression of urea cycle genes in mice subjected to either standard chow or a HFD was evaluated. As depicted in Figure **18D**, HFD consumption led to a significant down-regulation of mRNA levels associated with *Otc*, *Cps1*, *Ass1*, and *Nags*-encoding genes in the livers of *wild type* mice when compared to their counterparts on a regular chow diet. Notably, aligned with the observed resistance to hepatic steatosis, the loss of *Acod1* effectively countered these alterations imposed by fat overnutrition.

Due to the alterations at both the proteomic and transcriptional level observed in the enzymes of this metabolic route, the impact of *Acod1* deficiency on the levels of urea cycle metabolites in the livers of mice subjected to different dietary regimens was measured by LC-MS. As illustrated in Figure **18E**, no appreciable differences were noted in the steady-state levels of all urea cycle metabolites between *wild type* and *Acod1*$^{-/-}$ mice when fed a normal diet. Conversely, in alignment with the suppression of urea cycle gene expression, HFD consumption induced a reduction in the abundance of citrulline, argininosuccinate, and N-acetyl-glutamate- a major allosteric activator of the ammonia-detoxifying CPS1 enzyme. This led to an ensuing accumulation of ammonia in the liver (Fig. **18F**). Importantly, *Acod1* deficiency opposed these metabolic changes, resulting in a restoration of urea cycle function, further emphasizing the intricate regulatory role of *Acod1* in modulating the urea cycle in response to dietary challenges.

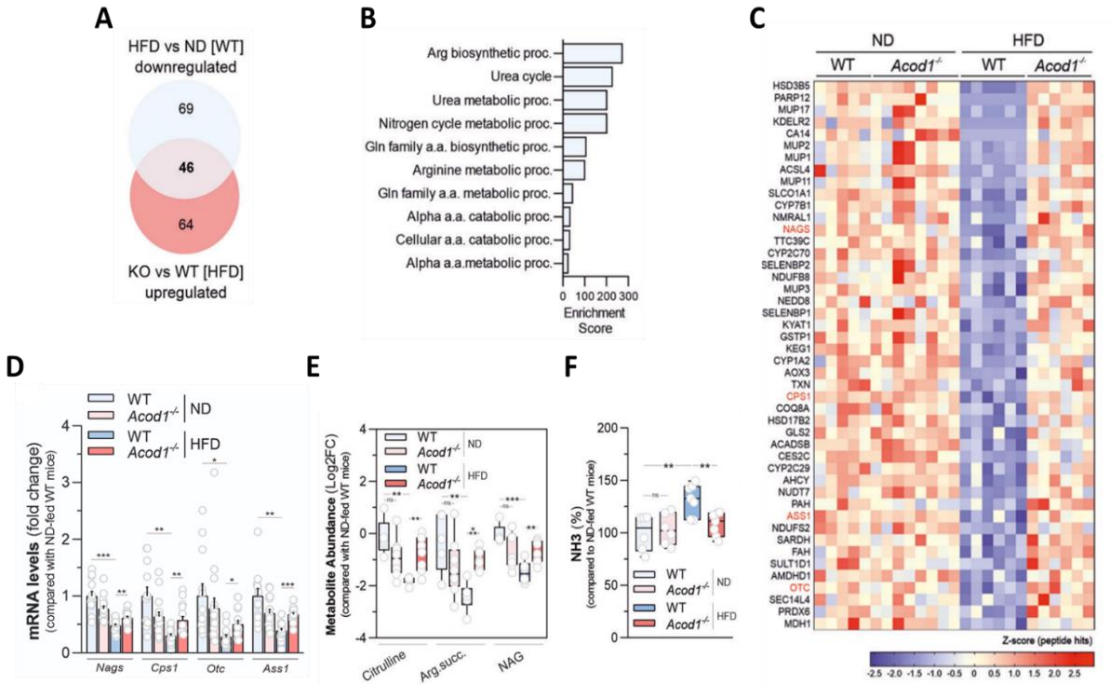

Figure 18. Acod1 loss rescues urea cycle dysfunctions induced by dietary lipid overload.

A. *Venn diagram (left) and (**B**) gene ontology (biological processes)-based functional enrichment analysis (right) of downregulated proteins in livers of WT mice fed with HFD compared with ND-fed mice (HFD vs ND [WT]) and rescued by Acod1 loss (Acod1$^{-/-}$ vs WT [HFD]).* ***C.*** *Heatmap of protein levels described in A.* ***D.*** *qPCR analysis of mRNA levels of the indicated genes in livers of WT and Acod1$^{-/-}$ mice fed with either ND or HFD for 16 weeks. Data as mean±s.e.m of n=12 (ND-fed WT), n=16 (ND-fed Acod1$^{-/-}$) and n=15 (HFD-fed) mice from three independent experiments.* ***E*** *Levels of the indicated urea cycle metabolites in liver of mice fed with either ND or HFD for 16 weeks. Data derive from n = 5 (ND-fed wild type), n = 8 (ND-fed Acod1$^{-/-}$), n = 6 (HFD-fed wild type), and n = 7 (HFD-fed Acod1$^{-/-}$) mice from two independent experiments; Arg.succ argininosuccinate, NAG N-Acetylglutamate.* ***F.*** *Levels of NH_3 in liver of mice fed with either ND or HFD for 16 weeks. Data derive from n = 6 (ND), n = 7 (HFD)-fed mice from two independent experiments. In E and F, boxes extend from 25th to 75th percentiles, black lines=median, whiskers=minimum to maximum. In (A) one-way ANOVA with Dunnett's multiple comparisons test compared to HFD-fed WT mice; In E, F): t-test; in (C) one-way ANOVA followed by Dunnett's multiple comparisons test, compared with HFD-fed WT. *P < 0.05; **P < 0.01; ***P < 0.001; ns not significant.*

Ammonia accumulation in the liver due to urea cycle dysfunction results in hepatic stellate cells activation, promoting the development and progression of fibrosis, a condition characterized by the excessive accumulation of extracellular matrix proteins,

including collagen. Therefore, it has been tested whether the observed improvement of urea cycle functions within livers isolated from *Acod1*$^{-/-}$ mice under an HFD regimen corresponded with concomitant alterations at the mRNA level of genes which are known to be upregulated during fibrosis. As depicted in Figure **19A**, HFD consumption led to an up-regulation of the mRNA levels associated with several collagen-encoding genes (*Col4A1, Col1A2, Col3A1, Col1A1, Timp1*) widely recognized as robust markers of tissue fibrosis in *wild type* mice. In contrast, *Acod1* deficiency counteracted the induction of this fibrotic gene signature (Fig. **19**). In sum, these findings underscore that the absence of *Acod1* protects mice against liver metabolic dysfunctions provoked by fat overnutrition.

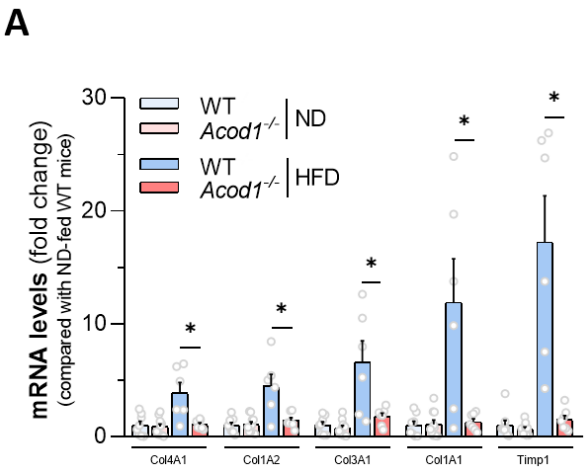

Figure 19. Acod1 ablation ameliorates fibrosis in mice under fat overnutrition.
*qPCR analysis of mRNA levels of the indicated genes in livers of mice fed with either a ND or HFD for 16 weeks. Data are presented as mean±s.e.m of n=8 (ND-fed WT), n=10 (ND-fed Acod1$^{-/-}$) and n=6 (HFD-fed WT), n=7 (HFD-fed Acod1$^{-/-}$) mice. One-way ANOVA with Dunnett's multiple comparisons test. *P < 0.05; **P < 0.01; ***P < 0.001.*

Acod1 loss positively impacts mice on HFD by enhancing metabolic activity

Obesity is fundamentally caused by a long-term positive disruption of energy balance, where energy intake exceeds energy expenditure. Therefore, to investigate the mechanisms by which *Acod1* loss offered protection to diet-induced obesity, food consumption and intestinal nutrient absorption were measured, as these factors are often primary contributors to obesity. However, the leaner phenotype in *Acod1* deficient mice

exposed HFD was not attributed to a decrease in food intake during both light and dark phases (Fig. **20A**) or alterations in the efficiency of nutrient absorption by the intestine (Fig. **20B**) as assessed by bomb calorimetry analyses, which measured the energy content of faeces to assess intestinal absorption capabilities.

Several hormones involved in the feedback mechanisms between the adipose tissue and the hypothalamus are central in regulating energy balance, appetite and food intake. Among them, leptin helps maintaining energy homeostasis and leptin resistance is a common characteristic of obesity, leading to increased food intake and weight gain. To investigate whether leptin levels were influenced by *Acod1* loss, plasma leptin levels were determined by multiplex bead-based assay. As shown in Fig**. 20C**, genetic ablation of *Acod1* did not impose any differences in circulating leptin levels both under a regular chow and HFD. Subsequently, it has been speculated that *Acod1* loss could impose changes in the basal adipogenic potential. To test this, pre-adipocytes were isolated from the iWAT of *wild type* and *Acod1*$^{-/-}$ mice, differentiated *in vitro* for 5 days and the accumulation of neutral lipids was evaluated by Oil red staining. As shown in Figure **20D,** no differences in the lipid content at both 0- and 5-days post differentiation were imposed by the genotype. Next, the expression levels of *Pparg and Cebpa*, critical genes involved in adipogenesis, in the same adipocytes were measured. Figure **20E** depicted that *Acod1* deficiency was dispensable in regulating their gene expression levels at both 0 and 5 days after differentiation.

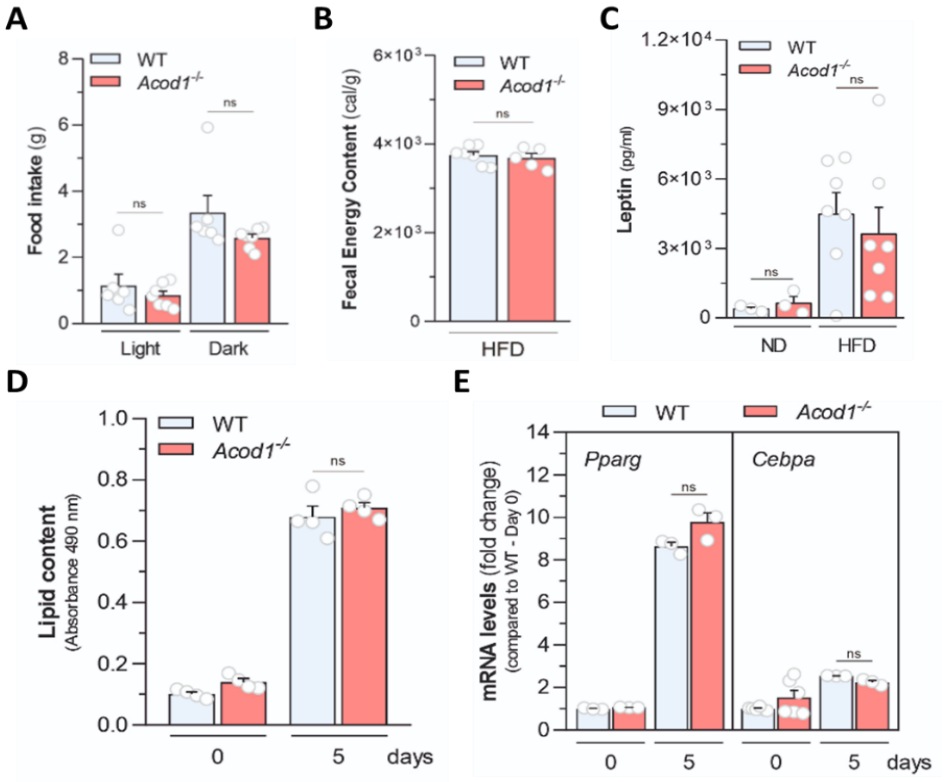

Figure 20. Impact of Acod1 loss on energy balance-regulating processes.
A*. Measurement of food intake of WT and Acod1$^{-/-}$ mice during light and dark hours after 16 weeks on HFD; n=6 (WT), n=7 (Acod1$^{-/-}$) mice. Data as mean±s.e.m from one representative experiment out of two independently executed.* ***B****. Bomb-calorimetry-mediated determination of energy content in stools of WT (n=7) and Acod1$^{-/-}$ (n=5) mice on HFD for 16 weeks. Data as mean±s.e.m from one representative experiment.* ***C.*** *Plasma leptin levels in WT and Acod1$^{-/-}$; n=3 (ND-fed), n=7 (HFD-fed) mice. Data as mean±s.e.m from one representative experiment out of two independently executed.* ***D****. Neutral lipid content (oil red staining) of adipocytes isolated from iWAT of WT and Acod1$^{-/-}$ mice, on day 0 and day 5 of differentiation in vitro; n= 4 replicates per group. Data as mean±s.e.m from one representative experiment out of three independently executed. (****E****) qPCR analysis of Pparg and Cebpa in WT and Acod1$^{-/-}$ adipocytes described in (C); n= 3-6 replicates per group. Data as mean±s.e.m from one representative experiment out of three independently executed. In (A-E): *P<0.05 (student t-test); ns: not significant.*

To further investigate the mechanism of resistance to diet-induced obesity in *Acod1*-deficient mice, Phenomaster metabolic cages were employed for an in-depth metabolic assessment of HFD-fed mice. These cages provide the capability to monitor each mouse in a controlled setting and this setup facilitate the simultaneous measurements of metabolic rates (indirect calorimetry), behaviours, and physiological responses in an

automated and synchronized manner. This approach is critical for the collection of detailed and systematic data, essential for understanding the metabolic dynamics at play. As reported in Figure **21A**, a marked increase in oxygen consumption across both light and dark phases in *Acod1*$^{-/-}$ mice was observed when compared to their *wild type* counterparts. This result was also reflected by a statistically significant increment in energy expenditure in the same mice under the same conditions (Fig. **21B**). To corroborate these data, other parameters were considered. In particular, the heightened metabolic rates in *Acod1*-deficient mice did not stem from changes in their fuel supply, as the respiratory quotient (RQ) and the respiratory exchange ratio (RER) were unaffected (Fig. **21C**). Moreover, the increase energy expenditure was also not attributable to differences in spontaneous locomotor activity (Fig. **21D**) between the two genotypes. These findings highlighted that the lack of *Acod1* prompted a heightened metabolic rate in response to a high-fat diet challenge in mice.

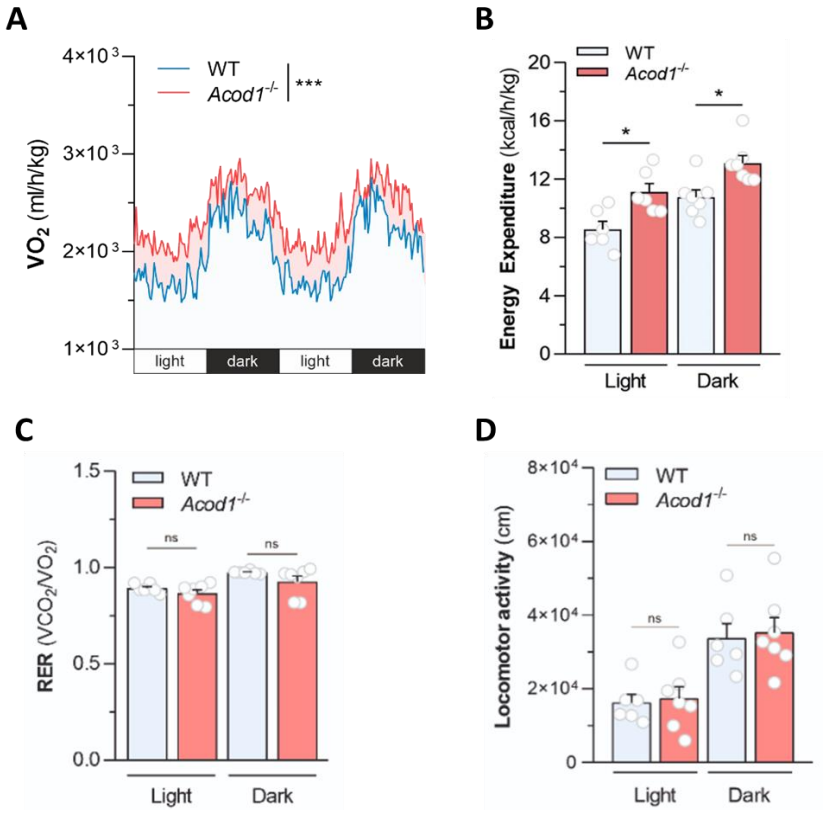

Figure 21. Acod1 deficiency ameliorates metabolic fitness challenged with dietary lipid overload

***A**. Whole-body O_2 consumption rate (VO_2) and energy expenditure rate (**B**) normalized on body weight of HFD-fed WT (n = 6) and Acod1$^{-/-}$ (n = 8) mice during light and dark hours (one representative experiment out of two independently executed). **C.** Respiratory exchange rate (RER) of WT and Acod1$^{-/-}$ mice described in (A); n=6 (WT), n=7 (Acod1$^{-/-}$) mice. Data as mean±s.e.m from one representative experiment out of two independently executed. **D**. Total locomotor activity (cm) of mice described in (A); n=6 (WT), n=7 (Acod1$^{-/-}$) mice. Data as mean±s.e.m from one representative experiment out of two independently executed. In (A) two-way ANOVA; in (B) data as mean±s.e.m; in (C), (D): student t-test. * P<0.05 (t-test); ns: not significant.*

Then, since adipose tissues are important contributors to energy homeostasis and considering the notable differences detected in their morphology, the contribution of fat depots to the higher energy consumption observed in *Acod1*$^{-/-}$ mice was defined. This was addressed by profiling by RNA-sequencing the gene expression changes in epididymal white adipose tissue (eWAT) isolated from HFD-fed mice, aiming to delineate the effects induced by *Acod1* loss. It is extensively reported in literature that the development of

obesity-related disorders is strictly associated with derailed adipocyte's mitochondrial functions (Heinonen et al., 2020; Rosen & Spiegelman, 2014). Accordingly, functional enrichment analysis of the 1124 genes downregulated in response to HFD and improved by *Acod1* loss revealed that mitochondrial functions and oxidative metabolism were the most impaired pathways (Fig. **22A**, **B**). Indeed, deficiency of *Acod1* determined a consistent amelioration of several genes involved in the citric acid cycle (*Mdh1b, Aco1, Dlst, Suclg2, Cs, Sdha, Dld, Idh3b, Ogdh*) and mitochondrial electron transport chain (*Ndufs1, Uqcrc2, Ndufv1, Ndufb8, Atp5b*) (Fig. **22C**). To validate these data, the gene expression level of the main inducer of mitochondrial oxidative metabolism was measured by real-time qPCR. *Acod1* loss rescued the mRNA level of the peroxisome proliferator-activated receptor gamma coactivator 1 alpha (Pgc-1α) which was decreased in *wild type* mice challenged with a HFD (Fig. **22D**). In addition, *Acod1* deletion led to a notable upregulation in the mRNA levels of genes implicated in neutral lipolysis (*Pnpla3, Lipe*) and mitochondrial fatty acid beta-oxidation pathways (*Echdc2, Echs1, Hsd17b10, Acad10, Acad11*), which were instead downregulated in the adipose tissue of *wild type* mice due to fat overnutrition as illustrated in Figure **22C**. When fatty acid influx exceeds the mitochondrial metabolic capacity, acyl-carnitines accumulate within the cell (McCann et al., 2021). As expected, high-fat diet led to the accumulation of major long-chain acyl-carnitines, such as palmitoyl-, oleoyl-, and stearoyl-carnitine, in the eWAT of *wild type* mice, which were instead normalized by the absence of *Acod1* (Fig. **22E**). This suggested that *Acod1* ablation enhanced oxidative metabolism during high-fat diet by increasing catabolic processes in the white adipose tissue.

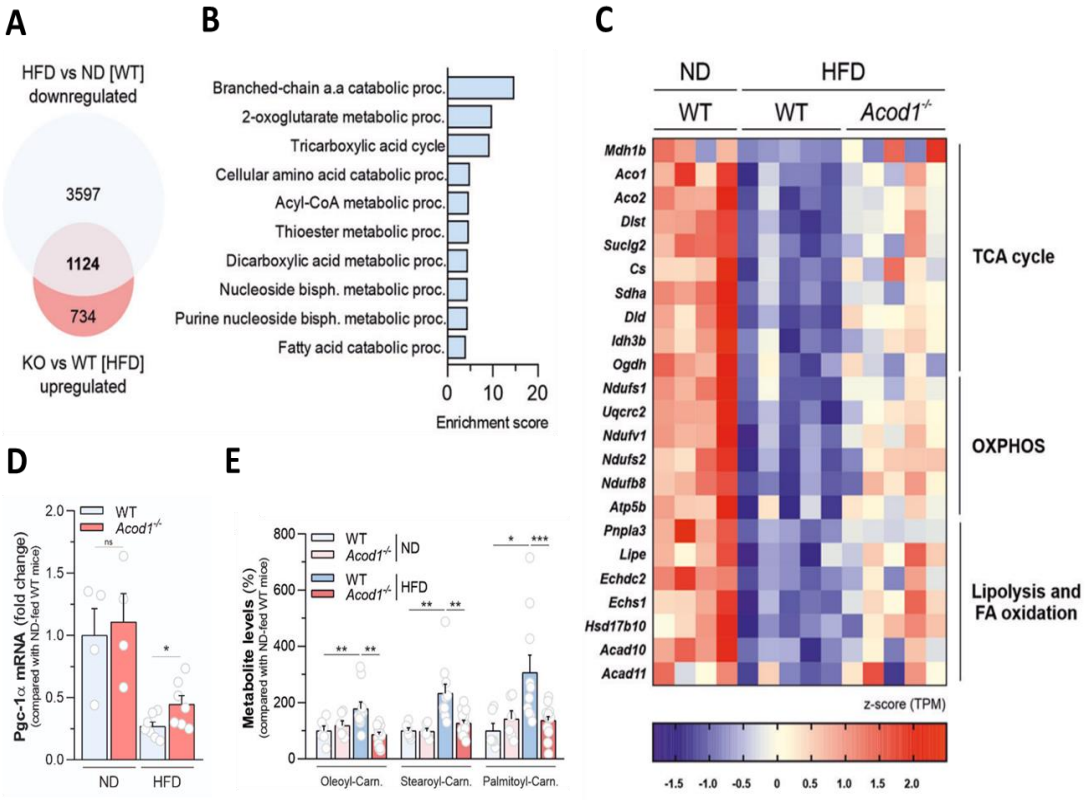

Figure 22. Acod1 ablation enhances catabolic processes during a high-fat diet in white adipose tissue.

A. *Venn diagram and* ***(B)*** *gene ontology (biological processes)-based functional enrichment analysis (right) of downregulated proteins in eWAT of WT mice fed with HFD for 16 weeks compared with ND-fed mice (HFD vs ND [WT]) and rescued by Acod1 loss (Acod1$^{-/-}$ vs WT [HFD]). Data derive from n = 4 (ND-fed WT) and n = 5 (HFD-fed) mice from one experiment.* ***C.*** *Heatmap depicting mRNA levels of selected genes related to tricarboxylic acid (TCA) cycle, oxidative phosphorylation (OXPHOS), lipolysis and fatty acid (FA) oxidation downregulated in eWAT of HFD-fed WT mice (HFD vs ND [WT]) and rescued by Acod1 loss (Acod1$^{-/-}$ vs WT [HFD]) Data derive from mice described in A: n = 4 (ND-fed WT) and n = 5 (HFD-fed) mice from one experiment.* ***D.*** *qPCR analysis of Pgc-1α (Ppargc1a) mRNA levels in eWAT of WT and Acod1$^{-/-}$ mice fed with either ND or HFD for 16 weeks; n=4 (ND-fed), n=7 (HFD-fed) mice. Data as mean±s.e.m from one representative experiment out of two independently executed.* ***E.*** *Acyl-carnitine levels in iWAT of mice fed with either ND (n = 6) or HFD (n = 10) from two independent experiments. Carn.: carnitine. In D *P<0.05 (t-test); ns: not significant; in E one-way ANOVA followed by Dunnett's multiple comparisons test compared to HFD-fed WT mice.*

Of profound importance in the context of obesity is the brown adipose tissue. Therefore, to determine its role in energy expenditure, several representative genes involved in catabolic processes were measured by real-time qPCR. In line with data derived from

WAT, *Acod1* loss determined an increased catabolic signature in the BAT isolated from *Acod1*$^{-/-}$ mice under HFD, as measured by gene expression analysis of several representative genes involved the central carbon metabolism (*Slc2a4, Aco2, Sdha, Suclg2*), triglyceride and fatty acid catabolism (*Pnpla3, Atgl, Cpt2, Cact, Acaa2, Hadha, Hadhb*) and mitochondrial biogenesis (*Nrf1, Tfam, Pgc1-α*) (Fig. **23A**). Moreover, the brown adipose tissue is a major contributor to energy expenditure by promoting adaptive thermogenesis via activation of uncoupling protein 1: UCP1 uncouples the oxidative respiratory chain of mitochondria that prevents ADP from synthesizing ATP, resulting in the release of energy in the form of thermal energy. To determine the impact of *Acod1* loss on adaptive thermogenesis, Ucp1 protein level was quantified by immunohistochemistry on sections of BAT obtained from *wild type* and *Acod1*$^{-/-}$ mice fed either with ND or HFD. As a result, a stronger Ucp1 immunostaining was observed in the BAT of HFD-fed *Acod1*$^{-/-}$ mice compared to their *wild type* counterparts (Fig. **23C**). On the contrary, no differences were imposed by the genotype under a regular chow. In line with immunohistochemical analysis, *Acod1* deficiency increased the mRNA levels of genes involved in adaptive thermogenesis such as *Ucp1, Ppar-γ* and *Cidea* in the brown adipose tissue compared to HFD-fed wild type mice (Fig. **23A** and Fig. **23B**). These results indicated that the BAT contributes to the augmented energy expenditure observed in *Acod1*$^{-/-}$ by engaging catabolic processes that sustain an increase adaptive thermogenesis.

In conditions of overfeeding, mature white adipocytes can undergo a trans-differentiation into beige adipocytes in a process referred to as white adipose tissue “browning”. Beige adipocytes can perform adaptive thermogenesis due to their expression of UCP1, thus increasing energy expenditure and reducing adiposity (Paulo & Wang, 2019). Therefore, gene expression level of *Ucp1* was measured in the iWAT of HFD-fed mice. Similarly to what observed in the BAT of *Acod1*$^{-/-}$, genetic ablation of *Acod1* resulted in a statistically significant upregulation of *Ucp1* mRNA levels in the iWAT of *Acod1* deficient mice compared to their *wild type* counterparts (Fig. **23D**). In line with this, data retrieved by RNA sequencing of iWAT of mice showed that, upon fat overnutrition, *Acod1* loss opposes the alterations of those genes involved in non-shivering thermogenesis elicited by dietary lipid overload in the iWATs isolated from *wild type* mice. Specifically, *Acod1* ablation counteracted the HFD-induced downregulation and upregulation of positive

(*Adrb3, Sctr, Trpv1, Ppargc1b, Cidea, Ebf2, Ppargc1a, Vegfa, Thra*) and negative (*Ffg9, Map2k6, Dhrs7b*) regulators of adaptive thermogenesis, respectively (Fig. **23E**). Importantly, upon HFD, *Acod1* was dispensable in modulating the expression level of several genes involved in beta-oxidation (*Cpt1a, Cpt2, Cact, Acaa2*), mitochondrial biogenesis (*Nrf1, Tfam, Pgc1a*) and oxidative mitochondrial metabolism (*Ucp2, Ucp3*) in both quadriceps (Fig. **23F**) and tibilias anterioris (Fig. **23G**) chosen as representative for lean mass. Together, these findings suggest that *Acod1* ablation enhances oxidative efficiency under conditions of fat overnutrition, primarily linked to increased catabolic activity in adipose tissues.

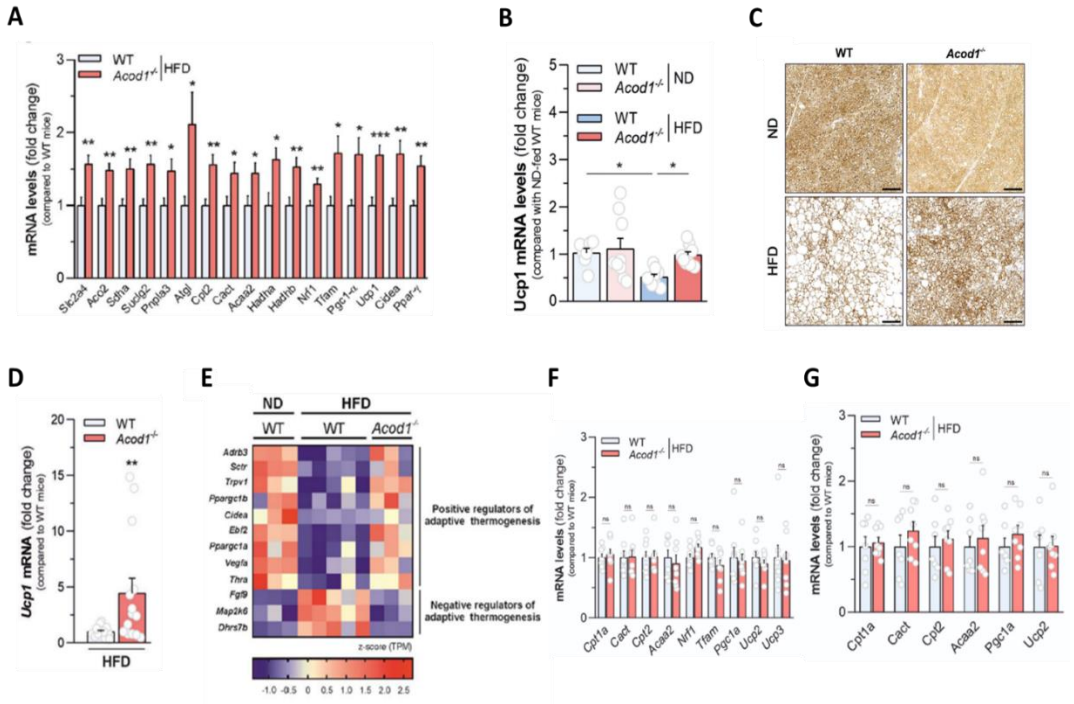

Figure 23. Acod1 loss enhances energy expenditure through activation of thermogenic processes in adipose tissues.

A*. qPCR analysis of mRNA levels of the indicated genes in BAT of mice HFD-fed WT (n = 6) and Acod1$^{-/-}$ (n = 8).* ***B.*** *qPCR analysis of Ucp1 mRNA levels in BAT of WT and Acod1$^{-/-}$ mice fed with either ND or HFD for 16 weeks. n = 7–9 per group from two independent experiments.* ***C****. Representative images of UCP1 immunohistochemical staining normalized to cell number in BAT of mice described in B.* ***D****. qPCR analysis of Ucp1 mRNA levels in iWAT of mice described in A; WT (n = 15), Acod1-/- (n = 14) mice from three independent experiments.* ***E****. Heatmap depicting mRNA levels of selected genes known as inducers (positive regulators) or inhibitors (negative regulators) of adaptive thermogenesis changed in iWAT of HFD-fed WT mice and rescued by Acod1 loss. Data derive from n = 3 (ND-fed WT), n = 5 (HFD-fed WT), and n = 3 (HFD-fed Acod1$^{-/-}$) mice from one experiment.*

F*. qPCR analysis of the indicated genes in quadriceps of WT and Acod1$^{-/-}$ mice on HFD for 16 weeks; n=8 mice per group. Data as mean±s.e.m from one representative experiment out of two independently executed.* ***G****. qPCR analysis of the indicated genes in tibialis anterior of WT and Acod1$^{-/-}$ mice on HFD for 16 weeks; n=7 (WT), n=8 (Acod1$^{-/-}$) mice. In (A, D) data as mean±s.e.m; in (A, D, F, G) student t-test; *P < 0.05; **P < 0.01; ***P < 0.001; ns: not significant. In B one-way ANOVA followed by Dunnett's multiple comparisons test compared to HFD-fed WT mice.*

Acod1 loss reduces obesity-associated inflammation in adipose tissues

Obesity is defined by a state of low-grade chronic inflammation that significantly impacts health outcomes. This condition is characterized by the activation and recruitment of proinflammatory immune cells, mostly macrophages, within the adipose tissues resulting in lipid deposition in ectopic sites, insulin resistance and impaired energy expenditure processes (Hildebrandt et al., 2022b).

Consistent with previous findings reported in literature (Basler et al., 2006; Michelucci et al., 2013), *in vitro* treatment with LPS upregulated *Acod1* mRNA levels in BMDMs isolated from *wild type* mice but not in their *Acod1*$^{-/-}$ counterparts, as expected (Fig **24A**). Moreover, *Acod1* ablated-BMDMs showed enhanced production of pro-inflammatory cytokines such as IL6 and IL1β upon LPS challenge (Fig **24B** and Fig. **24C**). Despite this, gene expression profiling of the macrophage marker F4/80 (used as a proxy for macrophage accumulation) by qPCR revealed an increased macrophage abundance in the eWAT, iWAT and colon of HFD-fed *wild type* mice, which was instead counteracted upon *Acod1* loss, indicative of a less macrophage accumulation in tissues derived from *Acod1*$^{-/-}$ mice (Fig. **24D**). On the contrary, no differences in *F4/80* gene expression were detected under a regular chow in mice.

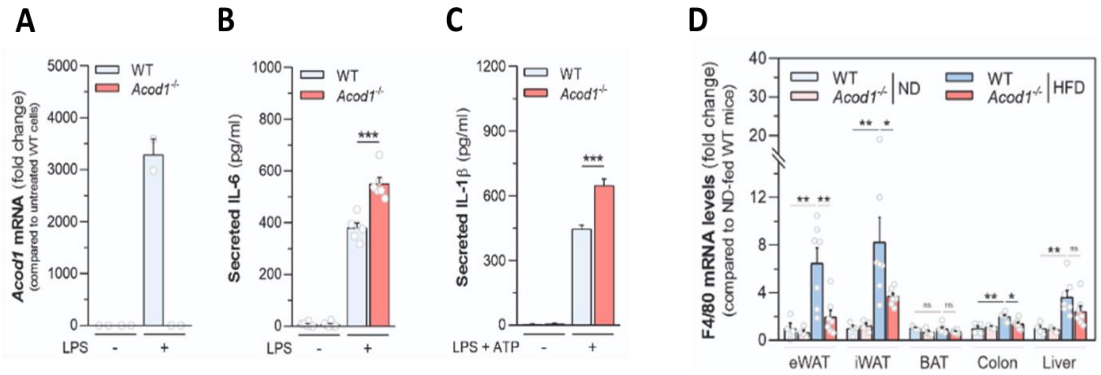

Figure 24. Acod1 impact on inflammation.
A*. qPCR analysis of Acod1 mRNA levels in resting and LPS-activated bone marrow-derived macrophages (BMDMs). Data as mean±s.e.m of n=2 technical replicates per condition from one experiment out of two independently executed.* ***B****. ELISA-mediated determination of IL-6 secreted in media of BMDMs treated as in A. Data as mean±s.e.m of n=6 technical replicates per condition from one experiment out of two independently executed.* ***C****. ELISA-mediated determination of IL-1β secreted in media of BMDMs treated as in A incubated with 2.5 mM ATP for additional 40 min for inflammasome activation. Data as mean±s.e.m of n=6 technical replicates per condition from one experiment out of two independently executed.* ***D****. qPCR analysis of F4/80 (Adgre1) mRNA levels in the indicated tissues from wild type and Acod1-/- mice fed with either ND or HFD for 16 weeks. Data as mean±s.e.m of n= 3-7 mice per group from one representative experiment. In (A, B) student t-test *P<0.05 **P<0.01 ***P<0.001; ns: not significant; in D one-way ANOVA followed by Dunnett`s T3 multiple comparison test compared with HFD-fed WT mice.*

Prompted by these differences, RNA-sequencing analysis was performed on the eWAT of mice to dissect the role of *Acod1* in the regulation of HFD-driven metabolic inflammation. Functional enrichment analysis of 1548 genes that were upregulated in the eWAT of *wild type* mice upon fat overnutrition and rescued by *Acod1* loss (Fig. **25A**), revealed that the restored transcriptional signature was mainly enriched with categories related to leukocyte activation and pro-inflammatory responses (Fig. **25B**). In particular, a gene expression signature indicative of an enhanced macrophage accumulation in fat depots, as demonstrated by the increase levels of several macrophage markers (*Adgre1*, *Lgals3*, *Trem2*, *Mrc1*, *Csf1r*, *Cd80*, *Cd86*, *Cd83*, *Lyz2*, *Cd14* and *Cd180*) and chemokines (*Ccl2*, *Ccl3*, *Ccl4*, *Ccl5*, *Ccl6*, *Ccl7* and *Ccl9*) promoting macrophage recruitment in tissues, was found in the eWAT isolated from HFD-challenged *wild type* mice and opposed by *Acod1* deficiency (Fig**. 25C**). A histological hallmark of the inflammatory process in the obese adipose tissue is the formation of crown-like structures (CLSs), formed by macrophages

infiltrating the adipose tissue and arranged around dead adipocytes. Consistent with the decrease macrophage accumulation, immunohistochemical detection of the macrophage marker F4/80 (encoded by *Adgre1*) revealed fewer crown-like structures in the eWAT isolated from HFD-fed *Acod1*$^{-/-}$ mice compared with *wild type* counterparts (Fig. **25D**). Furthermore, *Acod1* loss counteracted the expression of genes promoting pro-inflammatory activation of myeloid immune cells up-regulated in eWAT of *wild type* mice in response to HFD, such as *Sting1*, *Lacc1*, *Mif*, *Arl11*, *Zbp1*, several Toll-like receptors (*Tlr1*, *Tlr2*, *Tlr6*, *Tlr7*, *Tlr13*) and their interactor/adaptors (*Tril*, *MyD88* and *Ticam1*). In addition, *Acod1* deficiency opposed the transcriptional induction of genes encoding the pro-inflammatory cytokine *Tnf*, its super family members (*Tnfaip8l2*, *Tnfsfm13*, *Tnfsf12*, *Tnfaip2*, *Tnfsf13b*, *Tnfaip8*) and associated receptors (*Tnfrsf11a*, *Tnfrsf1b*, *Tnfrsf13b*, *Tnfrsf21*, *Tnfrsf12a*, *Tnfrsf23*, *Cd40*) promoted by dietary lipid overload in eWAT of *wild type* mice (Fig. **25C**).

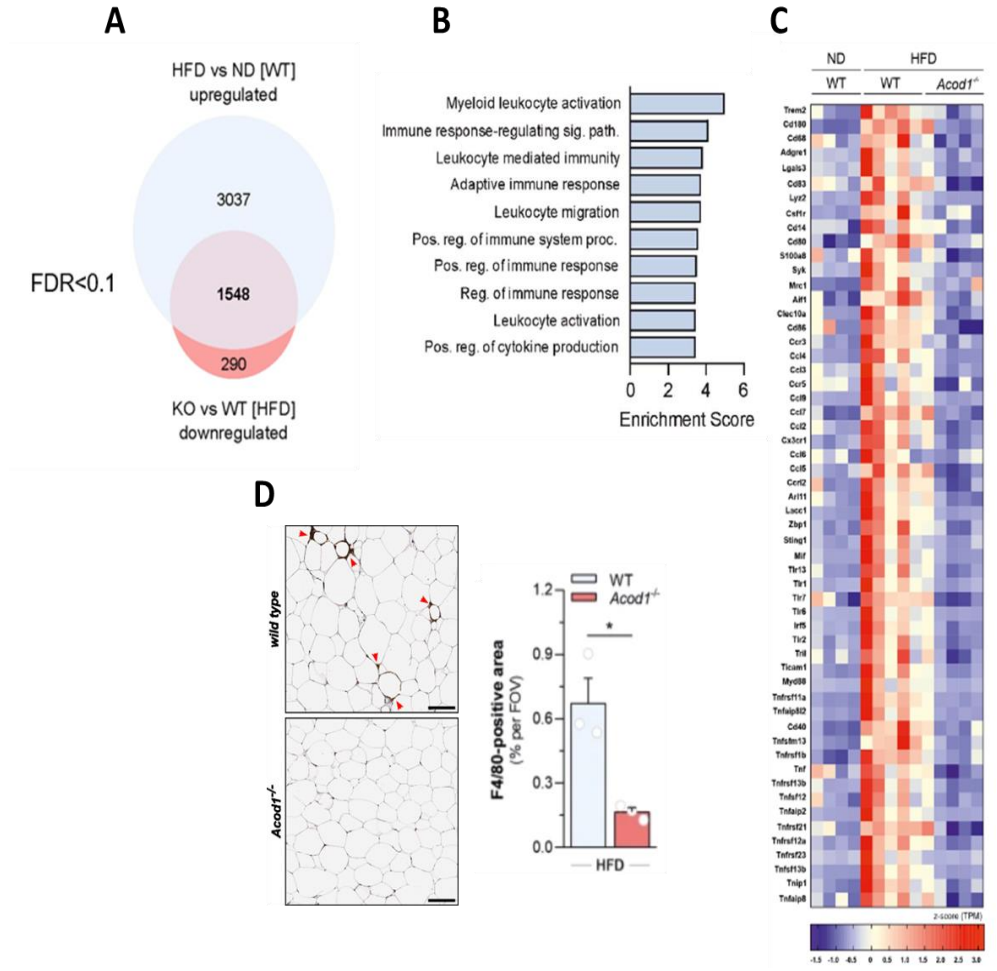

Figure 25. Acod1 ablation attenuates HFD-induced meta-inflammation in white adipose tissue.

A. *Venn diagram and (**B**)gene ontology (biological processes)-based functional enrichment analysis (right) of upregulated genes in eWAT of WT mice fed with HFD for 16 weeks compared with ND-fed mice (HFD vs ND [WT]) and rescued by Acod1 loss (Acod1$^{-/-}$ vs WT [HFD]). Data derive from n = 4 (ND-fed WT) and n = 5 (HFD-fed) mice from one experiment.* ***C.*** *Heatmap depicting the mRNA levels of selected genes defining macrophage markers, inflammatory cytokines and receptors, regulators of innate immunity, TLR signalling and TNF signalling upregulated in response to HFD (HFD vs ND [WT], FDR < 0.1) and rescued by Acod1 loss (Acod1$^{-/-}$ vs WT [HFD], FDR < 0.1) in eWAT. Data derive from mice described in A: n = 4 (ND-fed WT) and n = 5 (HFD-fed) mice from one experiment.* ***D.*** *Representative images (left) of immunohistochemistry staining for the macrophage marker F4/80 (Adgre1) in eWAT of WT and Acod1$^{-/-}$ mice after 16 weeks on HFD diet. Red arrows indicate crown-like structures. Quantification (right) of the F4/80-positive area per field of view (FOV) in images described in D. (n = 5 mice per group, average of 5 images each). Red arrows indicate crown-like structures. Bars, 100 μm. Data are represented as mean ± s.e.m. *P < 0.05 (t-test).*

Similarly to eWAT, a decreased pro-inflammatory transcriptional signature was retrieved by RNA-sequencing data of iWAT of mice. Functional enrichment analysis of 330 genes, upregulated upon HFD challenge and downregulated by *Acod1* loss (Fig. **26A**), showed that genetic ablation of *Acod1* rescued the levels of several macrophage markers (*Trem2, Adgre1, Cd68, Clec10a, Lgals3, Mrc1, Csf1r, S100a8*), chemokines (*Ccl2, Ccl7, Ccl9, Ccl6*) and pro-inflammatory mediators of myeloid cells (*Tril, Arl11*), which were instead increased in *wild type* mice upon fat overnutrition (Fig. **26B** and Fig. **26C**). Moreover, *Acod1* deficiency rescued the gene expression levels of some *Tnf* family members and receptors (*Tnfrsf21, Tnfrsf22, Tnfrsf12a*) (Fig. **26C**). In line with data obtained from the white adipose tissues, *Acod1* loss decreased *Il1b* mRNA levels in the brown adipose tissue (Fig. **26D**) and the circulating levels of pro-inflammatory cytokines such as Tnf, Il1β, Il6 compared with *wild type* mice (Fig. **26E**). Collectively, these data indicate that *Acod1* ablation protects from the HFD-driven metabolic inflammation.

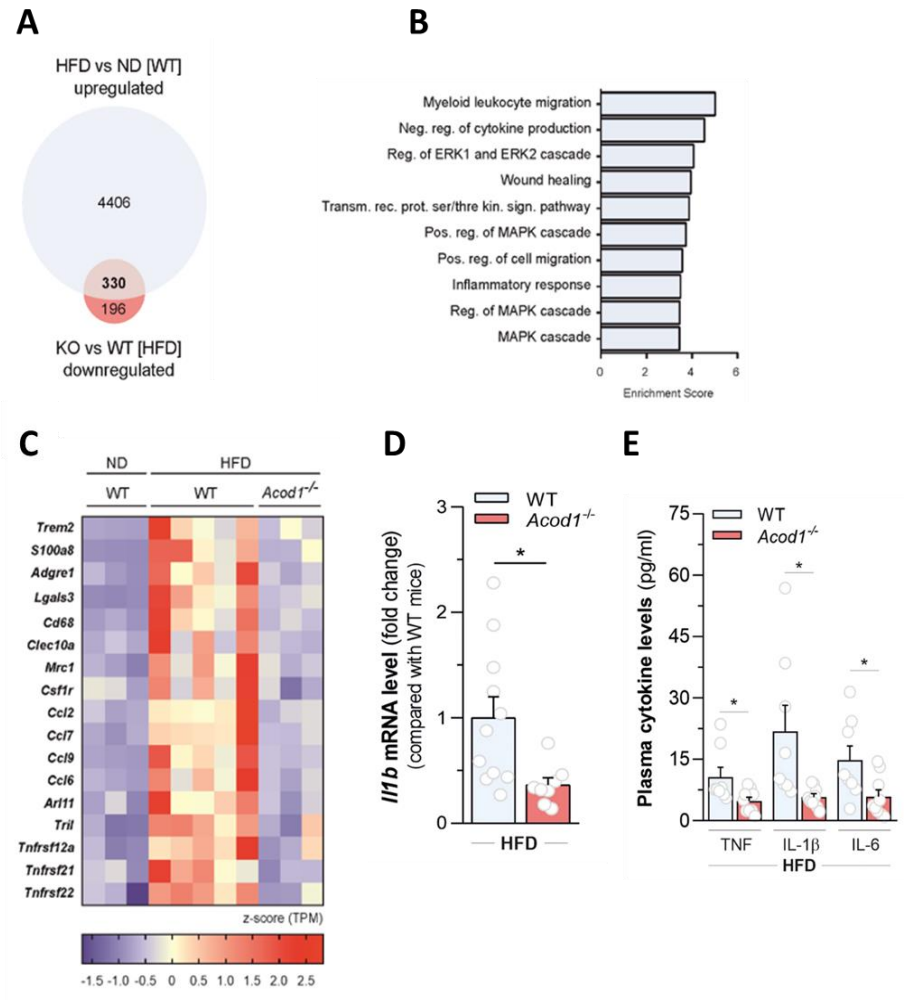

Figure 26. Acod1 ablation protects from the systemic HFD-driven metabolic inflammation.

A. *Venn diagram and (**B**) gene ontology (biological processes)-based functional enrichment analysis (right) of statistically significant (FDR<0.1) up-regulated genes in iWAT of WT mice in response to HFD (HFD vs ND [WT]) and rescued by Acod1 loss (Acod1$^{-/-}$ vs WT [HFD]). Data derive from n=3 (ND-fed WT), n=5 (HFD-fed WT) and n=3 (HFD-fed Acod1$^{-/-}$) mice from one experiment.* ***C***. *Heatmap depicting the mRNA levels of selected genes defining macrophage markers, inflammatory cytokines and receptors, regulators of innate immunity, TLR signaling and TNF signaling upregulated in response to HFD (HFDvsND in WT, FDR<0.1) and rescued by Acod1 loss (Acod1$^{-/-}$ vsWT in HFD, FDR<0.1) in iWAT. Data derive from mice described in (E): n=3 (ND-fed WT), n=5 (HFD-fed WT) and n=3 (HFD-fed Acod1$^{-/-}$) mice from one experiment.* ***D***. *qPCR analysis of Il1b mRNA levels in BAT of WT and Acod1$^{-/-}$ mice after 16 weeks on HFD diet. Data as as mean±s.e.m of n = 11 (WT) and n =n = 8 (Acod1$^{-/-}$) mice from two independent experiments.* ***E***. *Levels of the indicated pro-inflammatory cytokines in plasma of WT and Acod1$^{-/-}$ mice after 16 weeks on HFD diet. Data as as mean±s.e.m of n = 8 (WT) and n = 9 (Acod1$^{-/-}$) mice from two independent experiments. In (D, E) *P < 0.05 (t-test).*

Itaconate biosynthesis promotes gut microbiota changes associated with diet-induced obesity

The intestinal microbiota is fundamental in shaping host metabolism and it has been demonstrated that participates in the development and progression of obesity (Ley et al., 2005b; Zsálig et al., 2023). Alterations in the composition of the gut microbiota have been observed in obese individuals compared to lean subjects and these changes can be influenced by the diet and host-derived signals. In addition, itaconate is a well-recognized anti-microbial molecule by restricting the replication of many microbes via different mechanisms (Brogi et al., 2021). Building upon these insights, it was postulated that the changes in the inflammatory response observed in *Acod1*$^{-/-}$ mice were potentially secondary to alterations in gut microbiota imposed by *Acod1* ablation. Therefore, itaconate levels in stools of mice were measured. As a result, HFD induced itaconate accumulation in the faecal matter of *wild type* mice (0.66 mM) compared to ND-fed controls (Fig. **27A**). Moreover, it coincided with an upregulation of *Acod1* mRNA levels in the large intestine of the same mice (Fig. **27B**). To investigate whether *Acod1* deficiency might offer protection to diet-induced obesity through gut microbiota alterations, the bacterial composition of faecal microbiota isolated from *wild type* and *Acod1*$^{-/-}$ mice fed with either standard chow or HFD was profiled by using 16s ribosomal DNA sequencing. Alterations in the gut microbiota composition are characterized by changes in the *Bacteroidetes* to *Firmicutes* ratio, the two major intestinal phyla associated to metabolic health (Ley et al., 2006; Parks et al., 2013; Turnbaugh et al., 2008). This ratio is usually decreased due to the depletion of the *Bacteroidetes* proportion in faeces of both obese rodents and humans. In line with this, metagenomic analysis showed a decline in the *Bacteroidetes* proportion at the expense of *Firmicutes* in stools of *wild type* mice subjected to fat overnutrition. On the contrary, *Acod1* ablation mainly counteracted the reduction of the faecal *Bacteroidetes* abundance imposed by HFD (Fig. **27D** and Fig. **27E**). Consequently, the *Bacteroidetes* to *Firmicutes* ratio was decreased upon fat overnutrition in the faecal matter isolated from *wild type* mice and partially but significantly rescued by *Acod1* loss (Fig. **27C**). Under a regular chow, the genotype did not impose any difference in the faecal microbiota composition.

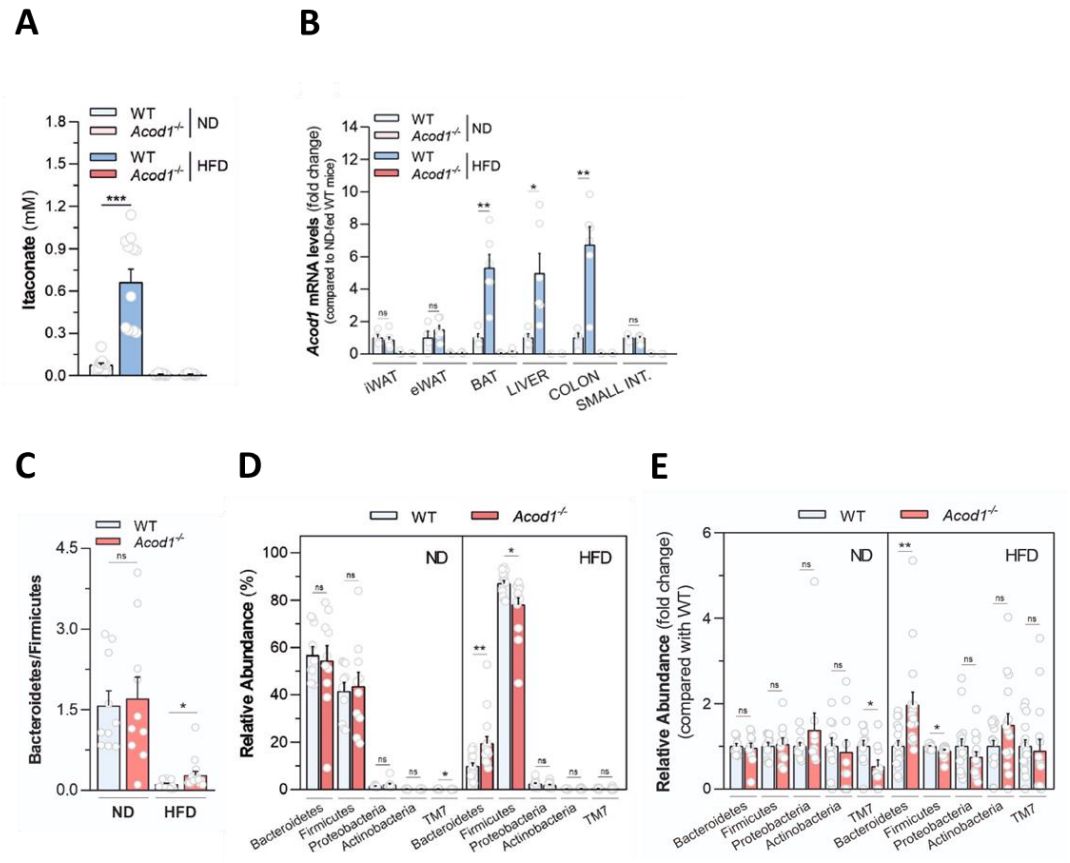

Figure 27. Acod1 exacerbates the impact of diet-induced gut dysbiosis.
A*. Faecal itaconate levels of WT and Acod1$^{-/-}$ mice fed for 16 weeks with ND or HFD. Data as mean±s.e.m. of n = 12 mice per group from three experiments independently executed.* ***B****. qPCR analysis of Acod1 mRNA levels in the indicated tissues from WT and Acod1$^{-/-}$ mice fed with ND (n = 4) or HFD (n = 6) for 16 weeks. Data as mean ± sem from one experiment out of two independently executed.* ***C****. Bacteroidetes to Firmicutes ratio in the fecal microbiota of WT and Acod1$^{-/-}$ mice fed for 16 weeks with ND or HFD. Data as mean±s.e.m. of n=10 (ND) or n=15 (HFD) mice from three experiments independently executed.* ***D.*** *Fractional analysis of the faecal bacterial composition at the phylum level of mice described in D. Data as mean±s.e.m. of n = 10 (ND) or n = 15 (HFD) mice from three independent experiments.* ***E****. Relative changes in the abundance of bacterial phyla in stools derived from mice described in D. Data as mean±s.e.m. of n=10 (ND) or n=15 (HFD) mice from three experiments independently executed. In (A, B, D, E, F): *P < 0.05; **P < 0.01; ***P < 0.001; ns not significant.*

To deeply investigate the impact of *Acod1* loss on faecal microbiota changes, unbiased abundance analyses at lower taxonomical levels were performed. Despite *Acod1* ablation elicited minor, although significant, effects on representation of *Ruminococcaceae* and *Desulfovibrionaceae* (belonging to the *Firmicutes* phylum), relative abundance

measurements revealed that the effect of *Acod1* loss was mostly associated with a significant increase in the abundance of bacterial families belonging to the *Bacteroidetes* phylum, such as *Bacteroidacae*, which ranked as the most statistically significant increased bacterial family in stools derived from *Acod1*$^{-/-}$ mice compared to HFD-fed *wild type* mice, *S24-7 (Muribaculaceae)*, *Erysipelotrichaceae* and *Porphyromonadaceae* families (Fig. **28A** and Fig. **28B**).

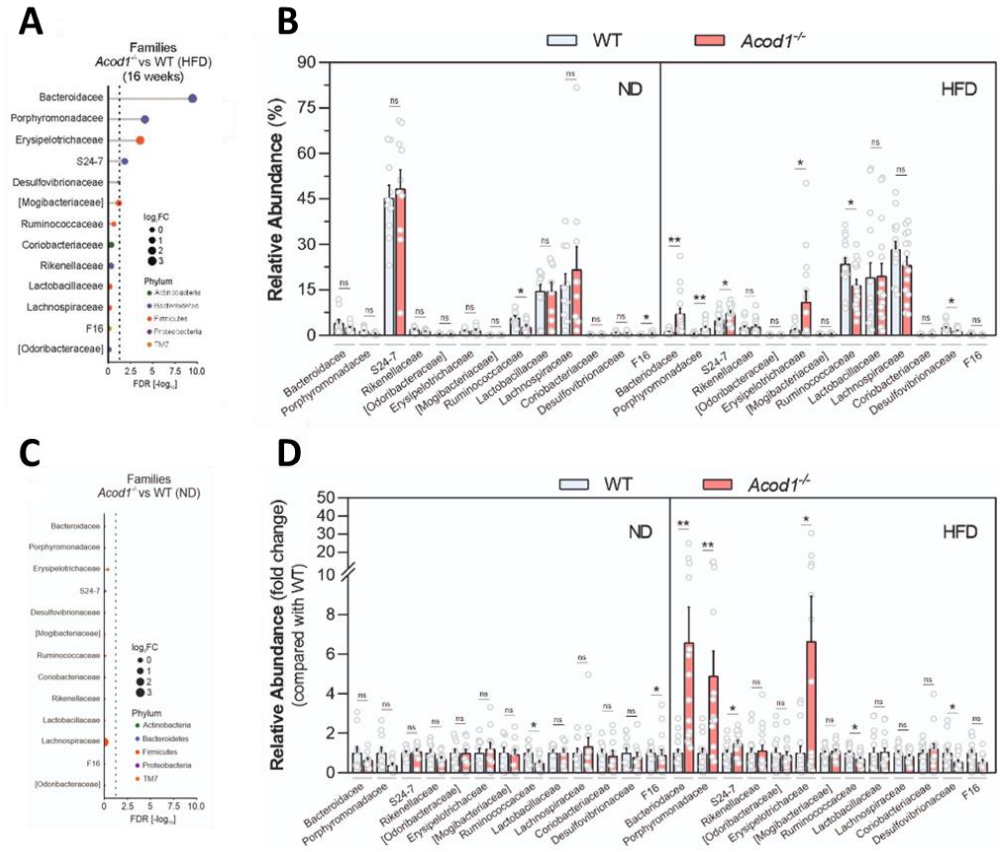

Figure 28. Acod1 ablation increases the abundance of Bacteroidetes families under high-fat diet.

A*. Differential abundance analysis (DESeq2) of the faecal bacterial composition at family level of WT (n = 15) and Acod1$^{-/-}$ (n = 15) mice fed with HFD for 16 weeks from three independent experiments. Dashed line indicates FDR = 0.05. The size of the dots indicates fold change (log2) and the colour indicates the phylum.* ***B****. Fractional analysis and relative changes (****D****) of the fecal bacterial composition at the family level of mice described in (A). Data as mean±s.e.m. of n=10 (ND) or n=15 (HFD) mice from three experiments independently executed.* ***C****. Differential abundance analysis (DESeq2) of the fecal bacterial composition at family level of WT (n=10) and Acod1$^{-/-}$ (n=10) mice fed with ND for 16 weeks from three experiments independently executed. Dashed line indicates FDR = 0.05. The size of the dots indicates fold change (log2), and the color indicates the phylum.*

Interestingly, *Bacteroides*, a genus within the *Bacteroidacee* family, was identified as the most statistically significant increased genus in the stools of *Acod1* deficient mice compared to *wild type* counterparts challenged with HFD (Fig. **29A** and Fig. **29B**). Members of these taxa have already been widely associated with protection against obesity and type 2 diabetes in both mice and humans (Jang et al., 2017; Palmas et al., 2021; J. Y. Yang et al., 2017a). Under a regular chow, the genotype did not impose major

differences neither at the family nor genus level (Fig. **28C**, **28D** and Fig. **29C**, **29D**).

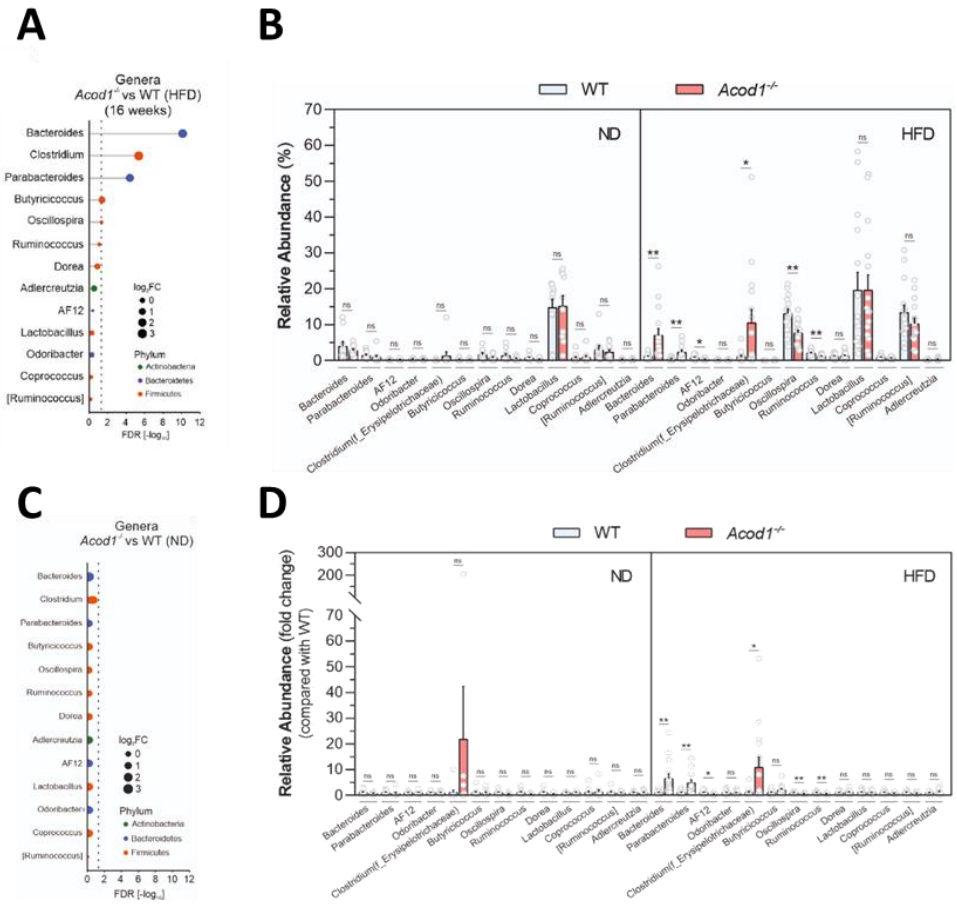

Figure 29. Acod1 deficiency increases the abundance of the Bacteroides genus under high-fat diet.

A*. Differential abundance analysis (DESeq2) of the faecal bacterial composition at genus level of WT (n = 15) and Acod1$^{-/-}$ (n = 15) mice fed with HFD for 16 weeks from three independent experiments. Dashed line indicates FDR = 0.05. The size of the dots indicates fold change (log2) and the colour indicates the phylum.* ***B****. Fractional analysis and relative changes (****D****) of the fecal bacterial composition at the genus level of mice described in A. Data as mean±s.e.m. of n=10 (ND) or n=15 (HFD) mice from three experiments independently executed.* ***C****. Differential abundance analysis (DESeq2) of the fecal bacterial composition at the genus level of WT (n=10) and Acod1$^{-/-}$ (n=10) mice fed with ND for 16 weeks from three experiments independently executed. Dashed line indicates FDR = 0.05. The size of the dots indicates fold change (log2) and the color indicates the phylum.*

Short chain fatty acids (SCFAs) are the end-products of the fermentation of dietary fibres by anaerobic gut microbes, mainly members of the *Bacteroidetes* phylum, and provide several health benefits to the host, with acetate, propionate, and butyrate being the most

abundant. Since fat overnutrition promotes gut dysbiosis which is linked to reduced production of SCFAs (Ríos-Covián et al., 2016; Schroeder & Bäckhed, 2016; Truax et al., 2018a), SCFAs levels were measured by GC/MS in the faecal matter isolated from mice under both a regular chow and HFD. In line with a more obesogenic faecal microbiota signature, fat overnutrition decreased the abundance of propionate and butyrate in the stools of *wild type* mice compared to their ND-fed controls. On the contrary, this decline was partially but significantly rescued upon *Acod1* loss (Fig. **30**). Importantly, the genotype did not impact the faecal levels of these metabolites under a normal diet.

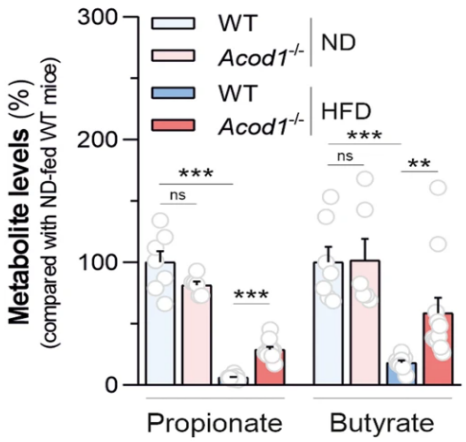

Figure 30. Acod1 loss rescues the drop in the abundance of SCFAs induced by HFD. *Levels of faecal SCFAs in mice fed for 16 weeks with ND or HFD. Data as mean±s.e.m. of n = 7 (ND-fed WT), n = 6 (ND-fed Acod1$^{-/-}$), n = 8 (HFD-fed WT), n = 11 (HFD-fed Acod1$^{-/-}$) mice from two experiments independently executed (student t-test; *P < 0.05; **P < 0.01; ***P < 0.001; ns not significant).*

Differently from what detected in the colon, *Acod1* mRNA levels were unaffected by the diet in the small intestine of *wild type* mice, as found by profiling gene expression of *Acod1* in several tissues involved in the pathogenesis of obesity (Fig. **12A**). Nonetheless, the small intestine microbiota is of major importance in regulating metabolism. Thus, to have a complete overview of microbiota changes occurring in the gastrointestinal tract, the bacterial composition of the small intestine isolated from mice fed with HFD was profiled by using 16s ribosomal DNA sequencing. Consistent with the unchanged *Acod1* gene expression levels detected in such tissue in response to dietary lipid overload, no

major differences were detected in the bacterial composition of the small intestines isolated from HFD-fed *Acod1*$^{-/-}$ and *wild type* mice (Fig. **31**). Overall, these findings suggested that alterations in the faecal microbiota influenced by *Acod1* primarily reflected changes occurring in the large intestine.

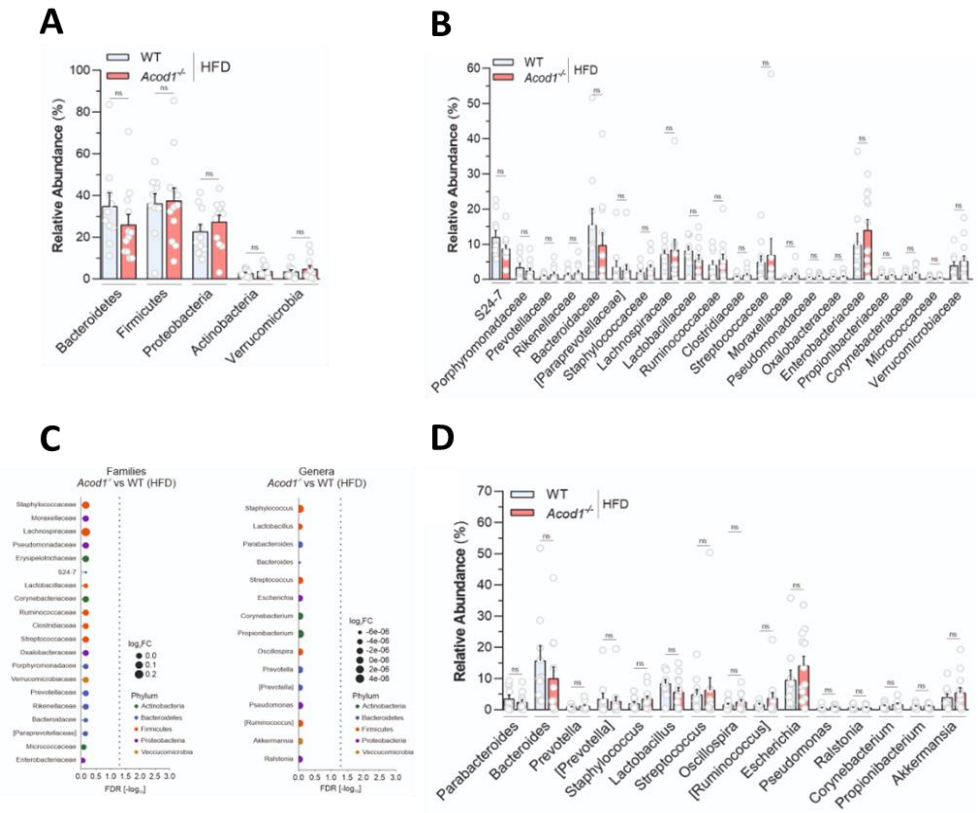

Figure 31. Acod1 loss does not alter the small intestine microflora.
A*. Fractional analysis of bacterial composition at the phylum level of the small intestine of WT and Acod1*$^{-/-}$ *mice fed for 16 weeks with HFD. Data as mean±s.e.m. of n=10 (WT) or n=12 (Acod1*$^{-/-}$*) mice from three experiments independently executed.* ***B****. Fractional analysis of bacterial composition at the family level of the small intestine of mice described in A. Data as mean±s.e.m. of n=10 (WT) or n=12 (Acod1*$^{-/-}$*) mice from three experiments independently executed.* ***C****. Differential abundance analysis (DESeq2) of the bacterial composition at family (left) and genus (right) level of WT (n=10) and Acod1*$^{-/-}$ *(n=12) mice fed with HFD for 16 weeks, from two experiments independently executed. Dashed line indicates FDR = 0.05. The size of the dots indicates fold change (log2) and the color indicates the phylum.* ***D****. Fractional analysis of bacterial composition at the genus level of the small intestine of mice described in A. Data as mean±s.e.m. of n=10 (WT) or n=12 (Acod1*$^{-/-}$*) mice from three experiments independently executed. ns: not significant (t-test).*

Itaconate supplementation induces an "obesity-like" microbiome

So far, results obtained from faecal microbiota analyses pointed toward an amelioration of the intestinal ecosystem, skewed by HFD towards an obesity-supporting profile, in response to *Acod1* ablation in the host. To substantiate these findings, it has been speculated that administration of high doses of itaconate, beyond the levels endogenously produced, on gut microbiota composition would lead to a more pronounced obesity-associated microbial signature and enhanced overall metabolic responses to HFD. Therefore, HFD-fed *wild type* mice were administered with supraphysiological doses of itaconate (20 mM) in drinking water throughout the experiment, compared to vehicle-treated counterparts and faecal microbiota changes were measured. The 5-fold increase of faecal itaconate levels detected in itaconate-treated mice (Fig. **32A**) was associated with an exacerbated depletion of the faecal abundance of *Bacteroidetes* (Fig. **32B**) and *Bacteroidetes* to *Firmicutes* ratio compared with vehicle-treated counterparts after 12 weeks of HFD (Fig. **32C**).

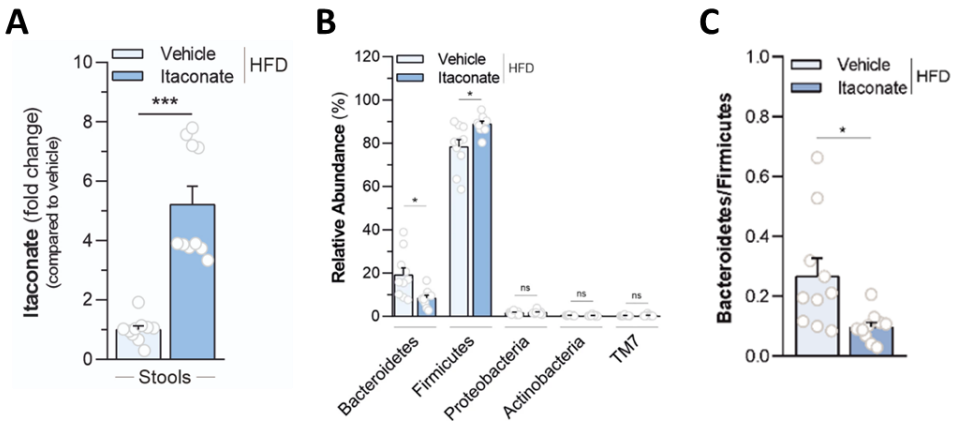

Figure 32. Itaconate supplementation induces an "obesity-like" gut microbiota.
***A**. Levels of itaconate in stools of HFD-fed WT mice treated with 20 mM itaconate in drinking water for 12 weeks. Data as mean±s.e.m. of n=10 mice per group from two independent experiments independently executed. **B**. Fractional analysis of the fecal bacterial composition at the phylum level of mice treated as in A. Data as mean±s.e.m. of n = 10 mice per group from two experiments independently executed. **C**. Bacteroidetes to Firmicutes ratio in the fecal microbiota of mice described in A. Data as mean±s.e.m. of n=10 mice per group from two experiments independently executed. In (A, B, C): student t-test; *P < 0.05; **P < 0.01; ***P < 0.001; ns not significant.*

By investigating the impact of itaconate supplementation at lower taxonomical levels, relative abundance measurements revealed that itaconate administration increased the faecal abundance of *Firmicutes*-belonging taxa such as *Lachnospiraceae, Ruminococcus and Coprococcus* (Fig. **33A** and Fig. **33B**) with respect to vehicle-treated mice. Nonetheless, the impact of itaconate supplementation on gut microbiota composition was mainly due to a significant reduced representation of *Bacteroidacee* and *Bacteroides* (Fig. **33C** and Fig. **33D**). These data indicated that itaconate effect opposed the major metagenomic changes elicited by genetic disruption of itaconate biosynthesis in HFD-fed mice.

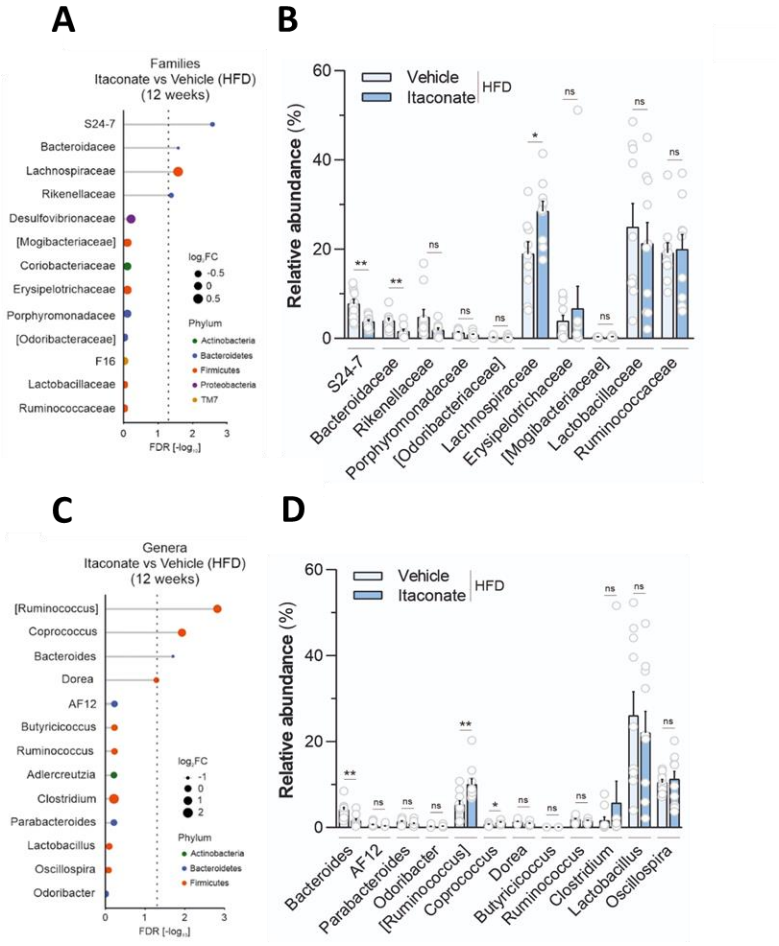

Figure 33. Itaconate supplementation reduces the abundance of Bacteroidetes families under high-fat diet.

***A**. Differential abundance analysis (DESeq2) comparing fecal bacterial composition at family and genus (**C**) levels of HFD-fed WT mice treated with 20 mM itaconate in drinking water for 12 weeks (n = 10 mice per group from two experiments independently executed). Dashed line indicates FDR = 0.05. The size of the dots indicates fold change (log2) and the color indicates the phylum. **B**. Fractional analysis of the fecal bacterial composition at the family and genus (**D**) level of mice described in A. Data as mean±s.e.m. of n=10 mice per group from two experiments independently executed. In (B, D): student t-test; *P<0.05; **P<0.01; ***P<0.001; ns: not significant.*

In line with the more obesity-like faecal microbial signature, itaconate treated mice gained significantly more weight compared to vehicle-treated mice (Fig. **34A**). This was reflected by an increased adiposity, as indicated by the increased weight of the brown adipose tissue, inguinal, perirenal and epididymal white adipose tissues, although the latter was not statistically significant (Fig. **34B**). Moreover, itaconate supplementation

aggravated insulin resistance (Fig. **34C**) and liver steatosis (Fig. **34D**), as demonstrated by the augmented liver weight and hepatic triglycerides accumulation, with respect to controls. Importantly, these effects were not tied to differences in the food consumed by mice in the two experimental groups (Fig. **34E**).

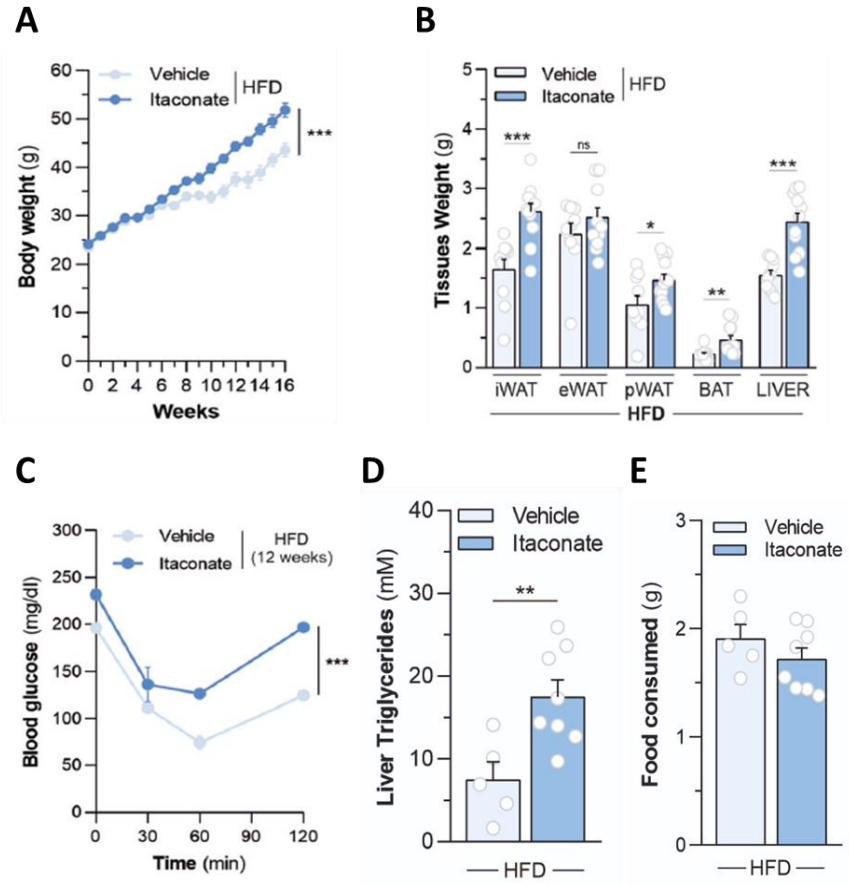

Figure 34. Itaconate supplementation aggravates obesity and associated metabolic outcomes.

A. *Body weight of HFD-fed WT mice treated with 20 mM itaconate in drinking water for the time indicated. Data as mean ± s.e.m. of n = 10 (vehicle) and n = 12 (itaconate)-treated mice from two experiments independently executed.* ***B*** *Tissue weights from mice escribed in A. Data as mean±s.e.m. of n = 10 (vehicle) and n = 12 (itaconate)-treated mice from two experiments independently executed.* ***C.*** *ITT in WT mice treated with 20 mM itaconate in drinking water for 12 weeks. Data as mean±s.e.m. of n = 5 (vehicle) and n = 7 (itaconate)-treated mice from one representative experiment out of two independently executed. Liver triglyceride content in wild type mice as treated in A after 16 weeks of HFD feeding. Data as mean±s.e.m. of n=5 (vehicle) and n=8 (itaconate)-treated mice from one representative experiment out of two independently executed.* ***D****. Food intake in HFD-fed WT mice as described in A. Data as mean±s.e.m of n=5 (vehicle) and n=8 (itaconate)-treated mice from one representative experiment out of two independently executed. In (A, C): two-way ANOVA; in (B, D, E): student t-test; *P<0.05; **P<0.01; ***P<0.001; ; ns: not significant.*

In addition, the expression levels of the urea cycle-encoding genes (*Nags, Cps1, Ass1*) were further downregulated in the liver of itaconate-treated mice, indicating an

exacerbation of liver functions due to itaconate overload (Fig. **35A**). Profiling of the macrophage marker *F4/80* in the adipose tissues revealed that itaconate supplementation induced an increased macrophage accumulation in the inguinal and epididymal white adipose tissues (Fig. **35B**).

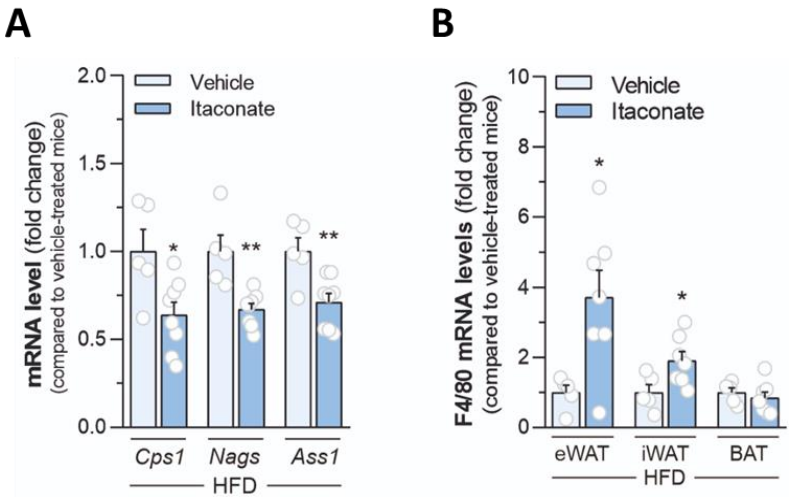

Figure 35. Effects of itaconate supplementation on urea cycle gene expression and macrophage accumulation.
A*. qPCR analysis of the indicated genes in liver of wild type mice treated with 20 mM itaconate in drinking water after 16 weeks of HFD feeding. Data as mean±s.e.m. of n=5 (vehicle) and n=8 (itaconate)-treated mice from one representative experiment out of two independently executed.* ***B****. qPCR analysis of F4/80 (Adgre1) in fat depots of wild type mice as described in A after 16 weeks of HFD feeding. Data as mean±s.e.m. of n=5 (vehicle) and n=7 (itaconate)-treated mice from one representative experiment out of two independently executed. Student t-test; *P<0.05; **P<0.01; ***P<0.001; ; ns: not significant.*

Since the effect on the faecal microbiota composition exerted by itaconate supplementation was specular to that induced by *Acod1* loss, mainly due to alterations in the faecal abundance of *Bacteroidetes*, it was speculated that itaconate could have a direct effect on this intestinal phylum. Therefore, faecal suspension of pooled stools derived from HFD-fed *wild type* mice were incubated *in vitro* either with increasing doses of itaconate starting from near physiologically relevant concentration (0.5, 1, 10, 20 mM) or vehicle for 48 hours in anaerobic atmosphere. Itaconate administration led to a dose-dependent decreased in the relative abundance of *Bacteroidetes* and the *Bacteroidetes* to *Firmicutes* ratio with respect to vehicle-treatment (Fig. **36A** and Fig. **36B**). Differently,

an increase in the relative abundance of *Firmicutes* occurred only at higher doses of itaconate (10 and 20mM). In line with this, the impact of itaconate application was mostly exerted by a dose-dependent decline in the *Bacteroidaceae* and *Bacteroides* proportion compared to vehicle-treated faecal cultures (Fig. **36C** and Fig. **36D**). Next, to validate these results, five pure bacterial strains representative of *Bacteroidaceae* family (*Bacteroides genus*) – *Bacteroides acidifaciens*, *Phocaeicola* (*Bacteroides*) *vulgatus*, *Phocaeicola* (*Bacteroides*) *dorei*, *Bacteroides thetaiotaomicron* and *Bacteroides uniformis*) found differently changed in the faecal microbiota analyses between *wild type* and *Acod1*$^{-/-}$ mice fed with HFD and already reported to have beneficial roles against metabolic disease (Gauffin Cano et al., 2012; R. Liu et al., 2017a; López-Almela et al., 2021; Ridaura et al., 2013b; J. Y. Yang et al., 2017b; Yoshida et al., 2018), were incubated *in vitro* with near physiologically relevant concentration of itaconate (0.5 mM) to evaluate the targeted impact of itaconate on these bacterial genera. Similarly to the effect of itaconate supplementation on faecal cultures, itaconate treatment restricted the growth of all five bacterial strains (Fig. **36E**). Overall, these findings indicate that itaconate, whether endogenously produced or exogenously administered, is essential in driving gut microbiota changes associated with diet-induced metabolic disease.

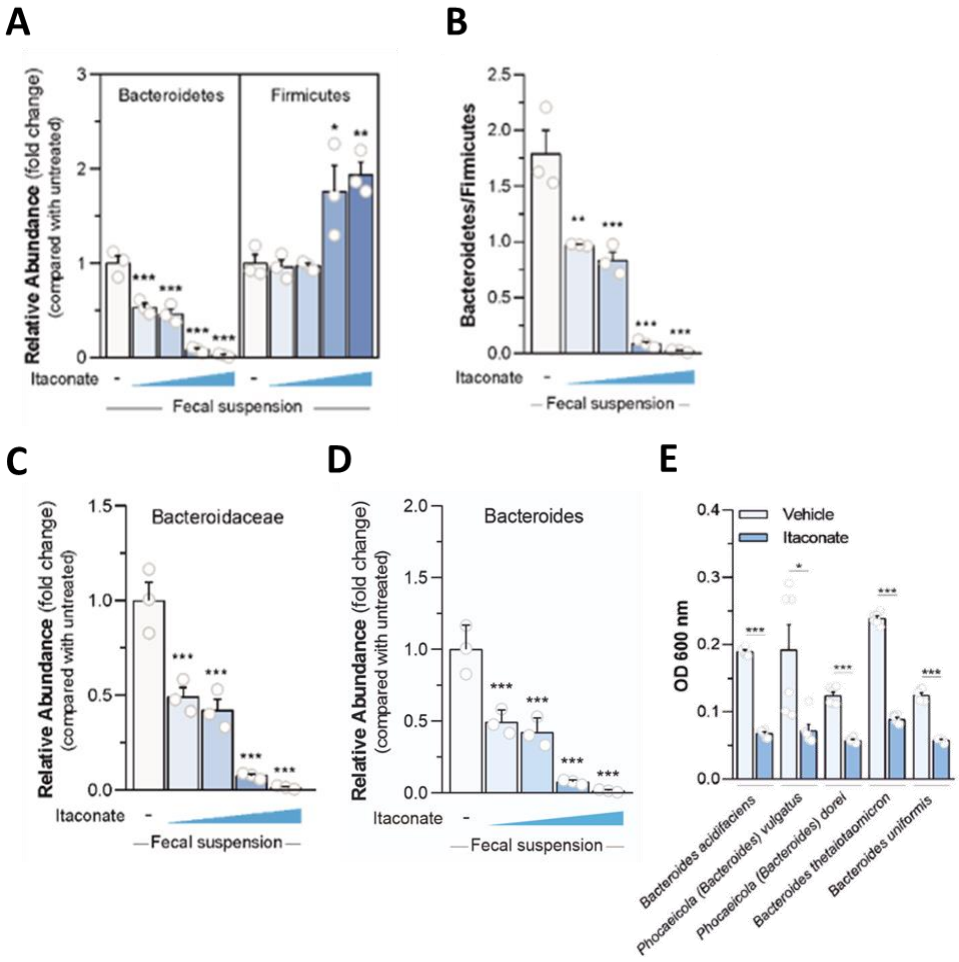

Figure 36. Itaconate inhibits the growth of Bacteoidetes-belonging taxa.
A*. Relative changes in abundance of Bacteroidetes and Firmicutes phyla measured in fecal suspensions, deriving from pooled stools of n= 6 HFD-fed WT mice, incubated in vitro either with itaconate (0.5, 1, 10, 20 mM) or vehicle (-) for 48 hours in anaerobic atmosphere. Data as mean±s.e.m. from n=3 independent experiments.* ***B****. Bacteroidetes to Firmicutes ratio measured in fecal suspensions described in A. Data as mean±s.e.m. from n=3 independent experiments.* ***C****. Relative changes in the abundance of Bacteroidaceae and Bacteroides (****D****) measured in fecal suspensions described in A. Data as mean±s.e.m. from n=3 independent experiments.* ***E****. Effect of itaconate (0.5 mM) treatment on growth (OD 600 nm) of five pure bacteria strains representative of the Bacteroidaceae family (Bacteroides genus), over 24 h of culture in anaerobic atmosphere, measured spectrophotometrically. Data as mean ± s.e.m. of n = 6 samples per condition from two independent experiments. In (A-D): one-way ANOVA followed by Dunnett`s T3 multiple comparison test compared with vehicle (-); in E student t-test; *P < 0.05; **P < 0.01; ***P < 0.001; ns not significant.*

Itaconate Biosynthesis: Sustaining Gut Microbiota Alterations and Driving Meta-Inflammation in Metabolic Disease

Low-grade inflammation is a key feature of metabolic disorders such as obesity, and recent evidence suggest that changes in the composition of the intestinal microflora may trigger its development (Ding et al., 2010; Scheithauer et al., 2020). In addition, data obtained so far demonstrated the essential role for itaconate biosynthesis in affecting gut microbiota composition but the degree to which gut microbiota alterations, resulting from the genetic disruption of itaconate biosynthesis, contributed to resistance to diet-induced obesity and its complications was still not clear. To address this, a faecal microbiota transplantation (FMT) experiment was performed on HFD-fed mice. Faeces collected from HFD-fed donor *wild type* and *Acod1*$^{-/-}$ mice were orally transferred, throughout the duration of the experiment, into HFD-fed recipient mice, of the reciprocal genotype and responses to overnutrition were measured (Fig. **37**).



Figure 37. Schematic representation of faecal microbiota transplantation (FMT)

Prior to receive the faecal matter from donor mice, recipient mice only were administered with a broad-spectrum antibiotic cocktail (50 μg/ml Streptomycin, 100 U/ml Penicillin) in drinking water for 3 days to lower the existing microbiota and favouring the following engraftment of donor microbiota (Bokoliya et al., 2021b). The abundance of bacteria in stools was determined by quantitative PCR-based measurement of bacterial 16S rRNA gene levels and Fig. **38A** shows that the antibiotic treatment was effective in lowering gut microbiota in both groups. By comparing the accumulation of body weight in mice, *wild type* recipient mice (*wild type* mice receiving stools from *Acod1*$^{-/-}$ donor mice) gained a similar weight with respect to *Acod1*$^{-/-}$ donor mice, which was significantly less compared

to their *wild type* donor counterparts (Fig. **38B**). Next, to understand whether the resistance to weight gain observed in *wild type* recipient mice was due to a decreased accumulation of fat, the weight of fat depots isolated from all mouse groups at the end of the experiment was measured. In line with the reduced body weight, *wild type* recipient mice showed a lower accumulation of adiposity compared to *wild type* donor littermates, as demonstrated by the considerable reduction in the weight of inguinal, epididymal and perirenal white fat depots as well as brown adipose tissue compared with *wild type* donor counterparts (Fig. **38C**). Then, to evaluate whether protection from diet-induced obesity offered by oral transfer of stools derived from *Acod1*$^{-/-}$ donor mice was associated with amelioration of systemic glucose homeostasis, an insulin tolerance test was performed on mice. As shown in Figure **38D**, *wild type* recipient mice had an improved tolerance to insulin overload compared to their *wild type* donor littermates, which was akin to the effect imposed by *Acod1* loss on insulin sensitivity. After, it was determined whether faecal transfer from *Acod1*$^{-/-}$ donor mice also conferred resistance to the development of liver steatosis and liver-associated dysfunctions. Necroscopic analysis revealed a decreased weight of livers isolated from *wild type* recipient mice with respect to *wild type* donor mice (Fig. **38C**). Moreover, quantitative determination of triglyceride content was assessed and as observed in Figure **38E**, livers derived from *wild type* recipient mice had lower accumulation of hepatic triglycerides compared to *wild type* donor mice, similarly to the effect induced by *Acod1* ablation upon HFD. To test whether the reduced steatotic phenotype observed in *wild type* recipient mice was also associated to an amelioration of liver urea cycle function, gene expression analysis of the genes encoding for urea cycle enzymes was performed. In line with the improvement of liver steatosis, faecal transfer from *Acod1*$^{-/-}$ donor into *wild type* recipient mice opposed the HFD-induced downregulation of urea cycle genes mRNA levels measured in *wild type* donor mice (Fig. **38F**). On the contrary, no major differences in body weight gain (Fig. **38B**), fat depot weight (Fig. **38C**), responsiveness to insulin (Fig. **38D**) as well hepatic lipid accumulation (Fig. **38E**) were observed in *Acod1*$^{-/-}$ recipient mice receiving stools from *wild type* counterparts, with respect to *Acod1*$^{-/-}$ controls.

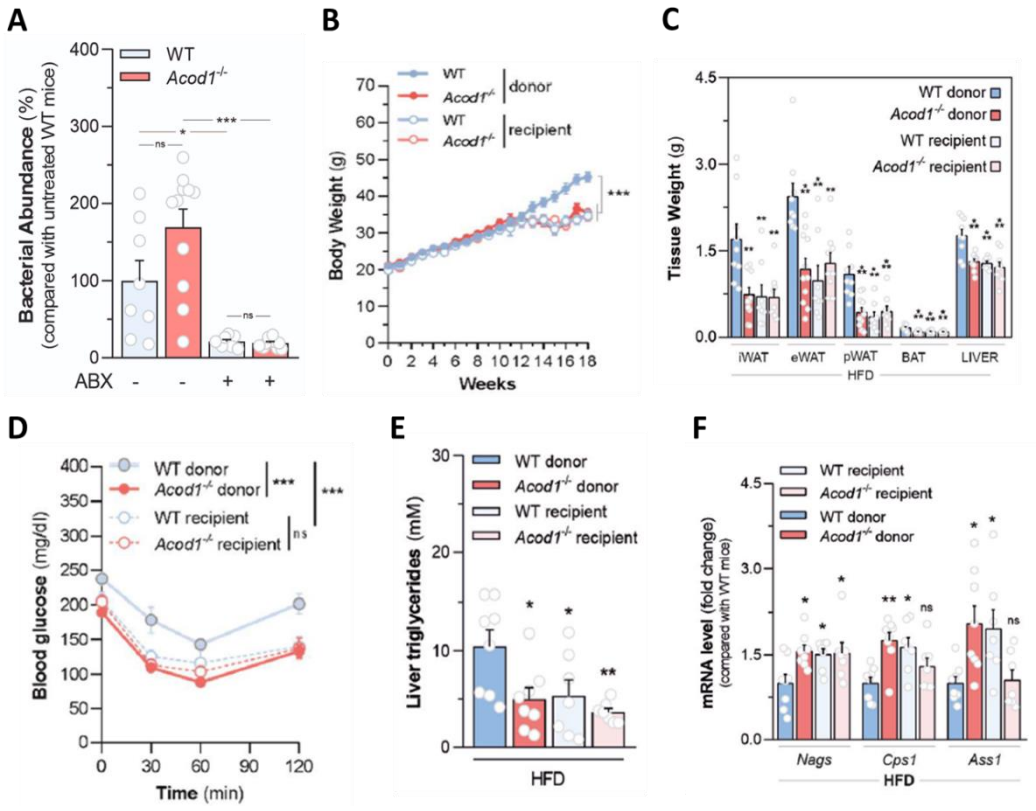

Figure 38. Faecal microbiota of Acod1-deficient mice offers transferable protection from metabolic disease and liver dysfunction.

A. *Abundance of bacteria in stools of WT (n=8) and Acod1$^{-/-}$ (n=11) recipient mice used in the FMT set-up measured before (-) and at the end (+) of antibiotics (ABX) treatment, determined by quantitative PCR-based measurement of bacterial 16S rRNA gene levels. Data as mean±s.e.m. from two experiments independently executed.* ***B***. *Body and tissue* (***C***) *weights of HFD-fed WT and Acod1$^{-/-}$ mice receiving either PBS (donor) or a fecal suspension from reciprocal genotypes (recipient). Data as mean ± s.e.m from n = 9 (WT donor), n = 11 (Acod1$^{-/-}$ donor), n = 8 (WT recipient) and n = 10 Acod1$^{-/-}$ recipient mice from two experiments independently executed.* ***D***. *ITT from mice treated as in B. Data as mean±s.e.m of n = 9 (WT donors), n = 11 (Acod1$^{-/-}$ donors), n = 8 (WT recipient) and n = 9 Acod1$^{-/-}$ recipient mice from two experiments independently executed.* ***E***. *Liver triglycerides and* (***F***) *qPCR analysis of indicated hepatic genes of mice treated as in A. Data as mean±s.e.m from n = 8 (donors) and n = 7 (recipient) mice from two independent experiments. In A: student t-test; in (B, D): two-way ANOVA; in (C, E, F): one-way ANOVA with Dunnett's multiple comparisons test compared with WT donor; *P < 0.05; **P < 0.01; ***P < 0.001; ns not significant.*

Since *wild type* recipient mice were protected from metabolic disturbances induced by fat overnutrition compared to their *wild type* donor counterparts, it has been investigated whether the transplant of faecal matter from *Acod1*$^{-/-}$ donor mice into *wild type* recipients would have attenuated the development of the low-grade inflammation. To test this, mRNA levels of pro-inflammatory mediators were measured by qPCR in the white and brown adipose tissues. Comparable to the amelioration of meta-inflammation conferred by *Acod1* loss, *wild type* recipient mice exhibited a dampened pro-inflammatory transcriptional signature in adipose tissues (Fig. **39A** and Fig. **39B**). Moreover, this decreased inflammatory state was associated with increased catabolic activity in adipose tissues, as demonstrated by the upregulation of several genes involved in energy expenditure-promoting processes in the BAT of *wild type* recipient mice compared to *wild type* donor littermates (Fig. **39C**).

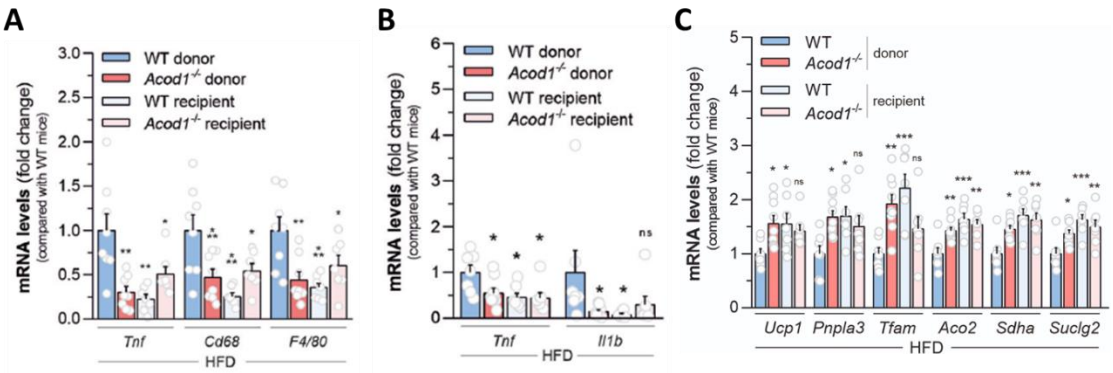

Figure 39. Faecal microbiota of Acod1-deficient mice opposes adipose tissues inflammation and altered catabolic activity induced by high-fat diet.
A*. qPCR analysis of indicated genes in eWAT of HFD-fed WT and Acod1*$^{-/-}$ *mice receiving either PBS (donor) or a fecal suspension from reciprocal genotypes (recipient). Data as mean±s.e.m from n = 8 (donors) and n = 7 (recipient) mice from two independent experiments.* ***B****,* ***C****. qPCR analysis of indicated genes in BAT of mice treated as in A. Data as mean±s.e.m from n = 7 (WT donor), n = 9 (Acod1*$^{-/-}$ *donor) and n = 7 (recipient) mice from two independent experiments. In (A-C): one-way ANOVA with Dunnett's multiple comparisons test compared with WT donor; *P < 0.05; **P < 0.01; ***P < 0.001; ns not significant.*

Despite the faecal microbiota transfer, *Acod1*$^{-/-}$ recipient mice exihibit the same extent of protection against diet-induced obesity and associated comorbidities with respect to *Acod1*$^{-/-}$ donor mice. This could be explained by the insufficient residual levels of

itaconate, present in the *wild type* stools gavaged, to affect gut microbiota composition of *Acod1*$^{-/-}$ recipients and their responses to HFD. To evaluate such possibility, the levels of itaconate in stools of both donor and recipient mice, collected at the end of the experiment, were determined. As shown in Figure **40A** the faecal microbiota transfer of *wild type* donor mice into *Acod1*$^{-/-}$ recipients resulted in faecal residual levels of itaconate comparable to those measured in *wild type* recipient mice. Another factor that could have contributed to the phenotype observed in *Acod1*$^{-/-}$ recipient mice could have been the intrinsic resistance of the *Acod1*$^{-/-}$ hosts to colonization of microbiota of *wild type* mice. To determine this, the faecal metagenomic compositions of donor and recipient mice, both before and after the transplant (at the end of the experiment) were profiled. No major differences in the bacterial composition of faecal microbiota were observed at any taxonomic level between the groups prior to faecal transplantation (Fig. **40B**, **C** and Fig. **40D**).

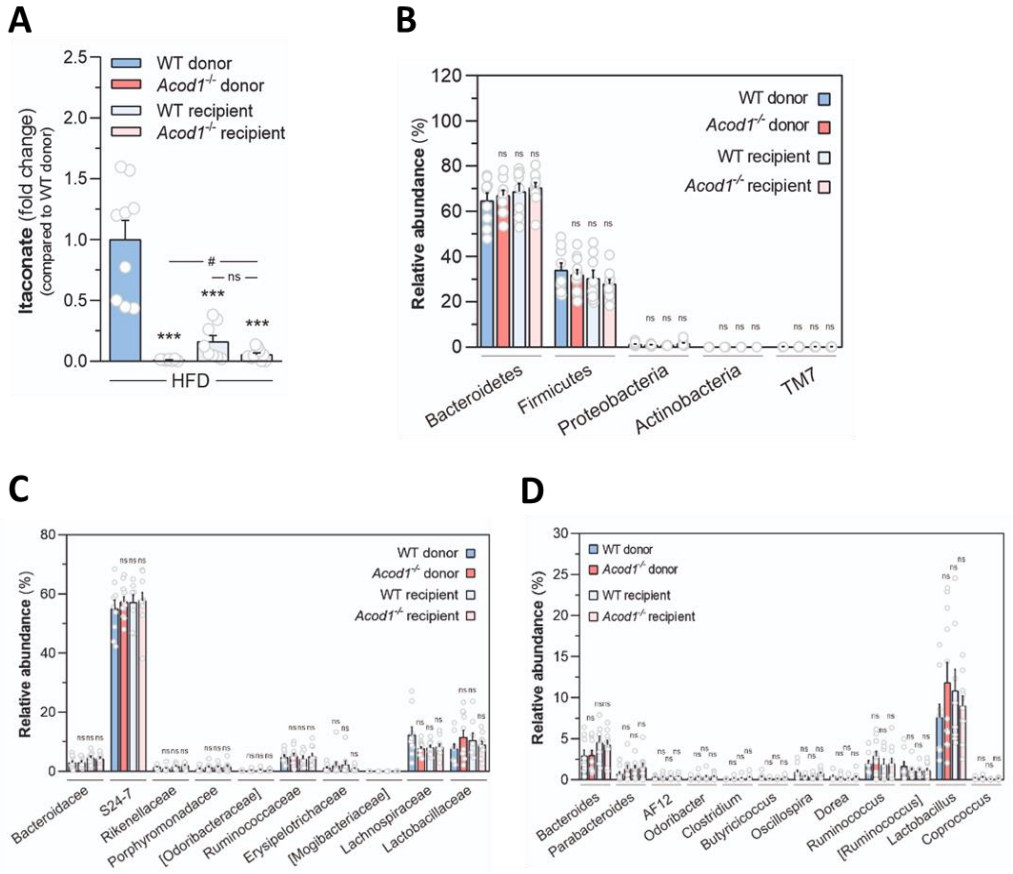

Figure 40. Gut microbiota before FMT.
***A**. Determination of itaconate levels in stools of HFD-fed WT and Acod1$^{-/-}$ mice receiving either PBS (donor) or a fecal suspension from reciprocal genotypes (recipient). Data as mean±s.e.m. of n=9 (WT donor), n=11 (Acod1$^{-/-}$ donor), n=8 (WT recipient), n=10 (Acod1$^{-/-}$ recipient) from two experiments independently executed. **B**. Fractional analysis of fecal bacterial composition at the phylum, family (**C**) and genus (**D**) level of WT and Acod1$^{-/-}$ donor and recipient mice assessed before the fecal microbiota transplantation (FMT). Data as mean±s.e.m. of n=9 (WT donor), n=11 (Acod1$^{-/-}$ donor), n=8 (WT recipient), n=10 (Acod1$^{-/-}$ recipient) from two experiments independently executed. In (A-D): one-way ANOVA followed by Dunnett`s T3 multiple comparison test compared with WT donor; *P<0.05; **P<0.01; ***P<0.001; in A $^{\#}$P<0.05 t-test; ns, not significant.*

In agreement with the unaffected disease severity, no significant differences were observed in the faecal microbiota composition of *Acod1*$^{-/-}$ recipients compared to *Acod1*$^{-/-}$ donor mice at the end of the experiment. On the other hand, a notable increase in the representation of *Bacteroidetes* in the faeces of *wild type* recipients compared to *wild type* donor counterparts at the conclusion of the experiment were detected (Fig. **41A**). Consistent with the phylum-level data, analyses conducted at the family and genus levels

revealed that the transplantation of stools collected from *Acod1*$^{-/-}$ donors led to elevated levels of *Bacteroidaceae* and *Bacteroides*—bacterial taxa linked to protection against metabolic disease—in *wild type* recipients compared to *wild type* donor mice, as represented by fractional analysis (Fig. **41B** and Fig. **41C**). Taken together, these data indicated a predominant protective effect of faecal microbiota from *Acod1*$^{-/-}$ mice against diet-induced obesity and associated comorbidities.

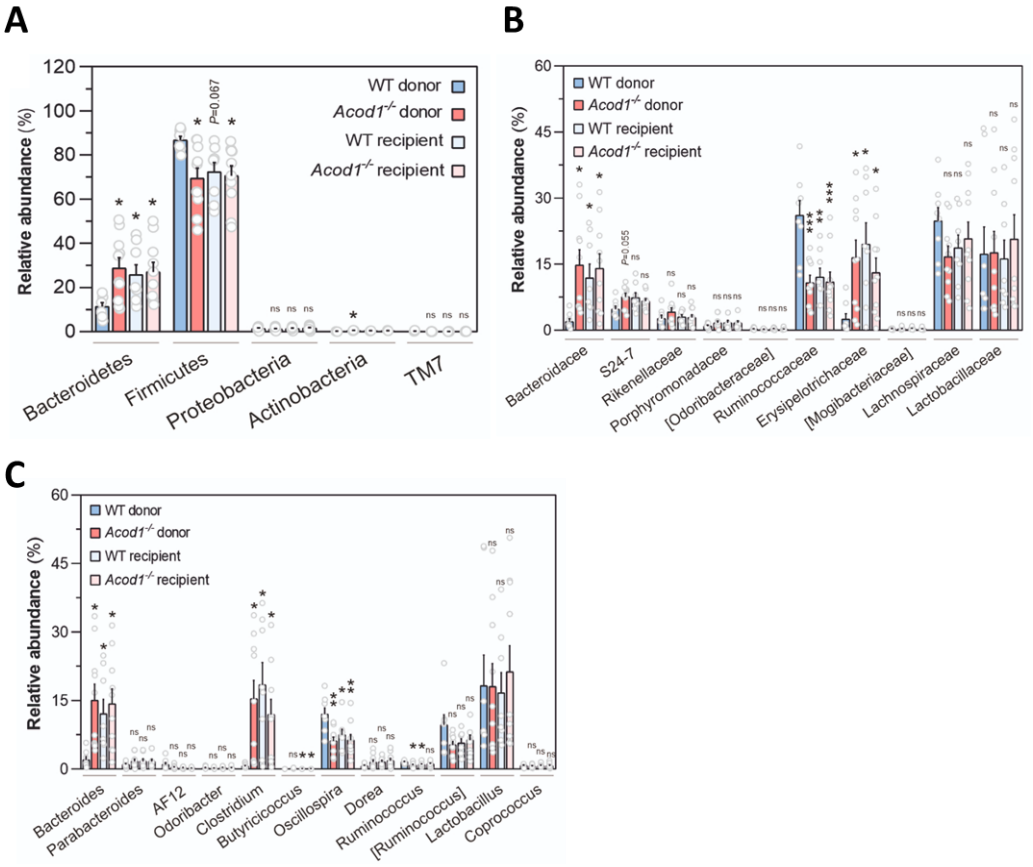

Figure 41. Gut microbiota after FMT.
A*. Fractional analysis of fecal bacterial composition at the phylum, family (**B**) and genus (**C**) level of WT and Acod1*$^{-/-}$ *donor and recipient mice receiving either PBS (donors) or a fecal suspension from reciprocal genotypes (recipients) assessed after 18 weeks of feeding with HFD. Data as mean±s.e.m. of n=8 (WT donor), n=10 (Acod1*$^{-/-}$ *donor), n=8 (WT recipient), n=10 (Acod1*$^{-/-}$ *recipient) from two experiments independently executed. In (A-C): one-way ANOVA followed by Dunnett`s T3 multiple comparison test compared with WT donor; *P<0.05; **P<0.01; ***P<0.001; ns, not significant.*

It has been extensively reported that high-fat diet exposure leads to gut dysbiosis which, in turn, impairs the gut barrier, thus increasing intestinal permeability. This has been termed “leaky gut” and plays a fundamental role in driving metabolic meta-inflammation (Brenchley & Douek, 2012). To assess whether the protection from metabolic inflammation provided by *Acod1* loss was linked to a preserved gut barrier, a fluorescein isothiocyanate dextran (FITC-dextran) assay was employed to measure intestinal permeability. FITC-dextran, a fluorescently labelled molecule, was administered orally to mice and its concentration was measured in plasma a few hours later. Notably, FITC-dextran is a large molecule (3–5 kDa) that typically cannot cross the epithelial barrier under normal conditions; thus, a higher concentration in plasma indicates increased gut permeability. As shown in Figure **42A**, high-fat diet enhanced gut barrier permeability in *wild type* mice compared to ND-fed controls as demonstrated by the significant increase in FITC-dextran intensity. On the contrary, *Acod1* deficiency normalized the FITC-dextran levels that were heightened upon fat overnutrition. Importantly, *wild type* recipient mice had a preserved gut barrier function as demonstrated by the statistically significant lower FITC-dextran levels in plasma compared to HFD-fed *wild type* donor mice. In line, results obtained from murine studies were supported by data retrieved from publicly available human colon datasets showing that the *ACOD1* mRNA levels was negatively correlated with the expression of genes related to gut-barrier function such as tight junction protein 1 and 2, occludin and myosin light chain kinase (Fig. **42B**). In addition, these genes were downregulated in obese compared to normal weight subjects (Fig. **42C**). Collectively these data demonstrate that itaconate biosynthesis supports gut microflora alterations, thereby driving low-grade inflammation and obesity associated metabolic disturbances in mice.

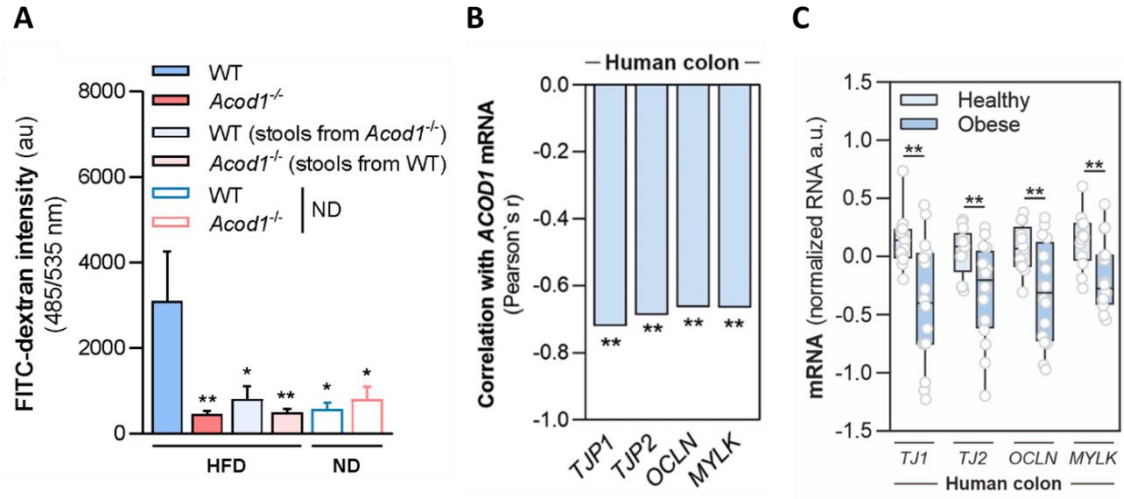

Figure 42. Effect and correlation of itaconate biosynthesis on gut permeability in mice and humans.

A*. Plasma FITC-dextran levels in ND-fed mice and in WT and Acod1-/- donor and recipient mice receiving either PBS (donors) or a fecal suspension from reciprocal genotypes (recipients) assessed after 18 weeks of feeding with HFD. Data as mean±s.e.m from n = 4 (ND), n = 7 (WT donor), n = 9 (Acod1-/- donor), n = 7 (WT recipient), and n = 8 (Acod1-/- recipient) mice from two independent experiments.* ***B****. Correlation analysis between mRNA of ACOD1 and the indicated genes in colon specimens of human obese (n = 16) subjects (GSE158237).* ***C****. mRNA levels of the indicated genes in colon of healthy (n=13) and obese (n=16) subjects (GSE158237). Boxes extend from 25th to 75th percentiles, black lines=median, whiskers=minimum to maximum. In A one-way ANOVA with Dunnett's multiple comparisons test compared with WT donor; *P < 0.05; **P < 0.01; ***P < 0.001; ns not significant.*

On the basis of data collected, we generated the working hypothesis illustrated in Figure 43.

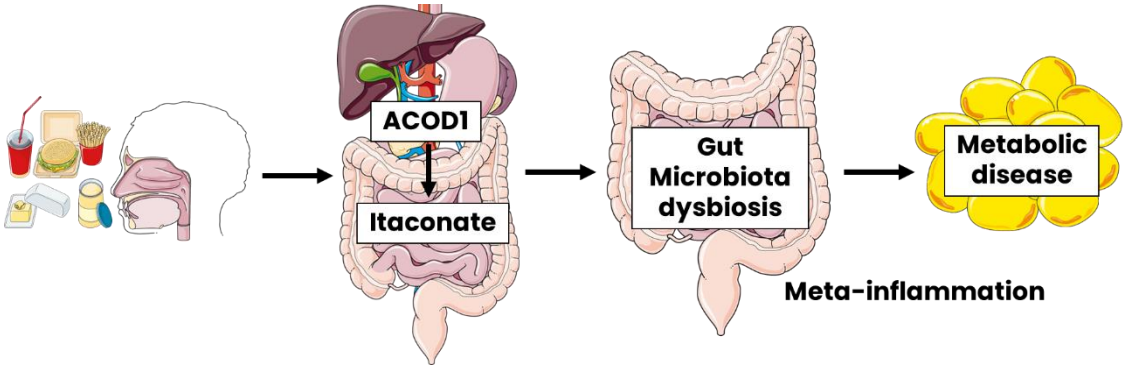

Figure 43. Working model
Created with Biorender

Acod1 loss protects against hepatocellular carcinoma development induced by Western diet

Liver cancer has been increasingly linked to obesity and NAFLD progression (Chen et al., 2012; Esposito et al., 2012; Lauby-Secretan et al., 2016). Indeed, hepatic dysfunctions induced by dietary lipid overload might promote the development of hepatocellular carcinoma. Despite protecting from obesity and associated comorbidities, it has been investigated whether genetic ablation of itaconate biosynthesis played a role in HCC development associated to diet-induced obesity. To this end, *Acod1*$^{-/-}$ mice have been administered with standardized Western diet (WD), containing high-fat, high-fructose and high-cholesterol, combined with a low dose of weekly peritoneal carbon tetrachloride (CCl_4) injections for 24 weeks, a condition promoting the progression of fatty liver to advanced fibrosis and HCC. This model mimics the histological, immunological and transcriptomic features of human disease (Tsuchida et al., 2018).

At the end of the experiment, mice underwent necroscopy and tumour burden was measured. Livers deriving from *Acod1* deficient mice showed a reduced tumour burden compared to their *wild type* counterparts (Fig. **44A**). In line with this, in response to WD/CCl_4 challenge, livers isolated from *wild type* mice were bigger compared to their *Acod1*$^{-/-}$ littermates (Fig. **44B**).

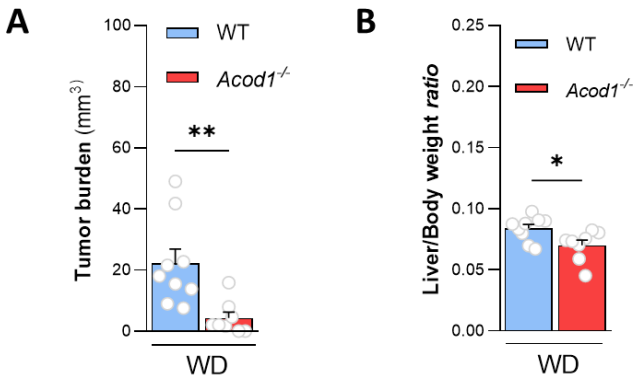

Figure 44. Acod1 loss protects against diet-induced HCC progression.
A*. Tumour burden measured in livers isolated from wild type and Acod1*$^{-/-}$ *mice fed with WD and injected with* CCl_4 *for24 weeks. Data as mean±s.e.m from ND-fed mice (n=4) and WD-fed mice (n=8) from one experiment.* ***B****. Liver/body weight ratio of mice treated as described in A. Data as mean±s.e.m from wild type (n=9) and Acod1*$^{-/-}$ *(n=8) from one experiment. In A, B: student t-test; *P < 0.05; **P < 0.01; ***P < 0.001; ns not significant.*

To determine whether *Acod1* was responsive to this treatment, *Acod1* expression was assessed in the malignant lesions originating in livers of *wild type* mice following WD/ CCl_4. As shown in Figure **45A,** the treatment determined an increase, although not significant, of *Acod1* mRNA level in the livers of *wild type* mice compared to their control littermates. Concomitantly, the increased *Acod1* expression was paralleled by a statistically significant heightened abundance of itaconate levels in the same livers as measured by LC-MS (Fig. **45B**).

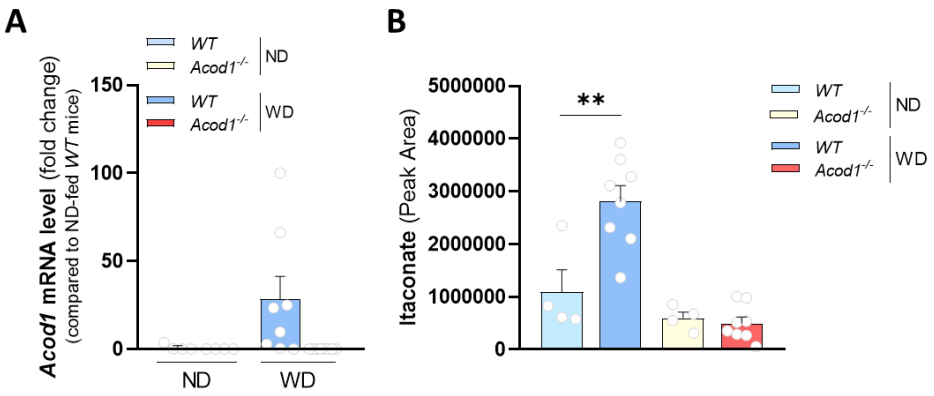

Figure 45. Acod1 is modulated by Western diet.
A*. Acod1 gene expression in livers isolated from wild type and Acod1$^{-/-}$ mice fed with WD and injected with CCl_4 for 24 weeks. Data as mean±s.e.m from ND-fed mice (n=4) and WD-fed mice (n=8) from one experiment.* ***B****. Itaconate abundance in livers of mice treated as described in A. Data as mean±s.e.m from wild type (n=9) and Acod1$^{-/-}$ (n=8) from one experiment. In A, B: student t-test; *P < 0.05; **P < 0.01; ***P < 0.001; ns not significant.*

Next, histological examination of liver sections stained with haematoxylin and eosin were performed to measure the impact of *Acod1* loss on diet-induced hepatic lipid accumulation. In line with the effect of genetic disruption of itaconate biosynthesis under HFD consumption, ablation of *Acod1* resulted in an obvious decrease in lipid droplets accumulating within hepatocytes following WD/ CCl_4 administration compared to their *wild type* littermates (Fig. **46A**). Since WD/ CCl_4 challenge has been reported to promote liver fibrosis, Sirius red staining on sections of liver specimens derived from experimental mice was performed. As shown in Figure **46B** and Figure **46C**, *Acod1* was dispensable in regulating the accumulation of the hepatic collagen deposition within livers of mice.

Overall, results collected so far, show that *Acod1* favours the development of obesity-induced HCC in mice.

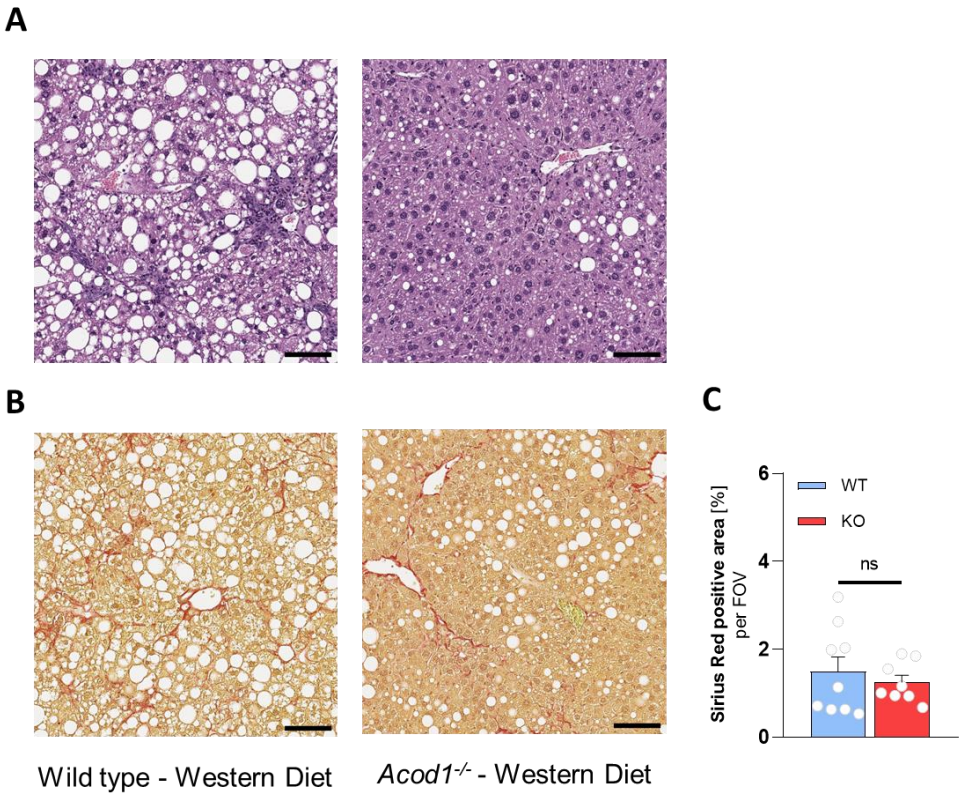

Figure 46. Impact of Acod1 loss on livers after WD/ CCl4 challenge.
***A**. Representative images of H&E staining of liver from wild type and Acod1$^{-/-}$ mice fed with WD and injected with CCl_4 for 24 weeks. **B**. Representative images of Sirius Red staining of livers of mice described as in (A). **C**. Quantification of hepatic collagen deposition in images described in Fig. 45B. Data as mean±s.e.m from ND-fed mice (n=4) and WD-fed mice (n=8) from one experiment, average of 5 images each). In C: student t-test; *P < 0.05; **P < 0.01; ***P < 0.001; ns not significant.*

Discussion

Obesity is a chronic condition characterized by the excessive accumulation of body fat, resulting from a sustained positive of energy balance (Hill et al., 2012; Redinger, 2007). Worldwide, obesity prevalence has reached epidemic dimensions becoming a major health concern due to the elevated risk of several medical conditions, including cardiovascular diseases and type 2 diabetes mellitus (T2DM). Moreover, one of the most common obesity-associated comorbidities is non-alcoholic fatty liver diseases (NAFLD), which ranges from abnormal hepatic lipid accumulation (steatosis) to non-alcoholic steatohepatitis (NASH) accompanied by inflammation and fibrosis, predisposing individuals to the development of hepatocellular carcinoma (HCC). As obesity progresses, excessive energy intake leads to adipose tissue dysfunction and, consequently, to ectopic lipid deposition in organs such as the liver and skeletal muscle. The dysregulated metabolism affecting central organs for glucose and lipid homeostasis paves the way for the development of a chronic low-grade inflammatory state, facilitating the onset of insulin resistance and disrupting the communication between central and peripheral pathways involved in maintaining energy balance and feeding behaviours. In addition, overnutrition negatively affects gut microflora, thus promoting dysbiosis of the intestinal ecosystem which, in turn, exacerbates inflammation and the obese phenotype. However, current therapeutic strategies against metabolic dysfunction associated with obesity show limited efficacy. **Therefore, understanding the adaptations of the metabolic machinery to nutritional perturbations induced by overnutrition might prevent life-threatening health conditions.**

The interplay of immune and metabolic responses to overnutritions is a well-established feature in the development of metabolic dysfunction associated with obesity (Saltiel & Olefsky, 2017). In this thesis, the role of itaconate, a molecule with potent immunomodulatory and anti-microbial properties, in the development of diet-induced obesity and associated comorbidities has been investigated. Specifically, itaconate is produced by the mitochondrial enzyme ACOD1 repurposing cis-aconitate from the tricarboxylic acid (TCA) cycle in response to inflammatory stimuli and infections, best described in macrophages (O'Neill & Artyomov, 2019; Scagliola et al., 2020; Ye et al., 2024b). Despite the anti-inflammatory role promoted by itaconate in several diseases, this work demonstrates that genetic disruption of itaconate biosynthesis offers protective

properties in diet-induced obesity and its major associated outcomes. In particular, *Acod1* deficiency mitigates the high fat diet (HFD)-induced alterations in systemic glucose homeostasis, hepatic steatosis, energy expenditure and meta-inflammation by preserving a healthy gut microbiota in mice. Thereby, this work unveils a novel and unexpected role of itaconate biosynthesis in the regulation of the systemic response to nutritional perturbations. Furthermore, this work highlights the initial, yet important, role of *Acod1* loss in the development of hepatocellular carcinoma in mice exposed to a hepatosteatotic diet, such as the Western diet, plus CCl_4 injections, paving the way for novel mechanisms underlying itaconate functions in the development of HCC.

To study the role of itaconate biosynthesis in the development of obesity and associated comorbidities, *Acod1* full-body knockout (*Acod1*$^{-/-}$) mice were challenged with a HFD containing 60% of calories from fat for 16 weeks, a condition sufficient to promote obesity and associated metabolic dysfunctions in *wild type* mice (Williams et al., 2014). Surprisingly, *Acod1* loss attenuated the body weight gain promoted by fat overnutrition compared to their *wild type* counterparts. In line with this, HFD-fed *Acod1*$^{-/-}$ mice exhibited lower accumulation of adiposity which was paralleled by attenuated adipocyte hypertrophy and brown adipose tissue (BAT) whitening with respect to *wild type* mice under the same dietary regimen. Also, *Acod1* deficiency opposes alterations in glucose homeostasis and insulin sensitivity elicited by fat overnutrition. Indeed, *Acod1*$^{-/-}$ mice exhibited lower fasting glycemia and insulinemia as well as an improved insulin response of peripheral tissues to intraperitoneal glucose overload compared to HFD-challenged *wild type* mice. To determine whether the protection against obesity and associated glucose dysfunctions observed in HFD-fed *Acod1*$^{-/-}$ mice was directly attributable to itaconate deficiency or to molecular pathways activated by enzyme deletion, near-physiologically relevant doses of itaconate were administered to HFD-fed *Acod1*$^{-/-}$ mice. As a result, itaconate administration reversed the effects of gene loss on body weight gain, adiposity and systemic glucose and insulin homeostasis, indicating that the protected phenotype was a consequence of itaconate itself. On a regular chow, genetic ablation of *Acod1* did not display any overt phenotype, maintaining overall body weight, glucose and insulin tolerance at comparable levels to *wild type* littermates. In support of this, a study conducted in 2004 demonstrated that administration of high doses of itaconate in normal

diet-fed rats neither elicited significant changes in weight nor altered their blood glucose levels under pair-feeding conditions. Moreover, a study published in 2024 reported similar findings, showing that C57BL6/J mice gavaged with itaconate for one month did not exhibit changes in body weight or fat mass when maintained on a regular diet (Z. Yu et al., 2024), demonstrating that itaconate per se is not sufficient to drive metabolic disease. In summary, these results demonstrate that disruption of itaconate biosynthesis protects mice from obesity and associated dysfunctions in glucose homeostasis when challenged with a fat diet.

The excessive energy intake leads to adipocyte dysfunction and subsequently ectopic lipid deposition in organs such as the liver. This paves the way for the development of a NAFLD, characterized by intrahepatic lipid accumulation, eventually accompanied by inflammation and fibrosis, which can ultimately progress into liver failure and HCC. Consistent with protection against obesity and alterations in systemic glucose homeostasis in response to HFD, *Acod1* deficiency mitigated hepatic steatosis by decreasing hepatic lipid accumulation, known to have causal roles in diet-induced hepatic insulin resistance (Magkos et al., 2012). In support of these results, proteomics data of liver specimens revealed that loss of *Acod1* counteracted the impact of dietary lipid overload on the hepatic proteome by impacting fatty acid biosynthesis and processing pathways in mice challenged with HFD but not after normal diet feeding. The impairment of the urea cycle, the metabolic route responsible for ammonia detoxification taking place primarily in the liver, due to hepatic fatty acid accumulation is well reported in NAFLD experimental models and patients (De Chiara et al., 2018). In line with this, *Acod1* ablation opposed the urea cycle dysfunctions induced upon dietary lipid overload in *wild type* mice, as demonstrated by proteomics and analytical chemistry-integrated approaches. Collectively, these results highlight the detrimental role of itaconate biosynthesis in the development of HFD-induced liver pathologies.

Since obesity arises from a long-term positive energy balance, it is crucial to investigate mechanisms influencing energy homeostasis. Firstly, it has been observed that the genotype did alter neither food intake, intestinal absorption capacity nor circulating leptin levels upon fat overnutrition in mice, which are often dysregulated in the obese state. Consequently, HFD-fed mice were subjected to indirect calorimetry by using Phenomaster metabolic cages to determine the impact of *Acod1* loss on their metabolic

activity. As a result, *Acod1* ablation protected mice from diet-induced obesity by stimulating energy expenditure. Importantly, this result was neither due to differences in preferential fuel supply utilization, as indicated by the unaffected respiratory exchange ratio, nor attributable to changes in spontaneous locomotor activity of mice. The obese state is characterized by derailed adipose tissue metabolism which affects whole-body metabolic health (Heinonen et al., 2020; Rosen & Spiegelman, 2014). Therefore, it was fundamental to explore the contribution of the adipose tissues to the higher metabolic rates imposed by *Acod1* deficiency upon HFD. Accordingly, transcriptional profiling after RNA-sequencing of the epididymal white adipose tissue (eWAT) showed that HFD impaired mitochondrial function and oxidative metabolic processes in *wild type* mice by downregulating the expression of genes involved in the TCA cycle, oxidative phosphorylation and fatty acid oxidation compared to normal diet-fed *wild type* controls. Moreover, fat overnutrition decreased the expression levels of genes involved in fatty acid catabolism and mitochondrial biogenesis in the BAT derived from *wild type* mice. Contrarily, these transcriptional changes were opposed by *Acod1* loss indicating that, upon fat overnutrition, disruption of itaconate biosynthesis played a key role in maintaining whole-body energy status by influencing adipose tissue metabolisms and mitochondrial function. In addition, BAT is a major contributor to energy expenditure due to the expression of uncoupling protein 1 (UCP1), an inner mitochondrial membrane protein dissipating energy stored in the mitochondrial electrochemical gradient as heat in a process called non-shivering (or adaptive) thermogenesis (X. Liu et al., 2022). By increasing UCP1 expression both at the transcriptional and protein level and by upregulating genes associated to non-shivering thermogenesis, *Acod1* ablation augmented energy expenditure in mice challenged with HFD. Moreover, *Acod1* deficiency opposed the HFD-induced changes in the expression levels of genes implicated in WAT browning, as retrieved by RNA-sequencing profiling of the iWAT of mice. Importantly, fatty acid catabolism and mitochondrial oxidative metabolism were not impacted by *Acod1* loss in muscles isolated from HFD-challenged mice. Collectively, these data demonstrated that genetic ablation of *Acod1* protects against diet-induced obesity by regulating energy dissipating processes in fat depots.

Fat overnutrition induces a systemic and persistent inflammatory state, which affects overall body energy balance. In line with the previous findings reported in literature

(Basler et al., 2006; Michelucci et al., 2013), *Acod1* responded consistently to LPS challenges *in vitro*. However, the epididymal white adipose tissues derived from *Acod1*$^{-/-}$ mice were characterized by lower infiltration of macrophages and emergence of crown-like structures, a hallmark of inflammation in obesity, compared to their *wild type* counterparts. Furthermore, *Acod1* loss decreased the transcriptional signature indicative of an inflammatory state observed in the adipose tissues deriving from *wild type* mice following dietary lipid overload. Beyond fat depots, *Acod1* loss attenuated systemic inflammation as demonstrated by reduced macrophage accumulation in the colon and decreased circulating pro-inflammatory cytokines in mice under fat overnutrition compared to their *wild type* counterparts. These findings were not in line with the well-established anti-inflammatory properties of itaconate in several clinical conditions (Ye et al., 2024a). Interestingly, recent studies have demonstrated that ACOD1 and itaconate biosynthesis might serve pro-inflammatory purposes, contradicting earlier findings in mouse models of sepsis. Specifically, the ACOD1/itaconate axis has been shown to worsen the outcomes of conditions such as polymicrobial sepsis and endotoxemia. Therefore, this shift in understanding adds complexity to its previously recognized immuneregulatory functions, revealing that its role may be context-dependent (Chen, Wu, et al., 2022; Wu et al., 2022). To elaborate on this, it was speculated that itaconate biosynthesis could facilitate systemic conditions promoting meta-inflammation in tissues, rather than simply suppressing immune cell activation. A key factor driving meta-inflammation in obesity and metabolic disease in the host is gut microbiota dysbiosis (Maslowski & MacKay, 2010; Scheithauer et al., 2020; Tilg & Kaser, 2011). In a healthy state, the gut microbiota regulates metabolism, immune function, and energy homeostasis (Hou et al., 2022b; Shreiner et al., 2015). However, factors like a high fat, low fiber diet or antibiotic use can disrupt gut microflora homeostasis (Lecuyer et al., 2021; Luck et al., 2015). An altered microbiota composition can lead to increased energy harvest from the diet, promoting weight gain and fat accumulation. Additionally, intestinal dysbiosis is associated with increased gut permeability, allowing bacterial endotoxins like lipopolysaccharides to enter the bloodstream (Shi et al., 2006), thus triggering a systemic inflammatory response, known as metabolic endotoxemia, which contributes to chronic low-grade inflammation. This further exacerbates insulin resistance and drives the progression of obesity and its related complications. Since itaconate is essential in

restricting replication of many microbes by regulating host-pathogen interactions (Brogi et al., 2021), itaconate levels were measured in stools from experimental mice. As a result, itaconate accumulated in the faecal matter of *wild type* mice subjected to a HFD, which paralleled the upregulation of *Acod1* mRNA levels in the large intestine compared to ND-fed *wild type* mice. Prompted by these data, the bacterial composition of faecal microbiota was profiled by using 16S ribosomal DNA to investigate whether *Acod1* deficiency might offer protection to diet-induced obesity through gut microbiota alterations. Several studies in literature reported that HFD decreases the *Bacteroidetes/Firmicutes* ratio, a microbial signature associated with obesity in both mice and humans (Ley et al., 2005; Parks et al., 2013; Turnbaugh et al., 2008). *Bacteroidetes* and *Firmicutes* are the two major phyla inhabiting the gut, with *Bacteroidetes* being associated with metabolic health and depleted in both obese rodents and humans (Ley et al., 2006; Sharma et al., 2018).Interestingly, genetic disruption of itaconate biosynthesis opposed this HFD-induced gut dysbiosis mainly by counteracting the decrease in the *Bacteroidetes* proportion. Unbiased analysis revealed that the most significantly increased bacterial family and genus in stools collected from *Acod1*$^{-/-}$ mice were *Bacteroidacae* and *Bacteroides*, respectively, which are frequently associated with a protection against obesity and type 2 diabetes (Jang et al., 2017; R. Liu et al., 2017; Palmas et al., 2021; Ridaura et al., 2013; J. Y. Yang et al., 2017). Moreover, the *Bacteroidetes* phylum has been considered one of the major producers of short-chain fatty acids (SCFAs), known to exert beneficial effects to the host (Agus et al., 2021; Ríos-Covián et al., 2016; Schroeder & Bäckhed, 2016; Truax et al., 2018a). In line with a less obesogenic microbial signature, *Acod1* loss rescued the levels of faecal SCFAs, decreased by dietary lipid overload in *wild type* mice. Importantly, SCFAs also preserve gut barrier integrity, thus preventing translocation of microbes and microbial products and obesity-associated inflammatory responses in the host caused by the increased intestinal permeability induced by diet-induced dysbiosis (Mariadason et al., 1997; Suzuki et al., 2008). In line with this, *Acod1* loss opposed the increased intestinal permeability promoted by fat overnutrition in *wild type* mice. Data retrieved from publicly available human colon datasets corroborate the results obtained in mouse studies, showing that the *ACOD1* mRNA levels negatively correlated with the expression of genes related to gut-barrier function such as tight junction protein 1 and 2, occludin and myosin light chain kinase and that these genes were

downregulated in obese compared to normal weight subjects. Taken together, these results point towards an amelioration of an obesity-associated intestinal ecosystem in the absence of *Acod1*. These findings were strengthened by the results obtained following administration of supraphysiological doses of itaconate (20mM) to *wild type* mice challenged with HFD. Specularly to *Acod1* loss, the increase of itaconate levels in HFD-fed *wild type* mice, beyond the levels endogenously produced, exacerbated the reduction in the abundance of *Bacteroidetes*, *Bacteroidaceae* and *Bacteroides* in stools compared to vehicle-treated controls. Consistent with a more obesity-like microbiome signature, itaconate supplementation enhanced obesogenic responses to HFD compared to controls. Based on these data and on the well-known anti-microbial functions of itaconate, *in vitro* experiments were conducted to address whether itaconate exerted a direct effect on the gut microflora. Firstly, faecal suspensions of pooled stools derived from HFD-fed *wild type* mice were treated with near-physiologically relevant concentration of itaconate (0.5-20 mM) in an anaerobic atmosphere. Interestingly, itaconate decreased the relative abundance of *Bacteroidetes*, *Bacteroidaceae* and *Bacteroides* in a dose-dependent manner compared to vehicle-treated controls. Furthermore, the *in vitro* growth of five pure bacterial strains representative of the *Bacteroidaceae* family, already reported to have beneficial roles against metabolic disease (Gauffin Cano et al., 2012; R. Liu et al., 2017a; López-Almela et al., 2021; Ridaura et al., 2013b; J. Y. Yang et al., 2017b; Yoshida et al., 2018), was inhibited by incubation with near-physiologically relevant concentration of itaconate (0.5 mM). This suggested that both the effect of gene loss and itaconate supplementation were reasonably attributable to a direct action of such molecule on these specific bacteria. Thus, it is conceivable that itaconate, once released into the intestinal lumen, can have a direct paracrine effect in skewing the balance among commensal bacteria in response to dietary changes.

To study the extent to which alterations in the gut microbiome due to disruption of itaconate biosynthesis account for resistance to diet-induced obesity a faecal microbiota transplantation experiment was conducted. Importantly, *Acod1* deficiency offered transferable protection against diet-induced obesity and associated comorbidities through amelioration of the intestinal ecosystem as demonstrated by our data. The transfer of faecal microbiota from HFD-fed *Acod1*$^{-/-}$ donor mice to *wild type* recipient mice provided protective effects against metabolic disease with respect to *wild type* donor mice.

Specifically, *wild type* recipients were characterized by a less pronounced obesity-associated microbial signature and thus by attenuation of adipose tissue accumulation, meta-inflammation, and obesity-associated metabolic dysfunctions at a level comparable to those measured in *Acod1*$^{-/-}$ donors. Notably, the genotype did not affect faecal bacterial composition of the experimental groups before the transplantation. **Taken together, such data demonstrate that the amelioration of the mouse gut ecosystem, influenced by HFD consumption, was not just the consequence of the protection from diet-induced obesity resulting from *Acod1* deficiency, but contributes causally to generate it.** Interestingly, the transfer of faecal microbiota from HFD-fed *wild type* donor mice to *Acod1*$^{-/-}$ recipient mice did not result in major changes in faecal microbiota composition and in the severity of metabolic disease, indicating that *Acod1* loss confers a dominant protective effect. This could be explained by an intrinsic resistance of the *Acod1*$^{-/-}$ hosts to the colonization of microbiota of *wild type* mice. A similar result has been obtained in different studies showing that one of the experimental groups exert resistance to gut microbiota colonization (either via FMT or co-housing of mice) (Chang et al., 2021; Laurans et al., 2018; Truax et al., 2018b). Consistent with this, no major differences were observed in the faecal microbiota composition of *Acod1*$^{-/-}$ recipients compared with *Acod1*$^{-/-}$ donor mice. It is reasonable to hypothesize that itaconate levels were insufficient to skew faecal microbiota composition of *Acod1*$^{-/-}$ recipient mice towards wild type profile, which is supported by the low levels of itaconate measured in stools of *Acod1*$^{-/-}$ recipient mice compared to those in *wild type* donors. Despite these data support this explanation, presently it is not possible to further explain the reasons of such colonization resistance. Overall, these data supported a novel role for itaconate biosynthesis in driving gut microflora composition towards an "obese-like" microbiota, causally contributing to diet-induced obesity in mice.

Recently, few studies have emerged reporting different findings compared to those presented in this thesis. A study led by Frieler and co-workers (Frieler et al., 2022) showed that genetic deficiency of *Acod1* did not elicit major changes on body weight but resulted in impaired glucose homeostasis in mice fed with HFD for a shorter time period (12 weeks) compared to the experimental settings implemented in this work (16 weeks). In addition, this study reported increased *Acod1* gene expression levels in adipose tissues

isolated from HFD-fed *wild type* mice. Furthermore, a study published in 2023 reported that *Acod1* deficiency aggravates NAFLD by modulating oxidative stress in livers via redox-sensitive AKT suppression in mice challenged with HFD for 14 weeks (X. Zhang et al., 2023). Differently to what have been reported by Frieler and colleagues, Zhang and co-workers showed that, upon HFD consumption, genetic ablation of *Acod1* exacerbates obesity and associated metabolic dysfunctions compared to their *wild type* counterparts. It is known that several factors can influence the experimental outcome of metabolic studies (Bastías-Pérez et al., 2020; Ericsson & Franklin, 2021). Therefore, the discrepancies observed can be explained by differences in the genetic background of mice, vivaria as well as other environmental conditions. It is worth noting that all these factors can directly affect the gut microbiota, thereby leading to inconsistent or conflicting results (Ericsson & Franklin, 2021). In 2023, Weiss and co-workers (Weiss et al., 2023) demonstrated that macrophage-derived itaconate modifies the oxidative profile and lipid metabolism of hepatocytes, thus exerting protective effects against NASH in mice utilizing the C57BL/6J substrain, differently from the mice used in this thesis (C57BL6N). Although C57BL6 mice are the most used mouse strain in biological studies, it is known that several genetically different substrains exist (Zurita et al., 2011), responding heterogeneously to experimental interventions such as HFD (Siersbæk et al., 2020). As an example, C57BL/6J are more glucose intolerant than the C57BL/6N background due to a functional deletion of exon 7–11 in the gene encoding nicotinamide nucleotide transhydrogenase (*Nnt*) (Nicholson et al., 2010). Moreover, NASH is induced by feeding mice with a high fat, high fructose and cholesterol-rich diet (Western diet) in combination with oral sucrose administration, known to induce a severe steatohepatitis in experimental models (Liang et al., 2018; Maretti-Mira et al., 2022; McGettigan et al., 2019), differently to the diet used in this thesis. Similarly, the lack of *Acod1* dampens Nrf2 activation, thereby aggravating liver fibrosis in mice treated with CCl4, a known hepatotoxic compound altering hepatic lipid metabolism and promotes HCC development (Fan et al., 2022). Therefore, the discrepancies observed in these studies can also be attributed to diet-dependent or nutrient-driven effects of itaconate. Furthermore, it is worth mentioning that Western diet can promote the pathogenesis of NASH through gut microbiota composition remodelling, indicating that those factors influencing gut microflora might impact the study outcome (M. Yang et al., 2023). It has been

demonstrated that itaconate ameliorates HFD-induced obesity and associated dysfunctions in glucose homeostasis in *wild type* mice treated with itaconate over a month (Z. Yu et al., 2024). Moreover, these data are corroborated by employing different obese mouse models, such as *ob/ob* and *db/db* mice, which lack functional leptin signalling. Specifically, itaconate counteracted obesity by enhancing thermogenic activation in BAT and increasing energy expenditure. It is worth noting that the experimental setting in this study with a short (5 weeks) but high dose (300 mg/kg/day) of intragastric itaconate treatment differed substantially to the approach used in this thesis (16 weeks, 20mM in drinking water). However, as discussed in this thesis, several factors could have contributed to the different outcomes reported in these studies compared to ours, suggesting that these discrepancies do not directly contradict our results.

Obesity is a major risk factor for NAFLD, a condition characterized by excessive fat accumulation in the liver, which can progress to NASH accompanied by fibrosis and to cirrhosis. The chronic liver inflammation and damage associated with NAFLD and NASH can ultimately progress into the development of HCC, the most common type of primary liver cancer and one of the leading causes of cancer-related deaths worldwide (Esposito et al., 2012; Kinsey & Lee, 2024; Sohn et al., 2021). As obesity rates continue to rise globally, the incidence of NAFLD and obesity-related HCC is increasing, highlighting the critical need for targeted interventions. Although ACOD1 has been found involved in several types of solid tumours, the connection between ACOD1 and HCC is still poorly understood. Recently, two papers have been published reporting a pro-tumorigenic role for the ACOD1/itaconate axis in hepatocarcinogenesis. In particular, Zhang and coworkers showed that ACOD1 promoted liver cancer development by induction of mitochondrial intrinsic apoptosis in hepatocytes in mice treated with N-nitrosodiethylamine (DEN) for 8 months (L. Zhang et al., 2023). Moreover, itaconate has been shown to promote HCC through induction of $CD8^+$ T cell exhaustion in the tumour microenvironment (Gu et al., 2023). In that work, Gu and colleagues performed three different orthotopic HCC mouse models: the hepatic portal vein injection of the murine hepatoma cell line Hepa1-6, the intraperitoneal injection of DEN plus carbon tetrachloride (CCl_4) and the hydrodynamic injection of plasmids containing the tumorigenic YAP^{5SA} in *wild type* and $Acod1^{-/-}$ mice. They observed that genetic ablation

of *Acod1* alleviated tumour burden compared to their *wild type* counterparts. Despite using a different mouse model for HCC tumorigenesis, preliminary results described in this thesis were in line with those reported in the literature. In particular, to study the role of obesity-induced HCC development, *Acod1* deficient mice have been administered with a standardized western diet (WD) combined with a low dose of weekly peritoneal carbon tetrachloride (CCl_4) injections for 24 weeks, a condition sufficient to promote the progression from fatty liver to advanced fibrosis and HCC. Importantly, this model mimics the histological, immunological and transcriptomic features of human disease (Tsuchida et al., 2018). After challenge with WD/CCl_4, *Acod1* loss protected mice against the development of HCC compared to their *wild type* counterparts. Furthermore, in line with data derived from the HFD experiments, *Acod1* ablation decreased liver weight and steatosis. However, no significant differences in liver fibrosis were measured. It is known that the gut microbiome might affect the development and progression of several cancers, including liver malignancies (Luo et al., 2022; Rajapakse et al., 2023). Regardless of the hepatocarcinogenesis mouse model used, HCC is reduced in gut-sterilised or germ-free mice (Schneider et al., 2022; Schwabe & Greten, 2020). Moreover, LPS-induced activation of toll-like receptors (Dapito et al., 2012; L. X. Yu et al., 2010), bile acid signalling (Yoshimoto et al., 2013) and SCFAs (Behary et al., 2021) have been linked to promoting HCC secondary to gut dysbiosis. Considering the effect of itaconate on gut microbiota phyla in obesity as previously described, it would be interesting to elucidate whether *Acod1* deficiency also affects tumour initiation and progression of HCC via modulation of the gut microbiota composition.

In conclusion, the results presented in this work support a novel role for itaconate biosynthesis in driving gut microflora composition towards an "obese-like" microbiota, causally contributing to diet-induced obesity in mice. Therefore, targeting ACOD1 can be a potential strategy to mitigate the inflammatory consequences of overnutrition. Indeed, it would be interesting to investigate the effects of small molecule inhibition of ACOD1 in diet-induced obese mice and one such molecule is citraconate, a naturally occurring itaconate isomer, which has been demonstrated to be the first occurring ACOD1 inhibitor (Chen, Elgaher, et al., 2022). Furthermore, data obtained in this thesis corroborate the existing literature reporting a detrimental role for itaconate in the development of HCC. As a result, additional studies will be necessary to unveil new

mechanisms by which itaconate influences HCC progression.

Materials and methods

Mice and treatments. Male C57BL/6 *Acod1*$^{-/-}$ (C57BL/6N-Acod1em1(IMPC)J/J) were bought from the Jackson Laboratory and bred in house. Mouse genotype was determined by amplification of DNA from tail biopsies by using Phire Tissue Direct PCR Master Mix (F170S, Thermo Scientific™) and allele-specific primers indicated by Jackson Laboratory (Table of primers). In experiments comparing *wild type* and *Acod1*$^{-/-}$ genotypes, experimental littermates were used and generated breeding *Acod1*$^{+/-}$ mice together. In experiments where only wild type littermates were used, they were generated by breeding *wild type* mice together. At weaning, all mice were separated according to the genotype and housed together in (at least two) different cages (multi-housed) until five weeks of age. Then, starting from five weeks of age, mice were individually caged, randomized, blindly allocated to experiment groups and fed with either a standard chow or high-fat diet (HFD) containing 60% of calories from fat (E15742-347, Charles River) for 16 weeks (if not otherwise stated throughout the main text or in each figure caption), with ad libitum access to water and food. For Western diet experiment, starting from five weeks of age, mice were individually caged, randomized, blindly allocated to experiment groups and fed with either a standard chow or Western diet (WD) (TD.120528, Envigo), containing high-fat, high-fructose and high-cholesterol, combined with a low dose of weekly intraperitoneal carbon tetrachloride (CCl_4) (289116, Sigma) injections for 24 weeks, with ad libitum access to water and food.

For itaconate treatments, mice received either 1 mM or 20 mM neutralized itaconate solution in drinking water ad libitum during HFD feeding, as indicated in the main text/figure captions. In all HFD-feeding experiments, body weight of mice was measured weekly. Tissues were collected at the end of each experiment for post-mortem analyses. The investigators were not blinded during experiments and outcome assessment.

RNA extraction and real-time qPCR. Total RNA from snap-frozen mouse tissues was extracted using TRIzol Reagent (15596026, Invitrogen) followed by purification by the ReliaPrep RNA Tissue Miniprep System (Z6111, Promega) according to manufacturer's instructions. For real-time qPCR analysis, total RNA was retro transcribed into complementary DNA using SuperScript VILO reverse transcriptase (11755-050, Invitrogen). cDNAs were mixed with PowerUp™ SYBR™ Green Master Mix (A25742, Applied Biosystems) and 200nM of both forward and reverse primers. A complete list of

all primers used, including the names and sequences, is reported in Table 1. qPCR was carried out using a CFX Connect Real-Time PCR System (BioRad) followed by melt curve analysis. The relative quantification of each mRNA was carried out with the comparative threshold cycle method using ribosomal protein S18 (*Rps18*) or β-actin (*Actb*) for normalization.

RNA-sequencing (RNA-seq). After RNA extraction, RNA integrity was confirmed by capillary electrophoresis (Fragment Analyzer, Agilent). Barcoded mRNA Libraries were prepared using NEBNext RNA Ultra II Directional Library Kit (New England Biolabs), following the manufacturer's instructions. Sequencing was performed on an Illumina NovaSeq instrument. The 3' adaptors were removed using cutadapt and trimmed reads with a length of less than 18bp were discarded. The trimmed reads were filtered with a contaminants database. The recovered nonmatching reads were aligned to the genome/transcriptome using STAR-align (v 2.4.2a) to the GENCODE reference genome build GRCm38.95. Genes with very low read counts were excluded from downstream analysis. The minimum threshold was set at 1 count per million mapped reads across all samples per tissue. Gene count tables were loaded into R (v 4.1.0) and differential gene expression analysis was performed using the DESeq2 workflow (Love et al., 2014). Row normalized z-scores of transcripts per million (TPMs) were used to plot the heatmaps.

Liver Proteomics. Frozen liver samples were powdered in liquid nitrogen using a ceramic mortar and pestle and lyophilized. Weighed tissue (approximately 2mg of each) was homogenized in freshly prepared high-salt buffer (50mM Tris-HCl, 3M NaCl, 25mM EDTA, 0.25% w/v CHAPS, pH 7.5) containing 1x protease inhibitor (Halt Protease Inhibitor, Thermo Scientific) at a concentration of 10mg/mL. Homogenization took place in a bead beater (Bullet Blender Storm 24, Next Advance, 1mm glass beads) for 3min at 4ºC. Samples were then spun for 20min at 18,000g at 4ºC and the supernatant removed and stored as Fraction 1. A fresh aliquot of high-salt buffer was added to the remaining pellet at 10mg/mL of the starting weight, vortexed at 4ºC for 15min, and spun for 15min. The supernatant was removed and stored as Fraction 2. This high-salt extraction was repeated once more to generate Fraction 3, after which freshly prepared guanidine extraction buffer (6 M guanidinium chloride adjusted to pH 9.0 with NaOH) was added at 10mg/mL and vortexed for 1h at RT. The samples were then spun for 15min, the supernatant removed and stored as Fraction 4. Fractions 1, 2, & 3 were combined, and all

fractions were stored at -20ºC until further analysis. Samples were digested according to the FASP protocol using a 10kDa molecular weight cutoff filter. In brief, 50ul of the samples were mixed in the filter unit with 8 Murea, 100mM ammonium bicarbonate (AB) pH 8.0, and centrifuged at 14 000g for 15min. The proteins were reduced with 10mM DTT for 30min at RT, centrifuged, and alkylated with 55mM iodoacetamide for 30min at RT in the dark. Following centrifugation, samples were washed 3× with urea solution, and 3× with 50 mM AB, pH 8.0. Protein digestion was carried out with sequencing grade modified Trypsin (Promega) at 1/50 protease/protein (wt/wt) at 37°C overnight. Peptides were recovered from the filter using 50mM AB. Samples were dried in Speed-Vac and desalted and concentrated on Thermo Scientific Pierce C18 Tip. A 20ul of each sample was loaded onto individual Evotips for desalting and then washed with 20µL 0.1% FA followed by the addition of 100µL storage solvent (0.1% FA) to keep the Evotips wet until analysis. The Evosep One system (Evosep, Odense, Denmark) was used to separate peptides on a Pepsep column, (150µm inter diameter, 15cm) packed with ReproSil C18 1.9 um, 120A resin. The system was coupled to the timsTOF Pro mass spectrometer (Bruker Daltonics, Bremen, Germany) via the nano-electrospray ion source (Captive Spray, Bruker Daltonics). The mass spectrometer was operated in PASEF mode. The ramp time was set to 100 ms and 10 PASEF MS/MS scans per topN acquisition cycle were acquired. MS and MS/MS spectra were recorded from m/z 100 to 1700. The ion mobility was scanned from 0.7 to 1.50 Vs/cm2. Precursors for data-dependent acquisition were isolated within ± 1 Th and fragmented with an ion mobility-dependent collision energy, which was linearly increased from 20 to 59 eV in positive mode. Low-abundance precursor ions with an intensity above a threshold of 500 counts but below a target value of 20000 counts were repeatedly scheduled and otherwise dynamically excluded for 0.4 min. MS/MS spectra were extracted from raw data files and converted into .mgf files using MS Convert (ProteoWizard, Ver. 3.0). Peptide spectral matching was performed with Mascot (Ver. 2.5) against the Uniprot mouse database (release 201701). Mass tolerances were +/- 15ppm for parent ions, and +/- 0.4 Da for fragment ions. Trypsin specificity was used, allowing for 1 missed cleavage. Met oxidation, Pro hydroxylation, protein N-terminal acetylation, and peptide N-terminal pyroglutamic acid formation were set as variable modifications with Cys carbamidomethylation set as a fixed modification. Scaffold (version 4.6, Proteome Software, Portland, OR, USA) was used to validate

MS/MS based peptide and protein identifications. Peptide identifications were accepted if they could be established at greater than 95.0% probability as specified by the Peptide Prophet algorithm. Protein identifications were accepted if they could be established at greater than 99.0% probability and contained at least two identified unique peptides. Total peptide hits were normalized via auto scale normalization and statistical analysis was performed using MetaboAnalyst 5 (Pang et al., 2022) to assess differentially expressed proteins between biological groups. Row normalized z-scores of peptide hits were used to plot the heatmaps.

Functional Enrichment Analyses. Over-representation analyses (ORA) of RNA-sequencing and proteomics data were performed with Shiny-GO 0.76 (Ge et al., 2020) by using Gene Ontology (GO) terms (Ashburner et al., 2000) and KEGG (Kanehisa et al., 2021). Only differentially expressed genes/proteins in response to HFD and rescued by Acod1 loss with an adjusted P value (FDR) <0.1 in both comparisons were considered. No threshold was set on the fold change as some of the genes/proteins might show moderate, yet biologically relevant changes.

Metabolite extraction and LC-MS. For metabolite determination, 40 mg of frozen tissue was dissociated in 1ml of ice-cold extraction solution, composed of methanol, acetonitrile, and water (5:3:2), using ceramic beads and a Precellys tissue homogenizer (Bertin Instruments) by 3 cycles of oscillations at 8000 RPM (45 seconds each paused by 30-second intervals) at 4ºC. After centrifugation (16,000g for 30min at 4°C), the supernatants were analysed by liquid chromatography-mass spectrometry (LC-MS) by using a Q Exactive Orbitrap mass spectrometer (Thermo Fisher Scientific) coupled with a Thermo Fisher Scientific Accela HPLC system, as previously described (Torretta et al., 2020). Data were acquired and analyzed with Thermo Xcalibur and Thermo LCquan 2.7 (Thermo Fisher Scientific) software, respectively. Absolute quantification of itaconate levels in stools of mice was determined by sample peak areas comparison to reference standards.

For measurements of free fatty acids in liver samples, an ultra-high pressure-liquid chromatography-mass spectrometry (UHPLC-MS – Vanquish and Q Exactive, Thermo Fisher) was used as previously reported (Nemkov et al., 2015). Briefly, liver samples were extracted in ice cold methanol:acetonitrile:water (5:3:2 v/v/v) at a concentration of 15mg/mL. Glass beads (1.0mm, BioSpec Products Inc. cat.# 11079110) were added to

each sample and samples were placed in the bead beater (GenoGrinder; SPEX, Metuchen, NJ) for 5 minutes at level 5 at 4°C. Samples were then vortexed for 30min at 4°C and centrifuged at 18,213 g for 10min at 4°C. Supernatants were processed for metabolomics analyses. Five microliters of sample extracts (diluted to 15mg/ml in extraction solution) were loaded onto a Kinetex XB-C18 column (150 × 2.1 mm i.d., 1.7 μm – Phenomenex). A 5 min gradient (5%–95% B, phase A: water + 0.1% formic acid and phase B: acetonitrile with + 0.1% formic acid for positive ion mode; 0%–100% B, phase A: 5% acetonitrile + 5mM ammonium acetate and phase B: 95% acetonitrile + 5mM ammonium acetate for negative ion mode) were used to elute metabolites. The mass spectrometer scanned in Full MS mode at 70,000 resolution in the 65–975 m/z range, 4 kV spray voltage, 45 sheath gas and 15 auxiliary gas, operated in negative and then positive ion mode (separate runs). Fatty acids assignment was performed against an in-house standard library, as reported (Nemkov et al., 2015, 2019).

Diglyceride profiling. Liver samples were collected and diglyceride profiling was performed via ultra-high pressure-liquid chromatography-mass spectrometry (UHPLC-MS – Vanquish and Q Exactive, Thermo Fisher Scientific). Briefly, liver samples were extracted in 100% ice cold methanol at a concentration of 15mg/mL of buffer. Glass beads were added to each sample and samples were placed in the bead beater (Bullet Blender Storm 24, Next Advance, 1mm glass beads) for 5 minutes at level 5 at 4°C. Samples were then vortexed for 30min at 4°C and then centrifuged at 18,213 g for 10 min at 4°C. 40uL of the sample extract and 40uL of 10mM ammonium acetate were then added to an autosampler vial. Five microliters of sample extracts were loaded onto a Acquity HSS T3 column (150 x 2.1mm i.d., 1.8μm). A 17 min gradient (25%-99% B, phase A: 75:25 water:acetonitrile + 5mM ammonium acetate, phase B: 50:45:5 isopropanol:acetonitrile:water + 5mM ammonium acetate) was used to elute the metabolites. The mass spectrometer scanned in Full MS mode at 70,000 resolution in the 150-1500 m/z range, 4 kV spray voltage, 45 sheath gas and 15 auxiliary gas, operated in negative mode. Metabolite assignment was performed against an in-house standard library, as reported (Nemkov et al., 2015, 2019).

Measurement of liver triglycerides and NH3. Triglycerides and NH3 levels were determined colorimetrically in 10mg of frozen liver tissues by using the Triglyceride Assay Kit (ab65336, Abcam) and Ammonia Assay Kit (ab83360, Abcam), respectively,

following manufacturer's instructions.

SCFA measurement. For short chain fatty acids (SCFA) measurement, 10mg of stools were homogenized in 400µl methanol-water (1:1, v/v) using ceramic beads and a Precellys tissue homogenizer (Bertin Instruments) by 3 cycles of oscillations at 8000 RPM (45 seconds each paused by 30-second intervals) at 4ºC. After centrifugation (16,000g for 15min at 4 °C), 200µl of the supernatants were transferred to a new microfuge tube and dried by SpeedVac. Dried tissue extracts were resuspended in 240µl of water and derivatized as previously reported (Tumanov et al., 2016). Briefly, each sample was mixed with 50µl of 1-propanol (34871, Sigma-Aldrich) and 50µl of pyridine (360570, Sigma-Aldrich) and incubated on ice for 5min. Then, 100 µl of 1 M sodium hydroxide was added, immediately followed by 30µl of methyl chloroformate (M35304, Sigma-Aldrich) and vigorous vortexing for 20s. Then, each sample was mixed with 300µl of methyl tert-butyl ether (650560, Sigma-Aldrich), vortexed for another 20 sec and centrifuged at 10,000g for 5min. 200µL microliters of the resulting upper layer was transferred to a gas-chromatography (GC) vial for analysis. Propyl derivatives of propionate and butyrate were analysed using an Agilent 7000 GC/MS provided with an Agilent 7890 GC chromatograph and 7693 autosampler (Agilent, CA, United states). High purity helium (99.999%) was the carrier gas with a column head pressure of 16.3 psi. The total flow and the septum purge flow rates were 24.9ml/min and 3mL/min, respectively. Injector was set at a temperature of 280 °C. Injection was made at an injection volume of 1µL in the split mode with a split ratio of 10:1. The chromatographic separation was performed on a Zebron ZB-1701P GC capillary column 30m X 0.25mm X 0.25µm film thickness (Cat. No. 7HG-G012-11, Phenomenex, CA, U.S.A). The oven temperature was set to 70°C initial temperature held for 2 min followed by a linear increase to 140°C at 10°C/min, followed by a more rapid increase to 182°C (held for 1 min) at 20°C/min then to 280°C at 50°C/min. The total run time was 16 minutes. The MS was operated in electron ionization (EI) mode at 70 eV and the interface was set to 300°C. Data was acquired in full scan made over the range of m/z = 25-200 with a scan time of 300ms. MS recording started at a cut-off of 1min. Data processing was performed using Agilent MassHunter Quantitative analysis software (Agilent, CA, United states). Initial compound annotation was performed by searching against NIST11 mass spectral library (National Institute of Standards and Technology, Gaithersburg, MD). The identity of the

propyl derivatives was further confirmed by comparison to reference standards using a combination of retention time and fragmentation pattern. Selected fragments were used for the quantitation of the propyl derivatives, which were 75.1 and 71.1 for propyl propionate and butyrate, respectively. The respective retention times were 3.55, and 4.95min.

Histology and image analyses. Formalin-fixed (HT501128, Sigma-Aldrich) paraffin-embedded sections were dewaxed and hydrated through graded decrease alcohol series. For histological analysis, slides were stained using standard protocols for Hematoxylin and Eosin (Mayer's Hematoxylin, BioOptica #05-06002/L and Eosin, BioOptica #05-10002/L). For immunohistochemistry (IHC), slides were immunostained with Automatic Leica BOND RX system (Leica Microsystems GmbH, Wetzlar, Germany). Antigen-retrieval was performed using sodium citrate or EDTA buffer at 100°C. For primary antibodies anti-F4/80 (dilution 1/500; F4/80 (D2S9R), Cell Signaling Technology, Inc.) and anti-UCP1 (1/500; ab10983, Abcam) antigen-retrieval was performed for 20 minutes at 100°C using sodium citrate buffer. For anti-CD8α (dilution 1/200; D4W2Z, #98941 Cell Signaling Technology, Inc.), anti-CD4 (dilution 1/100; D7D2Z, #25229 Cell Signaling Technology, Inc.) and anti-MPO (dilution 1/1000); EPR20257, ab208670, abcam) antigen retrieval was performed using EDTA buffer for 20 minutes at 100°C. The signals were developed with the Bond Polymer Refine Detection (Leica, DS9800). Bright-field images were acquired with an Aperio AT2 digital scanner (Leica Biosystems) and Aperio ImageScope software (v12.4.3.5008, Leica Biosystem). Image analysis was performed using ImageJ. Adipocyte size from WAT was determined using the Adiposoft plugin (Galarraga et al., 2012) (n=5 per group with an average of 5 images per tissue) and the F4/80 positive areas were quantified by binarization after colour deconvolution (n=3 per group with an average of 5 images per tissue). In BAT, lipid droplet particles were determined using thresholding and by applying limits for particle size and circularity to avoid inclusion of non-lipid droplet structures (n=3-4 per group with an average of 10 images per tissue). The UCP1 positive areas were determined by thresholding and normalized to the cell number (n=3 per group with an average of 3 images per tissue) per field of view. For livers, Sirius red stained images were color separated and the green channel was utilized for determining the Sirius red positive area via thresholding (*wild type* n = 9, *Acod1*$^{-/-}$ n = 8, 10 images per sample). For determining

the positively stained area after immunohistochemistry in liver sections, images were color deconvoluted (vectors=[H DAB]) and the positive area quantified via thresholding (n = 6 mice per group, 10 images per samples.

Glycemia and insulinemia determination. Blood was collected from the tail of overnight-fasted mice. Then, glucose and insulin levels were determined by using a handheld glucometer (Contour XT Meter, Ascensia Diabetes Care Italy) and a precoated ELISA Kit (EMINS, Invitrogen), respectively, according to the manufacturer's instructions.

Glucose and insulin tolerance test. For glucose-tolerance test (GTT), mice were fasted overnight before receiving an intraperitoneal injection of glucose solution (2g of glucose per kg body weight). For insulin tolerance test (ITT), mice received an intraperitoneal injection of insulin solution (0.75U of insulin per kg body weight) after 6-hours fasting. For both GTT and ITT, glycemia was determined at the indicated time points as above described.

Indirect calorimetry and activity measurements. Measurements of oxygen consumption (VO2), carbon dioxide (CO2) production, respiratory exchange ratio, energy expenditure, food intake and locomotor activity were performed using open-circuit indirect calorimetric chambers (PhenoMaster, TSE Systems, Bad Homburg, Germany). Mice were individually caged, fed with a HFD and acclimated to the chambers for 36h before experimental recordings. Calorimetric data show the average of 6 days or 6 nights. Energy expenditure and VO2 were calculated using the manufacturer's software and values were corrected for body mass. Total locomotor activity was measured using a 3-dimensional infrared light-beam.

Determination of total faecal energy excretion. Faecal energy content, used as a proxy for intestinal nutrient absorption capacity, was determined in 0.5g of frozen stools isolated from HFD-fed mice by bomb calorimetry (Phenomin facility).

16s ribosomal DNA gene sequencing and analysis. Total DNA was extracted from faecal samples of ND and HFD-fed mice using the QIAamp PowerFecal Pro DNA Kit (Qiagen), following manufacturer's instructions. The V3-V4 region of the 16s rRNA gene was amplified starting from 500ng of extracted DNA using the AccuPrime Taq DNA Polymerase (Invitrogen), the following primers: V3-16S-Fw: TCG TCG GCA GCG TCA GAT GTG TAT AAG AGA CAG CCT ACG GGN GGC WGC AG; V4-16S-Rev: GTC

TCG TGG GCT CGG AGA TGT GTA TAA GAG AGA CAG GAC TAC HVG GGT ATC TAA TCC; and the amplification protocol: 94°C for 2 min., 35 cycles of 94°C for 30sec, 56°C for 30sec, and 68°C for 1min and finally stored at 4°C. Amplicons were purified using the AMPure XP beads (Beckman Coulter, Brea, USA). A second PCR step was performed for indexing and add Illumina sequencing adapters to each sample. The Nextera XT Index Kit (Illumina) and the KAPA HiFi HotStart PCR Kit (KAPA Biosystem) were used following the amplification protocol: 95°C for 3min, 8 cycles of 95°C for 30sec, 55°C for 30sec, 72°C for 30sec, 72°C for 4min and then stored at 4°C. A second purification step with AMPure XP beads was performed to clean up the samples for preparing the final library. Purified DNA is quantified using the Qubit double-stranded DNA (dsDNA) HS Assay Kit on a Qubit 2.0 Fluorometer (Thermo Fisher) and then diluted and pooled following Illumina protocol. Sequencing is performed using the MiSeq Illumina platform with a 600 (2 X 300)-base pairs (bp) paired-end read protocol.

For the metagenomic profiling of the small intestines isolated from HFD-fed *wild type* and *Acod1*$^{-/-}$ mice, total DNA was extracted from small intestine samples of mice using the DNeasy Blood & Tissue Kits (Qiagen), following the manufacturer's instructions with these modifications: 180 uL of ATL and 20 uL of Proteinase K were added to a small piece of intestine and incubated for 10h at 56°C at 600 RPM in a thermomixer compact (Eppendorf). The DNA was lastly eluted in 60 uL of Buffer AE after an incubation of 5 minutes. Then, the V3-V4 region of the 16s rRNA gene was amplified starting from 500 ng of extracted DNA as described above. Amplicons were purified and sequenced using the MiSeq Illumina platform with a 600 (2 X 300)-base pairs (bp) paired-end read protocol as described above.

For all metagenomics analyses, FastQ files were processed using the Divisive Amplicon Denoising Algorithm 2 (DADA2) (Callahan et al., 2016) pipeline (version 1.26.0) to de-noise the sequences, remove chimeras and assign amplicon sequence variants (ASVs) using standard quality filter parameters (maxN=0, maxEE=2, truncQ=2, rm.phix=TRUE) and trimming 25 and 75 bases of the 3′ region of the forward and reverse reads, respectively. Taxonomic classification was performed implementing a naive Bayesian classifier approach using the Greengenes 13.8 database. Lowly abundant microbial taxa with a relative abundance of less than 0.01% in less than 75% of the samples were excluded from downstream analyses. Differential abundance analysis was performed

using the DESeq2 workflow (Love et al., 2014) on taxonomic levels and accurate estimation of log-fold changes was performed using the apeglm shrinkage estimator (version 1.20.0) (Zhu et al., 2019).

Treatment of faecal bacterial cultures with itaconate. Bacterial cultures were performed starting from faecal pool derived from 6 HFD-fed *wild type* mice. Each pool was resuspended and homogenized in 1.5 mL of BBL™ Brain Heart Infusion (BHI) culture medium (Becton, Dickinson and Company, BD) and then centrifuged for 2 minutes at 840Xg with Prism™ microcentrifuge (Labnet). One hundred microliters of obtained supernatants were transferred in four BHI vials containing 0.5, 1, 10 and 20 mM itaconate, respectively. One BHI vial supplemented with phosphate saline buffer was used as control of bacterial growth. All vials were placed at 37 °C in AnaeroJar 2.5 L Jar System (OXOID) and using Thermo Scientific™ Oxoid™ AnaeroGen™ 2.5L Sachet (Fisher Scientific) to generate an anaerobic atmosphere. Three samplings of 500 µL were carried out every two days from each vial and, finally, extraction of genetic material and sequencing were performed as described above.

Treatment of pure bacterial cultures with itaconate. The antimicrobial effect of the itaconate was tested on five pure bacteria strains belonging to *Bacteroidaceae* family (*Bacteroides* genus) obtained from DSMZ: *Bacteroides acidifaciens* (DSM 15896), *Phocaeicola vulgatus* (DSM 1447), *Phocaeicola dorei* (DSM 17855), *Bacteroides thetaiotaomicron* (DSM 2079) and *Bacteroides uniformis* (DSM 6597). Briefly, the freeze-dried bacteria pellets were rehydrated using 500ul of BBL™ Brain Heart Infusion (BHI) culture medium (Becton, Dickinson and Company, BD). To identify a single culture medium suitable for all the strains of interest, preliminary experimental growths were performed using 3 liquid media (BHI, Columbia, and Columbia supplemented with 5% defibrinated sheep blood). The Columbia medium allowed the growth of all bacteria tested and therefore it was chosen for next experiments. To test the effects of itaconate on the different strains, all bacteria were cultured in Columbia medium and 24h after colony inoculum, 50uL of bacterial suspensions were grown in 5mL of fresh Columbia medium either in the presence or absence of 0.5mM itaconate for further 24h at 37°C in anaerobic condition (in AnaeroJar 2.5 L Jar System (OXOID) with Thermo Scientific™ Oxoid™ AnaeroGen™ 2.5L Sachet (Fisher Scientific)). At the end of the experiment, bacteria abundance in all cultures was determined spectrophotometrically by measuring

absorbance (OD) at 600 nm by the Multiskan Go, Thermo Scientific™ (Fisher Scientific).

Plasma metabolic hormones and cytokines determination. Circulating levels of GLP-1, resistin, Leptin, TNF, IL-1B, and IL6 were determined by multiplex bead-based assay (Eve Technologies, Calgary, AB, Canada).

Measurement of intestinal permeability. Gut permeability was determined using the fluorescein isothiocyanate (FITC)–dextran assay. In brief, mice fed with HFD for 18 weeks were fasted for 4h and orally gavaged with 300mg/kg 4kDa FITC dextran (FD4-100MG Sigma-Aldrich) solubilized in sterile PBS. Four hours later, approximately 80µl of blood was collected and the relative levels of FITC dextran in plasma diluted 1:10 in PBS were measured by fluorescence spectroscopy (excitation at 485nm and emission at 535nm).

Measurement of faecal bacterial abundance. The content of bacteria in stools of mice was determined by quantitative PCR of the gene encoding bacterial 16S rRNA (Yao et al., 2022). Briefly, DNA was extracted from equal amount of faecal material derived from *wild type* and *Acod1*$^{-/-}$ mice before and at the end of antibiotics treatment, by the QIAamp PowerFecal Pro DNA Kit (Qiagen) following the manufacturer's instructions. For real-time qPCR analysis, the variable regions 3 and 4 (V3–V4) of 16S ribosomal ribonucleic acid (rRNA) gene were amplified starting from extracted genetic material. Amplification primers used were 16S_FW: TCG TCG GCA GCG TCA GAT GTG TAT AAG AGA CAG CCT ACG GGN GGC WGC AG and 16S_Rev: GTC TCG TGG GCT CGG AGA TGT GTA TAA GAG ACA GGA CTA CHV GGG TAT CTA ATCC. SYBR Green PCR Master mix (Applied Biosystem) and the following cycling conditions were used: 95°C for 2 min, 45 cycles of (95C for 20'', 56°C for 20'' and 72°C for 30''), 72° for 10 min. qPCRs were carried out using a 7900HT Fast Real-Time PCR System (Applied Biosystem). Serial dilutions of DNA from the E. coli DH5a strain were used as standard for absolute quantification of bacterial load in each sample.

Faecal microbiota transplantation. For faecal microbiota transfer (FMT), 5-week-old male *wild type* and *Acod1*$^{-/-}$ littermates were randomly divided in two groups: donors and recipients. Before the transplantation, recipient mice only were treated with a broad-spectrum antibiotic cocktail (50 µg/ml Streptomycin, 100 U/ml Penicillin) in drinking water for 3 days to lower existing microbiota and favour the following engraftment of donor microbiota, as previously described (Bokoliya et al., 2021c). Soon after antibiotics

removal, HFD feeding was started for all mice. Starting from the first day of HFD administration and throughout the whole experiment (18 weeks), recipient *wild type* and *Acod1*$^{-/-}$ mice were gavaged daily (4 consecutive times per week) with 200µl of a faecal slurry prepared by pooling stools freshly collected from their counterparts of reciprocal genotype in the donor group. As control, donor mice instead received 200µl of sterile PBS by oral gavage daily (4 consecutive times per week). In detail, faecal slurries were prepared by grinding stools pooled from either *wild type* or *Acod1*$^{-/-}$ donor mice in sterile PBS at the concentration of 100mg/ml. The slurries were then centrifuged at 300g for 2 min to discard insoluble materials and the supernatants used for gavaging recipient mice, as above described. Collection of stools, preparation of faecal slurries and mouse gavaging procedures were conducted under sterile conditions (under laminar flow hood).

***In vitro adipogenesis assay*.** Pre-adipocytes were isolated from iWAT collected from 8-week-old *wild type* and *Acod1*$^{-/-}$ mice fed with normal diet and digested in DMEM/F12 (D8437, Merck) supplemented with 100U/ml penicillin, 100mg/ml streptomycin and 1mg/ml collagenase IV (17104-019, Gibco) for 30min at 37°C by shaking. The cell suspension was filtered through a 70µm cell strainer and centrifuged 8min at 500g. Supernatant was removed and the pellet incubated with ACK Lysing Buffer (A10492-01, Gibco) for 5min at RT. Pre-adipocytes were resuspended in DMEM/F12 supplemented with 10% FBS, 4mM L-glutamine, 100U/ml penicillin and 100mg/ml streptomycin, seeded in 24-well plates (30,000 cells per well) and grown to confluence. Culture medium was replaced with differentiation medium containing 1µM dexamethasone (190040, MP Biomedicals), 0.5mM IBMX (I5879, Merck), 1µM rosiglitazione (R2408, Merck) and 5µg/ml insulin (Merck, I9278). After 72h, medium was replaced with medium containing 1µM rosiglitazione and 5µg/ml insulin. After 5 days cells were washed with PBS and lysed for RNA extraction or fixed with formalin solution (HT501128, Sigma-Aldrich) for 15min and stained with 0.3% Oil-Red-O solution (O1391, Sigma-Aldrich) for 15min. Air dried samples were destained with isopropanol and absorbance was measured at 490nm using a microplate reader (Bio-Rad) to determine lipid content.

***Generation and treatment of BMDMs*.** Bone marrow (BM)-derived macrophages (BMDMs) were prepared from 5-week-old CO2-euthanized C57BL/6N *wild type* and *Acod1*$^{-/-}$ mice as previously reported (Torretta et al., 2020). At the end of the differentiation, cultured BMDMs were stimulated with 100 ng/ml LPS (Enzo Life

Sciences) for 24h or with 2.5mM ATP for 40min after priming with LPS for 24h for inflammasome activation.

Enzyme-linked immunosorbent assay (ELISA). IL-1β concentrations and IL-6 levels in BMDMs culture medium were determined using IL-1 beta (88701376, Invitrogen) or IL-6 (88-7064-22, Invitrogen) mouse-uncoated ELISA Kits, respectively, according to the manufacturer's instructions. Absorbance was measured at a wavelength of 450nm, subtracting the values measured at 570nm, using a microplate reader (Bio-Rad).

Human datasets. The microarray GSE158237 (Garcia-Irigoyen et al., 2021) dataset integrates RMA normalized mRNA expression values from colonic biopsies and clinical data of human subjects with different degrees of body mass index (BMI). Healthy (BMI < 25 kg/m2, n = 13) and obese (BMI > 30 kg/m2, n = 16) subjects were included in the analysis. To correlate colonic ACOD1 mRNA levels and tolerance to glucose overload, relative changes in plasma glucose levels measured 2 h after bolus glucose administration were compared with their baseline levels. The RNAseq dataset GSE130970 (Hoang et al., 2019) contains transcriptomic profiles of 78 distinct human liver biopsies. Of these, 6 are histologically normal and 72 cover the full spectrum of non-alcoholic fatty liver disease (NAFLD) (assessed by NIDDK NASH CRN criteria (D. E. Kleiner et al., 2005). In both studies, data were tested for normality (Ashburner et al., 2000; Bokoliya et al., 2021c; Callahan et al., 2016; Galarraga et al., 2012; Ge et al., 2020; Kanehisa et al., 2021; Love et al., 2014; Nemkov et al., 2015, 2019; Pang et al., 2022; Torretta et al., 2020; Tumanov et al., 2016; Yao et al., 2022; Zhu et al., 2019).

Ethical approval of animal studies. All mice used in this study were bred and housed in individual ventilated cages in a barrier facility proactive in environmental enrichment under specific pathogen-free conditions in line with European Union regulations. All experimental animal procedures were approved by the Institutional Animal Committee of San Raffaele Scientific Institute.

Statistics and reproducibility. For each experiment, sample size was chosen based on similar experimental approaches reported in the literature. If not otherwise stated, data are expressed as mean ± s.e.m. and details about group sizes (n) and how many times each experiment was independently repeated is provided in each figure caption. When two groups were compared, statistical significance was evaluated by an unpaired, two-

tailed Student's t-test (referred to as t-test) and applying Welch's correction when variances between groups were significantly different. For multiple group analyses one-way ANOVA followed by Dunnett's multiple comparisons test or two-way ANOVA were performed. Mann-Whitney U-test (referred to as Mann–Whitney test) was applied in Supplementary Fig. 1D, E, as data were not normally distributed. Pearson's correlation was applied to determine the relationship between ACOD1 mRNA expression levels and alterations in plasma glucose or alterations in expression of genes related to intestinal permeability. All statistical analyses were performed using GraphPad Prism version 8.

***Data availability*.** Proteomics and RNAseq data are available at ProteoSAFe/MassIVE (MSV000090276) and GEO (GSE213632), respectively. All other data that support the findings in this study are stored at the IRCCS San Raffaele Scientific Institute and are available from the corresponding author upon reasonable request.

Gene name	Species	Forward primer	Reverse primer
Acod1	*Mus musculus*	TAATGGTGTTGCTGTTCA	AGCTAGGACAGCCCCAGAAAG
Actin	*Mus musculus*	CACTGTCGAGTCGCGTCCA	CATCCATGGCGAACTGGTGG
Adgre1 (F4/80)	*Mus musculus*	AAGACTGACAACCAGACGGC	CTGCCTCCACTAGCATCCAG
Ass1	*Mus musculus*	CACTCTACGAGGACCGCTATCT	CTCAAAGCGGACCTGGTCATTC
Cd68	*Mus musculus*	GGCGGTGGAATACAATGTGTCC	AGCAGGTCAAGGTGAACAGCTG
Cps1	*Mus musculus*	CATGGAACATCCAGCCGAATTGG	GATGGCACATCCTCAGAGCCTT
Nags	*Mus musculus*	GCCTGCGGAATAACAGTCAGAAG	TCCACGATGAGCCGAATCTGCT
Otc	*Mus musculus*	ACACTGTTTGCCTAGAAAGCCAG	CTTCTGGAGCACAGGTGAGTAG
Pnpla2 (Atgl)	*Mus musculus*	TTAGGAGGAATGCCCTGCTG	CGCACTGGTAGCATGTTGGA
Ppargc1a (Pgc1a)	*Mus musculus*	ATCACGTTCAAGGTCACCCTAC	TTCTGCTTCTGCCTCTCTCTCT
Rps18	*Mus musculus*	CACTTTTGGGGCCTTCGTG	GCAAAGGCCCAGAGACTCATT
Tnf	*Mus musculus*	GCCTCTTCTCATTCCTGCTT	TGGGAACTTCTCATCCCTTTG
Slc2a4	*Mus musculus*	GGTGTGGTCAATACGGTCTTCAC	AGCAGAGCCACGGTCATCAAGA
Aco2	*Mus musculus*	ACTGTGGCAGAGAAGGAAGGCT	CAATGCCTGCTTAGCCACAGCT
Sdha	*Mus musculus*	GAGATACGCACCTGTTGCCAAG	GGTAGACGTGATCTTTCTCAGGG
Suclg2	*Mus musculus*	AGCTCAAGGTGCCACTGGTAGT	GCTTTCTTGGCTGCATCCTCCA
Pnpla3	*Mus musculus*	GCACTTTCTTTGGCTGCTCG	CATTATACGGCCGAGAGGGAG
Cpt2	*Mus musculus*	GATGGCTGAGTGCTCCAAATACC	GCTGCCAGATACCGTAGAGCAA
Cact	*Mus musculus*	CAACCACCAAGTTTGTCTGGA	CCCTCTCTCATAAGAGTCTTCCG
Acaa2	*Mus musculus*	AGTCCCCCTACTGTGTCAGAAA	CCATCTCCTCATTGAAGTAGCC
Hadha	*Mus musculus*	ACCTCGGTGTAAAGCACAAAGT	GAGGTTTTGTCAGTGGTGATGA
Hadhb	*Mus musculus*	CACTGCGTTCTCATAGTCTGGC	GCCATTTGCTCCAGTGAGGAAG
Nrf1	*Mus musculus*	GGCAACAGTAGCCACATTGGCT	GTCTGGATGGTCATTTCACCGC
Tfam	*Mus musculus*	GAGGCAAAGGATGATTCGGCTC	CGAATCCTATCATCTTTAGCAAGC
Ucp1	*Mus musculus*	TGGTGAACCCGACAACTTCC	GGCCTTCACCTTGGATCTGAA
Cidea	*Mus musculus*	GGTGGACACAGAGGAGTTCTTTC	CGAAGGTGACTCTGGCTATTCC
Pparg	*Mus musculus*	GTACTGTCGGTTTCAGAAGTGCC	ATCTCCGCCAACAGCTTCTCCT
Il1b	*Mus musculus*	TGCCACCTTTTGACAGTGATG	ATGTGCTGCTGCGAGATTTG
Cpt1a	*Mus musculus*	AGATCAATCGGACCCTAGACAC	CAGCGAGTAGCGCATAGTCA
Ucp2	*Mus musculus*	TAAAGGTCCGCTTCCAGGCTCA	ACGGGCAACATTGGGAGAAGTC
Ucp3	*Mus musculus*	CAACTGTGCTGAGATGGTGACC	TGGCACAGAAGCCAGCTCCAAA
Gene	**Application**	**Primer sequence**	
Acod1	Genotyping	GTGGGGAGGGGAACTATGAG	
Acod1	Genotyping	ATTTGGAGGAACCCCATGAC	
Acod1	Genotyping	CAGCCTCTAAGCCAGACAGC	

Table 1. List of primers used

References

Adeva-Andany, M. M., Carneiro-Freire, N., Seco-Filgueira, M., Fernández-Fernández, C., & Mouriño-Bayolo, D. (2019). Mitochondrial β-oxidation of saturated fatty acids in humans. *Mitochondrion*, *46*, 73–90. https://doi.org/10.1016/J.MITO.2018.02.009

ADLER, J., WANG, S. F., & LARDY, H. A. (1957). THE METABOLISM OF ITACONIC ACID BY LIVER MITOCHONDRIA. *Journal of Biological Chemistry*, *229*(2), 865–879. https://doi.org/10.1016/S0021-9258(19)63691-4

Afzaal, M., Saeed, F., Shah, Y. A., Hussain, M., Rabail, R., Socol, C. T., Hassoun, A., Pateiro, M., Lorenzo, J. M., Rusu, A. V., & Aadil, R. M. (2022). Human gut microbiota in health and disease: Unveiling the relationship. *Frontiers in Microbiology*, *13*. https://doi.org/10.3389/FMICB.2022.999001

Agus, A., Clément, K., & Sokol, H. (2021). Gut microbiota-derived metabolites as central regulators in metabolic disorders. *Gut*, *70*(6), 1174–1182. https://doi.org/10.1136/GUTJNL-2020-323071

Aleffi, S., Petrai, I., Bertolani, C., Parola, M., Colombatto, S., Novo, E., Vizzutti, F., Anania, F. A., Milani, S., Rombouts, K., Laffi, G., Pinzani, M., & Marra, F. (2005). *Upregulation of Proinflammatory and Proangiogenic Cytokines by Leptin in Human Hepatic Stellate Cells*. https://doi.org/10.1002/hep.20965

Amin, T., & Mercer, J. G. (n.d.). *Hunger and Satiety Mechanisms and Their Potential Exploitation in the Regulation of Food Intake*. https://doi.org/10.1007/s13679-015-0184-5

Anachad, O., Taouil, A., Taha, W., Bennis, F., & Chegdani, F. (2023). The Implication of Short-Chain Fatty Acids in Obesity and Diabetes. *Microbiology Insights*, *16*, 117863612311627. https://doi.org/10.1177/11786361231162720

Apovian, C. M., Aronne, L., Rubino, D., Still, C., Wyatt, H., Burns, C., Kim, D., & Dunayevich, E. (2013). A Randomized, Phase 3 Trial of Naltrexone SR/Bupropion SR on Weight and Obesity-related Risk Factors (COR-II). *Obesity (Silver Spring, Md.)*, *21*(5), 935. https://doi.org/10.1002/OBY.20309

Asgharpour, A., Cazanave, S. C., Pacana, T., Seneshaw, M., Vincent, R., Banini, B. A., Kumar, D. P., Daita, K., Min, H. K., Mirshahi, F., Bedossa, P., Sun, X., Hoshida, Y., Koduru, S. V., Contaifer, D., Warncke, U. O., Wijesinghe, D. S., & Sanyal, A. J. (2016). A diet-induced animal model of non-alcoholic fatty liver disease and hepatocellular cancer. *Journal of Hepatology*, *65*(3), 579. https://doi.org/10.1016/J.JHEP.2016.05.005

Ashburner, M., Ball, C. A., Blake, J. A., Botstein, D., Butler, H., Cherry, J. M., Davis, A. P., Dolinski, K., Dwight, S. S., Eppig, J. T., Harris, M. A., Hill, D. P., Issel-Tarver, L., Kasarskis, A., Lewis, S., Matese, J. C., Richardson, J. E., Ringwald, M., Rubin, G. M., & Sherlock, G. (2000). Gene Ontology: tool for the unification of biology. *Nature Genetics*, *25*(1), 25. https://doi.org/10.1038/75556

Audano, M., Pedretti, · S, Caruso, · D, Crestani, · M, De Fabiani, · E, & Mitro, · N. (2022). Regulatory mechanisms of the early phase of white adipocyte differentiation: an overview. *Cellular and Molecular Life Sciences*, *79*, 139. https://doi.org/10.1007/s00018-022-04169-6

Bäckhed, F., Manchester, J. K., Semenkovich, C. F., & Gordon, J. I. (2007). Mechanisms underlying the resistance to diet-induced obesity in germ-free mice. *Proceedings of the National Academy of Sciences of the United States of America*, *104*(3), 979–984. https://doi.org/10.1073/PNAS.0605374104/SUPPL_FILE/INDEX.HTML

Bambouskova, M., Gorvel, L., Lampropoulou, V., Sergushichev, A., Loginicheva, E., Johnson, K., Korenfeld, D., Mathyer, M. E., Kim, H., Huang, L. H., Duncan, D., Bregman, H., Keskin, A., Santeford, A., Apte, R. S., Sehgal, R., Johnson, B., Amarasinghe, G. K., Soares, M. P., … Artyomov, M. N. (2018). Electrophilic properties of itaconate and derivatives regulate the IκBζ–ATF3 inflammatory axis. *Nature*, *556*(7702), 501. https://doi.org/10.1038/S41586-018-0052-Z

Bambouskova, M., Potuckova, L., Paulenda, T., Kerndl, M., Mogilenko, D. A., Lizotte, K.,

Swain, A., Hayes, S., Sheldon, R. D., Kim, H., Kapadnis, U., Ellis, A. E., Isaguirre, C., Burdess, S., Laha, A., Amarasinghe, G. K., Chubukov, V., Roddy, T. P., Diamond, M. S., … Artyomov, M. N. (2021). Itaconate confers tolerance to late NLRP3 inflammasome activation. *Cell Reports*, *34*(10). https://doi.org/10.1016/J.CELREP.2021.108756

Bankova, L. G., Lai, J., Yoshimoto, E., Boyce, J. A., Austen, K. F., Kanaoka, Y., & Barrett, N. A. (2016). Leukotriene E4 elicits respiratory epithelial cell mucin release through the G-protein-coupled receptor, GPR99. *Proceedings of the National Academy of Sciences of the United States of America*, *113*(22), 6242–6247. https://doi.org/10.1073/PNAS.1605957113/SUPPL_FILE/PNAS.201605957SI.PDF

Bansal, A. B., Patel, P., & Khalili, Y. Al. (2024). Orlistat. *XPharm: The Comprehensive Pharmacology Reference*, 1–3. https://doi.org/10.1016/B978-008055232-3.62333-5

Barberá, M. J., Schlüter, A., Pedraza, N., Iglesias, R., Villarroya, F., & Giralt, M. (2001). Peroxisome Proliferator-activated Receptor α Activates Transcription of the Brown Fat Uncoupling Protein-1 Gene. *Journal of Biological Chemistry*, *276*(2), 1486–1493. https://doi.org/10.1074/jbc.m006246200

Bartelt, A., & Heeren, J. (2013). Adipose tissue browning and metabolic health. *Nature Reviews Endocrinology 2013 10:1*, *10*(1), 24–36. https://doi.org/10.1038/nrendo.2013.204

Basler, T., Jeckstadt, S., Valentin-Weigand, P., & Goethe, R. (2006). Mycobacterium paratuberculosis, Mycobacterium smegmatis, and lipopolysaccharide induce different transcriptional and post-transcriptional regulation of the IRG1 gene in murine macrophages. *Journal of Leukocyte Biology*, *79*(3), 628–638. https://doi.org/10.1189/JLB.0905520

Bastías-Pérez, M., Zagmutt, S., Soler-Vázquez, M. C., Serra, D., Mera, P., & Herrero, L. (2020). Impact of Adaptive Thermogenesis in Mice on the Treatment of Obesity. *Cells 2020, Vol. 9, Page 316*, *9*(2), 316. https://doi.org/10.3390/CELLS9020316

BEGLINGER, C. (1994). Effect of cholecystokinin on gastric motility in humans. *Annals of the New York Academy of Sciences*, *713*(1), 219–225. https://doi.org/10.1111/J.1749-6632.1994.TB44068.X

Behary, J., Amorim, N., Jiang, X. T., Raposo, A., Gong, L., McGovern, E., Ibrahim, R., Chu, F., Stephens, C., Jebeili, H., Fragomeli, V., Koay, Y. C., Jackson, M., O'Sullivan, J., Weltman, M., McCaughan, G., El-Omar, E., & Zekry, A. (2021). Gut microbiota impact on the peripheral immune response in non-alcoholic fatty liver disease related hepatocellular carcinoma. *Nature Communications 2021 12:1*, *12*(1), 1–14. https://doi.org/10.1038/s41467-020-20422-7

Bhatti, J. S., Bhatti, G. K., & Reddy, P. H. (2017). Mitochondrial dysfunction and oxidative stress in metabolic disorders — A step towards mitochondria based therapeutic strategies. *Biochimica et Biophysica Acta (BBA) - Molecular Basis of Disease*, *1863*(5), 1066–1077. https://doi.org/10.1016/J.BBADIS.2016.11.010

Blanco, L. P., Patino-Martinez, E., Nakabo, S., Zhang, M., Pedersen, H. L., Wang, X., Carmona-Rivera, C., Claybaugh, D., Yu, Z. X., Desta, E., & Kaplan, M. J. (2022). Modulation of the Itaconate Pathway Attenuates Murine Lupus. *Arthritis & Rheumatology (Hoboken, N.J.)*, *74*(12), 1971–1983. https://doi.org/10.1002/ART.42284

Boffa, I. C., Vidali, G., Mann, R. S., & Allfrey, V. G. (1978). Suppression of histone deacetylation in vivo and in vitro by sodium butyrate. *Journal of Biological Chemistry*, *253*(10), 3364–3366. https://doi.org/10.1016/S0021-9258(17)34804-4

Bokoliya, S. C., Dorsett, Y., Panier, H., & Zhou, Y. (2021a). Procedures for Fecal Microbiota Transplantation in Murine Microbiome Studies. *Frontiers in Cellular and Infection Microbiology*, *11*, 711055. https://doi.org/10.3389/FCIMB.2021.711055/BIBTEX

Bokoliya, S. C., Dorsett, Y., Panier, H., & Zhou, Y. (2021b). Procedures for Fecal Microbiota Transplantation in Murine Microbiome Studies. *Frontiers in Cellular and Infection Microbiology*, *11*, 711055. https://doi.org/10.3389/FCIMB.2021.711055/BIBTEX

Bokoliya, S. C., Dorsett, Y., Panier, H., & Zhou, Y. (2021c). Procedures for Fecal Microbiota Transplantation in Murine Microbiome Studies. *Frontiers in Cellular and Infection*

Microbiology, *11*. https://doi.org/10.3389/FCIMB.2021.711055
Bournat, J. C., & Brown, C. W. (2010). Mitochondrial Dysfunction in Obesity. *Current Opinion in Endocrinology, Diabetes, and Obesity*, *17*(5), 446. https://doi.org/10.1097/MED.0B013E32833C3026
Brenchley, J. M., & Douek, D. C. (2012). Microbial Translocation Across the GI Tract. *Annual Review of Immunology*, *30*, 149. https://doi.org/10.1146/ANNUREV-IMMUNOL-020711-075001
Brogi, S., Zhu, X., Yu, L., Lin, J., Ren, J., Schwinn Gao, D., & Dai, Y. (2021). The Emerging Application of Itaconate: Promising Molecular Targets and Therapeutic Opportunities. *Frontiers in Chemistry | Www.Frontiersin.Org*, *1*, 669308. https://doi.org/10.3389/fchem.2021.669308
Brown, A. J., Goldsworthy, S. M., Barnes, A. A., Eilert, M. M., Tcheang, L., Daniels, D., Muir, A. I., Wigglesworth, M. J., Kinghorn, I., Fraser, N. J., Pike, N. B., Strum, J. C., Steplewski, K. M., Murdock, P. R., Holder, J. C., Marshall, F. H., Szekeres, P. G., Wilson, S., Ignar, D. M., … Dowell, S. J. (2003). The orphan G protein-coupled receptors GPR41 and GPR43 are activated by propionate and other short chain carboxylic acids. *Journal of Biological Chemistry*, *278*(13), 11312–11319. https://doi.org/10.1074/jbc.M211609200
Bugarith, K., Dinh, T. T., Li, A. J., Speth, R. C., & Ritter, S. (2005). Basomedial Hypothalamic Injections of Neuropeptide Y Conjugated to Saporin Selectively Disrupt Hypothalamic Controls of Food Intake. *Endocrinology*, *146*(3), 1179–1191. https://doi.org/10.1210/EN.2004-1166
Callahan, B. J., McMurdie, P. J., Rosen, M. J., Han, A. W., Johnson, A. J. A., & Holmes, S. P. (2016). DADA2: High-resolution sample inference from Illumina amplicon data. *Nature Methods*, *13*(7), 581–583. https://doi.org/10.1038/NMETH.3869
Camilleri, M. (2014). *PERIPHERAL MECHANISMS IN APPETITE REGULATION*. https://doi.org/10.1053/j.gastro.2014.09.016
Candela, M., Maccaferri, S., Turroni, S., Carnevali, P., & Brigidi, P. (2010). Functional intestinal microbiome, new frontiers in prebiotic design. *International Journal of Food Microbiology*, *140*(2–3), 93–101. https://doi.org/10.1016/J.IJFOODMICRO.2010.04.017
Canfora, E. E., Jocken, J. W., & Blaak, E. E. (2015a). Short-chain fatty acids in control of body weight and insulin sensitivity. *Nature Reviews Endocrinology 2015 11:10*, *11*(10), 577–591. https://doi.org/10.1038/nrendo.2015.128
Canfora, E. E., Jocken, J. W., & Blaak, E. E. (2015b). Short-chain fatty acids in control of body weight and insulin sensitivity. *NATURE REVIEWS | ENDOCRINOLOGY*, *11*, 577–591. https://doi.org/10.1038/nrendo.2015.128
Chakhtoura, M., Haber, R., Ghezzawi, M., Rhayem, C., Tcheroyan, R., & Mantzoros, C. S. (2023). Pharmacotherapy of obesity: an update on the available medications and drugs under investigation. *EClinicalMedicine*, *58*. https://doi.org/10.1016/J.ECLINM.2023.101882/ATTACHMENT/D28621A2-1891-4E0A-913D-EBCD11367A98/MMC1.DOCX
Chang, C. S., Liao, Y. C., Huang, C. T., Lin, C. M., Cheung, C. H. Y., Ruan, J. W., Yu, W. H., Tsai, Y. T., Lin, I. J., Huang, C. H., Liou, J. S., Chou, Y. H., Chien, H. J., Chuang, H. L., Juan, H. F., Huang, H. C., Chan, H. L., Liao, Y. C., Tang, S. C., … Kao, C. Y. (2021). Identification of a gut microbiota member that ameliorates DSS-induced colitis in intestinal barrier enhanced Dusp6-deficient mice. *Cell Reports*, *37*(8), 110016. https://doi.org/10.1016/J.CELREP.2021.110016/ATTACHMENT/52DF41DF-9A72-44A4-8C8C-B083AA1E52BB/MMC6.PDF
Charlton, M., Krishnan, A., Viker, K., Sanderson, S., Cazanave, S., McConico, A., Masuoko, H., & Gores, G. (2011). Fast food diet mouse: novel small animal model of NASH with ballooning, progressive fibrosis, and high physiological fidelity to the human condition. *American Journal of Physiology - Gastrointestinal and Liver Physiology*, *301*(5), G825. https://doi.org/10.1152/AJPGI.00145.2011
Chen, C., Zhang, Z., Liu, C., Sun, P., Liu, P., & Li, X. (2024). ABCG2 is an itaconate exporter

that limits antibacterial innate immunity by alleviating TFEB-dependent lysosomal biogenesis. *Cell Metabolism*, *36*(3), 498-510.e11. https://doi.org/10.1016/J.CMET.2023.12.015

Chen, F., Elgaher, W. A. M., Winterhoff, M., Büssow, K., Waqas, F. H., Graner, E., Pires-Afonso, Y., Casares Perez, L., de la Vega, L., Sahini, N., Czichon, L., Zobl, W., Zillinger, T., Shehata, M., Pleschka, S., Bähre, H., Falk, C., Michelucci, A., Schuchardt, S., … Pessler, F. (2022). Citraconate inhibits ACOD1 (IRG1) catalysis, reduces interferon responses and oxidative stress, and modulates inflammation and cell metabolism. *Nature Metabolism 2022 4:5*, *4*(5), 534–546. https://doi.org/10.1038/s42255-022-00577-x

Chen, F., Lukat, P., Iqbal, A. A., Saile, K., Kaever, V., Van Den Heuvel, J., Blankenfeldt, W., Büssow, K., & Pessler, F. (n.d.). *Crystal structure of cis-aconitate decarboxylase reveals the impact of naturally occurring human mutations on itaconate synthesis*. https://doi.org/10.1073/pnas.1908770116

Chen, F., Wu, R., Liu, J., Kang, R., Li, J., & Tang, D. (2022). The STING1-MYD88 complex drives ACOD1/IRG1 expression and function in lethal innate immunity. *IScience*, *25*(7), 104561. https://doi.org/10.1016/J.ISCI.2022.104561

Chen, F., Yalcin, I., Zhao, M., Chen, C., Blankenfeldt, W., Pessler, F., & Büssow, K. (2023). Amino acid positions near the active site determine the reduced activity of human ACOD1 compared to murine ACOD1. *Scientific Reports 2023 13:1*, *13*(1), 1–8. https://doi.org/10.1038/s41598-023-37373-w

Chen, L. L., Morcelle, C., Cheng, Z. L., Chen, X., Xu, Y., Gao, Y., Song, J., Li, Z., Smith, M. D., Shi, M., Zhu, Y., Zhou, N., Cheng, M., He, C., Liu, K. -Y, Lu, G., Zhang, L., Zhang, C., Zhang, J., … Ye, D. (2022). Itaconate inhibits TET DNA dioxygenases to dampen inflammatory responses. *Nature Cell Biology*, *24*(3), 353–363. https://doi.org/10.1038/S41556-022-00853-8

Chen, Y. J., Li, G. N., Li, X. J., Wei, L. X., Fu, M. J., Cheng, Z. L., Yang, Z., Zhu, G. Q., Wang, X. D., Zhang, C., Zhang, J. Y., Sun, Y. P., Saiyin, H., Zhang, J., Liu, W. R., Zhu, W. W., Guan, K. L., Xiong, Y., Yang, Y., … Chen, L. L. (2023). Targeting IRG1 reverses the immunosuppressive function of tumor-associated macrophages and enhances cancer immunotherapy. *Science Advances*, *9*(17). https://doi.org/10.1126/SCIADV.ADG0654

Chen, Y., Wang, X., Wang, J., Yan, Z., & Luo, J. (2012). Excess body weight and the risk of primary liver cancer: An updated meta-analysis of prospective studies. *European Journal of Cancer*, *48*(14), 2137–2145. https://doi.org/10.1016/j.ejca.2012.02.063

Chouchani, E. T., Pell, V. R., Gaude, E., Aksentijević, D., Sundier, S. Y., Robb, E. L., Logan, A., Nadtochiy, S. M., Ord, E. N. J., Smith, A. C., Eyassu, F., Shirley, R., Hu, C. H., Dare, A. J., James, A. M., Rogatti, S., Hartley, R. C., Eaton, S., Costa, A. S. H., … Murphy, M. P. (2014). Ischaemic accumulation of succinate controls reperfusion injury through mitochondrial ROS. *Nature*, *515*(7527), 431. https://doi.org/10.1038/NATURE13909

Chun, H. L., Lee, S. Y., Kim, K. H., Lee, C. S., Oh, T. J., & Ho Park, H. (2020). The crystal structure of mouse IRG1 suggests that cis-aconitate decarboxylase has an open and closed conformation. *PLoS ONE*, *15*(12). https://doi.org/10.1371/JOURNAL.PONE.0242383

Cinti, S., Mitchell, G., Barbatelli, G., Murano, I., Ceresi, E., Faloia, E., Wang, S., Fortier, M., Greenberg, A. S., & Obin, M. S. (2005). Adipocyte death defines macrophage localization and function in adipose tissue of obese mice and humans. *Journal of Lipid Research*, *46*(11), 2347–2355. https://doi.org/10.1194/JLR.M500294-JLR200

Ciofi, C., De Boer, M., Bruford, M. W., Hecht, M. K., Wallace, B., Macintyre, R. J., Lenk, P., Eidenmueller, B., Staudter, H., Wicker, R., & Wink, M. ; I. J. (2006). Human gut microbes associated with obesity. *Nature 2006 444:7122*, *444*(7122), 1022–1023. https://doi.org/10.1038/4441022a

Clemente-Suárez, V. J., Redondo-Flórez, L., Beltrán-Velasco, A. I., Martín-Rodríguez, A., Martínez-Guardado, I., Navarro-Jiménez, E., Laborde-Cárdenas, C. C., & Tornero-Aguilera, J. F. (2023). The Role of Adipokines in Health and Disease. *Biomedicines*, *11*(5). https://doi.org/10.3390/BIOMEDICINES11051290

Cong, B., Zhang, Q., & Cao, X. (2021). The function and regulation of TET2 in innate immunity and inflammation. *Protein & Cell*, *12*(3), 165–173. https://doi.org/10.1007/S13238-020-00796-6

Cordes, T., Lucas, A., Divakaruni, A. S., Murphy, A. N., Cabrales, P., & Metallo, C. M. (2020). Itaconate modulates tricarboxylic acid and redox metabolism to mitigate reperfusion injury. *Molecular Metabolism*, *32*, 122–135. https://doi.org/10.1016/J.MOLMET.2019.11.019

Cordes, T., Wallace, M., Michelucci, A., Divakaruni, A. S., Sapcariu, S. C., Sousa, C., Koseki, H., Cabrales, P., Murphy, A. N., Hiller, K., & Metallo, C. M. (2016). Immunoresponsive gene 1 and itaconate inhibit succinate dehydrogenase to modulate intracellular succinate levels. *Journal of Biological Chemistry*, *291*(27), 14274–14284. https://doi.org/10.1074/jbc.M115.685792

Cousin, B., Cinti, S., Morroni, M., Raimbault, S., Ricquier, D., Pénicaud, L., & Casteilla, L. (1992). Occurrence of brown adipocytes in rat white adipose tissue: molecular and morphological characterization. *Journal of Cell Science*, *103 (Pt 4)*(4), 931–942. https://doi.org/10.1242/JCS.103.4.931

Covey, S. D., Wideman, R. D., McDonald, C., Unniappan, S., Huynh, F., Asadi, A., Speck, M., Webber, T., Chua, S. C., & Kieffer, T. J. (2006). The pancreatic β cell is a key site for mediating the effects of leptin on glucose homeostasis. *Cell Metabolism*, *4*(4), 291–302. https://doi.org/10.1016/j.cmet.2006.09.005

Daniels, B. P., Kofman, S. B., Smith, J. R., Norris, G. T., Snyder, A. G., Kolb, J. P., Gao, X., Locasale, J. W., Martinez, J., Gale, M., Loo, Y. M., & Oberst, A. (2019a). The nucleotide sensor ZBP1 and kinase RIPK3 induce the enzyme IRG1 to promote an antiviral metabolic state in neurons. *Immunity*, *50*(1), 64. https://doi.org/10.1016/J.IMMUNI.2018.11.017

Daniels, B. P., Kofman, S. B., Smith, J. R., Norris, G. T., Snyder, A. G., Kolb, J. P., Gao, X., Locasale, J. W., Martinez, J., Gale, M., Loo, Y. M., & Oberst, A. (2019b). The nucleotide sensor ZBP1 and kinase RIPK3 induce the enzyme IRG1 to promote an antiviral metabolic state in neurons. *Immunity*, *50*(1), 64. https://doi.org/10.1016/J.IMMUNI.2018.11.017

Dapito, D. H., Mencin, A., Gwak, G. Y., Pradere, J. P., Jang, M. K., Mederacke, I., Caviglia, J. M., Khiabanian, H., Adeyemi, A., Bataller, R., Lefkowitch, J. H., Bower, M., Friedman, R., Sartor, R. B., Rabadan, R., & Schwabe, R. F. (2012). Promotion of Hepatocellular Carcinoma by the Intestinal Microbiota and TLR4. *Cancer Cell*, *21*(4), 504–516. https://doi.org/10.1016/j.ccr.2012.02.007

Day, C. P., & Saksena, S. (2002). Non-alcoholic steatohepatitis: Definitions and pathogenesis. *Journal of Gastroenterology and Hepatology (Australia)*, *17*(SUPPL. 3). https://doi.org/10.1046/J.1440-1746.17.S3.31.X

De Chiara, F., Heebøll, S., Marrone, G., Montoliu, C., Hamilton-Dutoit, S., Ferrandez, A., Andreola, F., Rombouts, K., Grønbæk, H., Felipo, V., Gracia-Sancho, J., Mookerjee, R. P., Vilstrup, H., Jalan, R., & Thomsen, K. L. (2018). Urea cycle dysregulation in non-alcoholic fatty liver disease. *Journal of Hepatology*, *69*(4), 905–915. https://doi.org/10.1016/j.jhep.2018.06.023

De Chiara, F., Thomsen, K. L., Habtesion, A., Jones, H., Davies, N., Gracia-Sancho, J., Manicardi, N., Hall, A., Andreola, F., Paish, H. L., Reed, L. H., Watson, A. A., Leslie, J., Oakley, F., Rombouts, K., Mookerjee, R. P., Mann, J., & Jalan, R. (2020). Ammonia Scavenging Prevents Progression of Fibrosis in Experimental Nonalcoholic Fatty Liver Disease. *Hepatology*, *71*(3), 874–892. https://doi.org/10.1002/HEP.30890

Degrandi, D., Hoffmann, R., Beuter-Gunia, C., & Pfeffer, K. (2009). The Proinflammatory Cytokine-Induced IRG1 Protein Associates with Mitochondria. *Https://Home.Liebertpub.Com/Jir*, *29*(1), 55–67. https://doi.org/10.1089/JIR.2008.0013

d'Errico, M., Pavlova, M., & Spandonaro, F. (2022). The economic burden of obesity in Italy: a cost-of-illness study. *The European Journal of Health Economics*, *23*(2), 177. https://doi.org/10.1007/S10198-021-01358-1

Ding, S., Chi, M. M., Scull, B. P., Rigby, R., Schwerbrock, N. M. J., Magness, S., Jobin, C., &

Lund, P. K. (2010). High-Fat Diet: Bacteria Interactions Promote Intestinal Inflammation Which Precedes and Correlates with Obesity and Insulin Resistance in Mouse. *PLoS ONE*, *5*(8). https://doi.org/10.1371/JOURNAL.PONE.0012191

Divella, R., Mazzocca, A., Daniele, A., Sabbà, C., & Paradiso, A. (2019). Obesity, Nonalcoholic Fatty Liver Disease and Adipocytokines Network in Promotion of Cancer. *International Journal of Biological Sciences*, *15*(3), 610. https://doi.org/10.7150/IJBS.29599

Eberhart, T., Stanley, F. U., Ricci, L., Chirico, T., Ferrarese, R., Sisti, S., Scagliola, A., Baj, A., Badurek, S., Sommer, A., Culp-Hill, R., Dzieciatkowska, M., Shokry, E., Sumpton, D., D'Alessandro, A., Clementi, N., Mancini, N., & Cardaci, S. (2024). ACOD1 deficiency offers protection in a mouse model of diet-induced obesity by maintaining a healthy gut microbiota. *Cell Death & Disease 2024 15:2*, *15*(2), 1–16. https://doi.org/10.1038/s41419-024-06483-2

Ericsson, A. C., & Franklin, C. L. (2021). The gut microbiome of laboratory mice: considerations and best practices for translational research. *Mammalian Genome*, *32*(4), 239. https://doi.org/10.1007/S00335-021-09863-7

Esposito, K., Chiodini, P., Colao, A., Lenzi, A., & Giugliano, D. (2012). Metabolic syndrome and risk of cancer: A systematic review and meta-analysis. *Diabetes Care*, *35*(11), 2402–2411. https://doi.org/10.2337/DC12-0336/-/DC1

Fan, K., Zan, X., Zhi, Y., Yang, Y., Hu, K., Zhang, X., Zhang, X., Zhao, S., Chen, K., Gong, X., Tian, R., & Zhang, L. (2022). Immune response gene 1 deficiency impairs Nrf2 activation and aggravates liver fibrosis in mice. *Biochemical and Biophysical Research Communications*, *607*, 103–109. https://doi.org/10.1016/J.BBRC.2022.03.110

Fasshauer, M., & Blüher, M. (2015). Adipokines in health and disease. *Trends in Pharmacological Sciences*, *36*(7), 461–470. https://doi.org/10.1016/J.TIPS.2015.04.014

Fei, N., & Zhao, L. (2012). An opportunistic pathogen isolated from the gut of an obese human causes obesity in germfree mice. *The ISME Journal 2013 7:4*, *7*(4), 880–884. https://doi.org/10.1038/ismej.2012.153

Flessa, C. M., Nasiri-Ansari, N., Kyrou, I., Leca, B. M., Lianou, M., Chatzigeorgiou, A., Kaltsas, G., Kassi, E., & Randeva, H. S. (2022). Genetic and Diet-Induced Animal Models for Non-Alcoholic Fatty Liver Disease (NAFLD) Research. *International Journal of Molecular Sciences*, *23*(24). https://doi.org/10.3390/IJMS232415791

Flint, H. J., Scott, K. P., Duncan, S. H., Louis, P., & Forano, E. (2012). Microbial degradation of complex carbohydrates in the gut. *Gut Microbes*, *3*(4), 289–306. https://doi.org/10.4161/GMIC.19897

Frieler, R. A., Vigil, T. M., Song, J., Leung, C., Goldstein, D. R., Lumeng, C. N., & Mortensen, R. M. (2022). Aconitate decarboxylase 1 regulates glucose homeostasis and obesity in mice. *Obesity*, *30*(9), 1818–1830. https://doi.org/10.1002/OBY.23509

Fritz, J. V., Desai, M. S., Shah, P., Schneider, J. G., & Wilmes, P. (2013). From meta-omics to causality: experimental models for human microbiome research. *Microbiome*, *1*(1), 14. https://doi.org/10.1186/2049-2618-1-14

Fritzen, A. M., Lundsgaard, A. M., & Kiens, B. (2020). Tuning fatty acid oxidation in skeletal muscle with dietary fat and exercise. *Nature Reviews Endocrinology 2020 16:12*, *16*(12), 683–696. https://doi.org/10.1038/s41574-020-0405-1

Galarraga, M., Campión, J., Munõz-Barrutia, A., Boqué, N., Moreno, H., Martínez, J. A., Milagro, F., & Ortiz-de-Solórzano, C. (2012). Adiposoft: automated software for the analysis of white adipose tissue cellularity in histological sections. *Journal of Lipid Research*, *53*(12), 2791–2796. https://doi.org/10.1194/JLR.D023788

Gamberi, T., Magherini, F., Modesti, A., & Fiaschi, T. (2018). Adiponectin Signaling Pathways in Liver Diseases. *Biomedicines*, *6*(2), 52. https://doi.org/10.3390/BIOMEDICINES6020052

Garcia-Galiano, D., Borges, B. C., Allen, S. J., & Elias, C. F. (2019). PI3K signaling in leptin receptor cells: role in growth and reproduction. *Journal of Neuroendocrinology*, *31*(5),

e12685. https://doi.org/10.1111/JNE.12685
Garcia-Irigoyen, O., Bovenga, F., Piglionica, M., Piccinin, E., Cariello, M., Arconzo, M., Peres, C., Corsetto, P. A., Rizzo, A. M., Ballanti, M., Menghini, R., Mingrone, G., Lefebvre, P., Staels, B., Shirasawa, T., Sabbà, C., Villani, G., Federici, M., & Moschetta, A. (2021). Enterocyte superoxide dismutase 2 deletion drives obesity. *IScience*, *25*(1). https://doi.org/10.1016/J.ISCI.2021.103707
Gauffin Cano, P., Santacruz, A., Moya, Á., & Sanz, Y. (2012). Bacteroides uniformis CECT 7771 ameliorates metabolic and immunological dysfunction in mice with high-fat-diet induced obesity. *PloS One*, *7*(7). https://doi.org/10.1371/JOURNAL.PONE.0041079
Ge, S. X., Jung, D., Jung, D., & Yao, R. (2020). ShinyGO: a graphical gene-set enrichment tool for animals and plants. *Bioinformatics (Oxford, England)*, *36*(8), 2628–2629. https://doi.org/10.1093/BIOINFORMATICS/BTZ931
Geurts, L., Lazarevic, V., Derrien, M., Everard, A., Van Roye, M., Knauf, C., Valet, P., Girard, M., Muccioli, G. G., François, P., de Vos, W. M., Schrenzel, J., Delzenne, N. M., & Cani, P. D. (2011). Altered Gut Microbiota and Endocannabinoid System Tone in Obese and Diabetic Leptin-Resistant Mice: Impact on Apelin Regulation in Adipose Tissue. *Frontiers in Microbiology*, *2*(JULY). https://doi.org/10.3389/FMICB.2011.00149
Gonzalez-Franquesa, A., & Patti, M. E. (2017). Insulin resistance and mitochondrial dysfunction. *Advances in Experimental Medicine and Biology*, *982*, 465–520. https://doi.org/10.1007/978-3-319-55330-6_25/FIGURES/4
Grabner, G. F., & Xie, H. ✉. (n.d.). *Lipolysis: cellular mechanisms for lipid mobilization from fat stores*. https://doi.org/10.1038/s42255-021-00493-6
Gray, S. L., Donald, C., Jetha, A., Covey, S. D., & Kieffer, T. J. (2010). Hyperinsulinemia precedes insulin resistance in mice lacking pancreatic beta-cell leptin signaling. *Endocrinology*, *151*(9), 4178–4186. https://doi.org/10.1210/EN.2010-0102
Gu, X., Wei, H., Suo, C., Shen, S., Zhu, C., Chen, L., Yan, K., Li, Z., Bian, Z., Zhang, P., Yuan, M., Yu, Y., Du, J., Zhang, H., Sun, L., & Gao, P. (2023). Itaconate promotes hepatocellular carcinoma progression by epigenetic induction of CD8+ T-cell exhaustion. *Nature Communications 2023 14:1*, *14*(1), 1–15. https://doi.org/10.1038/s41467-023-43988-4
Gulinac, M., Miteva, D. G., Peshevska-Sekulovska, M., Novakov, I. P., Antovic, S., Peruhova, M., Snegarova, V., Kabakchieva, P., Assyov, Y., Vasilev, G., Sekulovski, M., Lazova, S., Tomov, L., & Velikova, T. (2023). Long-term effectiveness, outcomes and complications of bariatric surgery. *World Journal of Clinical Cases*, *11*(19), 4504. https://doi.org/10.12998/WJCC.V11.I19.4504
Hall, C. J., Boyle, R. H., Astin, J. W., Flores, M. V., Oehlers, S. H., Sanderson, L. E., Ellett, F., Lieschke, G. J., Crosier, K. E., & Crosier, P. S. (2013). Immunoresponsive gene 1 augments bactericidal activity of macrophage-lineage cells by regulating β-oxidation-dependent mitochondrial ros production. *Cell Metabolism*, *18*(2), 265–278. https://doi.org/10.1016/j.cmet.2013.06.018
Hassnain Waqas, S. F., Noble, A., Hoang, A. C., Ampem, G., Popp, M., Strauß, S., Guille, M., & Röszer, T. (2017). Adipose tissue macrophages develop from bone marrow–independent progenitors in Xenopus laevis and mouse. *Journal of Leukocyte Biology*, *102*(3), 845–855. https://doi.org/10.1189/JLB.1A0317-082RR
He, A., Chen, X., Tan, M., Chen, Y., Lu, D., Zhang, X., Dean, J. M., Razani, B., & Lodhi, I. J. (2020). Acetyl-CoA Derived from Hepatic Peroxisomal β-Oxidation Inhibits Autophagy and Promotes Steatosis via mTORC1 Activation. *Molecular Cell*, *79*(1), 30-42.e4. https://doi.org/10.1016/j.molcel.2020.05.007
He, W., Henne, A., Lauterbach, M., Geißmar, E., Nikolka, F., Kho, C., Heinz, A., Dostert, C., Grusdat, M., Cordes, T., Härm, J., Goldmann, O., Ewen, A., Verschueren, C., Blay-Cadanet, J., Geffers, R., Garritsen, H., Kneiling, M., Holm, C. K., … Hiller, K. (2022). Mesaconate is synthesized from itaconate and exerts immunomodulatory effects in

macrophages. *Nature Metabolism 2022 4:5*, *4*(5), 524–533. https://doi.org/10.1038/s42255-022-00565-1

He, W., Miao, F. J. P., Lin, D. C. H., Schwandner, R. T., Wang, Z., Gao, J., Chen, J. L., Tlan, H., & Ling, L. (2004). Citric acid cycle intermediates as ligands for orphan G-protein-coupled receptors. *Nature 2004 429:6988*, *429*(6988), 188–193. https://doi.org/10.1038/nature02488

Heinonen, S., Jokinen, R., Rissanen, A., & Pietiläinen, K. H. (2020). White adipose tissue mitochondrial metabolism in health and in obesity. *Obesity Reviews*, *21*(2). https://doi.org/10.1111/OBR.12958

Hernández-Aguilera, A., Rull, A., Rodríguez-Gallego, E., Riera-Borrull, M., Luciano-Mateo, F., Camps, J., Menéndez, J. A., & Joven, J. (2013). Mitochondrial Dysfunction: A Basic Mechanism in Inflammation-Related Non-Communicable Diseases and Therapeutic Opportunities. *Mediators of Inflammation*, *2013*, 13. https://doi.org/10.1155/2013/135698

Hernández-Saavedra, D., & Stanford, K. I. (2019). The Regulation of Lipokines by Environmental Factors. *Nutrients*, *11*(10). https://doi.org/10.3390/NU11102422

Hildebrandt, X., Ibrahim, M., & Peltzer, N. (2022a). *Cell death and inflammation during obesity: â€œKnow my methods, WAT(son)â€•*. https://doi.org/10.1038/s41418-022-01062-4

Hildebrandt, X., Ibrahim, M., & Peltzer, N. (2022b). Cell death and inflammation during obesity: "Know my methods, WAT(son)." *Cell Death & Differentiation 2022 30:2*, *30*(2), 279–292. https://doi.org/10.1038/s41418-022-01062-4

Hill, J. O., Hauptman, J., Anderson, J. W., Fujioka, K., O'Neil, P. M., Smith, D. K., Zavoral, J. H., & Aronne, L. J. (1999). Orlistat, a lipase inhibitor, for weight maintenance after conventional dieting: a 1-y study. *The American Journal of Clinical Nutrition*, *69*(6), 1108–1116. https://doi.org/10.1093/AJCN/69.6.1108

Hill, J. O., Wyatt, H. R., & Peters, J. C. (2012). Obesity Energy Balance and Obesity How the Body Achieves Energy Balance. *Circulation*, *126*, 126–132. https://doi.org/10.1161/CIRCULATIONAHA.111.087213

Hoang, S. A., Oseini, A., Feaver, R. E., Cole, B. K., Asgharpour, A., Vincent, R., Siddiqui, M., Lawson, M. J., Day, N. C., Taylor, J. M., Wamhoff, B. R., Mirshahi, F., Contos, M. J., Idowu, M., & Sanyal, A. J. (2019). Gene Expression Predicts Histological Severity and Reveals Distinct Molecular Profiles of Nonalcoholic Fatty Liver Disease. *Scientific Reports*, *9*(1). https://doi.org/10.1038/S41598-019-48746-5

Hong-Zai, G., Qing-Chun, L., Zheng-Yao, J., & 管洪在关蛋白神经元而诱发多食. (2010). Ghrelin acts on rat dorsal vagal complex to stimulate feeding via arcuate neuropeptide Y/agouti-related peptide neurons activation. *Acta Physiologica Sinica*, *62*(4), 357–364. http://www.actaps.com.cn

Hooftman, A., Angiari, S., Hester, S., Corcoran, S. E., Runtsch, M. C., Ling, C., Ruzek, M. C., Slivka, P. F., McGettrick, A. F., Banahan, K., Hughes, M. M., Irvine, A. D., Fischer, R., & O'Neill, L. A. J. (2020). The Immunomodulatory Metabolite Itaconate Modifies NLRP3 and Inhibits Inflammasome Activation. *Cell Metabolism*, *32*(3), 468-478.e7. https://doi.org/10.1016/J.CMET.2020.07.016

Horwitz, A., & Birk, R. (2023). Adipose Tissue Hyperplasia and Hypertrophy in Common and Syndromic Obesity—The Case of BBS Obesity. *Nutrients*, *15*(15). https://doi.org/10.3390/NU15153445

Hotamisligil, G. S. (2006). Inflammation and metabolic disorders. *Nature 2006 444:7121*, *444*(7121), 860–867. https://doi.org/10.1038/nature05485

Hou, K., Wu, Z. X., Chen, X. Y., Wang, J. Q., Zhang, D., Xiao, C., Zhu, D., Koya, J. B., Wei, L., Li, J., & Chen, Z. S. (2022a). Microbiota in health and diseases. *Signal Transduction and Targeted Therapy 2022 7:1*, *7*(1), 1–28. https://doi.org/10.1038/s41392-022-00974-4

Hou, K., Wu, Z. X., Chen, X. Y., Wang, J. Q., Zhang, D., Xiao, C., Zhu, D., Koya, J. B., Wei, L., Li, J., & Chen, Z. S. (2022b). Microbiota in health and diseases. *Signal Transduction*

and Targeted Therapy 2022 7:1, *7*(1), 1–28. https://doi.org/10.1038/s41392-022-00974-4
Houten, S. M., & Wanders, R. J. A. (2010). A general introduction to the biochemistry of mitochondrial fatty acid β-oxidation. *Journal of Inherited Metabolic Disease*, *33*(5), 469–477. https://doi.org/10.1007/S10545-010-9061-2
Hu, L., Li, Z., Cheng, J., Rao, Q., Gong, W., Liu, M., Shi, Y. G., Zhu, J., Wang, P., & Xu, Y. (2013). Crystal Structure of TET2-DNA Complex: Insight into TET-Mediated 5mC Oxidation. *Cell*, *155*(7), 1545–1555. https://doi.org/10.1016/J.CELL.2013.11.020
Jamaluddin, M. S., Weakley, S. M., Yao, Q., & Chen, C. (2012). Resistin: functional roles and therapeutic considerations for cardiovascular disease. *British Journal of Pharmacology*, *165*(3), 622. https://doi.org/10.1111/J.1476-5381.2011.01369.X
Jang, H. B., Choi, M. K., Kang, J. H., Park, S. I., & Lee, H. J. (2017). Association of dietary patterns with the fecal microbiota in Korean adolescents. *BMC Nutrition*, *3*(1). https://doi.org/10.1186/S40795-016-0125-Z
Jung, S. M., Sanchez-Gurmaches, J., & Guertin, D. A. (2019). Brown Adipose Tissue Development and Metabolism. *Handbook of Experimental Pharmacology*, *251*, 3. https://doi.org/10.1007/164_2018_168
Kadowaki, T., Yamauchi, T., Kubota, N., Hara, K., Ueki, K., & Tobe, K. (2006). Adiponectin and adiponectin receptors in insulin resistance, diabetes, and the metabolic syndrome. *Journal of Clinical Investigation*, *116*(7), 1784. https://doi.org/10.1172/JCI29126
Kahn, B. B., Alquier, T., Carling, D., & Hardie, D. G. (2005). AMP-activated protein kinase: Ancient energy gauge provides clues to modern understanding of metabolism. *Cell Metabolism*, *1*(1), 15–25. https://doi.org/10.1016/j.cmet.2004.12.003
Kalogeris, T., Baines, C. P., Krenz, M., & Korthuis, R. J. (2016). Ischemia/Reperfusion. *Comprehensive Physiology*, *7*(1), 113. https://doi.org/10.1002/CPHY.C160006
Kanehisa, M., Furumichi, M., Sato, Y., Ishiguro-Watanabe, M., & Tanabe, M. (2021). KEGG: integrating viruses and cellular organisms. *Nucleic Acids Research*, *49*(D1), D545–D551. https://doi.org/10.1093/NAR/GKAA970
Kazankov, K., Jørgensen, S. M. D., Thomsen, K. L., Møller, H. J., Vilstrup, H., George, J., Schuppan, D., & Grønbæk, H. (2018). The role of macrophages in nonalcoholic fatty liver disease and nonalcoholic steatohepatitis. *Nature Reviews Gastroenterology & Hepatology 2018 16:3*, *16*(3), 145–159. https://doi.org/10.1038/s41575-018-0082-x
Keipert, S., & Jastroch, M. (2014). Brite/beige fat and UCP1 — is it thermogenesis? *Biochimica et Biophysica Acta (BBA) - Bioenergetics*, *1837*(7), 1075–1082. https://doi.org/10.1016/J.BBABIO.2014.02.008
Kennedy, E. A., King, K. Y., & Baldridge, M. T. (2018). Mouse Microbiota Models: Comparing Germ-Free Mice and Antibiotics Treatment as Tools for Modifying Gut Bacteria. *Frontiers in Physiology*, *9*(OCT), 1534. https://doi.org/10.3389/FPHYS.2018.01534
Khan, T., Muise, E. S., Iyengar, P., Wang, Z. V., Chandalia, M., Abate, N., Zhang, B. B., Bonaldo, P., Chua, S., & Scherer, P. E. (2009). Metabolic Dysregulation and Adipose Tissue Fibrosis: Role of Collagen VI. *Molecular and Cellular Biology*, *29*(6), 1575. https://doi.org/10.1128/MCB.01300-08
Khosravi, A., Yáñez, A., Price, J. G., Chow, A., Merad, M., Goodridge, H. S., & Mazmanian, S. K. (2014). Gut microbiota promote hematopoiesis to control bacterial infection. *Cell Host & Microbe*, *15*(3), 374–381. https://doi.org/10.1016/J.CHOM.2014.02.006
Kim, M. H., Kang, S. G., Park, J. H., Yanagisawa, M., & Kim, C. H. (2013). Short-Chain Fatty Acids Activate GPR41 and GPR43 on Intestinal Epithelial Cells to Promote Inflammatory Responses in Mice. *Gastroenterology*, *145*(2), 396-406.e10. https://doi.org/10.1053/J.GASTRO.2013.04.056
Kinsey, E., & Lee, H. M. (2024). Management of Hepatocellular Carcinoma in 2024: The Multidisciplinary Paradigm in an Evolving Treatment Landscape. *Cancers*, *16*(3). https://doi.org/10.3390/CANCERS16030666
Kirichenko, T. V., Markina, Y. V., Bogatyreva, A. I., Tolstik, T. V., Varaeva, Y. R., &

Starodubova, A. V. (2022). The Role of Adipokines in Inflammatory Mechanisms of Obesity. *International Journal of Molecular Sciences*, *23*(23). https://doi.org/10.3390/IJMS232314982

Kleiner, D. E., Brunt, E. M., Van Natta, M., Behling, C., Contos, M. J., Cummings, O. W., Ferrell, L. D., Liu, Y. C., Torbenson, M. S., Unalp-Arida, A., Yeh, M., McCullough, A. J., & Sanyal, A. J. (2005). Design and validation of a histological scoring system for nonalcoholic fatty liver disease. *Hepatology (Baltimore, Md.)*, *41*(6), 1313–1321. https://doi.org/10.1002/HEP.20701

Kleiner, S., Mepani, R. J., Laznik, D., Ye, L., Jurczak, M. J., Jornayvaz, F. R., Estall, J. L., Bhowmick, D. C., Shulman, G. I., & Spiegelman, B. M. (2012). Development of insulin resistance in mice lacking PGC-1α in adipose tissues. *Proceedings of the National Academy of Sciences of the United States of America*, *109*(24), 9635–9640. https://doi.org/10.1073/PNAS.1207287109/-/DCSUPPLEMENTAL

Kleinert, M., Clemmensen, C., Hofmann, S. M., Moore, M. C., Renner, S., Woods, S. C., Huypens, P., Beckers, J., De Angelis, M. H., Schürmann, A., Bakhti, M., Klingenspor, M., Heiman, M., Cherrington, A. D., Ristow, M., Lickert, H., Wolf, E., Havel, P. J., Müller, T. D., & Tschöp, M. H. (2018). Animal models of obesity and diabetes mellitus. *Nature Reviews Endocrinology 2018 14:3*, *14*(3), 140–162. https://doi.org/10.1038/nrendo.2017.161

Kloock, S., Ziegler, C. G., & Dischinger, U. (2023). Obesity and its comorbidities, current treatment options and future perspectives: Challenging bariatric surgery? *Pharmacology & Therapeutics*, *251*, 108549. https://doi.org/10.1016/J.PHARMTHERA.2023.108549

Kobayashi, E. H., Suzuki, T., Funayama, R., Nagashima, T., Hayashi, M., Sekine, H., Tanaka, N., Moriguchi, T., Motohashi, H., Nakayama, K., & Yamamoto, M. (2016). Nrf2 suppresses macrophage inflammatory response by blocking proinflammatory cytokine transcription. *Nature Communications 2016 7:1*, *7*(1), 1–14. https://doi.org/10.1038/ncomms11624

Kulak-Bejda, A., Bejda, G., & Waszkiewicz, N. (2021). Safety and efficacy of naltrexone for weight loss in adult patients – a systematic review. *Archives of Medical Science : AMS*, *17*(4), 940. https://doi.org/10.5114/AOMS.2020.96908

Kuo, P.-C., Weng, W.-T., Scofield, B. A., Furnas, D., Paraiso, H. C., Yu, I.-C., & Yen, J.-H. (n.d.). *Immunoresponsive gene 1 modulates the severity of brain injury in cerebral ischaemia*. https://doi.org/10.1093/braincomms/fcab187

Lahera, V., de las Heras, N., López-Farré, A., Manucha, W., & Ferder, L. (2017). Role of Mitochondrial Dysfunction in Hypertension and Obesity. *Current Hypertension Reports*, *19*(2), 1–9. https://doi.org/10.1007/S11906-017-0710-9/FIGURES/2

Lampropoulou, V., Sergushichev, A., Bambouskova, M., Nair, S., Vincent, E. E., Loginicheva, E., Cervantes-Barragan, L., Ma, X., Huang, S. C. C., Griss, T., Weinheimer, C. J., Khader, S., Randolph, G. J., Pearce, E. J., Jones, R. G., Diwan, A., Diamond, M. S., & Artyomov, M. N. (2016a). Itaconate Links Inhibition of Succinate Dehydrogenase with Macrophage Metabolic Remodeling and Regulation of Inflammation. *Cell Metabolism*, *24*(1), 158–166. https://doi.org/10.1016/J.CMET.2016.06.004

Lampropoulou, V., Sergushichev, A., Bambouskova, M., Nair, S., Vincent, E. E., Loginicheva, E., Cervantes-Barragan, L., Ma, X., Huang, S. C. C., Griss, T., Weinheimer, C. J., Khader, S., Randolph, G. J., Pearce, E. J., Jones, R. G., Diwan, A., Diamond, M. S., & Artyomov, M. N. (2016b). Itaconate Links Inhibition of Succinate Dehydrogenase with Macrophage Metabolic Remodeling and Regulation of Inflammation. *Cell Metabolism*, *24*(1), 158–166. https://doi.org/10.1016/j.cmet.2016.06.004

Lauby-Secretan, B., Scoccianti, C., Loomis, D., Grosse, Y., Bianchini, F., & Straif, K. (2016). Body Fatness and Cancer — Viewpoint of the IARC Working Group. *The New England Journal of Medicine*, *375*(8), 794. https://doi.org/10.1056/NEJMSR1606602

Laurans, L., Venteclef, N., Haddad, Y., Chajadine, M., Alzaid, F., Metghalchi, S., Sovran, B., Denis, R. G. P., Dairou, J., Cardellini, M., Moreno-Navarrete, J. M., Straub, M., Jegou, S.,

McQuitty, C., Viel, T., Esposito, B., Tavitian, B., Callebert, J., Luquet, S. H., … Taleb, S. (2018). Genetic deficiency of indoleamine 2,3-dioxygenase promotes gut microbiota-mediated metabolic health. *Nature Medicine 2018 24:8*, *24*(8), 1113–1120. https://doi.org/10.1038/s41591-018-0060-4

Lecuyer, E., Roy, T. Le, Gestin, A., Lacombe, A., Philippe, C., Ponnaiah, M., Hure, J. B., Fradet, M., Ichou, F., Boudebbouze, S., Huby, T., Gautier, E., Rhimi, M., Maguin, E., Kapel, N., Gerard, P., Venteclef, N., Garlatti, M., Chassaing, B., & Lesnik, P. (2021). Tolerogenic Dendritic Cells Shape a Transmissible Gut Microbiota That Protects From Metabolic Diseases. *Diabetes*, *70*(9), 2067–2080. https://doi.org/10.2337/DB20-1177

Lee, C. G. L., Jenkins, N. A., Gilbert, D. J., Copeland, N. G., & O'Brien, W. E. (1995). Cloning and analysis of gene regulation of a novel LPS-inducible cDNA. *Immunogenetics*, *41*(5), 263–270. https://doi.org/10.1007/BF00172150

Lee, Y. S., & Olefsky, J. (2021). Chronic tissue inflammation and metabolic disease. *Genes & Development*, *35*(5–6), 307. https://doi.org/10.1101/GAD.346312.120

Lee, Y. S., Wollam, J., & Olefsky, J. M. (2018). An Integrated View of Immunometabolism. *Cell*, *172*(1–2), 22–40. https://doi.org/10.1016/J.CELL.2017.12.025

Ley, R. E., Bäckhed, F., Turnbaugh, P., Lozupone, C. A., Knight, R. D., & Gordon, J. I. (2005a). Obesity alters gut microbial ecology. *Proceedings of the National Academy of Sciences of the United States of America*, *102*(31), 11070. https://doi.org/10.1073/PNAS.0504978102

Ley, R. E., Bäckhed, F., Turnbaugh, P., Lozupone, C. A., Knight, R. D., & Gordon, J. I. (2005b). Obesity alters gut microbial ecology. *Proceedings of the National Academy of Sciences of the United States of America*, *102*(31), 11070–11075. https://doi.org/10.1073/PNAS.0504978102

Ley, R. E., Turnbaugh, P. J., Klein, S., & Gordon, J. I. (2006). Microbial ecology: human gut microbes associated with obesity. *Nature*, *444*(7122), 1022–1023. https://doi.org/10.1038/4441022A

Li, S., Liu, M., Cao, S., Liu, B., Li, D., Wang, Z., Sun, H., Cui, Y., & Shi, Y. (2023). The Mechanism of the Gut-Brain Axis in Regulating Food Intake. *Nutrients*, *15*(17). https://doi.org/10.3390/NU15173728

Li, W., Li, Y., Kang, J., Jiang, H., Gong, W., Chen, L., Wu, C., Liu, M., Wu, X., Zhao, Y., & Ren, J. (2023). 4-octyl itaconate as a metabolite derivative inhibits inflammation via alkylation of STING. *Cell Reports*, *42*(3). https://doi.org/10.1016/j.celrep.2023.112145

Li, Z., Zheng, W., Kong, W., & Zeng, T. (123 C.E.). *Itaconate: A Potent Macrophage Immunomodulator*. https://doi.org/10.1007/s10753-023-01819-0

Liang, J. Q., Teoh, N., Xu, L., Pok, S., Li, X., Chu, E. S. H., Chiu, J., Dong, L., Arfianti, E., Haigh, W. G., Yeh, M. M., Ioannou, G. N., Sung, J. J. Y., Farrell, G., & Yu, J. (2018). Dietary cholesterol promotes steatohepatitis related hepatocellular carcinoma through dysregulated metabolism and calcium signaling. *Nature Communications 2018 9:1*, *9*(1), 1–13. https://doi.org/10.1038/s41467-018-06931-6

Liao, S. T., Han, C., Xu, D. Q., Fu, X. W., Wang, J. S., & Kong, L. Y. (2019). 4-Octyl itaconate inhibits aerobic glycolysis by targeting GAPDH to exert anti-inflammatory effects. *Nature Communications 2019 10:1*, *10*(1), 1–11. https://doi.org/10.1038/s41467-019-13078-5

Lichtenstein, G. R. (2013). Letter from the Editor. *Gastroenterology & Hepatology*, *9*(9), 552. /pmc/articles/PMC3983972/

Liu, R., Hong, J., Xu, X., Feng, Q., Zhang, D., Gu, Y., Shi, J., Zhao, S., Liu, W., Wang, X., Xia, H., Liu, Z., Cui, B., Liang, P., Xi, L., Jin, J., Ying, X., Wang, X., Zhao, X., … Wang, W. (2017a). Gut microbiome and serum metabolome alterations in obesity and after weight-loss intervention. *Nature Medicine*, *23*(7), 859–868. https://doi.org/10.1038/NM.4358

Liu, R., Hong, J., Xu, X., Feng, Q., Zhang, D., Gu, Y., Shi, J., Zhao, S., Liu, W., Wang, X., Xia, H., Liu, Z., Cui, B., Liang, P., Xi, L., Jin, J., Ying, X., Wang, X., Zhao, X., … Wang, W. (2017b). Gut microbiome and serum metabolome alterations in obesity and after weight-loss intervention. *Nature Medicine*, *23*(7), 859–868. https://doi.org/10.1038/NM.4358

Liu, X., Zhang, Z., Song, Y., Xie, H., & Dong, M. (2022). An update on brown adipose tissue and obesity intervention: Function, regulation and therapeutic implications. *Frontiers in Endocrinology*, *13*. https://doi.org/10.3389/FENDO.2022.1065263

Löffler, M. C., Betz, M. J., Blondin, D. P., Augustin, R., Sharma, A. K., Tseng, Y. H., Scheele, C., Zimdahl, H., Mark, M., Hennige, A. M., Wolfrum, C., Langhans, W., Hamilton, B. S., & Neubauer, H. (2021). Challenges in tackling energy expenditure as obesity therapy: From preclinical models to clinical application. *Molecular Metabolism*, *51*, 101237. https://doi.org/10.1016/J.MOLMET.2021.101237

Longo, M., Zatterale, F., Naderi, J., Parrillo, L., Formisano, P., Raciti, G. A., Beguinot, F., & Miele, C. (2019). *Molecular Sciences Adipose Tissue Dysfunction as Determinant of Obesity-Associated Metabolic Complications*. https://doi.org/10.3390/ijms20092358

Lönnqvist, F., Arner, P., Nordfors, L., & Schalling, M. (1995). Overexpression of the obese (ob) gene in adipose tissue of human obese subjects. *Nature Medicine 1995 1:9*, *1*(9), 950–953. https://doi.org/10.1038/nm0995-950

López-Almela, I., Romaní-Pérez, M., Bullich-Vilarrubias, C., Benítez-Páez, A., Gómez Del Pulgar, E. M., Francés, R., Liebisch, G., & Sanz, Y. (2021). Bacteroides uniformis combined with fiber amplifies metabolic and immune benefits in obese mice. *Gut Microbes*, *13*(1), 1–20. https://doi.org/10.1080/19490976.2020.1865706

Lorenz, M. C., & Fink, G. R. (2002). Life and Death in a Macrophage: Role of the Glyoxylate Cycle in Virulence. *Eukaryotic Cell*, *1*(5), 657. https://doi.org/10.1128/EC.1.5.657-662.2002

Love, M. I., Huber, W., & Anders, S. (2014). Moderated estimation of fold change and dispersion for RNA-seq data with DESeq2. *Genome Biology*, *15*(12). https://doi.org/10.1186/S13059-014-0550-8

Luck, H., Tsai, S., Chung, J., Clemente-Casares, X., Ghazarian, M., Revelo, X. S., Lei, H., Luk, C. T., Shi, S. Y., Surendra, A., Copeland, J. K., Ahn, J., Prescott, D., Rasmussen, B. A., Chng, M. H. Y., Engleman, E. G., Girardin, S. E., Lam, T. K. T., Croitoru, K., … Winer, D. A. (2015). Regulation of obesity-related insulin resistance with gut anti-inflammatory agents. *Cell Metabolism*, *21*(4), 527–542. https://doi.org/10.1016/j.cmet.2015.03.001

Lumeng, C. N., Bodzin, J. L., & Saltiel, A. R. (2007). Obesity induces a phenotypic switch in adipose tissue macrophage polarization. *Journal of Clinical Investigation*, *117*(1), 175. https://doi.org/10.1172/JCI29881

Lumeng, C. N., Deyoung, S. M., & Saltiel, A. R. (2007). Macrophages block insulin action in adipocytes by altering expression of signaling and glucose transport proteins. *Am J Physiol Endocrinol Metab*, *292*, 166–174. https://doi.org/10.1152/ajpendo.00284.2006.-Obesity

Luo, W., Guo, S., Zhou, Y., Zhao, J., Wang, M., Sang, L., Chang, B., & Wang, B. (2022). Hepatocellular Carcinoma: How the Gut Microbiota Contributes to Pathogenesis, Diagnosis, and Therapy. *Frontiers in Microbiology*, *13*, 873160. https://doi.org/10.3389/FMICB.2022.873160/BIBTEX

Magkos, F., Su, X., Bradley, D., Fabbrini, E., Conte, C., Eagon, J. C., Varela, J. E., Brunt, E. M., Patterson, B. W., & Klein, S. (2012). Intrahepatic diacylglycerol content is associated with hepatic insulin resistance in obese subjects. *Gastroenterology*, *142*(7). https://doi.org/10.1053/J.GASTRO.2012.03.003

Makki, K., Deehan, E. C., Walter, J., & Bäckhed, F. (2018). The Impact of Dietary Fiber on Gut Microbiota in Host Health and Disease. *Cell Host and Microbe*, *23*(6), 705–715. https://doi.org/10.1016/j.chom.2018.05.012

Mancabelli, L., Milani, C., Lugli, G. A., Turroni, F., Cocconi, D., van Sinderen, D., & Ventura, M. (2017). Identification of universal gut microbial biomarkers of common human intestinal diseases by meta-analysis. *FEMS Microbiology Ecology*, *93*(12). https://doi.org/10.1093/FEMSEC/FIX153

Maretti-Mira, A. C., Salomon, M. P., Hsu, A. M., Kanel, G. C., & Golden-Mason, L. (2022). Hepatic damage caused by long-term high cholesterol intake induces a dysfunctional restorative macrophage population in experimental NASH. *Frontiers in Immunology*, *13*,

968366. https://doi.org/10.3389/FIMMU.2022.968366/BIBTEX
Margetic, S., Gazzola, C., Pegg, G. G., & Hill, R. A. (2002). Leptin: a review of its peripheral actions and interactions. *International Journal of Obesity 2002 26:11*, *26*(11), 1407–1433. https://doi.org/10.1038/sj.ijo.0802142
Mariadason, J. M., Barkla, D. H., & Gibson, P. R. (1997). Effect of short-chain fatty acids on paracellular permeability in Caco-2 intestinal epithelium model. *Https://Doi.Org/10.1152/Ajpgi.1997.272.4.G705*, *272*(4 35-4). https://doi.org/10.1152/AJPGI.1997.272.4.G705
Marra, F., & Bertolani, C. (2009). Adipokines in liver diseases. *Hepatology (Baltimore, Md.)*, *50*(3), 957–969. https://doi.org/10.1002/HEP.23046
Maslowski, K. M., & MacKay, C. R. (2010). Diet, gut microbiota and immune responses. *Nature Immunology 2011 12:1*, *12*(1), 5–9. https://doi.org/10.1038/ni0111-5
Matzinger, D., Gutzwiller, J. P., Drewe, J., Orban, A., Engel, R., D'Amato, M., Rovati, L., & Beglinger, C. (1999). Inhibition of food intake in response to intestinal lipid is mediated by cholecystokinin in humans. *The American Journal of Physiology*, *277*(6). https://doi.org/10.1152/AJPREGU.1999.277.6.R1718
McCann, M. R., De la Rosa, M. V. G., Rosania, G. R., & Stringer, K. A. (2021). L-Carnitine and Acylcarnitines: Mitochondrial Biomarkers for Precision Medicine. *Metabolites 2021, Vol. 11, Page 51*, *11*(1), 51. https://doi.org/10.3390/METABO11010051
McFadden, B. A., & Purohit, S. (1977). Itaconate, an isocitrate lyase-directed inhibitor in Pseudomonas indigofera. *Journal of Bacteriology*, *131*(1), 136. https://doi.org/10.1128/JB.131.1.136-144.1977
McGettigan, B., McMahan, R., Orlicky, D., Burchill, M., Danhorn, T., Francis, P., Cheng, L. L., Golden-Mason, L., Jakubzick, C. V., & Rosen, H. R. (2019). Dietary Lipids Differentially Shape Nonalcoholic Steatohepatitis Progression and the Transcriptome of Kupffer Cells and Infiltrating Macrophages. *Hepatology*, *70*(1), 67–83. https://doi.org/10.1002/HEP.30401
McKinney, J. D., Höner Zu Bentrup, K., Muñoz-Elias, E. J., Miczak, A., Chen, B., Chan, W. T., Swenson, D., Sacchettini, J. C., Jacobs, W. R., & Russell, D. G. (2000). Persistence of Mycobacterium tuberculosis in macrophages and mice requires the glyoxylate shunt enzyme isocitrate lyase. *Nature*, *406*(6797), 735–738. https://doi.org/10.1038/35021074
Mechanick, J. I., Youdim, A., Jones, D. B., Garvey, W. T., Hurley, D. L., McMahon, M. M., Heinberg, L. J., Kushner, R., Adams, T. D., Shikora, S., Dixon, J. B., & Brethauer, S. (2013). Clinical Practice Guidelines for the Perioperative Nutritional, Metabolic, and Nonsurgical Support of the Bariatric Surgery Patient—2013 Update: Cosponsored by American Association of Clinical Endocrinologists, The Obesity Society, and American Society for Metabolic & Bariatric Surgery. *Obesity (Silver Spring, Md.)*, *21*(0 1), S1. https://doi.org/10.1002/OBY.20461
Michelucci, A., Cordes, T., Ghelfi, J., Pailot, A., Reiling, N., Goldmann, O., Binz, T., Wegner, A., Tallam, A., Rausell, A., Buttini, M., Linster, C. L., Medina, E., Balling, R., & Hiller, K. (2013). Immune-responsive gene 1 protein links metabolism to immunity by catalyzing itaconic acid production. *Proceedings of the National Academy of Sciences of the United States of America*, *110*(19), 7820–7825. https://doi.org/10.1073/PNAS.1218599110/-/DCSUPPLEMENTAL
Mills, E. L., Ryan, D. G., Prag, H. A., Dikovskaya, D., Menon, D., Zaslona, Z., Jedrychowski, M. P., Costa, A. S. H., Higgins, M., Hams, E., Szpyt, J., Runtsch, M. C., King, M. S., McGouran, J. F., Fischer, R., Kessler, B. M., McGettrick, A. F., Hughes, M. M., Carroll, R. G., … O'Neill, L. A. (2018). Itaconate is an anti-inflammatory metabolite that activates Nrf2 via alkylation of KEAP1. *Nature 2018 556:7699*, *556*(7699), 113–117. https://doi.org/10.1038/nature25986
Mills, E. L., Ryan, D. G., Prag, H. A., Dikovskaya, D., Menon, D., Zaslona, Z., Jedrychowski, M. P., H Costa, A. S., Higgins, M., Hams, E., Szpyt, J., Runtsch, M. C., King, M. S., McGouran, J. F., Fischer, R., Kessler, B. M., McGettrick, A. F., Hughes, M. M., Carroll,

R. G., … O, L. A. (2018). Itaconate is an anti-inflammatory metabolite that activates Nrf2 via alkylation of KEAP1 Europe PMC Funders Group. *Nature*, *556*(7699), 113–117. https://doi.org/10.1038/nature25986

Müller, T. D., Blüher, M., Tschöp, M. H., & DiMarchi, R. D. (2021). Anti-obesity drug discovery: advances and challenges. *Nature Reviews Drug Discovery 2021 21:3*, *21*(3), 201–223. https://doi.org/10.1038/s41573-021-00337-8

Muls, E., Kolanowski, J., & Scheen, A. (2001). The effects of orlistat on weight and on serum lipids in obese patients with hypercholesterolemia: a randomized, double-blind, placebo-controlled, multicentre study. *International Journal of Obesity 2001 25:11*, *25*(11), 1713–1721. https://doi.org/10.1038/sj.ijo.0801814

Napolitano, G., & Ballabio, A. (2016). TFEB at a glance. *Journal of Cell Science*, *129*(13), 2475–2481. https://doi.org/10.1242/JCS.146365/259795/AM/TFEB-AT-A-GLANCE

Naujoks, J., Tabeling, C., Dill, B. D., Hoffmann, C., Brown, A. S., Kunze, M., Kempa, S., Peter, A., Mollenkopf, H. J., Dorhoi, A., Kershaw, O., Gruber, A. D., Sander, L. E., Witzenrath, M., Herold, S., Nerlich, A., Hocke, A. C., van Driel, I., Suttorp, N., … Opitz, B. (2016). IFNs Modify the Proteome of Legionella-Containing Vacuoles and Restrict Infection Via IRG1-Derived Itaconic Acid. *PLOS Pathogens*, *12*(2), e1005408. https://doi.org/10.1371/JOURNAL.PPAT.1005408

Nemkov, T., D'Alessandro, A., & Hansen, K. C. (2015). Three-minute method for amino acid analysis by UHPLC and high-resolution quadrupole orbitrap mass spectrometry. *Amino Acids*, *47*(11), 2345–2357. https://doi.org/10.1007/S00726-015-2019-9

Nemkov, T., Reisz, J. A., Gehrke, S., Hansen, K. C., & D'Alessandro, A. (2019). High-Throughput Metabolomics: Isocratic and Gradient Mass Spectrometry-Based Methods. *Methods in Molecular Biology (Clifton, N.J.)*, *1978*, 13–26. https://doi.org/10.1007/978-1-4939-9236-2_2

Nguyen, N. T., Vu, S., Kim, E., Bodunova, N., & Phelan, M. J. (2016). Trends in utilization of bariatric surgery, 2009-2012. *Surgical Endoscopy*, *30*(7), 2723–2727. https://doi.org/10.1007/S00464-015-4535-9

Nguyen, T. M. D. (2020). Adiponectin: Role in Physiology and Pathophysiology. *International Journal of Preventive Medicine*, *11*(1), 136. https://doi.org/10.4103/IJPVM.IJPVM_193_20

Nicholson, A., Reifsnyder, P. C., Malcolm, R. D., Lucas, C. A., MacGregor, G. R., Zhang, W., & Leiter, E. H. (2010). Diet induced obesity in two C57BL/6 substrains with intact or mutant Nicotinamide Nucleotide Transhydrogenase (Nnt) gene. *Obesity (Silver Spring, Md.)*, *18*(10), 1902. https://doi.org/10.1038/OBY.2009.477

Nieto-Vazquez, I., Fernández-Veledo, S., Krämer, D. K., Vila-Bedmar, R., Garcia-Guerra, L., & Lorenzo, M. (2008). Insulin resistance associated to obesity: the link TNF-alpha. *Archives Of Physiology And Biochemistry*, *114*(3), 183–194. https://doi.org/10.1080/13813450802181047

Obradovic, M., Sudar-Milovanovic, E., Soskic, S., Essack, M., Arya, S., Stewart, A. J., Gojobori, T., & Isenovic, E. R. (2021). Leptin and Obesity: Role and Clinical Implication. *Frontiers in Endocrinology*, *12*. https://doi.org/10.3389/FENDO.2021.585887

O'Brien, P. E., Hindle, A., Brennan, L., Skinner, S., Burton, P., Smith, A., Crosthwaite, G., & Brown, W. (2019). Long-Term Outcomes After Bariatric Surgery: a Systematic Review and Meta-analysis of Weight Loss at 10 or More Years for All Bariatric Procedures and a Single-Centre Review of 20-Year Outcomes After Adjustable Gastric Banding. *Obesity Surgery*, *29*(1), 3. https://doi.org/10.1007/S11695-018-3525-0

Ohashi, K., Parker, J. L., Ouchi, N., Higuchi, A., Vita, J. A., Gokce, N., Pedersen, A. A., Kalthoff, C., Tullin, S., Sams, A., Summer, R., & Walsh, K. (2010). Adiponectin Promotes Macrophage Polarization toward an Anti-inflammatory Phenotype. *The Journal of Biological Chemistry*, *285*(9), 6153. https://doi.org/10.1074/JBC.M109.088708

Ohlsson, C., Mohan, S., Sjögren, K., Tivesten, Å., Isgaard, J., Isaksson, O., Jansson, J. O., & Svensson, J. (2009). The role of liver-derived insulin-like growth factor-I. *Endocrine*

Reviews, *30*(5), 494–535. https://doi.org/10.1210/ER.2009-0010

Olagnier, D., Brandtoft, A. M., Gunderstofte, C., Villadsen, N. L., Krapp, C., Thielke, A. L., Laustsen, A., Peri, S., Hansen, A. L., Bonefeld, L., Thyrsted, J., Bruun, V., Iversen, M. B., Lin, L., Artegoitia, V. M., Su, C., Yang, L., Lin, R., Balachandran, S., … Holm, C. K. (2018). Nrf2 negatively regulates STING indicating a link between antiviral sensing and metabolic reprogramming. *Nature Communications*, *9*(1). https://doi.org/10.1038/S41467-018-05861-7

Olagnier, D., Farahani, E., Thyrsted, J., Blay-Cadanet, J., Herengt, A., Idorn, M., Hait, A., Hernaez, B., Knudsen, A., Iversen, M. B., Schilling, M., Jørgensen, S. E., Thomsen, M., Reinert, L. S., Lappe, M., Hoang, H. D., Gilchrist, V. H., Hansen, A. L., Ottosen, R., … Holm, C. K. (2020). SARS-CoV2-mediated suppression of NRF2-signaling reveals potent antiviral and anti-inflammatory activity of 4-octyl-itaconate and dimethyl fumarate. *Nature Communications*, *11*(1). https://doi.org/10.1038/S41467-020-18764-3

Omede, A., Zi, M., Prehar, S., Maqsood, A., Stafford, N., Mamas, M., Cartwright, E., & Oceandy, D. (2016). The oxoglutarate receptor 1 (OXGR1) modulates pressure overload-induced cardiac hypertrophy in mice. *Biochemical and Biophysical Research Communications*, *479*(4), 708. https://doi.org/10.1016/J.BBRC.2016.09.147

O'Neill, L. A. J., & Artyomov, M. N. (2019). Itaconate: the poster child of metabolic reprogramming in macrophage function. *Nature Reviews Immunology 2019 19:5*, *19*(5), 273–281. https://doi.org/10.1038/s41577-019-0128-5

Palmas, V., Pisanu, S., Madau, V., Casula, E., Deledda, A., Cusano, R., Uva, P., Vascellari, S., Loviselli, A., Manzin, A., & Velluzzi, F. (2021). Gut microbiota markers associated with obesity and overweight in Italian adults. *Scientific Reports*, *11*(1), 5532. https://doi.org/10.1038/S41598-021-84928-W

Pan, J., Zhao, X., Lin, C., Xu, H., Yin, Z., Liu, T., & Zhang, S. (2014). Immune responsive gene 1, a novel oncogene, increases the growth and tumorigenicity of glioma. *Oncology Reports*, *32*(5), 1957–1966. https://doi.org/10.3892/or.2014.3474

Pang, Z., Zhou, G., Ewald, J., Chang, L., Hacariz, O., Basu, N., & Xia, J. (2022). Using MetaboAnalyst 5.0 for LC-HRMS spectra processing, multi-omics integration and covariate adjustment of global metabolomics data. *Nature Protocols*, *17*(8), 1735–1761. https://doi.org/10.1038/S41596-022-00710-W

Park, E. J., Lee, J. H., Yu, G. Y., He, G., Ali, S. R., Holzer, R. G., Österreicher, C. H., Takahashi, H., & Karin, M. (2010). Dietary and genetic obesity promote liver inflammation and tumorigenesis by enhancing IL-6 and TNF expression. *Cell*, *140*(2), 197. https://doi.org/10.1016/J.CELL.2009.12.052

Parks, B. W., Nam, E., Org, E., Kostem, E., Norheim, F., Hui, S. T., Pan, C., Civelek, M., Rau, C. D., Bennett, B. J., Mehrabian, M., Ursell, L. K., He, A., Castellani, L. W., Zinker, B., Kirby, M., Drake, T. A., Drevon, C. A., Knight, R., … Lusis, A. J. (2013). Genetic control of obesity and gut microbiota composition in response to high-fat, high-sucrose diet in mice. *Cell Metabolism*, *17*(1), 141–152. https://doi.org/10.1016/J.CMET.2012.12.007

Pati, S., Irfan, W., Jameel, A., Ahmed, S., & Shahid, R. K. (2023). Obesity and Cancer: A Current Overview of Epidemiology, Pathogenesis, Outcomes, and Management. *Cancers*, *15*(2). https://doi.org/10.3390/CANCERS15020485

Paulo, E., & Wang, B. (2019). Towards a Better Understanding of Beige Adipocyte Plasticity. *Cells*, *8*(12). https://doi.org/10.3390/CELLS8121552

Peloquin, J. M., & Nguyen, D. D. (2013). The microbiota and inflammatory bowel disease: Insights from animal models. *Anaerobe*, *24*, 102–106. https://doi.org/10.1016/J.ANAEROBE.2013.04.006

Perry, B., & Wang, Y. (2012). Appetite regulation and weight control: the role of gut hormones. *Nutrition and Diabetes*, *2*, 26. https://doi.org/10.1038/nutd.2011.21

Phelps, N. H., Singleton, R. K., Zhou, B., Heap, R. A., Mishra, A., Bennett, J. E., Paciorek, C. J., Lhoste, V. P., Carrillo-Larco, R. M., Stevens, G. A., Rodriguez-Martinez, A., Bixby, H., Bentham, J., Di Cesare, M., Danaei, G., Rayner, A. W., Barradas-Pires, A., Cowan, M.

J., Savin, S., … Ezzati, M. (2024). Worldwide trends in underweight and obesity from 1990 to 2022: a pooled analysis of 3663 population-representative studies with 222 million children, adolescents, and adults. *The Lancet*, *403*(10431), 1027–1050. https://doi.org/10.1016/S0140-6736(23)02750-2

Pires-Afonso, Y., Muller, A., Grzyb, K., Oudin, A., Yabo, Y. A., Sousa, C., Scafidi, A., Poli, A., Cosma, A., Halder, R., Coowar, D., Golebiewska, A., Skupin, A., Niclou, S. P., & Michelucci, A. (2022). Elucidating tumour-associated microglia/macrophage diversity along glioblastoma progression and under ACOD1 deficiency. *Molecular Oncology*, *16*(17), 3167–3191. https://doi.org/10.1002/1878-0261.13287

Pouwels, S., Sakran, N., Graham, Y., Leal, A., Pintar, T., Yang, W., Kassir, R., Singhal, R., Mahawar, K., & Ramnarain, D. (2022). Non-alcoholic fatty liver disease (NAFLD): a review of pathophysiology, clinical management and effects of weight loss. *BMC Endocrine Disorders*, *22*(1). https://doi.org/10.1186/S12902-022-00980-1

Qin, W., Qin, K., Zhang, Y., Jia, W., Chen, Y., Cheng, B., Peng, L., Chen, N., Liu, Y., Zhou, W., Wang, Y. L., Chen, X., & Wang, C. (2019). S-glycosylation-based cysteine profiling reveals regulation of glycolysis by itaconate. *Nature Chemical Biology 2019 15:10*, *15*(10), 983–991. https://doi.org/10.1038/s41589-019-0323-5

Quince, C., Walker, A. W., Simpson, J. T., Loman, N. J., & Segata, N. (2017). Shotgun metagenomics, from sampling to analysis. *Nature Biotechnology 2017 35:9*, *35*(9), 833–844. https://doi.org/10.1038/nbt.3935

Rada, P., González-Rodríguez, Á., García-Monzón, C., & Valverde, Á. M. (2020). Understanding lipotoxicity in NAFLD pathogenesis: is CD36 a key driver? *Cell Death & Disease 2020 11:9*, *11*(9), 1–15. https://doi.org/10.1038/s41419-020-03003-w

Rajapakse, J., Khatiwada, S., Akon, A. C., Yu, K. L., Shen, S., & Zekry, A. (2023). Unveiling the complex relationship between gut microbiota and liver cancer: opportunities for novel therapeutic interventions. *Gut Microbes*, *15*(2). https://doi.org/10.1080/19490976.2023.2240031

Ramracheya, R., Chapman, C., Chibalina, M., Dou, H., Miranda, C., González, A., Moritoh, Y., Shigeto, M., Zhang, Q., Braun, M., Clark, A., Johnson, P. R., Rorsman, P., & Briant, L. J. B. (2018). GLP-1 suppresses glucagon secretion in human pancreatic alpha-cells by inhibition of P/Q-type Ca2+ channels. *Physiological Reports*, *6*(17). https://doi.org/10.14814/PHY2.13852

Rangel-Azevedo, C., Santana-Oliveira, D. A., Miranda, C. S., Martins, F. F., Mandarim-de-Lacerda, C. A., & Souza-Mello, V. (2022). Progressive brown adipocyte dysfunction: Whitening and impaired nonshivering thermogenesis as long-term obesity complications. *The Journal of Nutritional Biochemistry*, *105*, 109002. https://doi.org/10.1016/J.JNUTBIO.2022.109002

Redinger, R. N. (2007). The Pathophysiology of Obesity and Its Clinical Manifestations. *Gastroenterology & Hepatology*, *3*(11), 856. /pmc/articles/PMC3104148/

Ren, K., Lv, Y., Zhuo, Y., Chen, C., Shi, H., Guo, L., Yang, G., Hou, Y., Tan, R. X., & Li, E. (2016). *Suppression of IRG-1 Reduces Inflammatory Cell Infiltration and Lung Injury in Respiratory Syncytial Virus Infection by Reducing Production of Reactive Oxygen Species*. https://doi.org/10.1128/JVI.00563-16

Ridaura, V. K., Faith, J. J., Rey, F. E., Cheng, J., Duncan, A. E., Kau, A. L., Griffin, N. W., Lombard, V., Henrissat, B., Bain, J. R., Muehlbauer, M. J., Ilkayeva, O., Semenkovich, C. F., Funai, K., Hayashi, D. K., Lyle, B. J., Martini, M. C., Ursell, L. K., Clemente, J. C., … Gordon, J. I. (2013a). Gut microbiota from twins discordant for obesity modulate metabolism in mice. *Science (New York, N.Y.)*, *341*(6150). https://doi.org/10.1126/SCIENCE.1241214

Ridaura, V. K., Faith, J. J., Rey, F. E., Cheng, J., Duncan, A. E., Kau, A. L., Griffin, N. W., Lombard, V., Henrissat, B., Bain, J. R., Muehlbauer, M. J., Ilkayeva, O., Semenkovich, C. F., Funai, K., Hayashi, D. K., Lyle, B. J., Martini, M. C., Ursell, L. K., Clemente, J. C., … Gordon, J. I. (2013b). Gut microbiota from twins discordant for obesity modulate

metabolism in mice. *Science (New York, N.Y.)*, *341*(6150). https://doi.org/10.1126/SCIENCE.1241214

Ridaura, V. K., Faith, J. J., Rey, F. E., Cheng, J., Duncan, A. E., Kau, A. L., Griffin, N. W., Lombard, V., Henrissat, B., Bain, J. R., Muehlbauer, M. J., Ilkayeva, O., Semenkovich, C. F., Funai, K., Hayashi, D. K., Lyle, B. J., Martini, M. C., Ursell, L. K., Clemente, J. C., … Gordon, J. I. (2013c). Gut microbiota from twins discordant for obesity modulate metabolism in mice. *Science*, *341*(6150). https://doi.org/10.1126/SCIENCE.1241214/SUPPL_FILE/RIDAURATABLES9.XLSX

Ríos-Covián, D., Ruas-Madiedo, P., Margolles, A., Gueimonde, M., De los Reyes-Gavilán, C. G., & Salazar, N. (2016). Intestinal Short Chain Fatty Acids and their Link with Diet and Human Health. *Frontiers in Microbiology*, *7*(FEB), 185. https://doi.org/10.3389/FMICB.2016.00185

Riquelme, S. A., Liimatta, K., Wong Fok Lung, T., Fields, B., Ahn, D., Chen, D., Lozano, C., Sáenz, Y., Uhlemann, A. C., Kahl, B. C., Britto, C. J., DiMango, E., & Prince, A. (2020). Pseudomonas aeruginosa utilizes host-derived itaconate to redirect its metabolism to promote biofilm formation. *Cell Metabolism*, *31*(6), 1091. https://doi.org/10.1016/J.CMET.2020.04.017

Roh, E., & Kim, M.-S. (2016). *Brain Regulation of Energy Metabolism*. https://doi.org/10.3803/EnM.2016.31.4.519

Rong, J. X., Qiu, Y., Hansen, M. K., Zhu, L., Zhang, V., Xie, M., Okamoto, Y., Mattie, M. D., Higashiyama, H., Asano, S., Strum, J. C., & Ryan, T. E. (2007). Adipose Mitochondrial Biogenesis Is Suppressed in db/db and High-Fat Diet–Fed Mice and Improved by Rosiglitazone. *Diabetes*, *56*(7), 1751–1760. https://doi.org/10.2337/DB06-1135

Rosen, E. D., & Spiegelman, B. M. (2014). What We Talk About When We Talk About Fat. *Cell*, *156*(1), 20–44. https://doi.org/10.1016/J.CELL.2013.12.012

Ruan, H., & Dong, L. Q. (2016). Adiponectin signaling and function in insulin target tissues. *Journal of Molecular Cell Biology*, *8*(2), 101. https://doi.org/10.1093/JMCB/MJW014

Ruetz, M., Campanello, G. C., Purchal, M., Shen, H., McDevitt, L., Gouda, H., Wakabayashi, S., Zhu, J., Rubin, E. J., Warncke, K., Mootha, V. K., Koutmos, M., & Banerjee, R. (2019). Itaconyl-CoA forms a stable biradical in methylmalonyl-CoA mutase and derails its activity and repair. *Science (New York, N.Y.)*, *366*(6465), 589. https://doi.org/10.1126/SCIENCE.AAY0934

Rui, L. (2014). *Energy Metabolism in the Liver*. https://doi.org/10.1002/cphy.c130024

Runtsch, M. C., Angiari, S., Hooftman, A., Wadhwa, R., Zhang, Y., Zheng, Y., Spina, J. S., Ruzek, M. C., Argiriadi, M. A., McGettrick, A. F., Mendez, R. S., Zotta, A., Peace, C. G., Walsh, A., Chirillo, R., Hams, E., Fallon, P. G., Jayamaran, R., Dua, K., … O'Neill, L. A. J. (2022). Itaconate and itaconate derivatives target JAK1 to suppress alternative activation of macrophages. *Cell Metabolism*, *34*(3), 487-501.e8. https://doi.org/10.1016/j.cmet.2022.02.002

Sakai, A., Kusumoto, A., Kiso, Y., & Furuya, E. (2004). Itaconate reduces visceral fat by inhibiting fructose 2,6-bisphosphate synthesis in rat liver. *Nutrition (Burbank, Los Angeles County, Calif.)*, *20*(11–12), 997–1002. https://doi.org/10.1016/J.NUT.2004.08.007

Sakers, A., De Siqueira, M. K., Seale, P., & Villanueva, C. J. (2022). Adipose tissue plasticity in health and disease. *Cell*, *185*(3), 419. https://doi.org/10.1016/J.CELL.2021.12.016

Saltiel, A. R., & Olefsky, J. M. (2017). Inflammatory mechanisms linking obesity and metabolic disease. *The Journal of Clinical Investigation*, *127*(1), 1–4. https://doi.org/10.1172/JCI92035

Sam, S., & Mazzone, T. (2014). Adipose tissue changes in obesity and the impact on metabolic function. *Translational Research*, *164*(4), 284–292. https://doi.org/10.1016/J.TRSL.2014.05.008

Sato, A., Nakashima, H., Nakashima, M., Ikarashi, M., Nishiyama, K., Kinoshita, M., & Seki, S. (2014). Involvement of the TNF and FasL Produced by CD11b Kupffer Cells/Macrophages in CCl4-Induced Acute Hepatic Injury. *PLoS ONE*, *9*(3), 92515.

https://doi.org/10.1371/JOURNAL.PONE.0092515
Savvi, S., Warner, D. F., Kana, B. D., McKinney, J. D., Mizrahi, V., & Dawes, S. S. (2008). Functional Characterization of a Vitamin B12-Dependent Methylmalonyl Pathway in Mycobacterium tuberculosis: Implications for Propionate Metabolism during Growth on Fatty Acids. *Journal of Bacteriology*, *190*(11), 3886. https://doi.org/10.1128/JB.01767-07
Sayar-Atasoy, N., Laule, C., Aklan, I., Kim, H., Yavuz, Y., Ates, T., Coban, I., Koksalar-Alkan, F., Rysted, J., Davis, D., Singh, U., Alp, M. I., Yilmaz, B., Cui, H., & Atasoy, D. (2023). Adrenergic modulation of melanocortin pathway by hunger signals. *Nature Communications 2023 14:1*, *14*(1), 1–15. https://doi.org/10.1038/s41467-023-42362-8
Scagliola, A., Mainini, F., & Cardaci, S. (2020). The tricarboxylic acid cycle at the crossroad between cancer and immunity. In *Antioxidants and Redox Signaling* (Vol. 32, Issue 12, pp. 834–852). Mary Ann Liebert Inc. https://doi.org/10.1089/ars.2019.7974
Scheithauer, T. P. M., Rampanelli, E., Nieuwdorp, M., Vallance, B. A., Verchere, C. B., van Raalte, D. H., & Herrema, H. (2020). Gut Microbiota as a Trigger for Metabolic Inflammation in Obesity and Type 2 Diabetes. *Frontiers in Immunology*, *11*, 571731. https://doi.org/10.3389/FIMMU.2020.571731/BIBTEX
Scheja, L., & Heeren, J. (2019). *The endocrine function of adipose tissues in health and cardiometabolic disease*. https://doi.org/10.1038/s41574-019-0230-6
Schmidt, G., & Richter, K. (2000). Expression pattern of XIRG, a marker for non-neural ectoderm. *Development Genes and Evolution*, *210*(11), 575–578. https://doi.org/10.1007/S004270000095
Schmitz-Peiffer, C., & Biden, T. J. (2008). *Protein Kinase C Function in Muscle, Liver, and-Cells and Its Therapeutic Implications for Type 2 Diabetes*. https://doi.org/10.2337/db07-1769
Schneider, K. M., Mohs, A., Gui, W., Galvez, E. J. C., Candels, L. S., Hoenicke, L., Muthukumarasamy, U., Holland, C. H., Elfers, C., Kilic, K., Schneider, C. V., Schierwagen, R., Strnad, P., Wirtz, T. H., Marschall, H. U., Latz, E., Lelouvier, B., Saez-Rodriguez, J., de Vos, W., … Trautwein, C. (2022). Imbalanced gut microbiota fuels hepatocellular carcinoma development by shaping the hepatic inflammatory microenvironment. *Nature Communications 2022 13:1*, *13*(1), 1–19. https://doi.org/10.1038/s41467-022-31312-5
Schrauwen, P., & Hesselink, M. K. C. (2004). Oxidative Capacity, Lipotoxicity, and Mitochondrial Damage in Type 2 Diabetes. *Diabetes*, *53*(6), 1412–1417. https://doi.org/10.2337/DIABETES.53.6.1412
Schroeder, B. O., & Bäckhed, F. (2016). Signals from the gut microbiota to distant organs in physiology and disease. *Nature Medicine 2016 22:10*, *22*(10), 1079–1089. https://doi.org/10.1038/nm.4185
Schulz, C., Perdiguero, E. G., Chorro, L., Szabo-Rogers, H., Cagnard, N., Kierdorf, K., Prinz, M., Wu, B., Jacobsen, S. E. W., Pollard, J. W., Frampton, J., Liu, K. J., & Geissmann, F. (2012). A lineage of myeloid cells independent of myb and hematopoietic stem cells. *Science*, *335*(6077), 86–90. https://doi.org/10.1126/SCIENCE.1219179/SUPPL_FILE/SCHULZGOMEZ1219179.AVI
Schuster, E. M., Epple, M. W., Glaser, K. M., Mihlan, M., Lucht, K., Zimmermann, J. A., Bremser, A., Polyzou, A., Obier, N., Cabezas-Wallscheid, N., Trompouki, E., Ballabio, A., Vogel, J., Buescher, J. M., Westermann, A. J., & Rambold, A. S. (2022). TFEB induces mitochondrial itaconate synthesis to suppress bacterial growth in macrophages. *Nature Metabolism 2022 4:7*, *4*(7), 856–866. https://doi.org/10.1038/s42255-022-00605-w
Schwabe, R. F., & Greten, T. F. (2020). Gut microbiome in HCC – Mechanisms, diagnosis and therapy. *Journal of Hepatology*, *72*(2), 230–238. https://doi.org/10.1016/J.JHEP.2019.08.016/ATTACHMENT/270C52F8-4F5B-41BB-B4E5-973724061BB6/DISCLOSURES.PDF
Schwartz, D. R., & Lazar, M. A. (2011). Human Resistin: Found in Translation From Mouse to

Man. *Trends in Endocrinology and Metabolism: TEM*, *22*(7), 259. https://doi.org/10.1016/J.TEM.2011.03.005
Sealy, L., & Chalkley, R. (1978). The effect of sodium butyrate on histone modification. *Cell*, *14*(1), 115–121. https://doi.org/10.1016/0092-8674(78)90306-9
Sender, R., Fuchs, S., & Milo, R. (2016). Are We Really Vastly Outnumbered? Revisiting the Ratio of Bacterial to Host Cells in Humans. *Cell*, *164*(3), 337–340. https://doi.org/10.1016/j.cell.2016.01.013
Sendra, M., Saco, A., Rey-Campos, M., Novoa, B., & Figueras, A. (2020). Immune-responsive gene 1 (IRG1) and dimethyl itaconate are involved in the mussel immune response. *Fish & Shellfish Immunology*, *106*, 645–655. https://doi.org/10.1016/J.FSI.2020.07.034
Sghir, A., Gramet, G., Suau, A., Rochet, V., Pochart, P., & Dore, J. (2000). Quantification of Bacterial Groups within Human Fecal Flora by Oligonucleotide Probe Hybridization. *Applied and Environmental Microbiology*, *66*(5), 2263–2266. https://doi.org/10.1128/AEM.66.5.2263-2266.2000
Shakespear, M. R., Halili, M. A., Irvine, K. M., Fairlie, D. P., & Sweet, M. J. (2011). Histone deacetylases as regulators of inflammation and immunity. *Trends in Immunology*, *32*(7), 335–343. https://doi.org/10.1016/j.it.2011.04.001
Sharma, V., Smolin, J., Nayak, J., Ayala, J. E., Scott, D. A., Peterson, S. N., & Freeze, H. H. (2018). Mannose Alters Gut Microbiome, Prevents Diet-Induced Obesity, and Improves Host Metabolism. *Cell Reports*, *24*(12), 3087–3098. https://doi.org/10.1016/J.CELREP.2018.08.064
Shi, H., Kokoeva, M. V., Inouye, K., Tzameli, I., Yin, H., & Flier, J. S. (2006). TLR4 links innate immunity and fatty acid-induced insulin resistance. *The Journal of Clinical Investigation*, *116*(11), 3015–3025. https://doi.org/10.1172/JCI28898
Shi, S., Blumenthal, A., Hickey, C. M., Gandotra, S., Levy, D., & Ehrt, S. (2005). Expression of Many Immunologically Important Genes in Mycobacterium tuberculosis-Infected Macrophages Is Independent of Both TLR2 and TLR4 but Dependent on IFN-αβ Receptor and STAT1. *The Journal of Immunology*, *175*(5), 3318–3328. https://doi.org/10.4049/JIMMUNOL.175.5.3318
Shi, X., Zhou, H., Wei, J., Mo, W., Li, Q., & Lv, X. (2022). The signaling pathways and therapeutic potential of itaconate to alleviate inflammation and oxidative stress in inflammatory diseases. *Redox Biology*, *58*, 102553. https://doi.org/10.1016/J.REDOX.2022.102553
Shinde, A. B., Song, A., & Wang, Q. A. (2021). Brown Adipose Tissue Heterogeneity, Energy Metabolism, and Beyond. *Frontiers in Endocrinology*, *12*, 651763. https://doi.org/10.3389/FENDO.2021.651763/BIBTEX
Shreiner, A. B., Kao, J. Y., & Young, V. B. (2015). The gut microbiome in health and in disease. *Current Opinion in Gastroenterology*, *31*(1), 69. https://doi.org/10.1097/MOG.0000000000000139
Siersbæk, M. S., Ditzel, N., Hejbøl, E. K., Præstholm, S. M., Markussen, L. K., Avolio, F., Li, L., Lehtonen, L., Hansen, A. K., Schrøder, H. D., Krych, L., Mandrup, S., Langhorn, L., Bollen, P., & Grøntved, L. (2020). C57BL/6J substrain differences in response to high-fat diet intervention. *Scientific Reports 2020 10:1*, *10*(1), 1–15. https://doi.org/10.1038/s41598-020-70765-w
Sjöström, L., Peltonen, M., Jacobson, P., Sjöström, C. D., Karason, K., Wedel, H., Ahlin, S., Anveden, Å., Bengtsson, C., Bergmark, G., Bouchard, C., Carlsson, B., Dahlgren, S., Karlsson, J., Lindroos, A. K., Lönroth, H., Narbro, K., Näslund, I., Olbers, T., … Carlsson, L. M. S. (2012). Bariatric Surgery and Long-term Cardiovascular Events. *JAMA*, *307*(1), 56–65. https://doi.org/10.1001/JAMA.2011.1914
Sohn, W., Lee, H. W., Lee, S., Lim, J. H., Lee, M. W., Park, C. H., & Yoon, S. K. (2021). Obesity and the risk of primary liver cancer: A systematic review and meta-analysis. *Clinical and Molecular Hepatology*, *27*(1), 157. https://doi.org/10.3350/CMH.2020.0176
Song, Z., Xiaoli, A. M., & Yang, F. (2018). *Regulation and Metabolic Significance of De Novo*

Lipogenesis in Adipose Tissues. https://doi.org/10.3390/nu10101383
Speakman, J. R. (2013). Measuring Energy Metabolism in the Mouse – Theoretical, Practical, and Analytical Considerations. *Frontiers in Physiology*, *4*. https://doi.org/10.3389/FPHYS.2013.00034
Stickel, F., & Hellerbrand, C. (2010). Non-alcoholic fatty liver disease as a risk factor for hepatocellular carcinoma: mechanisms and implications. *Gut*, *59*(10), 1303–1307. https://doi.org/10.1136/GUT.2009.199661
Su, C., Cheng, T., Huang, J., Zhang, T., & Yin, H. (2023). 4-Octyl itaconate restricts STING activation by blocking its palmitoylation. *Cell Reports*, *42*(9). https://doi.org/10.1016/j.celrep.2023.113040
Summers, S. A., Garza, L. A., Zhou, H., & Birnbaum, M. J. (1998). Regulation of Insulin-Stimulated Glucose Transporter GLUT4 Translocation and Akt Kinase Activity by Ceramide. *MOLECULAR AND CELLULAR BIOLOGY*, *18*(9), 5457–5464.
Suzuki, T., Yoshida, S., & Hara, H. (2008). Physiological concentrations of short-chain fatty acids immediately suppress colonic epithelial permeability. *British Journal of Nutrition*, *100*(2), 297–305. https://doi.org/10.1017/S0007114508888733
Swain #, A., Bambouskova #, M., Kim, H., Andhey, S., Duncan, D., Auclair, K., Chubukov, V., Simons, D. M., Roddy, T. P., Stewart, K. M., & Artyomov, M. N. (2020). *Comparative evaluation of itaconate and its derivatives reveals divergent inflammasome and type I interferon regulation in macrophages*. *2*(7), 594–602. https://doi.org/10.1038/s42255-020-0210-0
Tabuchi, C., & Sul, H. S. (2021). Signaling Pathways Regulating Thermogenesis. *Frontiers in Endocrinology*, *12*, 595020. https://doi.org/10.3389/FENDO.2021.595020/BIBTEX
Tchang, B. G., Aras, M., Kumar, R. B., & Aronne, L. J. (2021). Pharmacologic Treatment of Overweight and Obesity in Adults. *Endotext*. https://www.ncbi.nlm.nih.gov/books/NBK279038/
Thomas, D., & Apovian, C. (2017). Macrophage functions in lean and obese adipose tissue. *Metabolism: Clinical and Experimental*, *72*, 120. https://doi.org/10.1016/J.METABOL.2017.04.005
Thomas, F., Hehemann, J. H., Rebuffet, E., Czjzek, M., & Michel, G. (2011). Environmental and Gut Bacteroidetes: The Food Connection. *Frontiers in Microbiology*, *2*(MAY). https://doi.org/10.3389/FMICB.2011.00093
Tilg, H., & Kaser, A. (2011). Gut microbiome, obesity, and metabolic dysfunction. *The Journal of Clinical Investigation*, *121*(6), 2126. https://doi.org/10.1172/JCI58109
Tiraby, C., Tavernier, G., Lefort, C., Larrouy, D., Bouillaud, F., Ricquier, D., & Langin, D. (2003). Acquirement of brown fat cell features by human white adipocytes. *Journal of Biological Chemistry*, *278*(35), 33370–33376. https://doi.org/10.1074/jbc.M305235200
Tomlinson, K. L., Lung, T. W. F., Dach, F., Annavajhala, M. K., Gabryszewski, S. J., Groves, R. A., Drikic, M., Francoeur, N. J., Sridhar, S. H., Smith, M. L., Khanal, S., Britto, C. J., Sebra, R., Lewis, I., Uhlemann, A. C., Kahl, B. C., Prince, A. S., & Riquelme, S. A. (2021). Staphylococcus aureus induces an itaconate-dominated immunometabolic response that drives biofilm formation. *Nature Communications*, *12*(1). https://doi.org/10.1038/S41467-021-21718-Y
Topping, D. L., & Clifton, P. M. (2001). *Short-Chain Fatty Acids and Human Colonic Function: Roles of Resistant Starch and Nonstarch Polysaccharides*. http://physrev.physiology.org
Torretta, S., Scagliola, A., Ricci, L., Mainini, F., Di Marco, S., Cuccovillo, I., Kajaste-Rudnitski, A., Sumpton, D., Ryan, K. M., & Cardaci, S. (2020). D-mannose suppresses macrophage IL-1β production. *Nature Communications*, *11*(1). https://doi.org/10.1038/S41467-020-20164-6
Truax, A. D., Chen, L., Tam, J. W., Cheng, N., Guo, H., Koblansky, A. A., Chou, W. C., Wilson, J. E., Brickey, W. J., Petrucelli, A., Liu, R., Cooper, D. E., Koenigsknecht, M. J., Young, V. B., Netea, M. G., Stienstra, R., Sartor, R. B., Montgomery, S. A., Coleman, R.

A., & Ting, J. P. Y. (2018a). The Inhibitory Innate Immune Sensor NLRP12 Maintains a Threshold against Obesity by Regulating Gut Microbiota Homeostasis. *Cell Host and Microbe*, *24*(3), 364-378.e6. https://doi.org/10.1016/j.chom.2018.08.009

Truax, A. D., Chen, L., Tam, J. W., Cheng, N., Guo, H., Koblansky, A. A., Chou, W. C., Wilson, J. E., Brickey, W. J., Petrucelli, A., Liu, R., Cooper, D. E., Koenigsknecht, M. J., Young, V. B., Netea, M. G., Stienstra, R., Sartor, R. B., Montgomery, S. A., Coleman, R. A., & Ting, J. P. Y. (2018b). The Inhibitory Innate Immune Sensor NLRP12 Maintains a Threshold against Obesity by Regulating Gut Microbiota Homeostasis. *Cell Host and Microbe*, *24*(3), 364-378.e6. https://doi.org/10.1016/J.CHOM.2018.08.009/ATTACHMENT/31101BAA-F164-4796-A1C8-D412DF52EB17/MMC2.PDF

Tsuchida, T., Lee, Y. A., Fujiwara, N., Ybanez, M., Allen, B., Martins, S., Fiel, M. I., Goossens, N., Chou, H. I., Hoshida, Y., & Friedman, S. L. (2018). A Simple Diet- and Chemical-Induced Murine NASH Model with Rapid Progression of Steatohepatitis, Fibrosis and Liver Cancer. *Journal of Hepatology*, *69*(2), 385. https://doi.org/10.1016/J.JHEP.2018.03.011

Tumanov, S., Bulusu, V., Gottlieb, E., & Kamphorst, J. J. (2016). A rapid method for quantifying free and bound acetate based on alkylation and GC-MS analysis. *Cancer & Metabolism 2016 4:1*, *4*(1), 1–12. https://doi.org/10.1186/S40170-016-0157-5

Turnbaugh, P. J., Bäckhed, F., Fulton, L., & Gordon, J. I. (2008). Diet-induced obesity is linked to marked but reversible alterations in the mouse distal gut microbiome. *Cell Host & Microbe*, *3*(4), 213–223. https://doi.org/10.1016/J.CHOM.2008.02.015

Turnbaugh, P. J., Ley, R. E., Mahowald, M. A., Magrini, V., Mardis, E. R., & Gordon, J. I. (2006a). An obesity-associated gut microbiome with increased capacity for energy harvest. *Nature 2006 444:7122*, *444*(7122), 1027–1031. https://doi.org/10.1038/nature05414

Turnbaugh, P. J., Ley, R. E., Mahowald, M. A., Magrini, V., Mardis, E. R., & Gordon, J. I. (2006b). An obesity-associated gut microbiome with increased capacity for energy harvest. *Nature 2006 444:7122*, *444*(7122), 1027–1031. https://doi.org/10.1038/nature05414

Uddin, M. J., Joe, Y., Kim, S. K., Jeong, S. O., Ryter, S. W., Pae, H. O., & Chung, H. T. (2016). IRG1 induced by heme oxygenase-1/carbon monoxide inhibits LPS-mediated sepsis and pro-inflammatory cytokine production. *Cellular and Molecular Immunology*, *13*(2), 170. https://doi.org/10.1038/CMI.2015.02

Uysal, K. T., Wiesbrock, S. M., Marino, M. W., & Hotamisligil, G. S. (1997). Protection from obesity-induced insulin resistance in mice lacking TNF-α function. *Nature 1997 389:6651*, *389*(6651), 610–614. https://doi.org/10.1038/39335

Van de Peer, Y., Chapelle, S., & De Wachter, R. (1996). A quantitative map of nucleotide substitution rates in bacterial rRNA. *Nucleic Acids Research*, *24*(17), 3381–3391. https://doi.org/10.1093/NAR/24.17.3381

Villarroya, F., Peyrou, M., & Giralt, M. (2017). Transcriptional regulation of the uncoupling protein-1 gene. *Biochimie*, *134*, 86–92. https://doi.org/10.1016/J.BIOCHI.2016.09.017

Vinolo, M. A. R., Rodrigues, H. G., Nachbar, R. T., & Curi, R. (2011). Regulation of Inflammation by Short Chain Fatty Acids. *Nutrients*, *3*, 858–876. https://doi.org/10.3390/nu3100858

Wakil, S. J., & Abu-Elheiga, L. A. (2009). Fatty acid metabolism: target for metabolic syndrome. *Journal of Lipid Research*, *50*(Suppl), S138. https://doi.org/10.1194/JLR.R800079-JLR200

Wang, J. Y., Wang, Q. W., Yang, X. Y., Yang, W., Li, D. R., Jin, J. Y., Zhang, H. C., & Zhang, X. F. (2023). GLP−1 receptor agonists for the treatment of obesity: Role as a promising approach. *Frontiers in Endocrinology*, *14*. https://doi.org/10.3389/FENDO.2023.1085799

Weisberg, S. P., McCann, D., Desai, M., Rosenbaum, M., Leibel, R. L., & Anthony W. Ferrante, Jr. (2003). Obesity is associated with macrophage accumulation in adipose tissue. *Journal of Clinical Investigation*, *112*(12), 1796. https://doi.org/10.1172/JCI19246

Weiss, J. M., Davies, L. C., Karwan, M., Ileva, L., Ozaki, M. K., Cheng, R. Y. S., Ridnour, L. A., Annunziata, C. M., Wink, D. A., & McVicar, D. W. (2018). Itaconic acid mediates crosstalk between macrophage metabolism and peritoneal tumors. *The Journal of Clinical Investigation*, *128*(9), 3794–3805. https://doi.org/10.1172/JCI99169

Weiss, J. M., Palmieri, E. M., Gonzalez-Cotto, M., Bettencourt, I. A., Megill, E. L., Snyder, N. W., & McVicar, D. W. (2023). Itaconic acid underpins hepatocyte lipid metabolism in non-alcoholic fatty liver disease in male mice. *Nature Metabolism 2023 5:6*, *5*(6), 981–995. https://doi.org/10.1038/s42255-023-00801-2

Wellman, P. J. (2000). Norepinephrine and the control of food intake. *Nutrition*, *16*(10), 837–842. https://doi.org/10.1016/S0899-9007(00)00415-9

Willard, F. S., Douros, J. D., Gabe, M. B. N., Showalter, A. D., Wainscott, D. B., Suter, T. M., Capozzi, M. E., van der Velden, W. J. C., Stutsman, C., Cardona, G. R., Urva, S., Emmerson, P. J., Holst, J. J., D'Alessio, D. A., Coghlan, M. P., Rosenkilde, M. M., Campbell, J. E., & Sloop, K. W. (2020). Tirzepatide is an imbalanced and biased dual GIP and GLP-1 receptor agonist. *JCI Insight*, *5*(17). https://doi.org/10.1172/JCI.INSIGHT.140532

Williams, L. M., Campbell, F. M., Drew, J. E., Koch, C., Hoggard, N., Rees, W. D., Kamolrat, T., Ngo, H. T., Steffensen, I. L., Gray, S. R., & Tups, A. (2014). The Development of Diet-Induced Obesity and Glucose Intolerance in C57Bl/6 Mice on a High-Fat Diet Consists of Distinct Phases. *PLOS ONE*, *9*(8), e106159. https://doi.org/10.1371/JOURNAL.PONE.0106159

Winterhoff, M., Chen, F., Sahini, N., Ebensen, T., Kuhn, M., Kaever, V., Bähre, H., & Pessler, F. (2021). Establishment, validation, and initial application of a sensitive lc-ms/ms assay for quantification of the naturally occurring isomers itaconate, mesaconate, and citraconate. *Metabolites*, *11*(5). https://doi.org/10.3390/METABO11050270/S1

Wolf, M. J., Adili, A., Piotrowitz, K., Abdullah, Z., Boege, Y., Stemmer, K., Ringelhan, M., Simonavicius, N., Egger, M., Wohlleber, D., Lorentzen, A., Einer, C., Schulz, S., Clavel, T., Protzer, U., Thiele, C., Zischka, H., Moch, H., Tschöp, M., … Heikenwalder, M. (2014). Metabolic activation of intrahepatic CD8+ T cells and NKT cells causes nonalcoholic steatohepatitis and liver cancer via cross-talk with hepatocytes. *Cancer Cell*, *26*(4), 549–564. https://doi.org/10.1016/j.ccell.2014.09.003

Wren, A. M., Small, C. J., Ward, H. L., Murphy, K. G., Dakin, C. L., Taheri, S., Kennedy, A. R., Roberts, G. H., Morgan, D. G. A., Ghatei, M. A., & Bloom, S. R. (2000). The Novel Hypothalamic Peptide Ghrelin Stimulates Food Intake and Growth Hormone Secretion. *Endocrinology*, *141*(11), 4325–4328. https://doi.org/10.1210/ENDO.141.11.7873

Wu, Q., Ortegon, A. M., Tsang, B., Doege, H., Feingold, K. R., & Stahl, A. (2006). FATP1 Is an Insulin-Sensitive Fatty Acid Transporter Involved in Diet-Induced Obesity. *MOLECULAR AND CELLULAR BIOLOGY*, *26*(9), 3455–3467. https://doi.org/10.1128/MCB.26.9.3455-3467.2006

Wu, R., Chen, F., Wang, N., Tang, D., & Kang, R. (2020a). *ACOD1 in immunometabolism and disease*. https://doi.org/10.1038/s41423-020-0489-5

Wu, R., Chen, F., Wang, N., Tang, D., & Kang, R. (2020b). ACOD1 in immunometabolism and disease. *Cellular & Molecular Immunology*. https://doi.org/10.1038/s41423-020-0489-5

Wu, R., Liu, J., Wang, N., Zeng, L., Yu, C., Chen, F., Wang, H., Billiar, T. R., Jiang, J., Tang, D., & Kang, R. (2022). Aconitate decarboxylase 1 is a mediator of polymicrobial sepsis. *Science Translational Medicine*, *14*(659). https://doi.org/10.1126/SCITRANSLMED.ABO2028

Xiao, W., Wang, L., Xiao, R., Wu, M., Tan, J., & He, Y. (2011). Expression profile of human immune-responsive gene 1 and generation and characterization of polyclonal antiserum. *Molecular and Cellular Biochemistry*, *353*(1–2), 177–187. https://doi.org/10.1007/S11010-011-0784-7

Yahoo, N., Dudek, M., Knolle, P., & Heikenwälder, M. (2023). Role of immune responses in the development of NAFLD-associated liver cancer and prospects for therapeutic

modulation. *Journal of Hepatology*, *79*(2), 538–551. https://doi.org/10.1016/J.JHEP.2023.02.033/ATTACHMENT/7407D79D-77D0-4CD0-8B60-C4C78001C502/MMC1.PDF

Yamamoto, M., Yamazaki, S., Uematsu, S., Sato, S., Hemmmi, H., Hoshino, K., Kaisho, T., Kuwata, H., Takeuchi, O., Takeshige, K., Saitoh, T., Yamaoka, S., Yamamoto, N., Yamamoto, S., Muta, T., Takeda, K., & Akira, S. (2004). Regulation of Toll/IL-1-receptor-mediated gene expression by the inducible nuclear protein IκBζ. *Nature 2004 430:6996*, *430*(6996), 218–222. https://doi.org/10.1038/nature02738

Yang, A., & Mottillo, E. P. (n.d.). *Adipocyte Lipolysis: from molecular mechanisms of regulation to disease and therapeutics*. https://doi.org/10.1042/BCJ20190468

Yang, J. Y., Lee, Y. S., Kim, Y., Lee, S. H., Ryu, S., Fukuda, S., Hase, K., Yang, C. S., Lim, H. S., Kim, M. S., Kim, H. M., Ahn, S. H., Kwon, B. E., Ko, H. J., & Kweon, M. N. (2017a). Gut commensal Bacteroides acidifaciens prevents obesity and improves insulin sensitivity in mice. *Mucosal Immunology*, *10*(1), 104–116. https://doi.org/10.1038/MI.2016.42

Yang, J. Y., Lee, Y. S., Kim, Y., Lee, S. H., Ryu, S., Fukuda, S., Hase, K., Yang, C. S., Lim, H. S., Kim, M. S., Kim, H. M., Ahn, S. H., Kwon, B. E., Ko, H. J., & Kweon, M. N. (2017b). Gut commensal Bacteroides acidifaciens prevents obesity and improves insulin sensitivity in mice. *Mucosal Immunology*, *10*(1), 104–116. https://doi.org/10.1038/MI.2016.42

Yang, M., Qi, X., Li, N., Kaifi, J. T., Chen, S., Wheeler, A. A., Kimchi, E. T., Ericsson, A. C., Scott Rector, R., Staveley-O'Carroll, K. F., & Li, G. (2023). Western diet contributes to the pathogenesis of non-alcoholic steatohepatitis in male mice via remodeling gut microbiota and increasing production of 2-oleoylglycerol. *Nature Communications 2023 14:1*, *14*(1), 1–17. https://doi.org/10.1038/s41467-023-35861-1

Yanovski, S. Z., & Yanovski, J. A. (2014). Long-term Drug Treatment for Obesity: A Systematic and Clinical Review. *JAMA : The Journal of the American Medical Association*, *311*(1), 74. https://doi.org/10.1001/JAMA.2013.281361

Yanovski, S. Z., & Yanovski, J. A. (2015). Naltrexone-Extended Release plus Bupropion-Extended Release for Treatment of Obesity. *JAMA*, *313*(12), 1213. https://doi.org/10.1001/JAMA.2015.1617

Yao, B., Dong, T., Fu, A., Li, H., Jiang, C., Li, N., & Cai, S. (2022). Quantification and characterization of mouse and human tissue-resident microbiota by qPCR and 16S sequencing. *STAR Protocols*, *3*(4). https://doi.org/10.1016/J.XPRO.2022.101765

Yasuda, T., Masaki, T., Kakuma, T., & Yoshimatsu, H. (2003). Centrally administered ghrelin suppresses sympathetic nerve activity in brown adipose tissue of rats. *Neuroscience Letters*, *349*(2), 75–78. https://doi.org/10.1016/S0304-3940(03)00789-4

Ye, D., Wang, P., Chen, L. L., Guan, K. L., & Xiong, Y. (2024a). Itaconate in host inflammation and defense. *Trends in Endocrinology & Metabolism*, *35*(7), 586–606. https://doi.org/10.1016/J.TEM.2024.02.004

Ye, D., Wang, P., Chen, L.-L., Guan, K.-L., & Xiong, Y. (2024b). Feature Review Itaconate in host inflammation and defense. *Trends in Endocrinology & Metabolism*. https://doi.org/10.1016/j.tem.2024.02.004

Yi, P., & Li, L. J. (2012). The germfree murine animal: An important animal model for research on the relationship between gut microbiota and the host. *Veterinary Microbiology*, *157*(1–2), 1–7. https://doi.org/10.1016/J.VETMIC.2011.10.024

Yi, Z., Deng, M., Scott, M. J., Fu, G., Loughran, P. A., Lei, Z., Li, S., Sun, P., Yang, C., Li, W., Xu, H., Huang, F., & Billiar, T. R. (2020a). Immune-Responsive Gene 1/Itaconate Activates Nuclear Factor Erythroid 2-Related Factor 2 in Hepatocytes to Protect Against Liver Ischemia-Reperfusion Injury. *Hepatology*, *72*(4). https://doi.org/10.1002/hep.31147/suppinfo

Yi, Z., Deng, M., Scott, M. J., Fu, G., Loughran, P. A., Lei, Z., Li, S., Sun, P., Yang, C., Li, W., Xu, H., Huang, F., & Billiar, T. R. (2020b). Immune-Responsive Gene 1/Itaconate Activates Nuclear Factor Erythroid 2–Related Factor 2 in Hepatocytes to Protect Against Liver Ischemia–Reperfusion Injury. *Hepatology*, *72*(4), 1394–1411.

https://doi.org/10.1002/HEP.31147
Yoshida, N., Emoto, T., Yamashita, T., Watanabe, H., Hayashi, T., Tabata, T., Hoshi, N., Hatano, N., Ozawa, G., Sasaki, N., Mizoguchi, T., Amin, H. Z., Hirota, Y., Ogawa, W., Yamada, T., & Hirata, K. I. (2018). Bacteroides vulgatus and Bacteroides dorei Reduce Gut Microbial Lipopolysaccharide Production and Inhibit Atherosclerosis. *Circulation*, *138*(22), 2486–2498. https://doi.org/10.1161/CIRCULATIONAHA.118.033714
Yoshida, N., Yamashita, T., Osone, T., Hosooka, T., Shinohara, M., Kitahama, S., Sasaki, K., Sasaki, D., Yoneshiro, T., Suzuki, T., Emoto, T., Saito, Y., Ozawa, G., Hirota, Y., Kitaura, Y., Shimomura, Y., Okamatsu-Ogura, Y., Saito, M., Kondo, A., … Hirata, K. ichi. (2021). Bacteroides spp. promotes branched-chain amino acid catabolism in brown fat and inhibits obesity. *IScience*, *24*(11). https://doi.org/10.1016/J.ISCI.2021.103342
Yoshimoto, S., Loo, T. M., Atarashi, K., Kanda, H., Sato, S., Oyadomari, S., Iwakura, Y., Oshima, K., Morita, H., Hattori, M., Honda, K., Ishikawa, Y., Hara, E., & Ohtani, N. (2013). Obesity-induced gut microbial metabolite promotes liver cancer through senescence secretome. *Nature 2013 499:7456*, *499*(7456), 97–101. https://doi.org/10.1038/nature12347
You, H., Tan, Y., Yu, D., Qiu, S., Bai, Y., He, J., Cao, H., Che, Q., Guo, J., & Su, Z. (2022). The Therapeutic Effect of SCFA-Mediated Regulation of the Intestinal Environment on Obesity. *Frontiers in Nutrition*, *9*. https://doi.org/10.3389/FNUT.2022.886902
Younossi, Z. M., Golabi, P., Paik, J. M., Henry, A., Van Dongen, C., & Henry, L. (2023). The global epidemiology of nonalcoholic fatty liver disease (NAFLD) and nonalcoholic steatohepatitis (NASH): a systematic review. *Hepatology*, *77*(4), 1335–1347. https://doi.org/10.1097/HEP.0000000000000004
Yu, L. X., Yan, H. X., Liu, Q., Yang, W., Wu, H. P., Dong, W., Tang, L., Lin, Y., He, Y. Q., Zou, S. S., Wang, C., Zhang, H. L., Cao, G. W., Wu, M. C., & Wang, H. Y. (2010). Endotoxin accumulation prevents carcinogen-induced apoptosis and promotes liver tumorigenesis in rodents. *Hepatology (Baltimore, Md.)*, *52*(4), 1322–1333. https://doi.org/10.1002/HEP.23845
Yu, Z., Li, X., Quan, Y., Chen, J., Liu, J., Zheng, N., Liu, S., Wang, Y., Liu, W., Qiu, C., Wang, Y., Zheng, R., & Qin, J. (2024). Itaconate alleviates diet-induced obesity via activation of brown adipocyte thermogenesis. *Cell Reports*, *43*(5), 114142. https://doi.org/10.1016/j.celrep.2024.114142
Zeng, Y. R., Song, J. Bin, Wang, D., Huang, Z. X., Zhang, C., Sun, Y. P., Shu, G., Xiong, Y., Guan, K. L., Ye, D., & Wang, P. (2023). The immunometabolite itaconate stimulates OXGR1 to promote mucociliary clearance during the pulmonary innate immune response. *The Journal of Clinical Investigation*, *133*(6). https://doi.org/10.1172/JCI160463
Zhang, L., Dong, Y., Zhang, L., Wang, M., Zhou, Y., Jia, K., Wang, S., Wang, M., Li, Y., Luo, S., Lu, S., Fan, Y., Zhang, D., Yang, Y., Li, N., Yu, Y., Cao, X., & Hou, J. (2023). Mitochondrial IRG1 traps MCL-1 to induce hepatocyte apoptosis and promote carcinogenesis. *Cell Death & Disease*, *14*(9). https://doi.org/10.1038/S41419-023-06155-7
Zhang, X., Zhi, Y., Zan, X., Fan, K., Chen, K., Zhao, S., Dai, X., Li, L., Yang, Y., Hu, K., Gong, X., & Zhang, L. (2023). Immune response gene 1 deficiency aggravates high fat diet-induced nonalcoholic fatty liver disease via promotion of redox-sensitive AKT suppression. *Biochimica et Biophysica Acta (BBA) - Molecular Basis of Disease*, *1869*(4), 166656. https://doi.org/10.1016/J.BBADIS.2023.166656
Zhang, Z., Chen, C., Yang, F., Zeng, Y. X., Sun, P., Liu, P., & Li, X. (2022). Itaconate is a lysosomal inducer that promotes antibacterial innate immunity. *Molecular Cell*, *82*(15), 2844-2857.e10. https://doi.org/10.1016/J.MOLCEL.2022.05.009
Zhao, H., Teng, D., Yang, L., Xu, X., Chen, J., Jiang, T., Feng, A. Y., Zhang, Y., Frederick, D. T., Gu, L., Cai, L., Asara, J. M., Boland, G. M., Flaherty, K. T., Swanson, K. D., Liu, D., Rabinowitz, J. D., & Zheng, B. (2022). nature metabolism Myeloid-derived itaconate suppresses cytotoxic CD8 + T cells and promotes tumour growth Check for updates. *Nature Metabolism* |, *4*, 1660–1673. https://doi.org/10.1038/s42255-022-00676-9

Zhao, L., Zhang, F., Ding, X., Wu, G., Lam, Y. Y., Wang, X., Fu, H., Xue, X., Lu, C., Ma, J., Yu, L., Xu, C., Ren, Z., Xu, Y., Xu, S., Shen, H., Zhu, X., Shi, Y., Shen, Q., … Zhang, C. (2018). Gut bacteria selectively promoted by dietary fibers alleviate type 2 diabetes. *Science*, *359*(6380), 1151–1156. https://doi.org/10.1126/SCIENCE.AAO5774/SUPPL_FILE/AAO5774_ZHAO_SM.PDF

Zhao, Y., Liu, Z., Liu, G., Zhang, Y., Liu, S., Gan, D., Chang, W., Peng, X., Suh Sung, E., Gilbert, K., Zhu, Y., Wang, X., Zeng, Z., Baldwin, H., Ren, G., Weaver, J., Huron, A., Mayberry, T., Wang, Q., … Lu, X. (2023). Neutrophils resist ferroptosis and promote breast cancer metastasis through aconitate decarboxylase 1. *Cell Metabolism*, *35*, 1688-1702.e11. https://doi.org/10.1016/j.cmet.2023.09.004

Zhu, A., Ibrahim, J. G., & Love, M. I. (2019). Heavy-tailed prior distributions for sequence count data: removing the noise and preserving large differences. *Bioinformatics (Oxford, England)*, *35*(12), 2084–2092. https://doi.org/10.1093/BIOINFORMATICS/BTY895

Zsálig, D., Berta, A., Tóth, V., Szabó, Z., Simon, K., Figler, M., Pusztafalvi, H., & Polyák, É. (2023). A Review of the Relationship between Gut Microbiome and Obesity. *Applied Sciences 2023, Vol. 13, Page 610*, *13*(1), 610. https://doi.org/10.3390/APP13010610

Zurita, E., Chagoyen, M., Cantero, M., Alonso, R., González-Neira, A., López-Jiménez, A., López-Moreno, J. A., Landel, C. P., Benítez, J., Pazos, F., & Montoliu, L. (2011). Genetic polymorphisms among C57BL/6 mouse inbred strains. *Transgenic Research*, *20*(3), 481–489. https://doi.org/10.1007/S11248-010-9403-8/FIGURES/2

